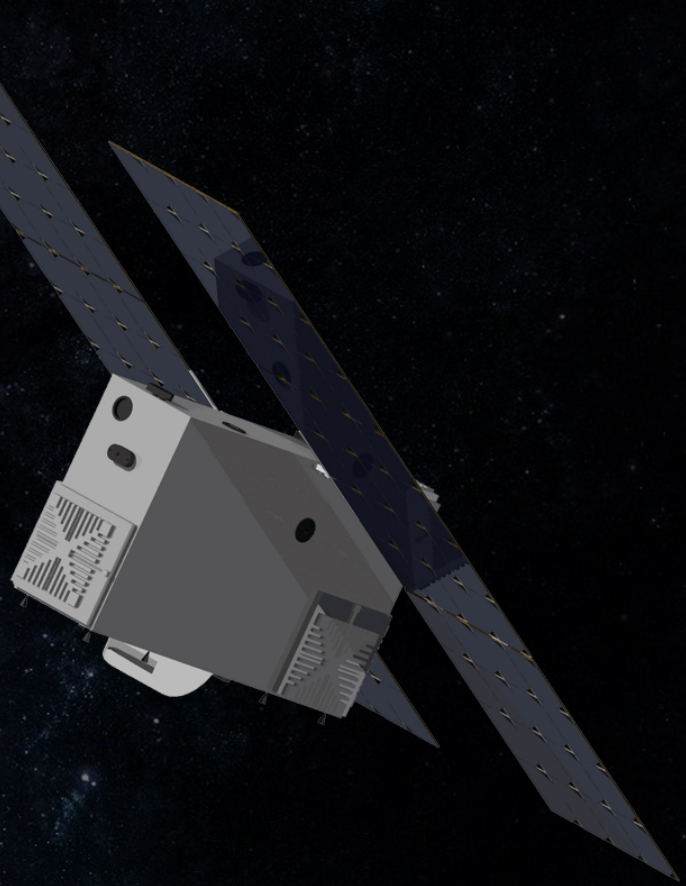


Final Report

Piggyback to Mars
Group S4



MICRO
PAVING THE WAY FOR INTERPLANETARY CUBESAT MISSIONS

*“Mars has been flown by, orbited, smacked into, radar examined, and rocketed onto,
as well as bounced upon, rolled over, shoveled, drilled into, baked and even blasted.
Still to come: Mars being stepped on.”*

– Buzz Aldrin, 2013

Final Report

Piggyback to Mars

by

Group S4

Students:	(M.E.A.)	El Akel, M.	4271548
	(M.F.)	Facchinelli, M.	4303040
	(G.H.)	Hirlav, G.	4135458
	(Y.F.H.)	Hu, Y.F.	4163095
	(E.K.)	Korhonen, E.	4272056
	(S.M.)	Mast, S.	4279425
	(A.N.)	Nawaz, A.	4276477
	(K.S.)	Samarawickrama, K.	4160568
	(M.v.S.)	van Strien, M.	4006240
	(D.T.)	Tol, D.	4290275
Tutor:	Dr. Ir.	van der Wal, W.	TU Delft, tutor
Coaches:	Dr. Ir.	Ellerbroek, J.	TU Delft, coach
	Ir.	Zhu, L.	TU Delft, coach

Cover page: Mars – NASA: <http://goo.gl/iHzUYt> [cited 24 June 2016]

Cover page: Terraforming of Mars – Wikipedia: <https://goo.gl/DmwsEI> [cited 24 June 2016]

Cover page: Stars – Chunoa: <http://goo.gl/ixC9xZ> [cited 24 June 2016]

Summary

MICRO (Mars Interplanetary Cubesat and Research Orbiter) is designed to be the first interplanetary cubesat to conduct a scientific mission on Mars in 2020. The mission aims at analysing the dust in Mars at specific location of interest to aid future manned mission. MICRO is developed as part of the 2016 Design Synthesis Exercise (DSE) by ten students at the Aerospace Engineering Faculty of Delft University of Technology.

Mars' atmosphere, as any other planet in the solar system, can be considered as a very hostile environment. Other than extreme temperatures and atmospheric properties, the surface of Mars is typically characterised by a thin layer of dust. While its effects have been studied by rovers on Mars, a lot still remains unknown. The dust is known to deposit on equipment posing operational and functional challenges. As dust particles vary in size, it might be hard to manage their removal from enclosed environments. For instance, contamination of living modules could pose a danger to future human settlers on Mars. Mapping of the dust can provide crucial information for future manned missions and help to comprehend the atmospheric radiative and chemical balance of Mars. In fact, dust particles as well as ice clouds on Mars are critical elements contributing to the weather system of Mars. Mapping their composition and spatial distribution could provide new insights into this convoluted system. Understanding of such a chaotic system, would not only be limited to Mars but could provide meteorological insight about Earth and other planets.

Analysis of microphysical dust and ice cloud properties on Mars is done by measuring properties of linear polarisation and the solar flux using SPEX (Spectropolarimeter for Planetary Exploration), which is selected as MICRO's scientific payload. The spectropolarimeter is a passive remote sensing instrument that measures these quantities as a function of single scattering sunlight angle in the wavelength range of 400 to 800 nm (2 nm intensity resolution). SPEX fits in almost a 1.5 unit module with no power consumption. The detector that has been selected is the HAWAII-H1RG along with the SIDECAR ASIC chip with a combined maximum power consumption of 1.5W.

The MICRO mission is a 6 unit micro-satellite designed to feature the SPEX as a payload to analyse the Martian surface. The advantage of a 6 unit micro-satellite is its low cost and high scientific gain. The high flexibility of the microsat enables it to be designed for a piggybacking option. MICRO mission is planned to be launched in 2020 with the GSLV III launcher with Mangalayan II satellite of the Indian Space Research Organisation as the host mission of MICRO. The duration of the mission 109 days, during which it orbits Mars 1330 times at 400 km altitude. MICRO undergoes a Sun synchronous quasi-polar orbit (inclination of 92.5 deg) which enables it to map the desired segments of the Martian surface.

MICRO has on-board capability to determine its attitude with three star trackers and four Sun sensors along with an inertial measurement unit. The attitude control is performed using four reaction wheels by Hyperion Technologies. Orbit determined using the aid of camera to detect the position with respect mars and scattering angle of sunlight. The propulsion system in MICRO is a dual unit Mono-propellant system called MPS 130 by Aerojet Rocketdyne. The system uses a green propellant AF-M315E to provide an specific impulse of 240 s. The two units have a combined capability to provide a ΔV of 248 ms^{-1} . One necessity of the mission is the ability to generate for all system and store power. The MICRO power subsystem uses high performance quadruple junction solar cells from Solarrow Technologies and has a total solar panel area of 0.215 m^2 . the power subsystem uses an array drive actuator for active sun tracking and maximum peak power generation. The two batteries implemented are MP14465 by SAFT gives the ability to perform during eclipse too.

MICRO obtains data using SPEX which is then processed by the on-board computer HT-CP 400.85 by Hyperion Technologies. The on-board computer has a power consumption of 0.5 W and delivers 500 MHz of processing capability. The data collected is transmitted back to Earth with the aid of a relay satellite Mars Reconnaissance Orbiter (MRO). communication is performed using five micro strip patch antennae, this enables to communicate independent of the orientation of the spacecraft. The telecommunication operates in the UHF band at 403 MHz to transmit and 435 MHz to receive telemetry. The 6U cubesat uses monocoque for load distribution and subsystem integration. Its structural panels guard the on-board systems from radiation, this is done by means of graded shielding composed of Tantalum and Aluminium. MICRO has a passive thermal control system, and capability to maintain temperature working temperature of -5°C to 27°C .

The MICRO mission address sustainability by means of using commercial off the shelf components and green propellant. In addition to the sustainable design solutions implemented, 3.16% of the budget is allocated for prosperity of the Earth and mankind by planting trees to compensate for the carbon foot print imposed at the launch. Finally, having the capability of sustaining the orbit for an estimated minimum of 167 Earth years, the COSPAR recommendations are met.

List of Symbols

Latin Symbols:

A	Cross-sectional area	[m ²]
a	Semi-major axis	[m]
B_n	Bandwidth	[Hz]
b	Albedo factor	[-]
b	Thruster arm length	[cm]
C	Consequence	[-]
C	Heat capacity	[J kg ⁻¹ K ⁻¹]
C_d	Drag coefficient	[-]
c	Speed of light	[m s ⁻¹]
D	Cubesat depth	[m]
D	Distance	[km]
D	Data size	[kB]
d	Orbital radius	[m]
E	Young's modulus	[GPa]
E	Energy	[Wh]
E_δ	Specific energy density	[Wh kg ⁻¹]
e	Eccentricity	[-]
F	Visibility factor	[-]
F	Safety factor	[-]
f	Frequency	[Hz]
g_0	Standard gravity	[m s ⁻²]
H	Angular momentum	[N m s]
h	Altitude	[km]
I_{sp}	Specific impulse	[s]
I	Mass moment of inertia	[kg m ²]
\mathbb{I}	Inertia tensor	[kg m ²]
i	Inclination	[deg]
J	Factor of oblateness	[-]
J	Solar intensity	[W m ²]
L	Cubesat length	[m]
L	Likelihood	[-]
l	Distance	[m]
m	Mass	[kg]
M	Mass fraction	[-]
M_δ	Specific mass density	[kg m ⁻²]
N	North	
P	Power	[W]
P	Load	[N]
\dot{Q}	Heat rate	[W]
q	Reflectance factor	[-]
r	Radius	[m]
R	Data/bit rate	[kB s ⁻¹]
R	Risk	[-]
R	Reliability	[-]
S	South	
S	Eclipse parameter	[m ²]
T	Temperature	[K]
T	Time	[s]
T	Period	[s]
T	Torque	[N m]
\mathbb{T}	Transformation matrix	[-]
U	One unit cubesat volume	[m ³]
U	RW imbalance factor	[gmm]
V	Velocity	[m s ⁻¹]
W	Cubesat width	[m]
W	Weight	[N]
X	Power transmission path efficiency	[-]
Z	Impedance	[Ω]

Greek Symbols:

α	Angle between MICRO and MRO	[deg]
α	Rotational acceleration	[rad s ⁻²]
α_s	Absorption factor	[-]
α_T	Thermal expansion coefficient	[μm m ⁻¹ °C ⁻¹]
γ	Flight path angle	[rad]
ΔV	Change in Velocity	[m s ⁻¹]
ϵ	Infrared emission factor	[-]
ϵ_{IR}	Infrared absorption factor	[-]
ϵ_r	Dielectric strength	[-]
η	Efficiency	[-]
θ	True anomaly	[rad]
λ	Carrier wavelength	[m]
μ	Standard gravitational parameter	[m ³ s ⁻²]
ρ	Air density	[kg m ⁻³]
σ_a	Axial normal stress	[N m ⁻²]
σ_l	Axial lateral stress	[N m ⁻²]
σ_b	Stephan-Boltzmann constant	[W m ⁻² K ⁻⁴]
θ	Solar incidence angle	deg
Υ	Longitude change equatorial ground track crossing	[deg]
Φ	Solar flux	[W m ⁻²]
Ψ	Eclipse parameter	[rad]
ω	Angular velocity	[rad s ⁻¹]
ω	Argument of perigee	[rad]
Ω	Ascending node	[rad]

Subscripts:

a	Aphelion
$aero$	Aerodynamic
avg	Average
b	Albedo
b	Burn
bat	Battery
$comm$	Communication
cr	Critical
D	Dynamic
D	Drag
e	Surface
ec	Eclipse
lat	Lateral
M	Mars
M	Mass
max	Maximum
MIC	MICRO
MS	Mars around Sun
p	Perihelion
$proc$	Processed
$prop$	Propellant
raw	raw
R, e	Receiver, effective
rev	Revised
s	System
s, p	Parallel system
S	Static
S	Sun
sol	Solar
SA	Solar array
sc	Solar cell/CIC
T, e	Transmitter, effective
t	Transfer Orbit
V	Volume

Abbreviations

ACU	Array Conditioning Unit	MIF	Mars Inertial Frame
ADC	Analog-to-Digital Converter	MOI	Mars Orbit Injection
ADN	Ammonium Dinitride	MRO	Mars Reconnaissance Orbiter
ADCS	Attitude Determination and Control Subsystem	n.a.	Not Available
AE	Faculty of Aerospace Engineering	NASA	National Aeronautics and Space Administration
AoLP	Angle of Linear Polarisation	NLR	Netherlands Aerospace Center
AODCS	Attitude and Orbit Determination and Control Subsystem	OBC	On-Board Computer
ASIC	Application-Specific Integrated Circuit	ODS	Orbit Determination Subsystem
AU	Astronomical Unit	OF	Orbital Frame
BWG	Beam Waveguide	OSI	Open Systems Interconnection
CAN	Controller Area Network	PC	Personal Communication
CCSDS	Consultative Committee Space Data Systems	PCB	Printed Circuit Board
CDH	Command and Data Handling	PCM	Pulse Code Modulation
CIC	Coverglass Interconnector and Cell	PDU	Power Distribution Unit
CMOS	Complementary Metal–Oxide–Semiconductor	PF	Perifocal Frame
CNSA	China National Space Administration	PMDC	Power Management, Distribution and Control
COSPAR	Committee on Space Research	PSK	Phase Shift Keying
COTS	Commercial Off-The-Shelf	R/T	Receptor and Transmitter
CPU	Central Processing Unit	RAM	Random Access Memory
CSD	Canisterized Satellite Dispenser	RBF	Remove Before Flight
CW	Continuous Waves	RF	Radio Frequency
DMIPS	Dhrystone Million Instructions Per Second	RHU	Radioisotope Heater Unit
DoLP	Degree of Linear Polarisation	RL	Return Loss
DSE	Design Synthesis Exercise	ROD	Review of Design
DSN	Deep Space Network	RTG	Radioisotope Thermoelectric Generator
DSS	Deep Space Station	RW	Reaction Wheel
EB	Engineering Budget	RX	Reception
EIRP	Equivalent Isotropic Radiated Power	S	South
EMC	Electromagnetic Compatibility	SAFT	Société des Accumulateurs Fixes et de Traction
EOL	End-of-Life	SADA	Solar Array Drive Actuator
EPS	Electrical Power Subsystem	SDRAM	Synchronous Dynamic Random Access Memory
ESA	European Space Agency	SF	Spacecraft Frame
FEM	Finite Element Method	SIDECAR	System for Image Digitization, Enhancement, Control And Retrieval
FOV	Field of View	SIF	Sun Inertial Frame
FPGA	Field-Programmable Gate Array	SPI	Serial Peripheral Interface
GMAT	General Mission Analysis Tool	SPENVIS	SPace ENVironment Information System
GCR	Galactic Cosmic Ray	SPEX	Spectropolarimeter for Planetary EXploration
GS	Ground Station	SS	Sun Sensor
GSLV	Geosynchronous Satellite Launch Vehicle	SSA	Sun Scattering Angle
G/T	Antenna Gain-to-Noise-Temperature	ST	Star Tracker
HAN	Hydroxyl Ammonium Nitrate	SRON	Stichting Ruimte Onderzoek Nederland
HGA	High-Gain Antenna	SVP	System Verification Plan
I ² C	Inter-Integrated Circuit	SWOT	Strengths, Weaknesses, Opportunities and Threats
ID	Identifier	T&C	Telemetry and Communication
IF	Inertial Frame	TCS	Thermal Control Subsystem
IFD	In-Flight Disconnect	TCXO	Temperature Compensated Crystal Oscillator
IMU	Inertial Measurement Unit	TEC	Thermal Expansion Coefficient
IR	Infra-Red Cleaning and Storage	TM	Telemetry
ISRO	Indian Space Research Organisation	TNO	Nederlandse Organisatie voor Toegepast Natuurwetenschappelijk Onderzoek
LIASON	Linked, Autonomous, Interplanetary Satellite Orbit Navigation	TRL	Technical Readiness Level
JTAG	Joint Test Action Group	TX	Transmission
LCL	Latching Current Limiter	UAE	United Arab Emirates
MB	Mega Byte	UHF	Ultra High Frequency
MCMF	Mars-Centred Mars-Fixed	ULA	United Launch Alliance
MCX	Micro Coaxial	UN	United Nations
MCU	Measurement Control Unit	U(S)ART	Universal (Synchronous) Asynchronous Receiver/Transmitter
MICRO	Mars Interplanetary Cubesat and Research Orbiter	USB	Universal Serial Bus
		V&V	Verification and Validation
		w.r.t.	With Respect To

Preface

Since the development of cubesats in 1999 by California Polytechnic State University and Stanford University, many cubesats have been launched into orbit. These tiny little cubesats prove to be of low cost, making them interesting subjects for academia. This document represents the Final Report for the Design Synthesis Exercise of group S4, written for the Aerospace Engineering at Technical University of Delft. Its purpose is to provide information to the principal tutor and the coaches, as well as any person who has a general interest in space missions related to cubesats.

We would like to express our gratitude towards our tutor Wouter van der Wal for giving us the opportunity to work on this exciting project. He allowed us a lot of freedom for coming up with our mission, which sparked our creativity we all could not develop during our bachelor. Furthermore, we would like to thank the coaches Joost Ellerbroek and Linyu Zhu for their general support and feedback on our report and progress. The occasional pop-ups and unplanned visits were great opportunities for us to ask questions.

We would like to thank Erin Mooij for the support and help during our first weeks of DSE, when our tutor was not able to be physically present. The OSCC members did a good job in organising the spring DSE of 2016. In addition, the OSSA did a great job in supporting the DSE projects.

We would like to thank Jasper Bouwmeester for his great insight in the design and features of cubesats in the many opportunities meetings of the first few weeks. Without his insight, we would not have a clear overview of a cubesat in general.

We would like to thank the team of experts who worked on SPEX: Jeroen Rietjens, Daphne Stam, Martijn Smit and Frans Snik. They have provided us with very detailed information and showed great support in our concept. Furthermore, they gave us the opportunity to talk with external experts and were willing to talk and collaborate with us during their free time, to assist us on our project.

Furthermore we are grateful for Bas Blank, Angelo Cervone and Barry Zandbergen for their expertise in their respective fields.

We are grateful for the companies Hyperion Technologies, Solar MEMS Technologies, Micro Aerospace Solutions for their help and feedback on cubesat components and providing us with detailed product specifications and capabilities.

Finally, we would like to thank the Delft University of Technology for providing facilities and a unique environment to develop and explore our talents and capabilities beyond space.

*Group S4
Delft, 28th June 2016*

Contents

Summary	ii
List of Symbols	iii
Abbreviations	iv
1 Introduction	1
I Mission Description	2
2 Market Analysis	3
2.1 Analysis of Emerging Markets	3
2.2 Scientific Mission	5
2.3 SWOT Analysis for MICRO	5
3 Scientific Mission	6
3.1 Scientific Background on Dust and Aerosols	6
3.2 Mission Overview and Considerations	6
3.3 Scientific Benefit	8
4 Payload	9
4.1 Scientific Payload: SPEX	9
4.2 Performance	11
5 Astrodynamic Characteristics	13
5.1 General Astrodynamics Characteristics	13
5.2 Mission Duration and Ground Track Optimisation	15
5.3 Nominal Mission Phase Simulation	17
5.4 Decay Rate and End-Of-Life	20
II Subsystem Design	22
6 Attitude and Orbit Determination and Control Subsystem	23
6.1 ADCS Design	23
6.2 ODS Design	28
6.3 Functional Flow Diagram	30
6.4 Layout	31
6.5 Control Operating Modes	31
6.6 Verification and Validation of Numerical Models	31
7 Propulsion Subsystem	33
7.1 Types of Propulsion Systems	33
7.2 Propulsion System Selection	36
7.3 Final Choice	36
7.4 Mission Operation	39
7.5 Recommendations	40
8 Command and Data Handling	41
8.1 Functions	41
8.2 On-Board Computer	41
8.3 Subsystem Data Interfaces	43
9 Telemetry and Communication	45
9.1 Proximity 1 Protocol	45
9.2 Subsystem Specifications	45
9.3 Transceiver Mechanism	47
9.4 Antenna	51
9.5 Quality Approach	54

10 Electrical Power Subsystem	55
10.1 Preliminary Trade-off Choices	55
10.2 Control Operating Modes and Subsystem Power Requirements	56
10.3 Solar Array Design	57
10.4 Power Storage	60
10.5 Power Management, Distribution and Control Subsystems	61
11 Bus Design	64
11.1 Structural Analysis	64
11.2 Thermal Control	68
11.3 Radiation	74
11.4 Verification and Validation of Numerical Models	79
12 Configuration and Layout	81
12.1 Deployment Mechanism	81
12.2 CAD Design	84
III System Performance	86
13 Technical Budgets	87
13.1 Mass Budget	87
13.2 Volume Budget	87
13.3 Comparison	88
13.4 ΔV Budget	88
14 Cost Budget	89
14.1 Cost Description	89
14.2 Cost Analysis	90
15 Requirements	91
15.1 Requirements and Compliance Matrices	91
15.2 Verification Methods	91
15.3 Cubesat Components	92
16 Sensitivity Analysis	96
16.1 Power Sensitivity Analysis	96
16.2 Launch Window Sensitivity	97
16.3 Host Mission Orbit Altitude	97
16.4 Feasibility and Robustness of the Design	98
17 Spacecraft System Characteristics	99
17.1 Mission Functional Flow Diagram	99
17.2 Cubesat Functional Breakdown Diagram	100
17.3 MICRO Specification Sheet	102
IV Mission Development	103
18 Assembly, Integration and Test	104
18.1 Assembly	104
18.2 Integration	105
18.3 Verification Phases	107
18.4 Logistics Diagram	109
19 Operations	111
19.1 Communication Flow	111
19.2 Ground Stations	112
19.3 Relay Satellite	114
19.4 Link Budgets	115
20 Sustainable Development	117
20.1 Sustainability of COTS	117
20.2 Green Propellant Advantage	117
20.3 Planetary Protection	117
20.4 MICRO Green Initiative	118

21 Risk Management	119
21.1 Statistics	119
21.2 Identification	119
21.3 Analysis	120
21.4 Mitigation.	122
21.5 Tracking.	123
22 Reliability, Availability, Maintainability and Safety	124
22.1 Reliability	124
22.2 Availability	125
22.3 Maintainability	125
22.4 Safety	126
23 Project Design and Development Logic	127
23.1 Design and Development Logic	127
23.2 Post-DSE Project Gantt Chart	128
24 Conclusion and Recommendations	130
A Reference Frames	132
B Parameters	134
C TCXO Instrument	135
D Link Budget Calculations	136
Bibliography	137

Introduction

Spacecraft development has evolved over the past two decades not only in terms of technology, but also in terms of size and mass. The purpose of cubesat development is to provide a standard for the design of micro-satellites to reduce development costs and time, increase accessibility to space and sustain frequent launches. The miniaturisation technology and its benefits have been demonstrated by cubesats orbiting Earth. However, this technology has not been demonstrated yet for interplanetary space missions.

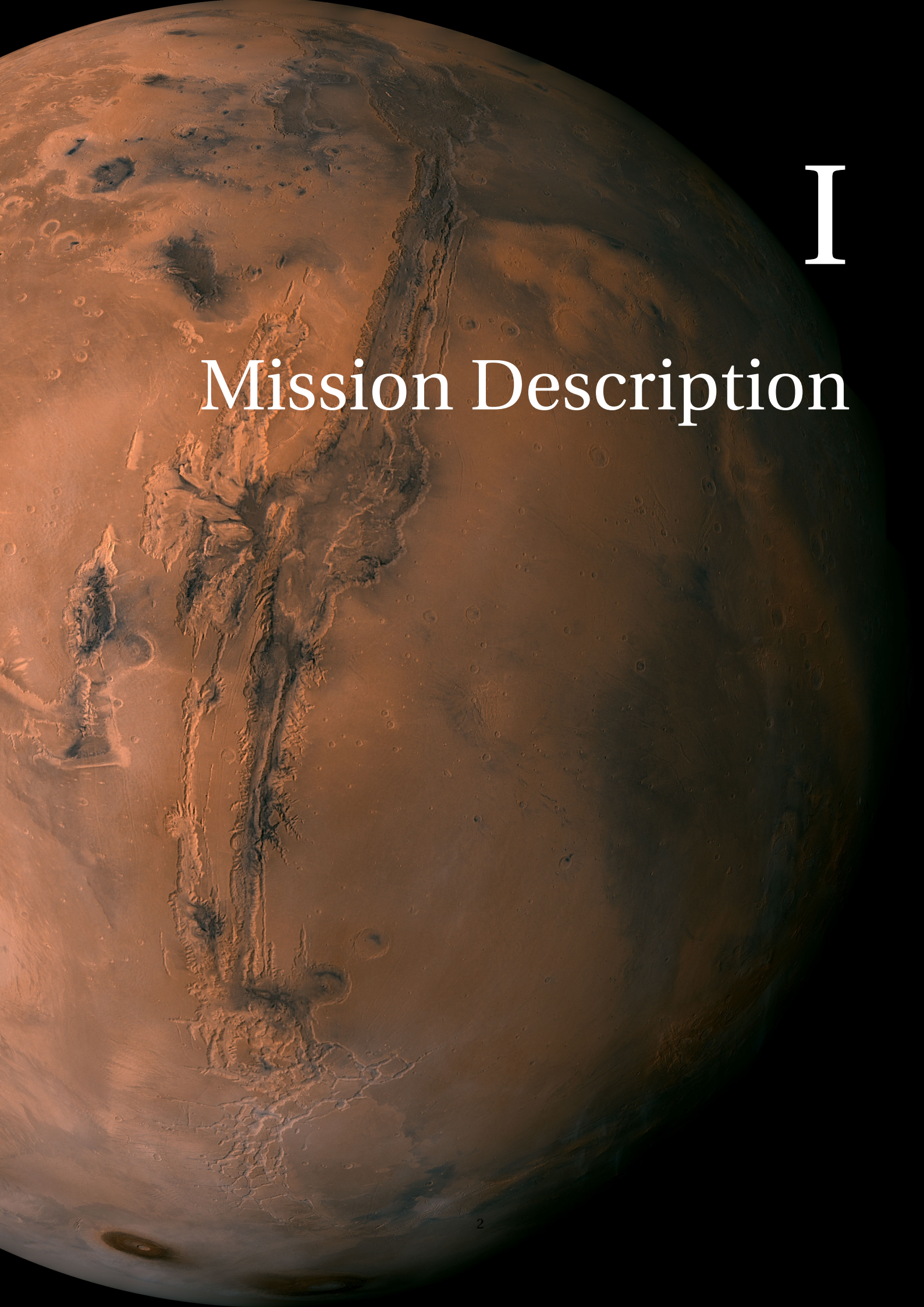
The aim of this DSE project is to design a cubesat mission that can join the launch of a larger mission, piggyback to Mars and successfully perform an interplanetary scientific mission. During the Mid-Term Report, several concepts were developed. The main outcome of the Mid-Term was to select one concept which will be further developed in this Final Report. The winning mission concept named MICRO, the Mars Interplanetary Cubesat and Research Orbiter, analyses the microphysical properties of dust on Mars using SPEX, the Spectropolarimeter for Planetary Exploration. There is a need to analyse the dust particles on Mars to aid in the selection of future Mars landing sites to protect the prospective astronauts and obtain knowledge on the properties of dust. The objective of the Final Report is to prove the feasibility and design of an interplanetary 6U cubesat, capable of performing a scientific mission on Mars with a lifetime budget of 10 million euro.

Part I gives a description of the mission. A market analysis is performed to select a scientific gap in Chapter 2. Chapter 3 will provide the reader with background information on the influence of dust on Mars and the scientific benefit for investigating the microphysical properties of dust on Mars. Furthermore, an overview of the mission is given in Chapter 3. The performance of the mission depend on the selected scientific payload, SPEX. The working principles, specifications and working principles are given in Chapter 4. Chapter 5 will detail on the mission duration and orbital parameters, dependent on the astrodynamic characteristics of MICRO.

Part II will elaborate on the design of the subsystems. Chapter 7 will select the propulsion subsystem. The Attitude and Orbit Determination and Control System works in conjunction with the propulsion system to provide knowledge and control of the attitude and orbit, elaborated in Chapter 6. Information and control of MICRO will be handled in the the Command and Data Handling Chapter 8. The data obtained from SPEX and subsystems have to be communicated back with the ground station, done by the telemetry subsystem in Chapter 9. The external lay-out is dominated by solar panels, designed in Chapter 10. The bus design which includes thermal and radiation handling are detailed in Chapter 11. The final configuration and lay-out is given in Chapter 12.

Part III will analyse the performance of the system. First the budgets are analysed, the technical budget in Chapter 13 and the cost budget in Chapter 14. Compliance with the determined requirements set up for MICRO are checked in Chapter 15. A sensitivity analysis is performed in Chapter 16 along with the feasibility of MICRO. Finally an overview of the spacecraft characteristics are given in Chapter 17.

Part IV goes into the development phases of the mission. The assembly, integration and testing phases along with the logistic diagram are given in Chapter 18. The operations of the ground station and Mars Reconnaissance Orbiter will be detailed in Chapter 19. Sustainable development was applied throughout the design of MICRO, elaborated in Chapter 20. The risks and mitigation strategies for MICRO are laid out in Chapter 21. The reliability, availability, maintainability and safety characteristics of the mission are discussed in Chapter 22. The design and development logic are given in Chapter 23 alongside the post DSE Gantt chart. Finally a conclusion about MICRO and recommendations are given in Chapter 24.



I

Mission Description

2

Market Analysis

Any project requires a market analysis in order to identify the objective opportunities for the developed product in the market and establish the competitive volume of the market for the product or for services the product can provide [W. Van Der Wal, pers. comm., 26th April 2016]. To do this, the current market should be analysed for comparable products or services and it should be assessed whether the new technology adds value to the market. In case of a scientific mission, the market analysis is a literature study on the scientific opportunities with respect to Mars. In Section 2.1, the emergence of new markets will be analysed. The MICRO mission was based on the prediction for future scientific missions to Mars and the corresponding scientific gaps elaborated in Section 2.2. Finally, a SWOT analysis for micro-satellites is given in Section 2.3

2.1. Analysis of Emerging Markets

The emergence of a new market is the result of the buyers demand which should be supplied by the sellers. One may wonder how the extent of the market for a product pertains to the extent of the demand for that product. This demand is most commonly expressed as the amount of a product or service that buyers would like to purchase for a certain price. The analysis of the correlation between the product/service and the public demand will be carried through two main parts in this section.

2.1.1. Launched Satellites

The current market for cubesats has been growing in the last decade to great extents and it is characterised by a rising popularity. There is an increasing number of initiatives from universities, state and private companies to design and launch cubesats. According to SpaceWorks¹ and Saint Louis University², the highest increase in the number of launched cubesats took place in 2012, with a 330% increase compared to 2011³. Because of this, the current market analysis will focus on the period starting from 2012, where the 23 launched cubesats have already been surpassed in 2016 (end of April). Furthermore, more than 80 % of the total number of launched cubesats were performed between 2012 and 2016. Year 2015 shows 215 cubesats launches, while 2016 shows 30 cubesat launches (up to end of April). Figure 2.1 displays the evolution of launched micro-satellites from 2012 onwards. One can notice that, up to 2014, the launch market for micro-satellites was using $\pm 90\%$ of all the available resources for launching cubesats. However, since 2015, a gap between the launched micro-satellites and the market capacity for launching has been linearly increasing. This is mainly due to the exponential rise of space missions, increasing the possibilities of piggybacking.

¹SpaceWorks Micro-satellite Market Analysis: <http://goo.gl/a08K8I> [cited 6 June 2016]

²Saint Louis Cubesat Database: <https://goo.gl/0WCTHh> [cited 6 June 2016]

³Small-satellite Market: <https://goo.gl/S2Xsqb> [cited 15 June 2016]

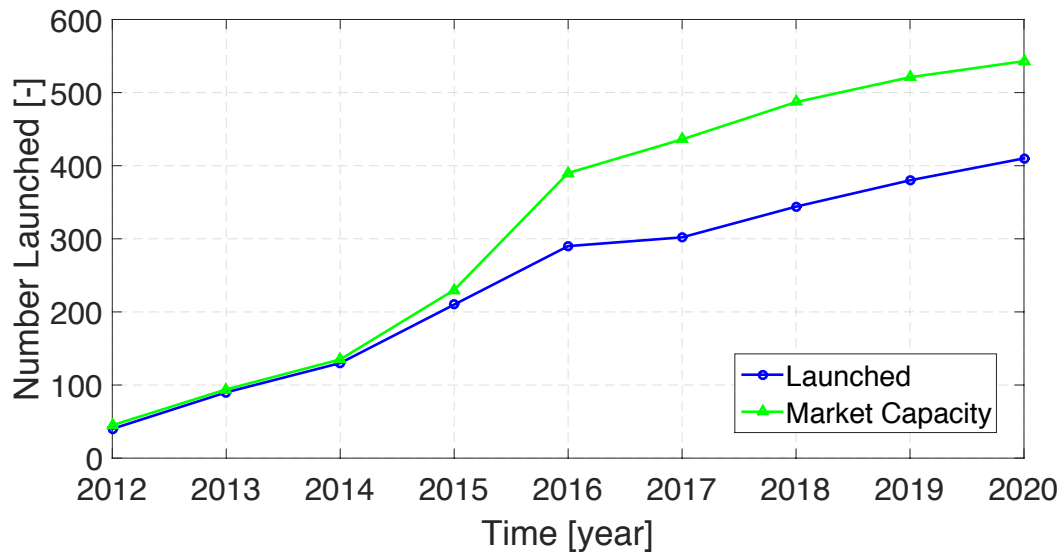


Figure 2.1: Launched micro-satellites

2.1.2. Current Market

An important factor to consider is the distribution of cubesat missions and initiators. If 2013 showed an approximately even distribution of launch initiatives between cubesat classes (i.e. commercial, governmental, military, university), 2014 and 2015 depict more than half of the launched cubesats for commercial purposes. Another crucial aspect for the market is the relation between the spacecraft class and the type of mission. The spacecraft class is given by the type of organisation that takes the initiative to design the cubesat, while the mission type is given by the purpose of the cubesat. The latter can be split into four main categories:

- *Earth observation*: mainly purposed for returning images of Earth, either for commercial purposes, for reconnaissance in case of military cubesats, or for general data, for the larger public.
- *Scientific*: the purpose is towards retrieving new scientific data or completing other science missions, where the collected data has to be clearly connected to end-user researchers; cubesats for educational purposes are included.
- *Communication*: the primary purpose is to relay communications between two points.
- *Technology development*: characterised by a clear purpose to test new technological capabilities.

From reference ² commercial cubesats focus on observation missions (85 %), which mainly consist of Earth imaging. University cubesat initiatives have an even share of scientific and technology demonstration missions (47 % each), mainly due to the educational nature of university cubesat initiatives and the scientific background of such missions. Military and governmental cubesats also rely on technology demonstration missions for cubesats (76 %). Therefore, from analysing the cubesat market from 2012 onwards, it can be concluded that the general purpose of cubesats is to demonstrate emerging technologies, with an evident emphasis on science and education for universities. Technology demonstration missions performed by cubesats are favourable because of their low cost, standardised design and continuous miniaturisation of technology, which makes such spacecraft ideal for high risk technology research and validation.

Furthermore, the market potential accounts for roughly 20 % of the market in 2015 and 25 % in 2016, predicted to grow to 30 % by 2018. This means that the current cubesat market has untapped potential for growth. It also has to be mentioned that there are more cubesats undergoing design and development without launching, either due to the lack of funds or launch opportunities, or because of the scope of the project.

As can be seen in Figure 2.2², which the distribution of cubesats according to the mission type, the micro-satellites encompass emerging technology, therefore their role over time has highly varied. At the beginning of their development, the use of micro-satellites was mainly focused on technology demonstration, as represented by the 55 % share of micro-satellite missions. A considerable interest was given for the scientific missions (21 %) while the communication and Earth observation missions were nearly equally distributed (10 % – 14 %).

However, since 2014, a considerable change of the mission distribution has been noticed, as described by Figure 2.2. The majority of the micro-satellites sent to space have as purpose to perform Earth observations. Over time, a decrease of technology demonstration cubesat mission (20 %) have been noted; which places this type of mission on the same level as the scientific purpose missions (17 %).

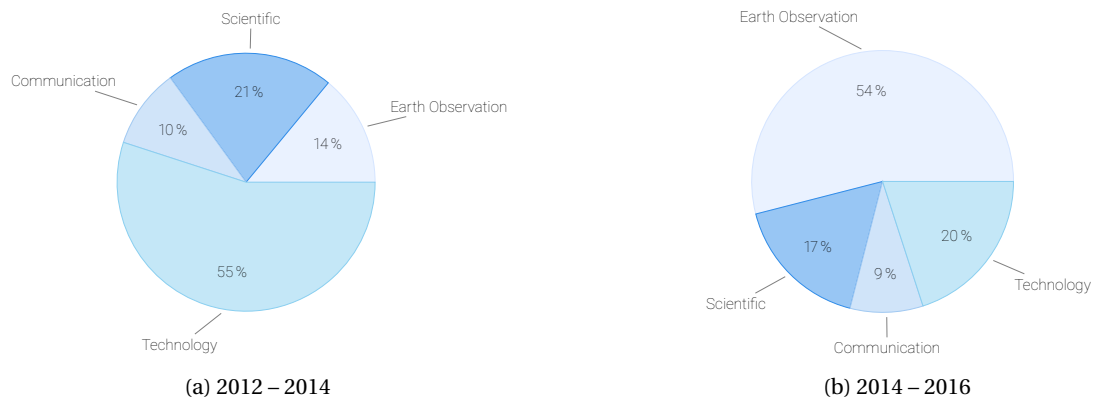


Figure 2.2: Mission type distribution: cubesats

2.2. Scientific Mission

Mars has been one of the target planets for satellite missions since the interplanetary explorations has become possible in the early seventies. However, some aspects of this planet still remain unknown. As shown by Figure 2.2, from the cubesats sent to space so far, a few contributions are meant for the scientific mission. Furthermore, despite growing interest from NASA and ESA, interplanetary cubesat missions have not flown yet. An analysis on the missions that have been performed and the eventual gaps for the scientific community has been done. Several missions to Mars would add a valuable contribution to the scientific community. Based on possible future mission [AFH⁺16], the feasible ones with a cubesat have been selected based on the availability of the instruments on the market. The selected mission, namely the dust analysis, will be explained in detail in Chapter 3.

2.3. SWOT Analysis for MICRO

In this section, a Strength, Weakness, Opportunities and Threats (SWOT) analysis for MICRO is shown in Table 2.1.

Table 2.1: SWOT analysis MICRO

	Helpful (to achieve the objective)	Harmful (to achieve the objective)
Internal origin (product/company attributes)	Rapid production and design Reduction in material and components used Lower costs Faster technological development High-risk, high-gain missions No concessions needed for payload design Higher efficiency Understanding of Martian climate Support to future Mars missions	Limited payload availability Available payloads with low scientific significance Concessions needed for sizing Dependency on host mission
External origin (environment/market attributes)	Possibility for higher risk missions Great for students Demonstration of new technologies Support to host mission Reproducible for other planets	Less capabilities Limited size Limited payload Creation of small-sized space debris

Scientific Mission

In this chapter, the scientific mission will be explained along with the method of conducting it. Background information on dust and aerosols is given in Section 3.1. The mission overview and considerations for performing the mission are given in Section 3.2. The scientific benefits to investigating the microphysical properties and distribution of these particles are finally given in Section 3.3. The aim is to fulfil the scientific gap found in Section 2.2.

3.1. Scientific Background on Dust and Aerosols

The surface of Mars is covered in a thin layer of dust. While its effects have been studied for decades, a lot still remains unknown. The dust on Mars is known to settle on rovers and other equipment, such as solar panels¹. The atmospheric dust has been found to be about $3\mu\text{m}$ [LWS⁺04] in diameter and these particles can cover the whole planet in an optically thick layer during massive dust storms [Can07]. Furthermore, the dust has been found to be quite abrasive which means it is a real hazard for equipment [FKS⁺99]. The dust storms thus make operations on the surface of Mars riskier due to the increased potential for damage caused by the dust. Dust storms are common and understanding them is crucial for the success of future Mars missions. In addition, studying microphysical properties (i.e. size, shape, composition) of atmospheric particles allows for better understanding of the weather and climate of a planet.

The dust itself is possibly a hazard to humans exploring Mars in the future. It might consist of silicates common on Mars that are highly reactive and could lead to severe health problems when inhaled². The physical characteristics of the dust could also cause trouble: the dust is possibly statically charged and thus sticky³ in addition to the particles' small size. This makes it hard to get rid of which leads to the dust being brought inside airlocks with the astronauts, leading to exposure. The charged state of the dust can also possibly be harmful for any electronics in the astronauts' suits or other machinery. The characteristics of the dust should be investigated before manned missions to Mars are launched to minimise the health risks to the astronauts. NASA is currently developing the capabilities needed to send humans to Mars in the 2030s which rely on the Orion mission⁴.

Some aerosols can act as cloud condensation particles, having an effect on and increasing the formation of clouds [H⁺11]. The aerosols can attract water droplets. These small droplets increase the lifetime of clouds and hence influence the effect of clouds on the climate. The aerosols thus influence the climate of Mars and have an effect on weather phenomena, such as dust devils and ice clouds. These dust devils can sometimes be local, existing for a day and going 1 km into the atmosphere. But sometimes, they can occur regionally or cover the whole planet in dust storms of up to 60 km [Can07].

3.2. Mission Overview and Considerations

The primary goal of the mission is to support the selection process for future Mars landing sites. The current rovers and most planned future landing sites are located between 30°S to 30°N latitude. One of the criteria for selecting the future Mars base locations is that there should not be enough dust to cause problems. Therefore the first priority will be to investigate these locations to determine the characteristics and distribution of the dust present.

¹NASA Dust: <http://goo.gl/BtZGF2> [cited 3 May 2016]

²Mars Dust Toxicity: <https://goo.gl/qr4JRZ> [cited 3 May 2016]

³Mars Dust Hazards: <https://goo.gl/VAXIaE> [cited 3 May 2016]

⁴Humans on Mars: <http://www.nasa.gov/content/nasas-journey-to-mars> [cited 26 May 2016]

The interesting locations can be found in Figure 3.1 which is adapted from NASA⁵. The locations indicated are obtained either from landing sites considered for Curiosity⁵ or the ExoMars rover⁶. These locations are representative of the suitable landing sites since they were considered for major rover missions. These locations are located around the equator. The same equatorial area is also observed to have a lot of iceclouds⁷. During an orbit around Mars, one location will be investigated and the data produced will be sent to the relay satellite. If multiple locations are located very close to each other, such as Holden and Eberswalde, they will be measured during the same orbit if possible. The same location can also be measured again after a period of time or orbit, to see if anything new happened or changed. The repeat time per location is random and therefore careful observation scheduling will be planned by the ground station as discussed in Subsection 19.2.3. For example, multiple measurements are needed to investigate a suitable Mars base location. One cannot conclude from one measurement whether a site is more suitable than the other, because there could be temporal changes. Some aspects for an ideal location would be that the area considered does not change much in time, not a lot of dust storms occur and the microphysical properties of dust allow for the placement of a future Mars base.

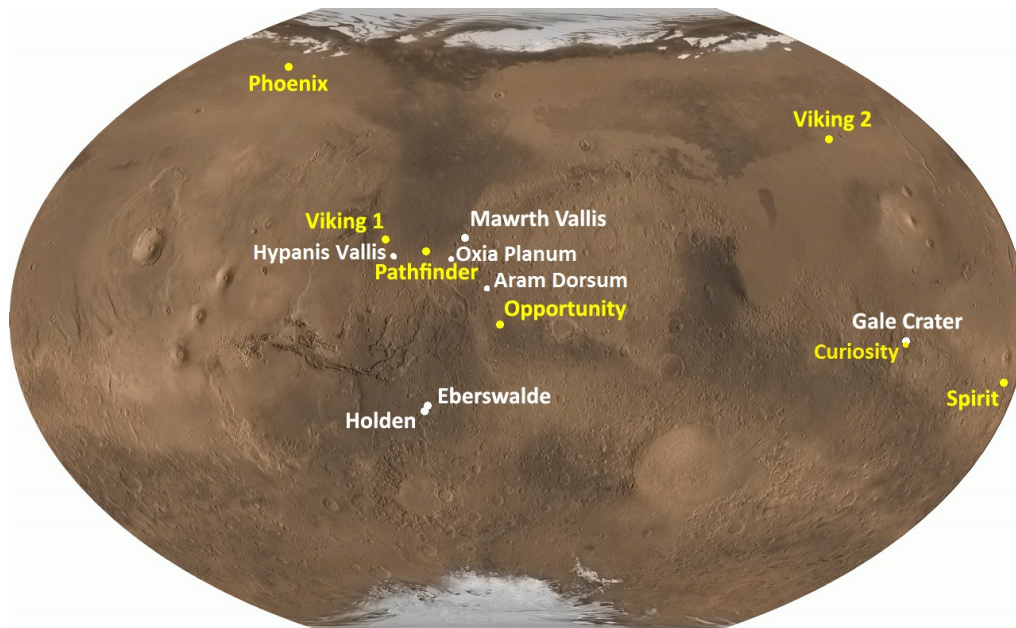


Figure 3.1: Location of sites and rovers

After performing the primary mission, the mission could be of supportive nature. For example by validating the data obtained from an existing Mars rover by measuring the microphysical properties of dust at the location of measurements done by the rover. Measurement locations can also be determined for example by making a survey among Mars scientists, to select the location which they think is interesting to investigate. Other possible options for measurements are the polar regions due to the fact that most of the dust present would be brought there by dust storms [D. Stam, pers. comm., May 2016]. If the dust present at the polar regions corresponds with dust from a different location, then one can conclude the dust has been or originated from that location. This would then provide some information on the climate of Mars. The previous presence of water can also be investigated by doing measurements on sites where dark streaks occur. The size distribution of dust depends on the geological history. More fine dust particles are usually distributed in the centre of rivers. Further exploration of dark streaks provides more clues to the location, origin and flow direction of ancient Mars rivers. In case there is a dust storm along the track of the satellite and it is known by the ground control in advance, commands can be sent to the spacecraft to take measurements of the storm and alter the mission. If no special areas of interest are along the ground track of the cubesat and there is a possibility of sending data, equatorial areas can also be measured to produce more scientific data. Mapping of the equatorial areas is useful as they are the most suitable for landing due to the moderate temperatures.

The obtained scientific data can be processed on-board to reduce the amount of data that has to be sent back. This processing reduces the size of the data generated by the detector. From time to time, the validity of the on-board processing has to be checked. Thus the raw data has to be sent back to Earth to perform the validation process. There is a possibility that certain unexpected spectra will be measured which requires an adaptation in the reduction

⁵Curiosity Landing Sites: <http://mars.nasa.gov/msl/mission/timeline/prelaunch/landingsiteselection/> [cited 1 June 2016]

⁶ExoMars Recommended Landing Sites: <http://goo.gl/CVBk91> [cited 1 June 2016]

⁷Ice Clouds: <http://goo.gl/Eypiyj> [cited 23 June 2016]

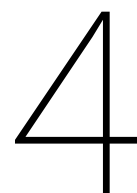
algorithm [D. Stam, pers. comm. May 2016]. The mission performance and the spatial coverage will depend on the total amount of data produced by SPEX explained in Section 4.2. The amount of data depends on the available memory given in Chapter 8, the astrodynamic characteristics given in Chapter 5 and the amount of data that can be sent back or received by the antennae in Chapter 9.

3.3. Scientific Benefit

Investigating the composition and spatial distribution of dust is both interesting for the science community and a necessity if human occupation of Mars is made a reality. There are too many uncertainties regarding the dust to be certain about its safety for the astronauts, such as its chemical properties and particle size and shape. This is an opportunity for a cubesat mission to investigate the dust and contribute to the future of space travel. Knowledge on location of the formation and occurrence of dust storms allows for better selection for the location of future Mars bases. Conducting the research with a small satellite is not only cheaper but offers some unique possibilities. The mission can be conducted with an inexpensive 6U cubesat and the orbits could be made riskier without endangering the large investment of large Mars missions. The science return of the mission would in any case be highly beneficial for future considerations. The SPEX instrument will be able to provide knowledge on the microphysical properties of the particles in the Martian atmosphere [H⁺11]. Besides understanding the dust particles, SPEX also allows for simultaneously studying the H₂O or CO₂ ice crystals that form thin clouds high in the atmosphere [SSL08]. This is because the instrument has 2 limb viewing angles which are pointed towards the limb atmosphere whilst the 7 viewing angles are pointed towards the surface as explained in Subsection 4.1.1.

Moreover, the climate on Earth is a combination of several weather phenomena. These weather phenomena cannot be zoned out individually on Earth and are difficult to simulate. Dust storms found on Earth also occur on Mars. However, the occurrence of these dust storms on Earth can have a multitude of reasons. On Mars, there are less weather phenomena and factors which can cause them. The study of the individual weather phenomena (e.g. the dust storms on Mars) provides insight into elements of the Earth's climate [H⁺11]. Understanding the interaction of tiny aerosols with the clouds gives better understanding of the climate on Mars but also on Earth. The use of artificial nanoparticles can ultimately enable manipulation of the climate.

Investigating the landing sites of current Mars rovers and future locations for Mars bases provides scientific support. The cubesat can observe the area around current rovers and further narrow down interesting locations to explore by the rovers. These rover landing sites are located near interesting places which provide a science return in terms of for example potential microbiological life and historical geological features. Interesting and promising locations for these rovers can be scouted and sites with high interest can be selected for the rover to explore.



Payload

This chapter describes the scientific payload along with the working principles in Section 4.1. The performance of the SPEX payload in conjunction with the subsystems is given in Section 4.2.

4.1. Scientific Payload: SPEX

SPEX (Spectropolarimeter for Planetary EXploration) is a spectropolarimeter developed in the Netherlands by various researchers from SRON [H⁺11]. It has been specifically designed for observing the microphysical properties of aerosols on Mars from space. In this section the working principle of the instrument is explained along with its specifications and the required electronics.

4.1.1. SPEX Working Principle

SPEX measures three properties: the degree of linear polarisation (DoLP), the angle of linear polarisation (AoLP) and the flux of the sunlight [FREQ-SS-PL1, 15]. These measurements are done over the whole spectrum of the instrument from visible to near-infrared: 400 to 800 nm [H⁺11] [FREQ-SS-PL2, 15] with a spectral resolution of 20 nm [FREQ-SS-PL3, 15]. The instrument has nine different viewing directions: seven for measuring dust [FREQ-SS-PL4, 15] and two limb directions for simultaneously measuring the particles in the ice clouds [Laa09] [FREQ-SS-PL5, 15]. This means that each pixel on the surface is measured seven times at seven different scattering angles. The AODCS, Attitude and Orbit Determination and Control Subsystem, will determine the scattering angle of the sunlight as described in Subsection 6.3. From the variance of the three measured quantities with the scattering angle, the characteristics of the dust and ice particles can be deduced. This requires that the scattering angles corresponding with each viewing direction are known at all times, provided by the AODCS in Chapter 6. The whole spectrum from 400 to 800 nm from the nine apertures is observed simultaneously and imaged by the detector. Additionally, information on the DoLP, AoLP and the flux in all directions is obtained at the same time. This provides information on the microphysical aerosol properties on Mars [FREQ-SS-PL6, 15]. Remarkably, SPEX uses no moving parts for the polarisation optics which makes it more reliable during its operational life [H⁺11]. The instrument's ability to measure the wide range of wave lengths and its polarisation properties simultaneously is an added strength to the instrument, simply because no physical changes or adjustments are required between subsequent measurements. The functional breakdown structure can be found in Figure 17.3 in Section 17.2.

4.1.2. SPEX Specifications

The SPEX instrument has been FEM analysed for thermal, stiffness and strength calculations [H⁺11]. The mechanical design is aimed at operation in space and survival of launch vibrations and has been validated to at least technical readiness level, TRL 6. SPEX does not require active alignment of optical elements through modern production techniques such as spark eroding and diamond turning [H⁺11]. The specifications for SPEX can be found in Table 4.1, taken from references [H⁺11, Laa09, SSL08]. For clarification, the SPEX instrument does not house any electronics and is solid state. The electronic system and power consumption are based off of the detector. The specifications of the detector, HAWAII H1RG, can be found in Table 4.2 [BAB⁺11] and was used in the baseline SPEX [DGA⁺10]. The detector includes a companion SIDECAR ASIC (application-specific integrated circuit) chip, which "reduces the complexity, volume and power needed to interface with the detector and reduces the output data from the detector" [DGA⁺10] the specifications for the detector and chip are taken from [BAB⁺11, BBG⁺08, LBGX07, DGA⁺10]. All the components of the SPEX, including the HAWAII H1RG and SIDECAR ASIC are rated 100 krad or greater [DGA⁺10]. SPEX is shown in Figure 4.1 [VMH⁺11].

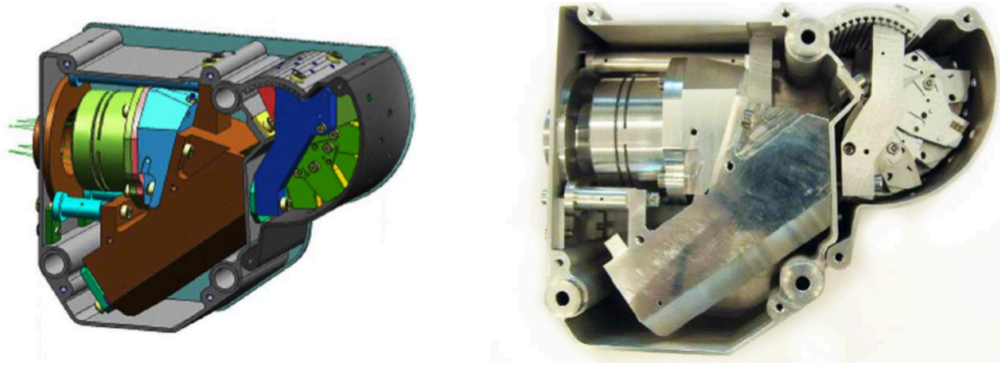


Figure 4.1: Schematic of SPEX (left) and the built instrument (right)

Table 4.1: SPEX specifications

Parameter	Value	Unit
Mass excluding electronics	0.9	[kg]
Maximum power consumption	0	[W]
Spectral range	400 – 800	[nm]
Spectral resolution for polarisation	20	[nm]
Spectral resolution for intensity	2	[nm]
Total amount of viewing directions	9	[–]
Amount of limb viewing directions	2	[–]
Viewing directions	0, ± 14 , ± 28 , ± 42 , ± 56	[–]
FOV for each viewing direction along-track	1	[deg]
FOV for each viewing direction cross-track	7	[deg]
Polarisation sensitivity	0.005	[–]
Relative polarisation accuracy	5	[%]
Dimension	152x115x63	[mm]
Pointing accuracy required	<1800	[arcsec]
Pointing knowledge required	<360	[arcsecs ⁻¹]
Operational temperature	-10 to 30	[°C]
TRL	6+	[–]
Cost	1.9	[M€]

Table 4.2: HAWAII H1RG and SIDECAR ASIC specifications

Parameter	Value	Unit
Total mass	<0.1	[kg]
Total maximum power consumption	<1.5	[W]
Sensor type	CMOS	[–]
Resolution	1024x1024	[–]
ADC	12 and 16	[bit]
Pixel size	18	[μm]
Total dimension	45x45x20	[mm]
Operating temperature	-243 to 27	[°C]
TRL HAWAII H1RG	9	[–]
TRL SIDECAR ASIC	6	[–]
Cost HAWAII H1RG	1.8	[M€]
Cost SIDECAR ASIC with firmware	1.5	[M€]

From Table 4.1, the requirement on pointing accuracy [FREQ-SS-AO3, Ch. 15] is derived.

4.1.3. Temperature Calibration

The temperature inside the cubesat can not be assumed to be constant and gradients can occur over the length of the SPEX optics. For this reason it is extremely important to quantify the effect of varying temperatures on the

measurements. This is done on the ground before the assembly of the cubesat. To do the temperature calibration, temperature sensors are put on both ends of the instrument. The temperature is then varied along the range expected to be encountered when taking scientific measurements, the operational temperature range.

The measurements being taken are known beforehand so that variations can be identified in the DoLP and AoLP.

The effects of a temperature gradient over the instrument are also checked. Based on the results of the calibration, the measurements taken during the mission can be properly analysed when the corresponding instrument temperatures are known [M. Smit and F. Snik, pers. comm. 13th June 2016].

Technical Readiness Level

The technical readiness level is currently between 6 and 7 [Snik, pers. comm., 13th May 2016] for the SPEX instrument found in [H⁺11] which is confirmed by [DGA⁺10]. Successful completion of NASA's TRL 5 implies that the system has undergone the verification and validation process¹. Since every component is above TRL 5, going through the verification and validation process for the scientific payload is not needed.

Processed Data Size

The detector is directly interfaced to the SIDECAR ASIC chip, which contains a programmable microcontroller. The chip handles the in-flight data processing. The principle described in this section by Martijn Smit [pers. comm., 2nd June 2016] is assumed to have an oversampling factor of two along the swath width, resulting in 15 ground pixels along swath width. It is assumed to have no oversampling along track, thus one ground pixel along track. For every viewing angle the degree of polarisation and radiance at a number of wavelengths needs to be known [vH14]. The amount of wavelengths needed to retrieve the aerosol properties is 5 [Smit, pers. comm., 2nd June 2016]. The DoLP is a value between 0 and 1, which is wanted with a precision of about 0.001. This leads to a dynamic range of 1000, which needs at least 10 bits to represent. However, the SIDECAR ASIC has 12 and 16 bit depth capabilities, done by the analogue to digital converter (ADC), to handle the bit conversion. Thus to represent the dynamic range of polarisation, 12 bits are used. The radiance has a larger dynamic range, hence 16 bits are used to represent it. The processed data size, D_{proc} is equal to the total amount of viewing angles multiplied with the ground pixel along swath multiplied with the ground pixel along track multiplied with the number of wavelengths sampled multiplied with the total bit depth required. The total bit depth required is 12 plus 16, 12 for the polarisation and 16 for the radiance. The processed data size per measurement is thus $D_{proc} = 2363 \text{ B} = 18904 \text{ bit}$. The data processing will be handled by the on-board computer given in Chapter 8.

4.2. Performance

This section calculates the minimal amount of measurements needed to be taken for the largest site. The amount of measurements that have to be taken per site depends on the size of the largest interesting landing sites from Figure 3.1, the length of the landing sites can be found in Table 4.3. When the largest site can be measured, one guarantees that the smaller sites can be measured too. The amount of measurements needed to investigate the sites depend on the orbital velocity which is 3.36 km s^{-1} from Subsection 5.1.3 and the landing sites^{2 3 4 5 6 7} [Gre12]. The largest site to investigate is thus Mawrth Vallis.

Table 4.3: Site sizes

Site	Largest dimension [km]
Aram Dorsum	80
Eberswalde	65
Gale Crater	154
Holden	140
Hypanis Vallis	104
Mawrth Vallis	636
Oxia Planum	300

Each measurement taken gives a raw data file. This size is the resolution of the detector multiplied with the required bit depth. For the raw data, no processing will be done, thus the highest bit depth has to be taken as a

¹NASA TRL: https://esto.nasa.gov/files/trl_definitions.pdf [cited 1 June 2016]

²Aram Dorsum: <http://exploration.esa.int/mars/54722-aram-dorsum/> [cited 8 June 2016]

³Eberswalde: <http://goo.gl/CEikuM> [cited 8 June 2016]

⁴Gale Crater: http://www.nasa.gov/mission_pages/msl/news/msl20110722.html [cited 8 June 2016]

⁵Holden: <http://goo.gl/aaxUKE> [cited 8 June 2016]

⁶Hypanis Vallis: <http://exploration.esa.int/mars/54712-hypanis-vallis/> [cited 8 June 2016]

⁷Oxia Planum: <http://exploration.esa.int/mars/54724-oxia-planum/> [cited 8 June 2016]

minimum. The highest bit depth required is 16, to represent the radiance. Hence the raw data size per measurement is $D_{raw} = 16778 \text{ kbit}$. The raw data has to be stored on the flash memory before it can be processed. After processing the raw data, it goes back to the flash memory from where it is sent to the MRO. Thus the amount of measurements that can be taken in one sequence, is dependent on the size of the flash memory.

To have sufficient amount of detail of Mawrth Vallis, an oversampling rate of two is desired. The ground pixel size along-track is 7 km from Subsection 5.1.3. Thus taking into account the orbital velocity, measurements have to be taken at 1 Hz. The total amount of measurements needed is then simply the length of Mawrth divided by the orbital velocity. This means a total of 190 measurements are needed to map the largest site, Mawrth Vallis. The required memory size to store 190 raw measurements is 3188 Mbit. From Subsection 8.2.3 the total memory that was selected is 512 MB or 4096 Mbit. This is enough to store all the data. The time it takes to process the raw measurements is about 10 seconds [M. Smit and F. Snik, pers. comm. 13th June 2016]. In conclusion, it will take a maximum of 4 minutes to take a series of 190 measurements and process the data, afterwards the data can be sent to MRO or a new sequence of measurements can start.

From time to time, the raw data has to be sent back to Earth as explained in Section 3.2. Iterating the amount of raw data which can be sent, whilst still having an achievable link budget, is 6 raw images. The total amount of data for sending 6 raw images is 12.6 MB or 100668 kbit. The command for sending the raw files will come from Earth. When the scientific payload starts-up, the detector has to acquire focus, thus the first four measurements are discarded due to inaccuracy [M. Smit and F. Snik, pers. comm., 13th June 2016].

Due to the current configuration of SPEX, the cubesat has to be slightly angled. This tilting of the cubesat will be done by the AODCS system, as explained in Subsection 6.1.3. The spacecraft with SPEX will fly over a certain site and the same ground pixel will eventually be observed at 9 different scattering angles. Figure 4.2 shows a model of MICRO flying over a certain site on Mars. In the middle of the figure, it is indicated that the same region is measured by the foremost and aftmost ground-pointing viewing angle.

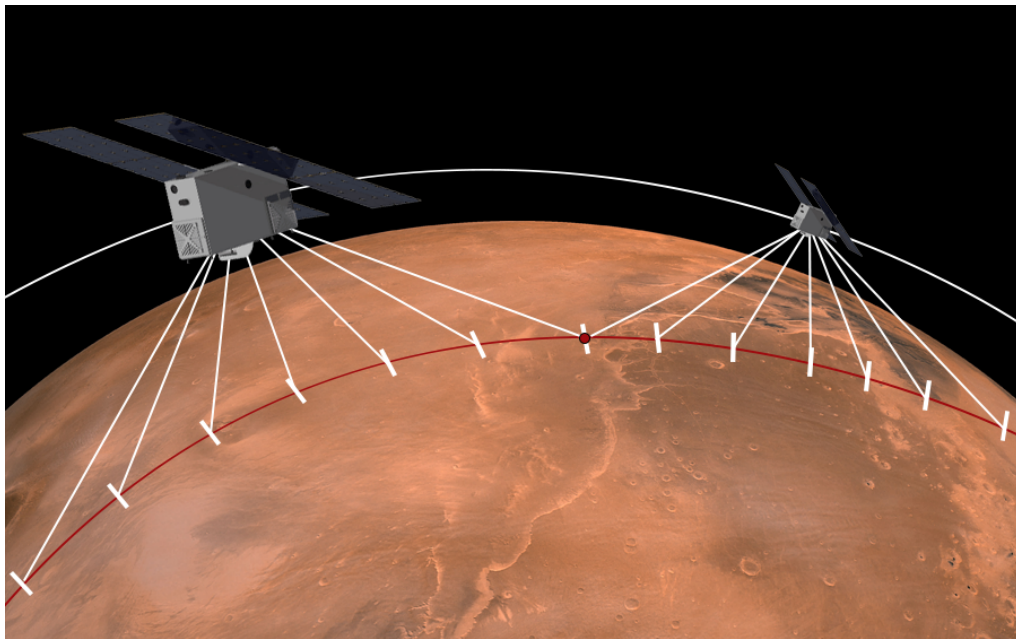


Figure 4.2: Measurements along track by SPEX as MICRO flies along its orbit

Astrodynamic Characteristics

Essential to the functionality of any space mission are the astrodynamic characteristics of its respective space vehicle(s). This chapter broadly outlines all relevant astrodynamic characteristics of the MICRO mission. Firstly, Section 5.1 describes the general characteristics of the mission that can be determined analytically including the transfer to Mars and the host mission selection. Secondly, the nominal mission duration and the ground track of the mission are determined in Section 5.2. Thirdly, Section 5.3 outlines the simulation of the nominal mission phase. Finally, the decay rate of MICRO and the end-of-life strategy of the mission are depicted in Section 5.4. To ensure the reproducibility of the obtained results, essential astrodynamic parameters used throughout this chapter can be found in Table B.1a of Appendix B.

5.1. General Astrodynamics Characteristics

This section describes the general astrodynamic characteristics of MICRO that can be derived using basic orbital analysis techniques and trade-offs. The initial orbital characteristics established in the Midterm Report [AFH⁺16] are updated and some of them briefly repeated (such as the transfer to Mars and the host mission selection).

5.1.1. Transfer to Mars

A crucial aspect of any mission to Mars is the interplanetary transfer to get there. A cubesat has a possibly great benefit with regards to this transfer in the sense that it could piggyback with another larger spacecraft. It is assumed that the cubesat piggybacks with another Mars mission during the launch phase. The trade-off that has to be made is whether the cubesat detaches from the host spacecraft before setting course to Mars and uses its own propulsion system to do the transfer or if it piggybacks along with the main mission until it reaches Mars.

In the Midterm Report [AFH⁺16] it was determined that performing a solo transfer to Mars would require a ΔV of 5.7 km s^{-1} . This assumes a Hohmann transfer to Mars from a 185 km parking orbit around Earth to a circular orbit around Mars of 400 km, which is a regular science orbit¹. This budget resulted from the summation of the ΔV manoeuvres at Earth and at Mars (See Table 5.1).

Table 5.1: Required ΔV for manoeuvres at Earth and Mars to perform a Hohmann transfer orbit from Earth to Mars

ΔV	Earth ΔV_1	Mars ΔV_2	Total ΔV_T	Unit
Value	3.616	2.081	5.697	[km s^{-1}]

Using the rocket equation (5.1) [LWH09], the required propellant fraction can be calculated to perform the total ΔV .

$$M_{Prop} = 1 - e^{-\frac{\Delta V}{I_{sp} g_0}} \quad (5.1)$$

Using the most efficient types of propulsion like electric, magnetic or ion propulsion which could have a specific impulse of up to 2500 s [Cer15], a propellant mass fraction of 0.21 would be required. This does not even include the propulsion system itself (dry mass).

¹Exomars Trace Gas Orbiter and Schiaparelli Mission: <http://exploration.esa.int/mars/46124-mission-overview/> [cited 4 May 2016]

It is clear that the propulsion system would impose major constraints on the design of the cubesat in terms of volume, mass and power. The advantage of piggybacking clearly outweighs its disadvantages: possible hazard to host mission, host needs more propellant, less launch options and no use of an RTG (radioisotope thermoelectric generator) or pyrotechnics. Therefore, it is decided that the cubesat will piggyback a planned mission to Mars and will detach from it when the host is in its nominal mission orbit resulting in requirement [OREQ-M-HO3, Ch. 15].

5.1.2. Host Mission and Launcher Selection

Knowing that MICRO will piggyback on another mission, the next logical step is the selection of the host mission and its respective launcher. The available missions that are currently in development^{2 3 4 5 6 7 8} are presented in Table 5.2.

Table 5.2: Future Mars missions in development

Mission	Insight	Red Dragon	Mangalyaan 2	Mars Hope	Mars 2020	ExoMars Rover	2020 Chinese Mars Mission
Launch	5 May 2018	2018	July 2020	July 2020	July 2020	July 2020	2020
Craft Type	Lander	Lander	Orbiter	Orbiter	Rover	Rover	Orbiter, rover
Space Agency	NASA	SpaceX	ISRO	UAE	NASA	ESA	CNSA

Of the missions shown above, four intend to land a spacecraft on the surface of Mars and will not include an orbiter. Insight, Red Dragon, Mars 2020 and ExoMars are all lander missions. These missions do not go into a circular orbit around Mars before entering the atmosphere and landing on the surface. Straight from their interplanetary trajectory, they dive into the atmosphere and do not slow down beforehand. This approach is common for lander and rover missions⁹. The discrepancy between the velocity of a circular orbit around Mars and the approach velocity of a lander mission is approximately 2 km s^{-1} . This amount of ΔV is too large to be achieved by a cubesat using high-thrust propulsion systems (required to slow down the cubesat within a relatively short time-frame). Therefore, those lander missions can be discarded as viable options.

Subsequently, the only available missions to piggyback are Mars Hope, Mangalyaan 2 and the Chinese Mars mission. Since ISRO is the only space agency out of the three which has demonstrated a successful mission to Mars (Mars Orbiter Mission)¹⁰, this mission is deemed more reliable. Furthermore, the UAE and the CNSA only provide scarce information on their missions. Based on these considerations, the Mangalyaan 2 mission is selected as the host mission with its launcher GSLV III¹¹ resulting in requirements [OREQ-M-HO2, Ch. 15] and [CREQ-M-SC1, Ch. 15].

5.1.3. Orbital Characteristics and Insertion

Since no information is available on the orbital characteristics of the Mangalyaan 2 mission, it is assumed that the cubesat is deployed from the host in a Sun-synchronous orbit around Mars within an altitude range of 200–500 km. These characteristics are common for Mars missions^{12 13 14 15} and is therefore a valid assumption. Nonetheless, a sensitivity analysis is carried out in Chapter 16 with respect to this assumption to find out what the impact is on the mission if MICRO is not deployed within this altitude range. This is because the altitude of the orbit of MICRO has a big impact on the success of the mission.

To perform the mission, the SPEX instrument is selected as payload (see Chapter 4). This instrument was submitted as a scientific payload instrument for the ExoMars Trace Gas Orbiter [H⁺11] which has a circular orbit of 400 km¹⁵. Therefore, to operate the payload in the conditions for which it was initially designed, the target orbit is a circular orbit of 400 km altitude similar to the ExoMars Trace Gas Orbiter. In this orbit, MICRO will have a velocity of 3.36 km s^{-1} .

²Insight: <http://insight.jpl.nasa.gov/home.cfm> [cited 29 May 2016]

³Red Dragon: <http://tinyurl.com/gpaslst> [cited 29 May 2016]

⁴Mangalyaan 2: <http://tinyurl.com/jeluvvtj> [cited 29 May 2016]

⁵Mars Hope: <http://tinyurl.com/zgqd2k4> [cited 29 May 2016]

⁶Mars 2020: <http://tinyurl.com/jx2aha9> [cited 29 May 2016]

⁷ExoMars Rover: <http://tinyurl.com/zgxhkcq> [cited 29 May 2016]

⁸2020 Chinese Mars Mission: <http://tinyurl.com/jspk9zc> [cited 29 May 2016]

⁹Curiosity Landing: <http://goo.gl/8FygS2> [cited 19 May 2016]

¹⁰Mars Orbiter: <http://goo.gl/pIv1Pj> [cited 19 May 2016]

¹¹Launcher Mangalyaan 2: <http://tinyurl.com/jkvxjaw> [cited 29 May 2016]

¹²Mars Reconnaissance Orbiter: https://www.nasa.gov/mission_pages/MRO/main/ [cited 31 May 2016]

¹³Mars Odyssey: <http://mars.nasa.gov/odyssey/> [cited 31 May 2016]

¹⁴Mars Global Surveyor: <http://mars.jpl.nasa.gov/mgs/> [cited 31 May 2016]

¹⁵Trace Gas Orbiter: <http://exploration.esa.int/mars/46475-trace-gas-orbiter/> [cited 31 May 2016]

Sun-Synchronous Orbit

Additionally, a polar orbit is required since the intention is to have the possibility of mapping any part of Mars. Also, a Sun-synchronous orbit is favourable for many reasons. The satellite would encounter the same lighting conditions throughout the mission which greatly simplifies analysis with respect to power and thermal control [Noo15b]. The observed surface also experiences the same illumination throughout the mission which ensures consistent data. To achieve this orbit, use is made of the J_2 -effect of Mars. The basic requirement is that the angular rotation of the orbit is equal to the angular orbital rotation of Mars around the Sun such that the orientation of the orbit remains constant with respect to the Sun as expressed by Equation (5.2a) [Noo15b]. The angular rotation of the orbit from the above equation depends on the J_2 of Mars like mentioned before and is expressed by Equation (5.2b) [Noo15b]. Furthermore, the orbital periods of Mars around the Sun and MICRO around Mars can be determined using Equation (5.2c) [Noo15b].

$$\dot{\Omega} = \frac{2\pi}{T_{MS}} \quad (5.2a) \quad \dot{\Omega} = \frac{\Delta\Omega_{2\pi}}{T} = -3\pi J_2 \left(\frac{r_M}{a(1-e^2)} \right)^2 \cos(i) \frac{1}{T} \quad (5.2b) \quad T = 2\pi \sqrt{\frac{a^3}{\mu}} \quad (5.2c)$$

From the above equations and using the astrodynamic parameters shown in Table B.1a, the orbital period of the satellite is determined to be 117 min and 50 s and the required inclination is 92.5 deg resulting in requirement [OREQ-M-ORB2, Ch. 15], approximately a polar orbit. Note that the orbital parameters used in Equation (5.2b) relate to MICRO's orbit around Mars. Using the orbital period of the satellite and basic geometry, it is determined that the satellite is in eclipse for 27 min and 22 s per orbit.

ΔV Orbit Insertion

Now that the initial orbital parameters have been set and assumptions are made with respect to the deployment, the required ΔV for orbit insertion can be determined. The largest possible altitude manoeuvre is one from 200 km until 400 km based on the insertion range defined earlier and the target orbit. Additionally, the largest possible inclination change is one from approximately 93.5 deg to the target of 92.5 deg based on the reference missions^{16 17 18}. To have the most conservative budget for orbit insertion, the ΔV required for a Hohmann transfer from a circular orbit of 200 km and inclination 93.5 deg to a circular orbit of 400 km and inclination 92.5 deg is determined. Equation (5.3a) represents the required ΔV to get into the transfer orbit with the initial inclination and (5.3b) gives the ΔV to get in the required circular orbit with an inclination of 92.5 degrees [Noo15b].

$$\Delta V_1 = \sqrt{\mu \left(\frac{2}{a_1} - \frac{1}{a_t} \right)} - \sqrt{\frac{\mu}{a_1}} \quad (5.3a) \quad \Delta V_2 = \sqrt{\mu \left(\frac{3}{a_2} - \frac{1}{a_t} \right)} - 2\mu \sqrt{\frac{1}{a_t} \left(\frac{2}{a_2} - \frac{1}{a_t} \right)} \cdot \cos(\Delta\theta) \quad (5.3b)$$

In the above equations, μ is the standard gravitational parameter of Mars and a_2 is the target semi-major axis of MICRO both defined in Table B.1a. a_1 is the assumed initial deployment orbit semi-major axis (3585 km), a_t is the semi-major axis of the transfer orbit (3685 km) and $\Delta\theta$ is the inclination change (1 deg). The results of the calculations are presented in Table 5.3.

Table 5.3: Required ΔV for manoeuvre from 200 km circular orbit with inclination 93.5 deg to 400 km circular orbit with inclination 92.5 deg

ΔV	Pericentre ΔV_1	Apocentre ΔV_2	Total ΔV_T	Unit
Value	46.61	74.26	120.9	[ms ⁻¹]

Subsequently, the required ΔV for orbit insertion is 120.9 ms⁻¹.

5.2. Mission Duration and Ground Track Optimisation

One of the most crucial astrodynamic characteristics that relates to all the spacecraft subsystems, operations and cost is the mission duration. The mission duration is mainly driven by the goal to map the interesting sites of Mars, the payload that is used and the astrodynamic characteristics of the selected orbit.

As mentioned in Chapter 3, interesting locations from a scientific point of view are selected to be analysed by MICRO. Since these locations are scattered over different locations on Mars (see Figure 3.1), the ground track of the cubesat is designed in such a way that it covers the surface of Mars twice. Firstly, it is interesting from a scientific point of view to cover the selected locations multiple times. It would allow the detection of dust storms, ice clouds et cetera. Analysing their temporal behaviour would add a lot of scientific value to the mission. Secondly, during slow

¹⁶Mars Reconnaissance Orbiter: https://www.nasa.gov/mission_pages/MRO/main/ [cited 31 May 2016]

¹⁷Mars Odyssey: <http://mars.nasa.gov/odyssey/> [cited 31 May 2016]

¹⁸Mars Global Surveyor: <http://mars.jpl.nasa.gov/mgs/> [cited 31 May 2016]

manoeuvres the payload will be deactivated and will not map for some time. The payload might also be deactivated when transmitting data to MRO, which would act as a relay satellite. Depending on when the payload is activated and deactivated, the selected locations can be mapped twice. Subsequently, for each selected pixel (corresponding to the selected locations mentioned in Chapter 3) to be analysed by MICRO, a minimum of two data points in time will be obtained.

The field of view of the SPEX instrument is 7 deg across the track and 1 deg along the track of the cubesat per viewing direction [H⁺11]. In combination with the altitude and basic geometry of the orbit, the swath width is 48.93 km and the pixel size along the track is 6.98 km. From the pixel size, the requirement for orbit determination accuracy [FREQ-SS-AO8, Ch. 15] is derived. Additionally, the change in longitude per orbit when crossing the equator of Mars can be determined using Equation (5.4).

$$\Upsilon = 2\pi \frac{T}{T_{M_{sol}}} \quad (5.4)$$

where T is the orbital period of the cubesat and $T_{M_{sol}}$ is the length of a solar day on Mars both defined in Table B.1a. Υ is the change in longitude when the ground track of the cubesat crosses the equator each orbit. For illustrative purposes, Υ is indicated in Figure 5.1. Note that this figure is created with GMAT, General Mission Analysis Tool¹⁹ which will be discussed in the next section.

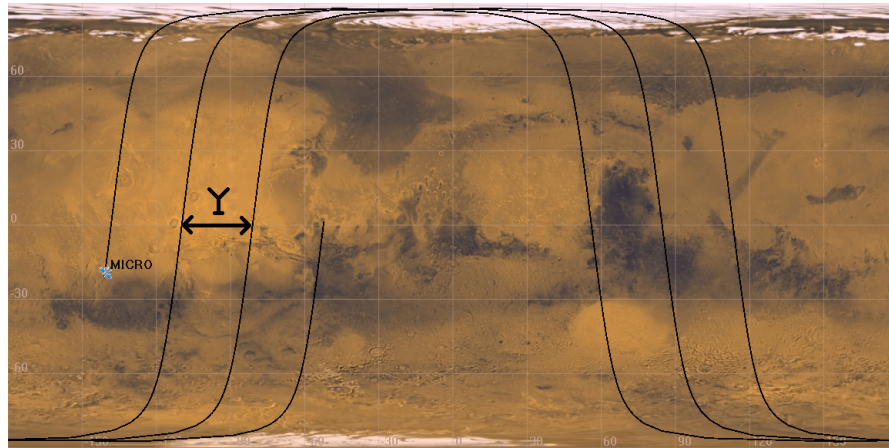


Figure 5.1: Ground track of MICRO for a few orbits

The value of Υ is determined to be 28.67 deg. An array of longitudinal values for the ground track is generated for every equatorial pass of the satellite. The raw array is sorted to draw the differences in between individual elements of the array. The differences are accumulated in a separate array until the maximum difference converges to the swath width. This method ensures that the planet is mapped at least once. Applying this procedure²⁰ results in a required number of 1217 orbits to map the entire planet at least once.

To illustrate the method even further, Figure 5.2 shows the longitudes of the equatorial crossings for 20 orbits. This plot was also generated analytically by hand to verify the code, which is deemed sufficient since the code only contains 21 lines. The maximum distance between two longitudes is 28.67 deg which corresponds to a distance 1694 km on the surface of Mars. Clearly the number of orbits needs to be increased further until this distance decreases below the swath width.

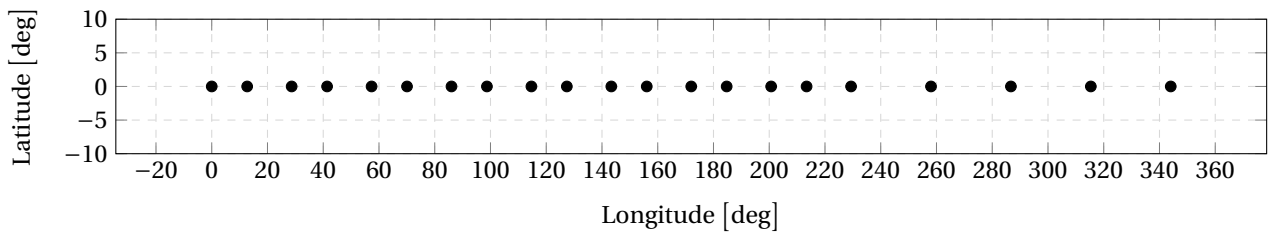


Figure 5.2: Longitudes of equatorial ground track crossings for 20 orbits of MICRO

¹⁹General Mission Analysis Tool: <https://gmat.gsfc.nasa.gov/> [cited 13 June 2016]

²⁰Duration Optimisation Code: <http://tinyurl.com/zjh92cm> [cited 13 June 2016]

To map the planet twice, the number of orbits can be doubled which results in 2434 orbits or the simulation can be run again until the maximum difference between the ground tracks converges to half the swath width. It results that the latter requires a total of 1330 orbits. This corresponds to a total mission duration of 109 days (see requirement [CREQ-M-SC4, Ch. 15]), which is believed to be a realistic result for a cubesat mission with only one payload.

5.3. Nominal Mission Phase Simulation

Since analytical calculations only allow the determination of the most basic astrodynamics characteristics, it is required to simulate the orbit of MICRO to study the effects of the perturbations on the orbit and to analyse the temporal behaviour of the Keplerian elements. Furthermore, it allows the analysis of the visibility of MICRO with respect to its relay-satellite.

5.3.1. Background Information GMAT

To perform the simulation of the nominal mission phase of MICRO, GMAT is selected as astrodynamics analysis tool. The General Mission Analysis Tool is a space trajectory optimisation and mission analysis system developed by a team of NASA, private industry, public and private contributors and is used for real-world mission support, engineering studies, as a tool for education and public engagement [The15]. It is designed to model, optimise and estimate spacecraft trajectories in flight regimes ranging from Earth and lunar orbits to interplanetary trajectories and other deep space applications²¹.

To model space missions in GMAT, resources need to be created such as spacecraft, propagators, optimizers et cetera [JHWK09]. All of these resources can be configured to meet the mission needs of MICRO. After the configuration (or initialisation of the simulation) is done in Subsection 5.3.2, the nominal mission phase can be simulated.

5.3.2. Initialisation of Simulation

In this subsection, each resource used for the mission will be treated in tables to ensure a comprehensive overview of the initial parameters used in the simulation.

Spacecraft

The initial spacecraft and orbit parameters are shown in Table 5.4 for MICRO and some initial settings related to the spacecraft can be found in Table 5.5.

The first three parameters of Table 5.4 follow from the results of Section 5.1.3. The right ascension is determined to be 227 deg by trial and error using the simulation and ensuring that the orbital plane of the spacecraft is parallel to the node connecting Mars and the Sun (resulting in requirement [OREQ-M-ORB3, Ch. 15]). This ensures a simple configuration of the spacecraft and especially its solar panels. Both the argument of periapsis and the true anomaly can be any arbitrary value because the orbit of MICRO is circular and it is not important at what true anomaly MICRO starts its nominal mission phase. The mass of the spacecraft is set at its specification value, the drag coefficient is 2.2 for cubesats [UNA13], the reflectivity coefficient is determined to be 0.91 in consideration with the thermal control engineer (see Section 11.2) and the drag area of the cubesat is determined from the maximum area of the cubesat and its solar panels in consideration with the power engineer (see Chapter 10).

Table 5.4: Spacecraft and orbit parameters of MICRO

Parameter	Value	Unit
Semimajor axis	3785	[km]
Eccentricity	0	[–]
Inclination	92.5	[deg]
Right Ascension	227	[deg]
Argument of Periapsis	0	[deg]
True Anomaly	178	[deg]
Mass	10	[kg]
Drag Coefficient	2.2	[–]
Reflectivity Coefficient	0.91	[–]
Drag/SRP Area	0.3	[m ²]

Table 5.5: Spacecraft and orbit settings of MICRO

Setting	Input
Epoch Format	UTCGregorian
Epoch	15 Feb 2021
Coordinate System	Mars Inertial
State Type	Keplerian
Attitude Model	Nadir Pointing

It is assumed that Mangalyaan 2 will be launched in July 2020 based on the planned missions of Table 5.2 and that

²¹GMAT Wiki Home: <http://gmatcentral.org/> [cited 2 June 2016]

it will arrive between January and March 2021²². Therefore, 15 February 2021 is chosen as epoch (see Table 5.4). A Mars Inertial Frame is selected for the simulation as defined in Appendix A. The MRO is also simulated to retrieve information on visibility of MICRO. It is assumed to have a polar orbit²³ and an altitude of 24213 km²⁴. Apart from these two parameters, all the others are put in similar to MICRO's, which is justifiable because the exact orbital perturbations on MRO are not relevant.

Propagator

The final object which needs to be initialised in GMAT is the propagator which actually performs the simulation. All relevant orbital perturbations are simulated which are shown in Table 5.6. This includes a high-order gravity model from [mar95], all relevant third-body perturbations, solar radiation pressure and even relativistic corrections. The only relevant perturbation which is not included in the GMAT software is the atmospheric drag acting on the cubesat. This is treated separately in Section 5.4. The simulation will be run for 109 days defined as the nominal mission duration.

Table 5.6: Propagator settings

Setting	Input
Propagator Type	Runge Kutta
Central Body	Mars
Gravity Model	Mars 50-C
Order and Degree Gravity Model	10
Atmosphere Model	Not Available
Point Masses	Sun, Jupiter
Solar Radiation Pressure Model	Spherical
Relativistic Correction	Yes

5.3.3. Results and Discussion

The 3D model of the orbits of MICRO and MRO are visualised in Figure 5.3. This figure already serves as a means to check whether the correct orbits are simulated. Everything complies with what was defined earlier: both MRO and MICRO have polar orbits, MRO's altitude is a lot larger than MICRO's orbit, the node connecting the Sun and Mars lies in the same plane as MICRO's orbit and both spacecraft are orbiting Mars.

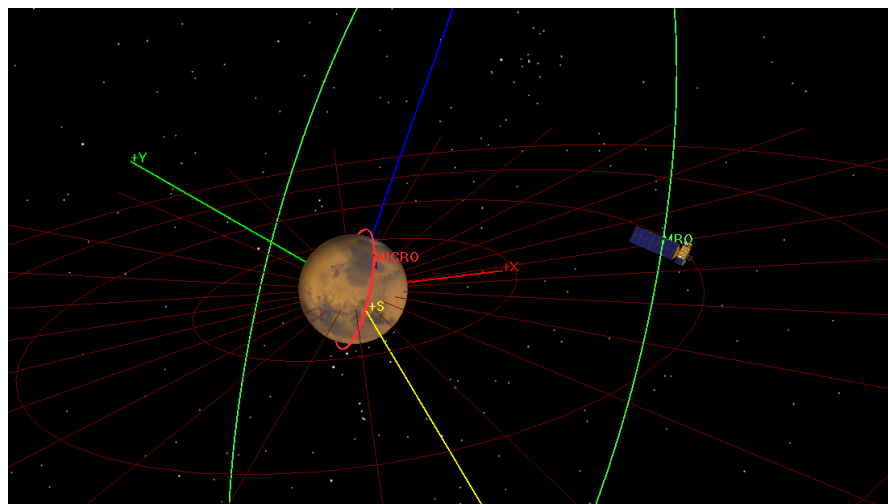


Figure 5.3: Visualisation of nominal mission phase simulation. The inner orbit is that of MICRO while the outer one is that of MRO. The Mars Inertial Frame is also visible as well as the ecliptic plane and the nadir connecting the Sun and the centre of Mars.

Altitude Variations

Many different orbital parameters have been investigated using this simulation and are not all relevant to this report. Therefore, the most interesting result will be discussed. When plotting the altitude of MICRO versus time, it became clear that there are large oscillations of the altitude over time. These can be categorised as large period oscillations

²²Mars 2020 Arrival Time: <http://tinyurl.com/jqk4k28> [cited 13 June 2016]

²³MRO Polar Orbit: <http://tinyurl.com/zedxrtu> [cited 13 June 2016]

²⁴MRO Altitude: <http://tinyurl.com/jfytztk> [cited 13 June 2016]

shown in Figure 5.4 and short period oscillations shown in Figure 5.5.

The large period oscillations are caused by the J_3 -effect of Mars. It quantifies the gravitational force caused by the imperfect symmetry of Mars around its equatorial plane [Bro59], also known as the north-south acceleration. Equation (5.5) [Cho02] defines how much it affects the eccentricity of MICRO's orbit per orbit

$$\Delta e = -\frac{1}{2} \frac{J_3}{J_2} \left(\frac{r}{a} \right) \sin(i) \sin(\omega) \quad (5.5)$$

where r is the radius of Mars, a is the semi-major axis of MICRO, i is the inclination of MICRO and ω is the argument of periapsis all defined in Table B.1a and Table 5.4. On Figure 5.4, it is clear that the large period oscillations in altitude result from the oscillation in eccentricity. Subsequently, the altitude of MICRO does not stay exactly at 400 km, but varies within a range of 336-473 km. Fortunately, the SPEX instrument is designed to operate within an altitude range of 300-500 km [H⁺11] resulting in requirement [OREQ-M-ORB1, Ch. 15], so no orbit maintenance is required to counteract these disturbances over the mission duration.

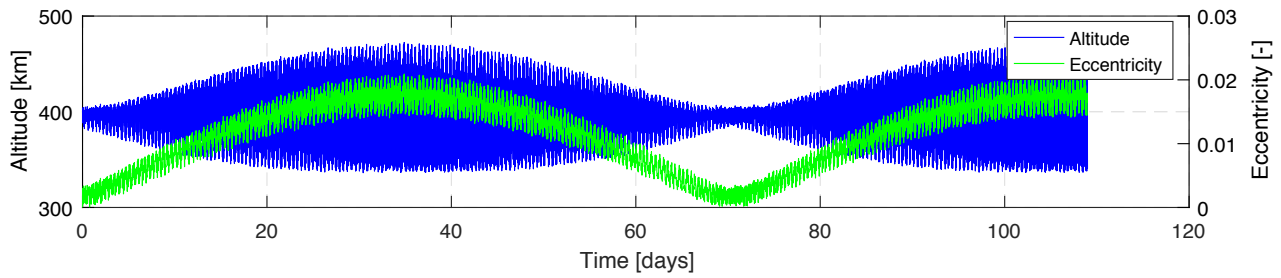


Figure 5.4: Altitude and eccentricity variation over mission duration

The obtained results are not unexpected. The Martian dichotomy is a known characteristic of the planet²⁵. The two hemispheres are more different from each other than any other planet in the solar system and their elevations differ from 1 to 3 km. Furthermore, the average thickness of the Martian crust is 45 km, with 32 km in the northern lowlands and 58 km in the southern highlands [NZW⁺04]. All these disparities between the northern and southern hemisphere give rise to the large altitude variations of MICRO.

The small period oscillations shown in Figure 5.5 are mainly caused by the variations in topography of Mars since it is not a perfect sphere. Additionally, the solar radiation pressure, the third-body perturbations and the non-uniform gravity field of Mars have a small contribution to these oscillations.

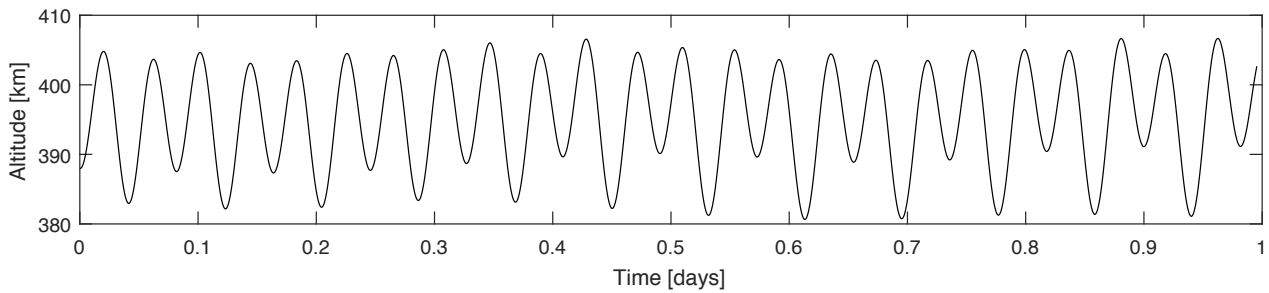


Figure 5.5: Small period oscillations of MICRO's altitude shown for day 1 of the nominal mission phase

Visibility

Like mentioned before, the transmission of the obtained data to MRO is crucial to the mission success. Therefore, it is essential to quantify how much time per orbit MICRO is in sight of MRO and not eclipsed by Mars. Figure 5.6 shows the orbits of MICRO and MRO. Since both spacecraft are approximately in the same plane, the diagram can be used to analyse visibility. The angle α is the angle between MICRO and MRO. It is clear from the diagram that α needs to be smaller than α_{max} so that MICRO is visible to MRO. Using basic geometry, α_{max} is determined to be 109.5 deg.

²⁵Martian Dichotomy: <http://tinyurl.com/jn334on> [cited 13 June 2016]

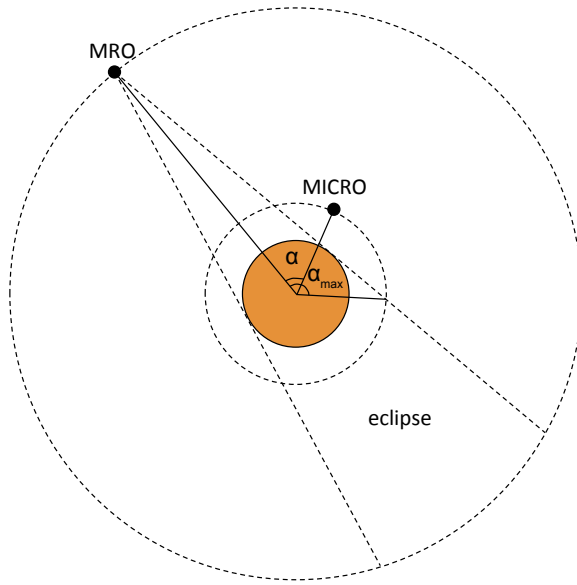


Figure 5.6: Visibility diagram of MICRO with respect to MRO (not to scale)

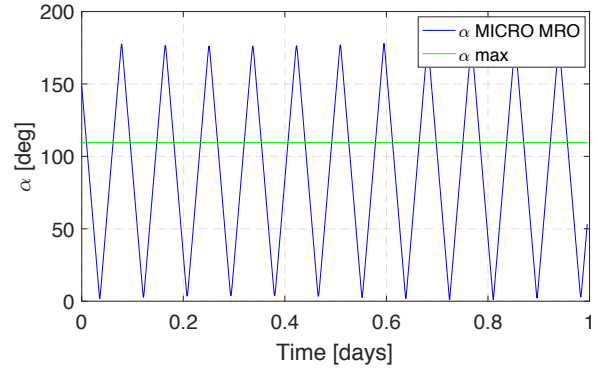


Figure 5.7: Visibility simulation output results: MICRO is visible to MRO when α is smaller than α_{max} ($0 < \alpha < 180$)

Using GMAT, the X, Y and Z coordinates of both spacecraft as a function of time can be outputted in a text-file. By applying the cosine-rule, the angle α is calculated. The results of the simulation over the 1 day are shown in Figure 5.7. The communication time slots occur whenever the α -curve is below the α_{max} -curve. The minimum communication time (T_{comm}) between MICRO and MRO per orbit is 4390 s. This conservative value is used for the communication time between the two spacecraft throughout this report.

5.3.4. Verification and Validation

Whenever using external software, it is essential to establish that it has been properly verified and validated. This is to ensure the legitimacy of the output results. The GMAT software has undergone an extensive verification and validation, V&V effort in 2014 [HQC⁺14]. The V&V-effort involved 10 full time engineers and developers over a time span of 18 calendar months. After this effort, it was concluded that GMAT is the best tested system encountered at NASA by the involved engineers and developers. The results show excellent agreement with industry-standard baseline systems. Finally, the V&V-effort resulted in the flight qualification of GMAT. To indicate the validity of GMAT even further, the software has an extensive flight heritage and contributed to the following missions [Hug15]: ARTEMIS, LRO, LCROSS, OSIRIS-REx, MMS, MAVEN, TESS and ACE.

To validate the simulation results specifically, the communication time described in the previous subsection is compared to what is expected analytically. The fraction $\frac{\alpha_{max}}{180 \text{ deg}}$ multiplied with the orbital period should approximately be the communication time when evaluating Figure 5.6. This results in a value of 4301 s of communication time. This is only a 2 percent difference compared to the result obtained with the simulation, hence validating the simulation results.

5.4. Decay Rate and End-Of-Life

Like mentioned previously, the simulation performed with GMAT does not include the perturbing effect of Mars' atmosphere on the spacecraft. However, if it can be determined that the perturbations are negligible over the nominal mission duration, then the simulation is valid. This section will analyse the orbital decay during the nominal mission phase and until end-of-life.

The only perturbing effect that the atmosphere has on the spacecraft with respect to astrodynamics is a drag force defined by Equation (5.6) [And10].

$$F_{aero} = \frac{1}{2} \rho V^2 A_r C_D \quad (5.6)$$

To quantify the effect of the atmospheric drag on the orbit, Equation (5.7) is used [WL10]. It describes the change in semimajor axis per orbit.

$$\Delta a_{rev} = \frac{-2\pi C_D A_r \rho a^2}{m} \quad (5.7)$$

To determine the decay rate and the minimum time that MICRO keeps orbiting Mars, the altitude of MICRO can easily be modelled. By determining the decrease in altitude per orbit using Equation (5.7), the altitude can be plotted as function of time until MICRO decays into the Martian atmosphere (see Figure 5.8). The drag coefficient, drag area and mass of the spacecraft can be found in Table 5.4. Mars-GRAM [mar01] is used as the atmospheric density model which gives the density as a function of altitude at the equator of Mars during equinox and local noon time. From Figure 5.4, the minimum orbital altitude is 336 km. However, selecting this altitude as the initial altitude for the orbital decay simulation would be too conservative since most of the time, the altitude is larger than this minimum value. Therefore the root-mean square value [The] of the altitude oscillations is selected which gives an initial altitude of 355 km for the simulation.

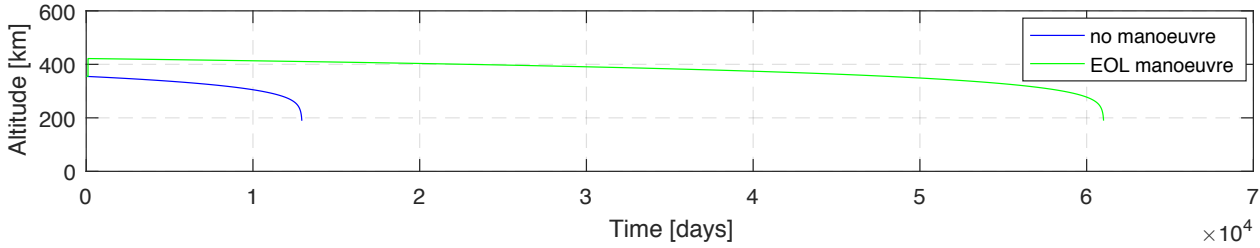


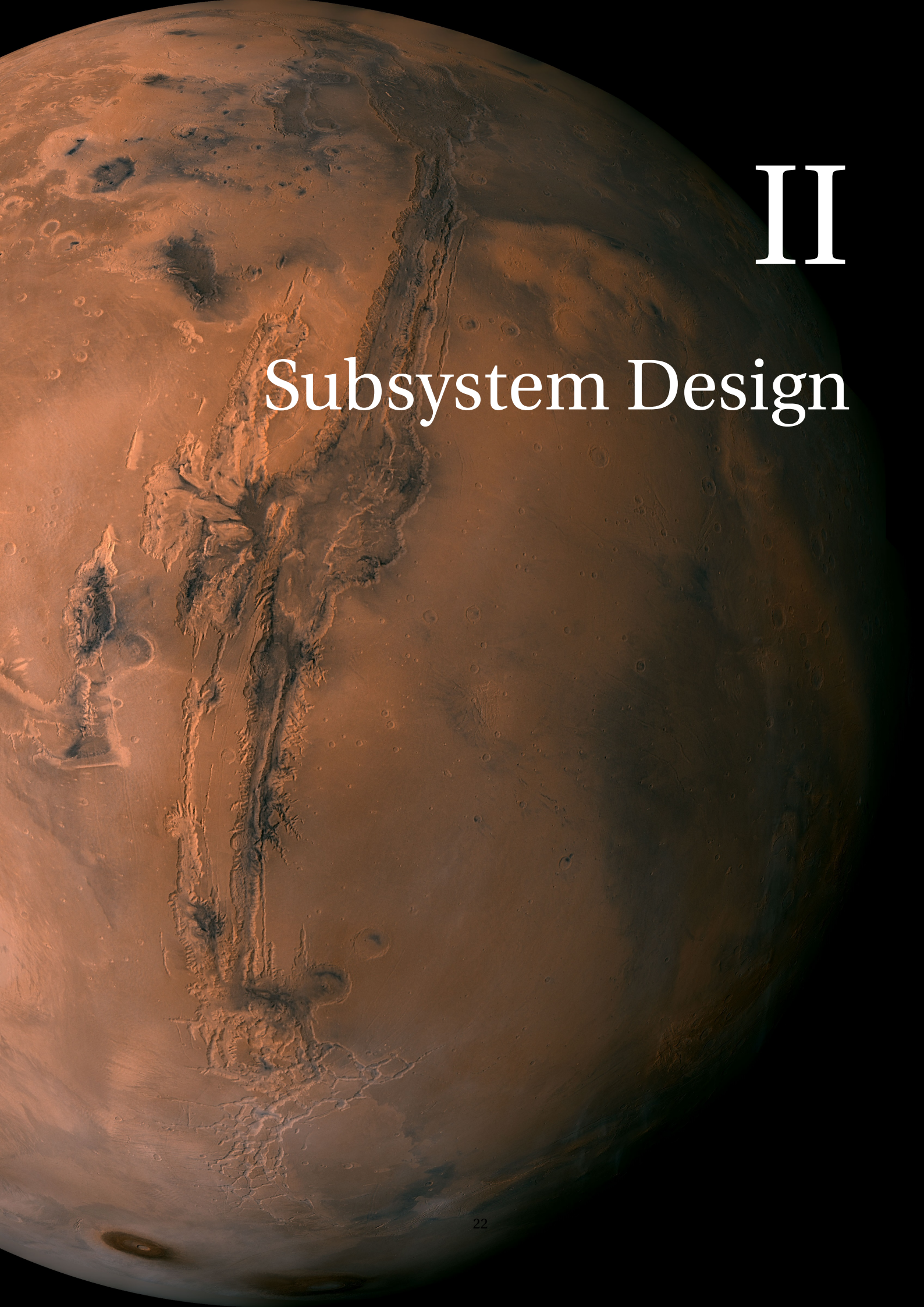
Figure 5.8: Decay of MICRO due to atmospheric drag

Without the application of an end-of-life manoeuvre, MICRO is expected to decay into the atmosphere 35 years after the start of the mission as can be seen on Figure 5.8. This does not comply with the COSPAR recommendations on planetary protection which states that an impact with Mars should be avoided over a time period of 50 years with a certainty of at least 99 percent²⁶ (see requirement [OREQ-M-ORB4, Ch. 15]). Therefore, an end-of-life manoeuvre will be performed to keep MICRO in orbit for at least 50 years with a high certainty. With a ΔV of 30 m s^{-1} , a Hohmann transfer manoeuvre can be performed to increase the orbital altitude with 67 km at the end-of-life. As can be seen on Figure 5.8, this manoeuvre drastically extends the time that MICRO will orbit Mars. The total duration is extended to 167 years which is well within the posed recommendation with sufficient certainty.

For the nominal mission phase, which is only 109 days, the effect of atmospheric drag is negligible. The effect on the orbit is a maximum decrease in altitude of 325 m with respect to the start of the mission. This justifies the assumption made at the beginning of this section.

The most essential results obtained throughout this chapter are summarised in Table 17.1.

²⁶Avoid Impact Mars: <https://planetaryprotection.nasa.gov/missiondesign/> [cited 16 June 2016]



II

Subsystem Design

Attitude and Orbit Determination and Control Subsystem

The AODCS is the subsystem that provides the spacecraft with attitude and orbit information. Its role is also extended on controlling the attitude, by means of both actuators and thrusters. This chapter is structured as follows. First the design of the attitude determination and control subsystem will be discussed, in Section 6.1. Then, in Section 6.2, the orbit determination subsystem will be treated, including a trade-off among the possible OD methods. This will be followed by the flow diagram of this subsystem, in Section 6.3, and by a description of the layout of the instruments chosen, in Section 6.4. Then, Section 6.5 will focus on the selection of said instruments for each control operating mode and to conclude, verification and validation of the numerical models used will be carried out, in Section 6.6.

6.1. ADCS Design

This section will focus on the determination and control of the spacecraft's attitude.

6.1.1. Disturbances

The attitude of a spacecraft is highly influenced by disturbances. These disturbances are divided into internal and external. The external ones, for an orbit around Mars, are *i)* solar radiation, *ii)* atmospheric drag and *iii)* gravity gradient. The internal disturbances, on the other hand, mainly depend on the manufacturing uncertainties, such as *i)* thruster misalignment, *ii)* thruster output mismatch, *iii)* reaction wheel imbalance, *iv)* liquid slosh and *v)* other subsystems dependant factors [WL11, UNA13, Eye90].

Modelling of the disturbances is required for the design of a well-performing ADC subsystem. The implementation of the GMAT software from NASA, already used for astrodynamical simulations in Chapter 5 is not possible, since it does not model for attitude perturbations. For this reason, a numerical model of the orbit of the cubesat is generated. The purpose of this model is to solely quantify the maximum disturbances acting on the spacecraft. To do so, the program has to take into account the following elements:

- Orbit of Mars around the Sun
- Orbit of the cubesat around Mars
- Atmospheric model of Mars and solar radiation
- Mass moment of inertia and dimensions

The orbital characteristics of Mars and the spacecraft, were computed by giving a initial conditions on both location and velocity. After this, the motion about the influencing body (Sun for Mars and Mars for Phobos and the S/C), was determined with the Lagrange coefficients method [Cur05, p. 79]. The equations for the orbital simulation are omitted, since the focus of this section will be put more on attitude disturbances. However, the full version of the code is publicly available at ¹. Note that, in this section, vectors are displayed in bold and with the reference frame they are described in as superscript. For details on these frames, see Appendix A.

The 3D perturbations are described by Equations (6.1) [UNA13, WL11, HL69, LWH09]. Equation (6.1a) models the solar radiation torques, (6.1b) the aerodynamic torques and (6.1c) the gravitational torques, where all the vector are expressed in components of the spacecraft frame, SF.

$$\mathbf{T}_{\text{sol}}^{SF} = -\left(1 + q\right) \frac{\Phi}{c} A \mathbf{l}_{\text{sol}}^{SF} \times \hat{\mathbf{d}}^{SF} \quad (6.1a)$$

$$\mathbf{T}_{\text{aero}}^{SF} = -\frac{1}{2} \rho V^2 C_d A_{\text{aero}} \mathbf{l}_{\text{aero}}^{SF} \times \hat{\mathbf{v}}^{SF} \quad (6.1b)$$

$$\mathbf{T}_{\text{grav}}^{SF} = 3\mu \frac{\hat{\mathbf{d}}^{SF} \times (\mathbb{I}^{SF} \hat{\mathbf{d}}^{SF})}{d^3} \quad (6.1c)$$

¹ADCS Simulation: <https://github.com/mfacchinelli/ADCS-simulation> [cited 28 May 2016]

Aerodynamic and gravitational torques are always present, whereas the solar pressure disturbances are only affecting the attitude if the spacecraft is in sunlight. To determine if the satellite is in eclipse, Equation (6.2) [Noo15a] is used.

$$\text{if } \begin{cases} \Psi > \pi/2 \\ S > 0 \end{cases} \text{ then, satellite is in eclipse.} \quad (6.2)$$

The values of Ψ and S are found using Equations (6.3a) and (6.3b) [Noo15a], respectively.

$$\Psi = \cos^{-1} \left(\frac{\mathbf{d}_{\text{Mars}}^{IF} \cdot \mathbf{d}_{\text{SC}}^{IF}}{d_{\text{Mars}} d_{\text{SC}}} \right) \quad (6.3a)$$

$$S = R^2 (1 + e \cos \vartheta)^2 + a^2 (1 - e^2)^2 (\cos^2 \Psi - 1) \quad (6.3b)$$

Moreover, \mathbb{I} from Equation (6.1c) represents the mass moment of inertia tensor, where for simplicity the cross-terms are assumed to be zero (implying that there is symmetry in the structure). It can be found with the aid of Equations (6.4a) and (6.4b). The most right-hand side term of the latter equation stands for the Huygens-Steiner theorem, which is used for the computation of the inertia contribution of the cubesat's solar array. For this computation, more assumptions are made, such as constant mass over time and fixed position of solar array (i.e. deployed parallel to the y -axis of the cubesat).

$$\mathbb{I}^{SF} = \begin{bmatrix} I_{xx} & 0 & 0 \\ 0 & I_{yy} & 0 \\ 0 & 0 & I_{zz} \end{bmatrix} \quad (6.4a)$$

$$I_{ii} = I_{ii,0} + m d_i^2 \quad \text{for } i \in [x, y, z] \quad (6.4b)$$

For the determination of the mass moment of inertia, the satellite is assumed to be a 6U cubesat with uniformly distributed mass and with the solar array positioned at the top (on the surface facing the negative z -axis), with the long axis (of the solar array) along the y -axis of the spacecraft.

The last effects to account for are the internal torques. These, as stated before, arise from manufacturing and assembly errors and internal dynamics. However, in this report only reaction wheel imbalance (both static and dynamic) will be treated. This is because they are the most influential internal torques and are usually even larger than external ones [Eye90, p.28], especially for missions where the external disturbances are rather small. In addition, the modelling of other internal disturbances, requires very accurate knowledge of the mechanical and dynamical characteristics of the spacecraft structure, which at this stage has not been achieved. On the other hand, for the propulsion system, it is known that the design of the tank is such that liquid slosh is minimised, if not cancelled, making the modelling of this disturbance not necessary. The equations for the static and dynamic disturbances are given in Equations (6.5a) and (6.5b), respectively [UNA13].

$$\mathbf{T}_{RW,S}^{SF} = U_S \left[\omega_x^2 \mathbf{I}_{RW}^{SF} \times \begin{pmatrix} 0 \\ \sin \omega_x t \\ \cos \omega_x t \end{pmatrix} + \omega_y^2 \mathbf{I}_{RW}^{SF} \times \begin{pmatrix} \cos \omega_y t \\ 0 \\ \sin \omega_y t \end{pmatrix} + \omega_z^2 \mathbf{I}_{RW}^{SF} \times \begin{pmatrix} \sin \omega_z t \\ \cos \omega_z t \\ 0 \end{pmatrix} \right] \quad (6.5a)$$

$$\mathbf{T}_{RW,D}^{SF} = U_D \left[\omega_x^2 \begin{pmatrix} 0 \\ \sin \omega_x t \\ \cos \omega_x t \end{pmatrix} + \omega_y^2 \begin{pmatrix} \cos \omega_y t \\ 0 \\ \sin \omega_y t \end{pmatrix} + \omega_z^2 \begin{pmatrix} \sin \omega_z t \\ \cos \omega_z t \\ 0 \end{pmatrix} \right] \quad (6.5b)$$

In Equations (6.5), U_S and U_D are called the static and dynamic reaction wheel imbalance factors. Their values are given by the manufacturer and are usually in the order of $1 \times 10^{-10} \text{ N s}^2$ and $1 \times 10^{-10} \text{ N m s}^2$ [UNA13]. As can be noted, these equations also depend on the rotational rate of each of the wheels, thus ω_x , ω_y and ω_z . The rotation speeds increase over time and depend on the total disturbance torque

$$\mathbf{T}^{SF} = \mathbf{T}_{\text{sol}}^{SF} + \mathbf{T}_{\text{aero}}^{SF} + \mathbf{T}_{\text{grav}}^{SF} + \mathbf{T}_{RW,S}^{SF} + \mathbf{T}_{RW,D}^{SF}.$$

The value of $\boldsymbol{\omega}_{RW}$, hence the vector containing the rotational velocities of the three wheels, is determined with Equations (6.6), where for sake of clarity the superscripts are removed from the vectors, since they are all expressed in SE.

$$\dot{\boldsymbol{\omega}}_{RW} = \mathbb{I}^{-1} \mathbf{T} \quad (6.6a)$$

$$\boldsymbol{\omega}_{RW} = \int \dot{\boldsymbol{\omega}}_{RW} dt \quad (6.6b)$$

Whenever one of the components of $\boldsymbol{\omega}_{RW}$ reaches the maximum rotational speed set by the manufacturer, momentum dumping will occur along that axis.

The final steps to be undertaken by the simulation are the computation of the propellant mass used for attitude corrections and the ΔV estimation. These can be found with Equations (6.7a) [WL11, p.583] and (6.7b) [Cer15], respectively.

$$m_{\text{prop}} = \frac{2}{I_{sp} g_0 I_{\text{prop}}} \int T dt \quad (6.7a)$$

$$\Delta V = I_{sp} g_0 \ln \left(\frac{m_0}{m_0 - m_{\text{prop}}} \right) \quad (6.7b)$$

For Equation (6.7a), T refers to the magnitude of the instantaneous torque and dt to the time step used for the simulation.

6.1.2. Sensors

Attitude determination is carried out with the aid of sensors. The type of required sensors is driven by the mission and payload specifications. From Chapter 4, it is known that the the SPEX instrument has a required pointing accuracy of 360 arcsec [FREQ-SS-AO3, Ch. 15]. The selection of the sensors was carried out in the Midterm Report [AFH⁺16, p.32]. From consulting various manufacturers websites^{2 3 4 5 6 7 8 9} and reports about previous cubesats missions [QMC14, UNA13], a preliminary sizing of the ADC subsystem was performed.

The sensors that have ultimately been selected are shown in Table 6.1. The values of the ST-200 were taken from Hyperion Technologies¹⁰ [S. Engelen, pers. comm. 30th May 2016], the ones of the nanoSSOC-A60 from Solar MEMS Technologies¹¹ and for the IMU, Inertial Measurement Unit, from Micro Aerospace Solutions¹².

Table 6.1: Selected sensors (values refer to one unit only)

Type	Name	Number [–]	Accuracy [arcsec]	Slew Tolerance [deg s ^{−1}]	Drift [arcsec s ^{−1}]	Mass [g]	Volume [cm ³]	Power [mW]
ST	ST-200	3	30 (3 σ)	0.3	n.a.	50	35	600
SS	nanoSSOC-D60	4	1800 (3 σ)	25	n.a.	6.5	3.6	76
IMU	MASIMU02	1	n.a.	n.a.	12	60	98.3	600

There are a few differences between the sensors in Table 6.1 and the sensors selected during the preliminary sizing [AFH⁺16]. The first difference is the number of star trackers (ST). The previous configuration consisted of two star tracker (with the same specifications as in Table 6.1) and one fine Sun sensor (SS) with an accuracy of 360 arcsec (1 σ), as a redundancy. Since its accuracy is only determined with a precision of 1 σ , the sensor was replaced with a more precise star tracker. These star trackers have a high accuracy and a mass that is 1.5 times lower than that of the Sun sensors previously selected.

The limiting factor of the ST-200 (as for every star tracker) is the very low slew tolerance. In case of the ST-200 the maximum slew rate after which the instrument cannot provide accurate measurements is of 0.3 deg s^{−1}. To determine attitude information also when the spacecraft is rotating at higher velocities (for instance after separation from the host), coarse Sun sensors have been selected as back-up. Having a slew rate of 25 deg s^{−1}, it is safe to assume that the sensor will be able to acquire attitude data to be used by the processor to initiate the actuators [FREQ-SS-AO5, Ch. 15]. In fact, the rotational rate of 6U cubesats after deployment is approximately 10 deg s^{−1} [Cor15a, p.7]. The reason behind the selection of four Sun sensors is because only three surfaces are lit at a time, hence only three sensors provide data. Since the spacecraft will likely be rotating about multiple axes, placing a Sun sensor on all sides accounts for all possible attitudes. The two remaining sides are accounted for by the solar cells, which also act as coarse Sun sensors, with an accuracy of 1.85 deg s^{−1}¹³.

Finally, an IMU is also present. Once the spacecraft is initially stabilised, the IMU will be able to provide very accurate and high frequency data with respect to an inertial reference. How the IMU and the other sensors work together is explained in Section 6.3.

6.1.3. Actuators

In the Midterm Report [AFH⁺16], it was determined that the ΔV requirement for attitude control is not dependent on the momentum storage of the reaction wheels (RW). Therefore, the main drivers for the selection of actuators are mass, power and frequency of momentum dumping. A preliminary trade-off was already carried out in the Midterm Report [AFH⁺16, p.35], however, since then, a new and better component was found. Its main advantage is the lower frequency of momentum discharge. The more momentum discharges, the more the measurements done by the payload will be interrupted. With the previous component, the frequency of discharge was 60 day^{−1},

²Sinclair Interplanetary: <http://goo.gl/pqAzfK> [cited 30 May 2016]

³Blue Canyon Tech: <http://goo.gl/QoZvZj> [cited 30 May 2016]

⁴CubeSatShop: <http://goo.gl/beY8da> [cited 30 May 2016]

⁵Space Micro: <http://goo.gl/1QM06l> [cited 30 May 2016]

⁶Berlin Space Technologies: <http://goo.gl/yvBOLN> [cited 30 May 2016]

⁷Solar Mems Technologies: <http://goo.gl/y5eVD1> [cited 30 May 2016]

⁸Micro Aerospace Solutions: <http://goo.gl/PXiX1e> [cited 30 May 2016]

⁹Maryland Aerospace: <http://goo.gl/fc87Ui> [cited 30 May 2016]

¹⁰ST-200 Data Sheet: <http://goo.gl/J9sIfj> [cited 30 May 2016]

¹¹nanoSSOC-A60 Data Sheet: <http://goo.gl/02qKVva> [cited 30 May 2016]

¹²MASIMU02 Data Sheet: <http://www.micro-a.net/imu-tmpl.html> [cited 30 May 2016]

¹³IMM4J CIC Data Sheet: <http://goo.gl/XEA6p> [cited 2 June 2016]

which, upon further investigation, is reputed to be unacceptable. On the other hand, with the new reaction wheel it is reduced to approximately 1 day^{-1} (where for both cases the unit [day] refers to Earth days). Furthermore, the instrument presented a very high maximum rotational rate: $10 \times 10^3 \text{ rpm}$ compared to the new $5 \times 10^3 \text{ rpm}$. This, although might seem a positive characteristic, actually increases the internal torques. Looking at Equations (6.5), the reaction wheel-dependent disturbances are highly influenced by the rotational rates, being proportional to the square of ω .

The instrument selected and its specifications can be seen in Table 6.2. Its characteristics were taken from the producer, namely Hyperion Technologies¹⁴.

Table 6.2: Inertia wheels specifications

Name	Number [–]	Momentum [mNm s]	Rotation Rate [rpm]	Mass Inertia [kg m ²]	Mass [g]	Volume [cm ³]	Power [mW]
HT-RW400.30	4	30	5000	5.73×10^{-5}	210	68.75	650

As it can be noticed from Table 6.2, the number of selected actuators is four. Their placement is as follows: one actuator per axis and a fourth one aligned in a tetrahedral configuration. Even though tetrahedral configurations are not recommended by the producer [S. Engelen, pers. comm. 30th May 2016], due to the high degradation of the instrument after long usage, it was decided to still go for this arrangement. The reason behind this decision is that the mission duration is relatively small (109 days as specified in Chapter 5). It is therefore expected that, should a reaction wheel fail in the early stages of the mission, the degradation of the fourth redundant wheel is not high enough to bring to another failure.

Furthermore, the reaction wheels provide for the attitude change needed to rotate the spacecraft by 30 deg about the y-axis, during scientific measurements, as explained in Chapter 4.

The very last elements used in the ADC subsystem are the thrusters. These are used for momentum dumping once the maximum rotational speed of one of the wheels is reached. Using vector thrusters, allows for control about one single axis at a time, and therefore for more freedom in the attitude control. For more information on the type of thruster selected and their specifications, refer to Chapter 7.

6.1.4. Attitude Control Operations

In this section, an overview of the functions performed by the attitude control of the spacecraft is given.

- **Disturbance Counteraction**

The role of the reaction wheels is to make sure that the spacecraft is always pointing in the required direction. The RWs start rotating slowly, as the disturbances start affecting the attitude of the cubesat.

- **Rotation of Cubesat**

The rotation of 30 deg is attained by increasing the torque of the reaction wheels until half of the required angle is achieved. Then, the reaction wheels decelerate to bring the rotation to a stop, once the angle is reached. The time required for this rotation is approximately 41.5 ms, when the reaction wheels are assumed to start from rest. The time taken will be roughly 1.7 s if the reaction wheels are rotating at maximum speed. These times were computed by solving Equation (6.8) for t and then by multiplying the result by two.

$$\frac{1}{2} \alpha_{RW} t^2 + \omega_{RW} t - \frac{\vartheta}{2} = 0 \quad (6.8)$$

In Equation (6.8), ϑ represents the 30 deg rotation angle and $\alpha_{RW} = 35 \text{ rad s}^{-2}$ the rotational acceleration of the wheels, provided by the manufacturer¹⁴. It is now evident that the time taken to rotate the spacecraft does not affect the selection of the RWs. This is because the time taken is very short, no matter the initial rotational velocity of the RWs.

6.1.5. Simulation Results and Recommendations

The simulation was run for 2, 121 and 1330 orbits. The initial conditions for Mars were the ones corresponding to its position and velocity on the 15th of February 2021, i.e. the day of arrival as stated in Chapter 5. In Table B.1b in Appendix B, information about the following can be found: orbital parameters the cubesat was assumed to be inserted in, components specifications, cubesat and environmental parameters. The value for the reaction wheel parameters were given by Hyperion Technologies [S. Engelen, pers. comm. 30th May 2016], the atmospheric density was taken from [nas01, p.1-3], the drag coefficient from [UNA13, p.5], the propulsion data from Chapter 7 and the reflectance factor of TiO_x (the element constituting the outer layer of the solar cells) from [Rau80, p.247]. The other values were computed (e.g. mass inertia and area) for the worst case scenario.

¹⁴HT-RW400.30 Data Sheet: <http://goo.gl/J9sIfj> [cited 30 May 2016]

For the position of centre of solar and atmospheric pressures, where both assumed to be the furthest from centre of mass, but in opposite directions. This way it was found that the torques would sum up, instead of cancelling each other (resulting in the worst case scenario). For the reaction wheels, the position is also set as the furthest from the centre of gravity. However, which corner in the bus structure is not of importance, since the perturbing torques oscillate due to the sinusoidal nature of the equations representing them (recall Equations (6.5)).

The results for the simulation of 2 orbits are shown in Figure 6.1. External torques and total torques are shown in Figures 6.1a and 6.1b, respectively.

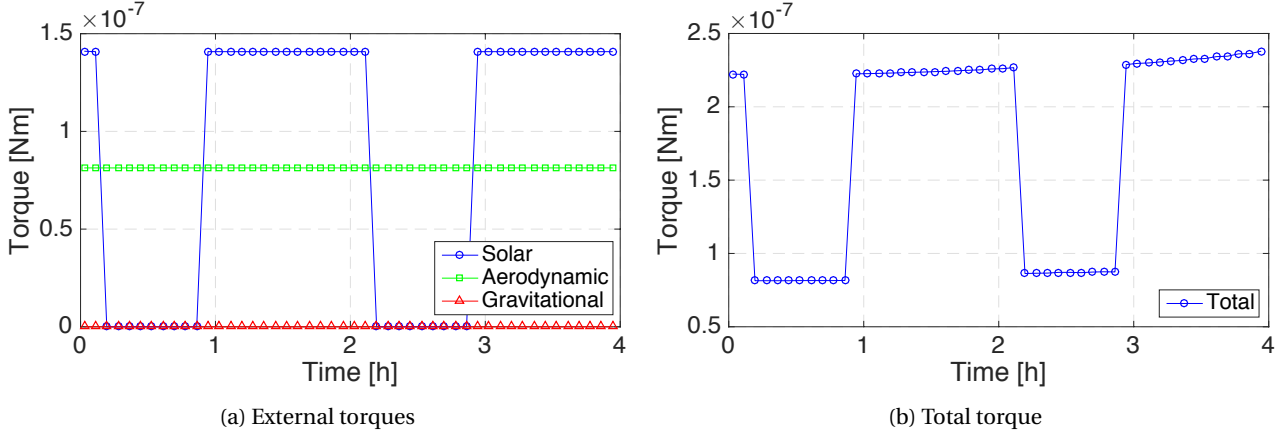


Figure 6.1: Magnitudes of perturbing torques for 2 orbits

The plots in Figure 6.1a show that the solar torque goes from constant to zero with constant intervals. These intervals represent the eclipses of the orbit, meaning that during eclipses no solar torque is experienced. Another important feature to notice is the absence of gravitational torque. This is due to the fact that the spacecraft is assumed to be perfectly aligned with the gravitational field of Mars (the z -axis is always pointing toward the centre of Mars, since the orbit is circular), therefore the cross product in Equation (6.1c) turns out to be zero. Finally, from Figure 6.1b, the magnitude of the total torque is majorly influenced by the external perturbations. This can be explained by considering that the internal torques caused by the reaction wheels are small at the very start of the mission, since they are yet to start rotating at significant rates. Small fluctuations, however already start affecting the graph, as can be seen just before the 2 h mark.

To observe the effect of the reaction wheels, one must take a look at the results of a longer simulation. As an example, the results for 121 orbits (corresponding to roughly ten Earth days) can be examined. The value of 10 days was chosen to give an overview of how the system will behave in the long run, due to the repetitive behaviour of the RW rotation. In addition, a very long time span gives very cluttered result, which are caused by the oscillating nature of the results. The outcome of the simulation are shown in Figure 6.2a for the reaction wheel torque and Figure 6.2b for the total torque.

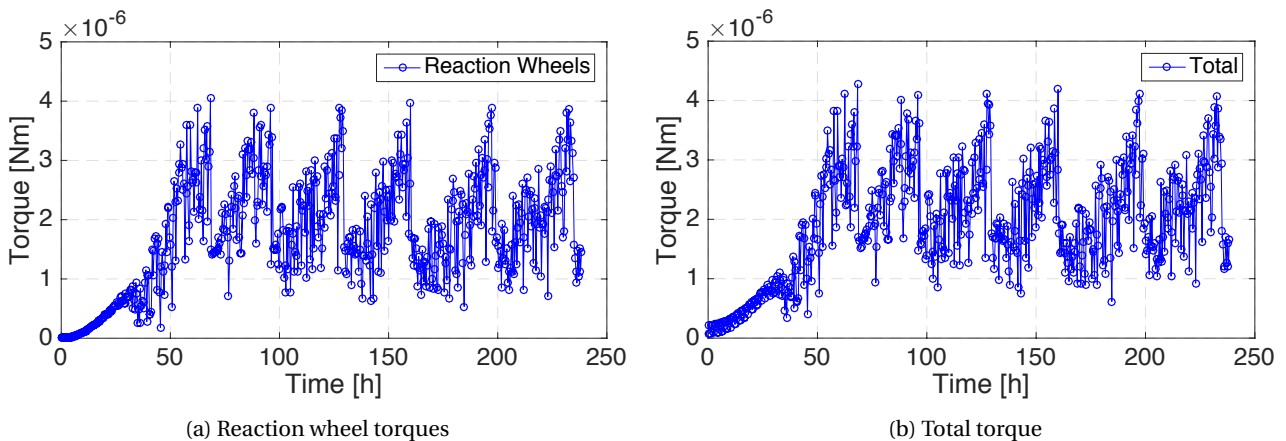


Figure 6.2: Magnitudes of perturbing torques for 121 orbits

It is now clear that the disturbance from the very components that should counteract the effect of disturbances, actually contribute the most to it. In fact, comparing Figure 6.2a with Figure 6.2b, one can see that the plots show a lot of similarity, but the plot for the total torque is slightly shifted upwards by the external torques. These results

are not so unexpected, especially for a satellite orbiting a relatively small planet, like Mars, and with actuators with moderate imbalance coefficients [Eye90, p.28]. Moreover, although the overall slope of the graphs remain roughly constant, after the torque reaches about 4×10^{-6} N m, there is a 'reset' in the torque value. The reason for this can be found in the mechanism regulating the reaction wheel rotation. When the reaction wheels reach the maximum rotational rates (i.e. they attain the maximum angular momentum storage), momentum dumping is takes place. Due to momentum dumping the disturbance torques and rotational rates of the reaction wheels are brought back to zero. Of course not all the reaction wheels reach saturation at the same time. Thus, the total torque does not actually reach zero. Taking a look at the rotational rates, this becomes very clear. The rotational rates of the reaction wheels are depicted in Figure 6.3 for all axes.

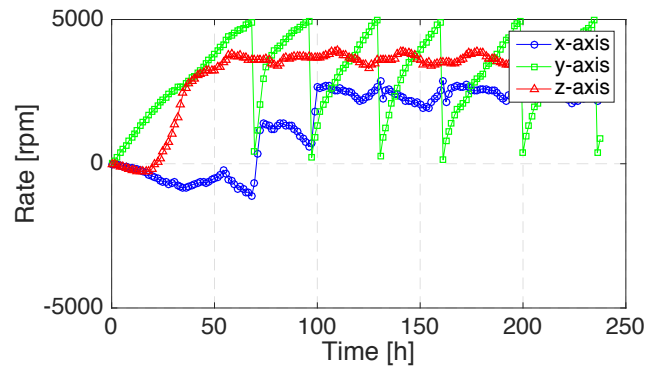


Figure 6.3: Rotational rates

To conclude, the results of the simulation after 1330 orbits are given. These are shown in Table 6.3. Since the values of torques is very oscillatory, the root mean square (RMS) is given, instead of a simpler arithmetic average.

Table 6.3: Results for 1330 orbits

RMS Torque [$\mu\text{N m}$]	Max. Torque [$\mu\text{N m}$]	Tot. Dumpings [—]	Freq. Dumpings [day^{-1}]	ΔV [m s^{-1}]	Critical Axis [—]
2.28	4.62	65	0.6	18.65	y

Although the torques in Table 6.3 refer to magnitudes, it was found (through the simulation) that the maximum value of torques is always exerted on the y-axis. This fact can also be seen by looking back at Figure 6.3. As one can clearly notice from this plot, momentum dumping (hence the reaching of the maximum rotational speed of the RW) is only necessary along y.

As a recommendation for future improvements, the following implementations are suggested:

- Addition of Kalman filter for noise reduction
- Addition of control operating modes
- Addition of thrusters and their misalignment
- Variation of area exposed to solar radiation
- Rotation of the spacecraft about the y-axis
- Switch to tetrahedral configuration for RW
- J2 effects of Mars for sun-synchronous orbits

6.2. ODS Design

The perturbations acting on the spacecraft are not only confined to attitude disturbances. Even the spacecraft orbit is affected. In particular, the main perturbations are:

- Third-body
- Solar radiation
- Aerodynamic
- Gravitational (i.e. J_2 and J_3 effects)
- Relativistic

All these disturbances were analysed in Chapter 5 and it was determined that the effects on the orbit are [Cur05]:

- Rotation of the orbit, due to J_2 effect
- Eccentricity oscillations, resulting in orbit height variations between 336 and 473 km, due to J_3 effect
- Decay of the orbit over a long time span (see Chapter 5 for more details), due to aerodynamic effects

The effects of the other disturbances were found to be negligible. Furthermore, from reference [H⁺11, p.4], it is known that the optimal altitude range for the SPEX instrument is from 300 km to 500 km. Clearly, then the altitude variations due to the oblateness of Mars, although they do affect the orbit, do not negatively affect the measurements of the SPEX instrument. With this in mind, it was decided that orbit control of the spacecraft would not be necessary.

On the other hand, for proper insertion into the defined orbit and for proper mapping of the planet, the cubesat needs to know its position. Usually, orbit determination for interplanetary satellites is done on Earth, with the use of trackers such as the DSN, Deep Space Network [HB07, p.1]. However, more ways exist for such purpose.

6.2.1. Orbit Determination Methods

Not being able to communicate directly with Earth, orbit determination becomes a challenging task to perform. Three methods have been found to be effective for such purpose: LiAISON method, radar and visual ranging [S. Engelen, pers. comm. 2nd June 2016] [HB07, HLB06]. These methods will be briefly described in the following paragraphs.

LiAISON

LiAISON navigation, or Linked, Autonomous, Interplanetary Satellite Orbit Navigation, uses satellite-to-satellite tracking as the only source of orbit determination [HB07, HLB06]. The only restriction of the LiAISON navigation is that one of the satellites using this method has to be in an orbit of locally unique size and shape. An example of such an orbit is a halo orbit, i.e. a three-dimensional and periodic orbit positioned near the Lagrange points of the Sun-Mars system [How84], which is very difficult to achieve due to the high non-linearity of the equations of motion [CGMM04, p.15]. Furthermore, the orbits of the spacecraft have to be separated by relatively large distances and cannot be coplanar.

Although the accuracy achieved by this method is very high (in the order of 10 m) [HLB06], the application requires very restricting conditions, which are not available at Mars.

Radar Ranging

A similar method to the LiAISON can be used, by using other Martian orbiters, as radar reflectors.

To determine its position, the cubesat would send signals to at least six satellites already orbiting Mars. Available satellites around Mars equipped with UHF, Ultra High Frequency, antennas are MRO¹⁵, MAVEN¹⁶, Mars Express¹⁷, Mars Odyssey¹⁸ and more. The use of six satellites is necessary for the detection of outliers and for better accuracy. This accuracy highly depends on the resolution and synchronisation of the time-keeping device present in the OBC, On-Board Processor. Even an error of 1 ms gives a distance uncertainty of 300 km. Other factors to be known are the time taken from reception and transmission of the satellites and also their position. All these conditions do not make this method unfeasible, but definitely add many constraints.

Visual Ranging

The final method is visual ranging. With visual ranging, it is meant that a nadir facing camera will take pictures of the Martian surface and compare it with an on-board features map of Mars. Based on the field of view and the surface features detected both latitude, longitude and altitude can be determined. The advantage of this method is that it is completely autonomous, meaning that it does not depend on other spacecraft or ground stations. Furthermore, the only instrument required is a high resolution camera, which (taking the IM-200 from Hyperion Technologies as reference¹⁹) can be very small and light: 44 cm³ and 50 g.

In case of local bad weather conditions, since the orbital position of the spacecraft does not have to be known at every instant, it can be extrapolated based on the previous known positions with the aid of the IMU's accelerometers, until new information is available. Furthermore, since Martian dust storms are rather mild²⁰, the surface is still visible through the dust, making detection of very prominent feature still possible.

6.2.2. Trade-off

The weights chosen for the trade-off are the following:

- Independence – 3
- Required instrumentation – 1.5
- Availability of experts – 1.5
- Readiness level – 1

An explanation of each criteria is given below:

- **Independence**

This parameter was given the highest weight since the autonomy of the system makes for a more reliable system. Due to the smaller amount of satellites orbiting Mars, it is possible that for long periods the position of the satellite cannot be determined properly.

¹⁵MRO Antennas: <http://goo.gl/CCs0Tb> [cited 2 June 2016]

¹⁶MAVEN Spacecraft Statistics: <http://goo.gl/n2Yh8J> [cited 2 June 2016]

¹⁷Mars Express Fact Sheet: <http://goo.gl/M1Ke6M> [cited 2 June 2016]

¹⁸Mars Odyssey Telecommunications: <http://goo.gl/TfMKn5> [cited 2 June 2016]

¹⁹IM-200 Specifications: <http://goo.gl/ifQgOn> [cited 3 June 2016]

²⁰NASA The Fact and Fiction of Martian Dust Storms: <http://goo.gl/McHK8h> [cited 14 June 2016]

- **Required extra instrumentation**

All the above methods require extra instrumentation. For LiAISON and radar ranging, being very similar concepts, require a Cross-link Transceiver [CSD01, p.136]. For LiAISON its purpose is to communicate with the other satellites and to determine the distance. For radar, it is used for distance determination and clock synchronisation. Finally, for Visual ranging, an extra camera is needed. This parameter is negatively affected by high mass, volume and cost of the above-listed instruments.

- **Availability of experts**

Implementation of these methods requires expertise. The only method that allows for consultation with local experts is the visual determination (Hyperion Technologies).

- **Readiness level**

Being still an experimental proposal, LiAISON has a low readiness level. Moreover, the lack of satellites in unique orbits around Mars, account for another downside of this method. Radar, despite being broadly used on Earth, has never been used in space. The last method, namely visual ranging, has already been tested on Earth [WL10, p.507].

Accuracy is not considered for the trade-off, since its value is very low [FREQ-SS-AO7, Ch. 15] and is not driving the design.

Table 6.4: Trade-off for orbit determination

Method	Independence	Instruments	Experts	Readiness
LiAISON	[U]	[E]	[B]	[U]
Radar	[B]	[E]	[B]	[B]
Visual	[E]	[G]	[E]	[G]

Legend [E] Excellent [G] Good [B] Barely acceptable [U] Unacceptable

Clearly, from Table 6.4 visual ranging is the best option. Not only it is independent from other systems, but there is also availability of experts in Delft. For the correct operation of this method, the IM-200 camera that was introduced above, is the one that is used, since with its purchase also the operating algorithms are provided [S. Engelen, pers. comm. 2nd June 2016].

Making a sensitivity analysis on the trade-off, it can be seen that changing the weight of the criteria will not change the results. Moreover, when considering some extra categories, such as cost and power consumption, it becomes clear that visual ranging is still the most favourable. For instance, the extra cost of visual ranging is the price of a small and compact camera, whereas for the other two criteria, collaboration with other satellites is necessary, which might require investments and/or purchase of communication channels.

6.3. Functional Flow Diagram

Figure 6.4 shows the functional flow diagram of the AODCS for the nominal control operating mode.

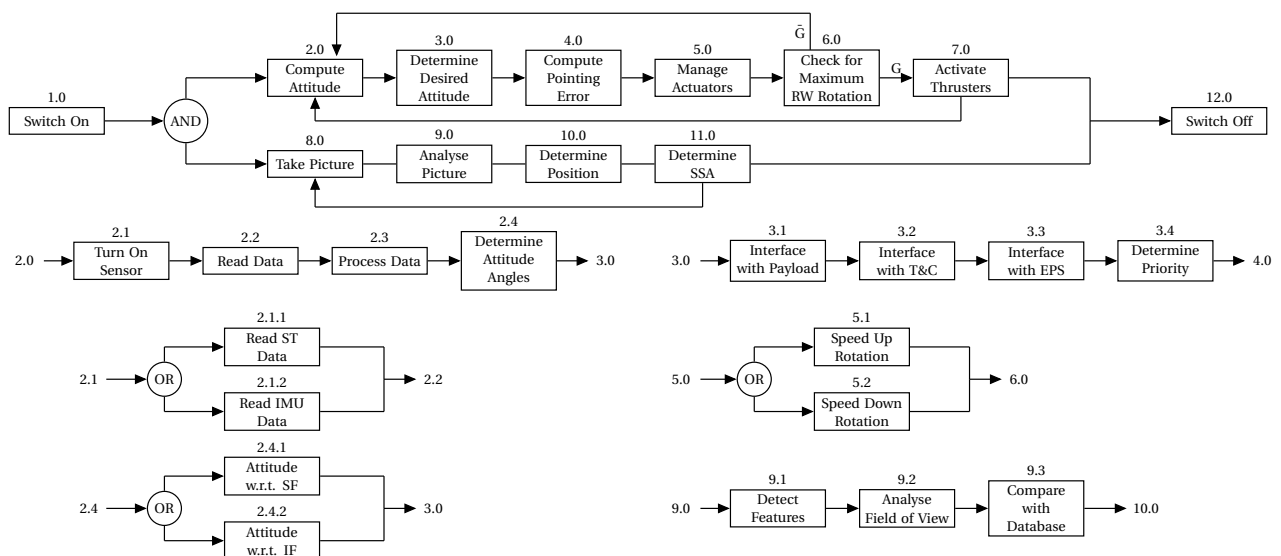


Figure 6.4: AODCS flow diagram

The diagram in Figure 6.4 is describing the working mechanism of the AODC subsystem. First the focus will be put on the ADCS, then on the ODS. From the figure one can see that, after switch on (as soon as the spacecraft enters the acquisition mode), the satellite will immediately start computing the attitude, doing so in real time [FREQ-SS-AO6, Ch. 15]. Figure 6.4 only focuses on the nominal operating mode, however, for the acquisition mode, for instance, the only difference stands in the fact that also sun sensors are used for attitude determination.

In the nominal mode, the use of the STs and the IMU is alternated approximately every 10 s. This means that at first the STs determines the attitude, by comparing the pattern of stars in the picture taken, with the on-board catalogue, then the IMU takes over. For 10 s the IMU is the only source of attitude determination. The switching between STs and IMU, is done to save power and to generate less data, to be processed by the OBC. The value of 10 s was taken from the drift of the selected IMU. Its value is 12 arcsec s^{-1} , which means that the IMU will give an attitude with an uncertainty of 360 arcsec in 30 s. To make sure that the pointing error build up never overcomes the required accuracy, the value of 10 s was chosen. The operation of the RWs and thrusters was already mentioned in Subsection 6.1.3. The OD subsystem only consists of a camera. This camera takes pictures of the surface of Mars and, by comparing the image to a database on-board, the OBC determines the position of the spacecraft. Before this comparison, the image has to be analysed to look for prominent features in the field of view. Of course the camera will give information on latitude, longitude and altitude w.r.t. Mars' surface, thus in the Mars-centred Mars-fixed (MCMF) frame. Transformation between this frame and the Mars inertial frame, or MIF, is given in Appendix A.

Finally, the last task that the ODS performs is to determine the Sun scattering angle (SSA). This angle represents the angular distance between the sun and the spacecraft, centred on the surface of Mars, as described in Chapter 4.

6.4. Layout

Regarding the layout, to achieve a very accurate pointing of the SPEX instrument, the STs should be attached to SPEX itself [S. Engelen, pers. comm. 30th May 2016]. In this manner, thanks to the high stiffness of SPEX's enclosure, the STs will undergo less vibrations and will determine the attitude of the payload itself, instead of of the whole cubesat. In addition, the STs should be placed along three perpendicular axes. In this way, the required accuracy will be achieved in all directions, something that is required for the achievement of accurate measurements. Would a ST fails, the third one could still provide data from a perpendicular axis. Furthermore, for the positioning of the RWs, the closer they are to the centre of gravity, the lower the parameter I_{RW} from Equation (6.5a) and the lower the internal disturbances caused by static imbalance.

After a personal interaction with one of the lead engineers at Hyperion Technologies [S. Engelen, pers. comm. 2nd June 2016], it was determined that all the components can be assembled by them. The dimension of the whole ADCS module would become of about 0.6U and with a total mass of approximately 1 kg. This choice, other than simplifying testing and making the components more compact, reduces the price and avoids the creation of the required algorithms. The creation of the ADC algorithm is one of the most crucial elements in the design of an ADC subsystem. With the use of the algorithms and the ADCS module from Hyperion Technologies, the reliability of this subsystem increases exponentially. Furthermore, these algorithms make the ADCS completely autonomous. The only information that needs to be provided is the desired pointing direction of the spacecraft.

6.5. Control Operating Modes

The ADC subsystem will be activated depending on which control operating mode is currently active. Table 6.5 shows in which mode the sensors and actuators are switched on (I) or off (O).

Table 6.5: AODCS instruments used for each mode

Subsystem	Modes									
	Separation	Insertion	Acquisition	Nominal	Slew	Search	Wait	Safe	Special	Comm
Star Trackers	O	O	I	I	O	I	O	O	I	I
Coarse Sun Sensors	O	O	I	O	O	O	O	I	O	O
IMU	O	O	I	I	I	I	O	O	I	I
Inertia Wheels	O	O	O	I	I	I	O	I	I	I
Camera	O	O	I	I	O	I	O	O	I	O

For more information about each mode, refer to Chapter 10. The selection in Table 6.5 fulfils requirements [FREQ-SS-AO1, FREQ-SS-AO2, FREQ-SS-AO4, Ch. 15].

6.6. Verification and Validation of Numerical Models

Verification of the numerical model used for the attitude disturbances computations, was carried out in the following way. First the correct functioning of the equations used for torque calculations was determined by substituting each

parameter one by one with zeros. The results of these tests are shown in Table 6.6.

Table 6.6: Verification with ‘zeros’ substitution

Parameter	Expectation	Compliance
$\mathbf{d} = \mathbf{0}$	$V \rightarrow \infty$ and no simulation	✓
$A = 0$	No torques	✓
$\mathbf{l} = \mathbf{0}$	No torques	✓
U_D and $U_S = 0$	No internal torques	✓
$\Phi = 0$	No solar torque	✓
$\rho = 0$	No aerodynamic torque	✓
$C_d = 0$	No aerodynamic torque	✓

Secondly, the values of torques were computed by hand to verify their correct usage. The parameters in Table B.1b are still the values used, however for position and velocities the initial conditions were implemented, hence

$$\mathbf{d}_0^{SF} = [0, 0, 3.7935 \times 10^6]^T \text{ m} \quad \text{and} \quad \mathbf{V}_0^{SF} = [3.359 \times 10^3, 0, 0]^T \text{ ms}^{-1}.$$

The comparison between the hand calculations and the simulation results is done in Table 6.7. For the computation by hand of the propellant mass, the RMS value of the disturbance torque was used. This is the reason why the values do not match exactly.

Table 6.7: Verification with hand calculations

Parameter	Calculation	Simulation	Unit	Compliance
Solar torque	$[-0.35, 1.19, 0]^T \times 10^{-7}$	$[-0.353, 1.201, 0]^T \times 10^{-7}$	[Nm]	✓
Aerodynamic torque	$[0, 6.45, 3.23]^T \times 10^{-8}$	$[0, 6.454, -3.223]^T \times 10^{-8}$	[Nm]	✓
Gravitational torque	$[0, 0, 0]^T$	$[0, 0, 0]^T$	[Nm]	✓
Propellant mass	92.0	78.9	[g]	✓
Period	7099.8	7095.9	[s]	✓

Validation, was done by comparing the orbital details of both Mars and the satellite with the results given by the software used in Chapter 5, i.e. GMAT by NASA. It turns out that, not taking into account the J_2 and J_3 effects, the orbital radius of the cubesat remains constant over time, instead of displaying the pattern visible in Chapter 5. Therefore, the software is valid.

Propulsion Subsystem

This chapter describes the propulsion subsystem needed on board of the cubesat for the MICRO mission. The analysis of this subsystem has been carried out through four main parts. First, a primary selection of the propulsion types will be carried out in Section 7.1. Then, in Section 7.2 will deal with the second trade-off leading to a final engine selection. The system architecture and each individual component and its function will be explained in Section 7.3. The mission operation will be described and the functionality of the propulsion system to the mission will be defined. 7.4. Finally, in Section 7.5, some recommendations for the propulsion system are stated.

7.1. Types of Propulsion Systems

An initial trade off was performed in the first stages of the propulsion design, as explained in the Midterm Report [AFH⁺16]. In this previous analysis, the different types of propulsion have been considered and identified as feasible or not for the dust mission on Mars.

In order to determine the feasibility of the mission several criteria have been taken into account. Firstly a ΔV budget needs to be defined, shown in the Table 7.1

Table 7.1: Total ΔV Budget]

ΔV [m s ⁻¹]			
Orbit Insertion	Reaction Control	EOL Manoeuver	Total
121	19	30	170

The other contributing factors to the first selection include;

- Existing technology for cubesat applications
- Power and mass requirements for a cubesat [FREQ-SS-PR5, Ch. 15]
- Orbit insertion performance [FREQ-SS-PR1, Ch. 15]
- Attitude control performance [FREQ-SS-PR2, Ch. 15]
- Volume requirement [FREQ-SS-PR7, Ch. 15]

An overview of the types of propulsion, the selection criteria and the feasibility of each option can be seen in Table 7.2. In this table, the symbol I has been used if the propulsion type meets the criterion, and O if it does not.

Table 7.2: Propulsion type selection

Propulsion Category	Type	Existing Technology	Mass Requ.	Power Requ.	Orbit Insertion	Attitude Control	Feasibility
Electrothermal	Cold Gas						
	Mono-prop.						
	Bi-prop.						
	Resistojet						
Electrostatic	Arcjet	O	O	O			O
	RIT			O			O
	Kaufman	O	O	O			O
Electromagnetic	Hall Thruster	O	O	O			O
	FEEP						
	PPT						

In this mission, it has been decided to use commercial-off-the-shelf technology as designing a new propulsion concept would be a high risk with respect to the time constraint of a launch in the year 2020. Development of a propulsion system will involve extensive research and development along with thorough testing, causing the final product to be significantly time consuming to achieve technical readiness level and more expensive than COTS(commercial off-the-shelf) components. Based on Table 7.2, a first selection has been made and different available models of propulsion systems have been investigated. For each of the models, the ΔV has been calculated based on the rocket equation, which is given in Equation (7.1).

$$\Delta V = I_{sp} g_0 \ln \left(\frac{M_0}{M_{dry}} \right) \quad (7.1)$$

These models and their specific characteristics can be seen in Table 7.3. It is important to realise the propulsion system comes with two types modes; the primary mode high ΔV manoeuvres such as orbit insertion and reaction control mode. systems consisting the capability of both modes are known as dual modes. For the different models selection, only dual modes have been considered in order to meet the attitude control requirement . One could use a combination of one primary and one dual mode propulsion system. However, this option would have led to a higher mass, power and adaptability issues than using a system that can perform both modes.

Table 7.3: COTS propulsion systems

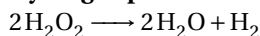
Manufacturer	Model	Type	Mode	ΔV [ms ⁻¹]
AEROJET	MPS-130	Mono-propellant	Dual	120
AEROJET	MPS-120XW	Mono-propellant	Dual	166
AEROJET	MPS-120	Mono-propellant	Dual	81
AEROJET	MPS-120XL	Mono-propellant	Dual	200
Busek	BmP-200	PPT	Dual	21
Busek	MRJ	Resistojet	Dual	37
Vacco	Hybrid Mips	Mono-propellant/Cold gas	Dual	143
Vacco	Marco MiPS	Cold gas	Dual	83
Vacco	Standard MiPS	Cold gas	Dual	25.83
Vacco	E&M MiPS	Cold gas	Dual	32.7

7.1.1. Propellant Types

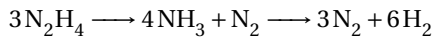
It is clear from Table 7.3 that Cold gas propulsion and Resistojet propulsion cannot provide the required ΔV (170 ms⁻¹) for the mission. This leaves the most suitable option as to use mono-propellant propulsion systems. The mono-propellant propulsion system consists of a propellant that undergoes decomposition with an exothermic reaction and uses this energy to accelerate these particles through a nozzle. The propulsion system can be operated in both steady state mode and pulse mode to provide low impulse bits. The main advantage of using a mono-propellant propulsion system for this mission is its low power consumption and high performance. The mono-propellant systems can provide the required ΔV for this mission with limited power and mass budgets. A typical mono-propellant system consists of a pressurised tank where the propellant is stored, feed system to distribute and control the flow, catalytic converter or heating element to decompose the propellant and finally a nozzle to accelerate the exhaust gases.

The types of mono-propellant that are used in space industry are limited. However, some of the most common types of propellant include hydrogen peroxide and Hydrazine. However, some systems mentioned in Table 7.3 uses the following Ammonium Dinitramide (ADN) and Hydroxylammonium Nitrate (HAN) based propellant known as AF-M315E which are green propellant. The mentioned propellants decompose in the following fundamental manner shown below;

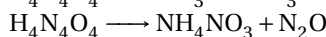
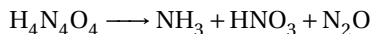
Hydrogen peroxide



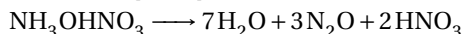
Hydrazine



ADN [YTY05]



AF-315ME [SK15]



Note that the above equation for ADN is not a stoichiometric equation, but just shows a phase of decomposition to show its products and by-products. Decomposition reactions varies resulting different by-products depending on multiple criteria, such as pressure and the temperature of the reaction.

The AF-M315E is a HAN based propellant, exact solvents to form this propellants and decomposition reaction is unknown. This is due to proprietary composition of AF-M315E [RAS13].

Hydrogen peroxide is the lowest performance propellant amongst the three. A major issue for hydrogen peroxide is storability because it is acidic and corrosive properties. Hydrogen peroxide has many negative aspects including the ability to self-decompose and increase system pressure, hence making it very undesirable for a long duration mission. Due unavailability of COTS products and lower performance hydrogen peroxide is omitted at this point as a possible choice of propellant. Hydrazine propellant is widely used in spacecraft, the Aerojet MPS 120XL is a hydrazine based propulsion system. In comparison to hydrogen peroxide it has greater performance increment of 30 % [LWH09]. Hydrazine uses Shell 405 catalyst commonly (32 % iridium with alumina); this triggers the decomposition of hydrazine. Hydrazine is a widely used propellant in spacecraft. However the drawbacks of Hydrazine is mainly due to its toxicity, Hydrazine is a well known carcinogenic¹ as well as pose a great threat to the environment if it poorly handled.

ADN has 24 % higher density and 6 % higher performance than hydrazine [LWH09]. ADN is used in liquid form by making a solution with alcohols (acetone, methanol and ethanol) or water. FLP106 is a liquid water based fuel consisting of 60.4 % ADN and has a theoretical I_{sp} of 259 s [LW11]. VACCO Mips ADN hybrid propulsion system cannot provide the sufficient ΔV of 169 ms^{-1} for orbit insertion and maintenance for MICRO. Simply because it uses two propellants. Though the current development of ADN thrusters is limited to contribute to the requirements of MICRO (this is due to low ΔV), ADN has a high performance compared to hydrazine, but the only dual mode COTS product is the VACCO Hybrid MIPS². The AF-315ME is new green propellant developed by U.S. Air Force Research Laboratory, This propellant is used in the Aerojet MPS 130. AF-315ME has 13 % higher theoretical I_{sp} and 63 % density- I_{sp} than hydrazine [TLZC13]. The HAN based AF-315ME is a ionic liquid in state (HAN dissolved to form a AF-M315E). the propellant is known for low toxicity level and can be handled in open containers³. The low toxicity level reduces the cost of handling propellant. Low toxicity permits the university to allow the propellant to be handled by students. Based on the components found in Table 7.3, a first selection can be done for meeting the ΔV requirements. Indeed, for the orbit insertion, the propulsion system shall have a ΔV of at least 120.9 ms^{-1} ; while for the end-of-life the ΔV shall be at least 19 ms^{-1} (Chapter 6) and ΔV for end-of-life solution 30 ms^{-1} (Chapter 5). This leads to a final required ΔV of at least 169.9 ms^{-1} . Based on these requirements, only the following configurations provided the ΔV required and fulfilled the requirements as shown in Table 7.4.

Table 7.4: Propulsion systems configuration

Manufacturer	Model	units	Isp	ΔV [m/s]	Propellant	Power W
AEROJET	MPS-130	2	240	248	AF-M315E	4
AEROJET	MPS-120XL	1	215	200	Hydrazine	8

¹Occupational Safety and Health Guideline for Hydrazine: <http://www.cdc.gov/niosh/docs/81-123/pdfs/0329.pdf> [cited 6 June 2016]

²VACCO Hybrid MIPS: <http://www.cubesat-propulsion.com/hybrid-adn-delta-v-rscs-system/> [cited 6 June 2016]

³NASA Green Propellant Infusion Mission Project: <https://goo.gl/YcYp5J> [cited 6 June 2016]

7.2. Propulsion System Selection

As explained in Section 7.1, a propellant has been realised leading to two feasible options, namely the MPS-120XL and two units of MPS-130 by Aerojet Rocketdyne. The purpose of this section is to select the best option of the MICRO mission by the use a complete final trade-off. For selecting the best option, several criteria have been taken into account.

1. ΔV (trade off weight of 20 %) this is to comply with requirements[FREQ-SS-PR1, FREQ-SS-PR2, FREQ-SS-PR3 Ch. 15]
2. Mass (trade off weight of 20 %)this is to comply with requirement [FREQ-SS-PR5, Ch. 15]
3. Power(trade off weight of 15 %) this is to comply with requirement [FREQ-SS-PR4, Ch. 15]
4. Adaptability (trade off weight of 20 %) this is ensure the subsystem can integrate into the structure of MICRO with minimum hindrance for other subsystem.
5. sustainability (trade off weight of 10 %) This is to make sure to mitigate any dangers or harm caused by the use of system to environment or people
6. Impulse bit (trade off weight of 10 %) This is to comply with [FREQ-SS-PR6, Ch. 15] ensures that the system can deliver high accuracy impulse for the reaction control system.

Table 7.5: Final trade-off between between MPS 120XL and MPS 130

System	ΔV [m/s]	Mass [kg]	Power [W]	Adapt- ability	Sustain- ability	Impulse- bits [Ns]
MPS 120XL	[G] 198.9	[E] 3.2	[E] 4	[U] Incompatible arrangement	[B] Toxic	[G] 0.0048
MPS 130	[E] 235	[G] 4.8	[G] 8	[G] Compatible	[G] Low Toxicity	[G] 0.003

Legend [E] Excellent [G] Good [B] Barely acceptable [U] Unacceptable

7.3. Final Choice

Based on the trade-off realised in Section 7.2, two units of MPS 130 was selected to perform this mission⁴. Figure 7.1 shows MPS 130 propulsion unit and the MR-143 thruster along with the fuel and pressurant tanks. The disadvantage of handling hydrazine as propellant due to its toxic properties, especially for a student involved mission. Hence the MPS 130 with its low toxic green propellant makes it ideal for this mission. The ability adapt MPS 120 XL was not feasible with the layout of the 6U cubesat, The MPS 120 XL which is a 10 x 10 x 22.4cm this could not be fitted in the current layout of the spacecraft, primarily due the shape of the SPEX payload. Adapting MPS 120 X with SPEX instrument would cause the cubesat to violate 6U requirement. Hence the most appropriate with respect to adaptable was using MPS 130. Hence the MPS 130 has an advantage of the Using two units of finally,MPS-130 gives the ability to use favourable thruster arrangements and adds redundancy with 4 extra thrusters. MPS-130.

In this section the specifications will be discussed, followed by the specific engine architecture and the integration mechanism. Then, the engine will operation during the different phases of the mission will be briefly discussed. Finally, recommendation for the propulsion subsystem will be discussed, as it is a critical subsystem for the mission.

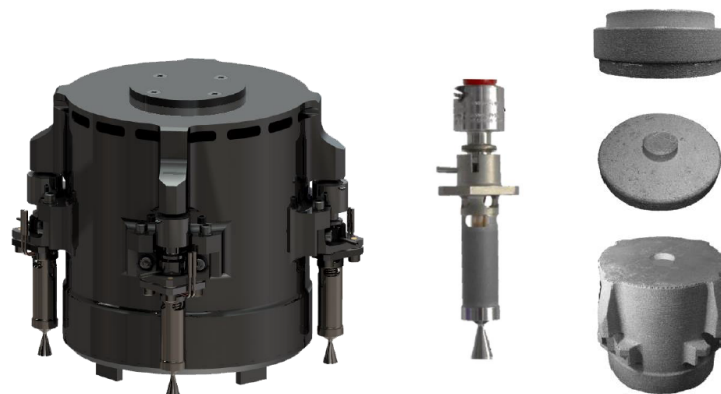


Figure 7.1: MPS 130 system, MR143 thruster and propellant system [CSOM13]

⁴Cubesat High Impulse Adaptable: <http://www.rocket.com/cubesat/mps-130> [cited 7 June 2016]

7.3.1. Specifications

The propulsion system specification has been summarised in Table 7.6 the data is obtain using top level specification sheet from Aerojet Rocketdyne [Roc15].

Table 7.6: Propulsion system specification

Aerojet MPS 130		
		Units
Mass	4.8	kg
Propellant Mass	1	kg
Specific Impulse	240	s
Thrust max	<1.5	N
Power Startup	4	W
Power Operational	1	W
Voltage Startup	6	V
Voltage Operational	2	V
Temperature	-5 to 50	°C
Operational Pressure	34-9 to 5.4	bar

Table 7.7: Thruster configuration

Axis	Rotation around axis	Thrusters
X	+	A4 & B3
X	-	A1 & B2
Y	+	A1 & A\$
Y	-	B2 & B3
Z	+	A1 & B3
Z	-	B2 & A4

7.3.2. Propulsion System Architecture

The propulsion system architecture is shown in Figure 7.2. It consists of a pressurant tank, pressurized by Nitrogen this can be seen on right corner of the Figure 7.1. The pressurant is then used to pressurise the propellant via a piston in the tank. The propellant is then flushed through the feedsystem to the thruster. The thrusters decompose and accelerate the flow.

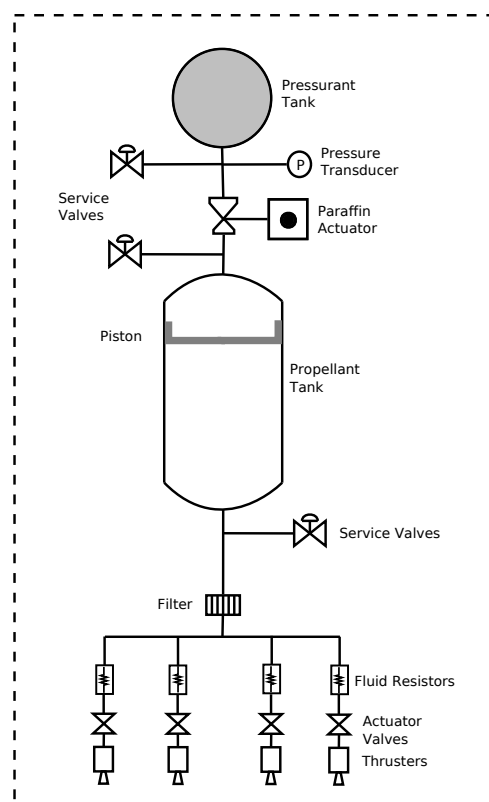


Figure 7.2: MPS 130 architecture [CSOM13]

7.3.3. Propellant Storage

Propellant storage is a critical element of the propulsion system. The storage needs to provide the propulsion system with ability to store and operate the propellant at the desired pressures. The storage tank needs to prevent leak of the propellant at all phases of the mission. Propellant sloshing give rise to disturbance in the spacecraft. In MPS 130 a piston is used in the seen on the Figure 7.2, this piston is used to prevent propellant sloshing by pressing using the pressurant tank. The the liquid propellant (AF-315ME) is oriented to the bottom of the tank using the piston, making it possible to blow-down the propellant through the feed system. The advantage of this system is prevention of propellant sloshing which can cause internal disturbance to the vehicle. The total system pressure ranges from 34.5 bar to 5.9 bar [Roc15].

7.3.4. Feed System

The feed system is responsible for propellant transportation and distribution. The feed system consists of a pressurant tank which is primarily use to pressurise the propellant. The pressurant tank is used to help maintain the feed pressure, the pressurant tank uses a inert gas to increase the feed pressure. The MPS 130 uses nitrogen as pressuring, the advantage of nitrogen is its large molecular size reduces the leaks for a long duration mission in comparison to a pressurant as helium which has smaller molecular size [LWH09]. The feed system consists of two paraffin actuated pressurant isolation devices are used to keep the system safe from the pre-launch all the way to cubesat deployment phase [CSOM12]. The service valve allows filling and dumping of Nitrogen and AF-M315E. The location of three service valves enables the user to identify any leaks across the isolation devices by measuring the the pressure using the a connection to the service valves. The fluid resistor is used before the thruster to customise the thrust depending on the mission requirements [CSOM12].

7.3.5. Thrusters

The propulsion system consists of 8 thruster, four of them are dedicated for primary and four of the thruster in the four corners of the cubesat are used for reaction control system shown in Figure 7.4. The thrusters are vectored five degrees inwards as shown in Figure 7.3 this provides the ability to perform rotation around Z axis as shown in Figure 7.4. The thruster configuration for each axis is define in Table 7.7. The thrusters are used to accelerate the flow and achieve a higher exhaust velocity. Mono-propellant thrusters consists a propellant inlet and the performance can be adjusted using a injector. Multiple configurations of the injector contribute to the performance of the thruster such as the injection angle (swirl angle), size of the orifice and the amount of offices. Varying the above will be result in changes to propellant mass flow and injection pattern. The propellant is then injected to a catalytic chamber where the propellant undergoes decomposition and the hot expanding gases is accelerated through a nozzle to achieve a high exhaust velocity. The catalyst used was EL-Formed Iridium Foam Catalyst [CSOM14]. The MPS-130 system uses four Aerojet MR-143 thrusters [CSOM14] shown in Figure 7.1. The chamber and nozzle composed out of Rhenium and coated with Iridium using EL-Form [CSOM14]. The EL-Form process gives the thruster the ability to withstand heat up to 2200 °C⁵.

7.3.6. Integration Mechanism

In order to integrate the system in to the cubesat it is required to know the attachment mechanism. The attachment mechanism require to be precise to avoid thruster misalignment. Due to limited information available about MPS 130 the attachment mechanism of the module is unknown. However according to publications made by Aerojet MPS family it safe to assumed that an adaptable payload mounting interface is used, it consist of four attachment on four sides of the frame, this is used to mount the propulsion system to the structure of the cubesat, This feature can be seen in Figure 7.4. However if the attachment can be custom made to the frame to reduce a joining mechanism, this can reduce mass of the system. The highest encountered forces on the adaptable mounting mounting mechanism is during the launch of the cubesat, this will result in 200.12 N axially and 70.63 N laterally. An even distribution of load on each attachment point will result in lower loads of 25.01 N axially and 35.32 N laterally on each attachment. The schematics of the adaptable mounting is not available due the unknown size of diameter of attachment hole and the thickness the stress can vary.

⁵EL-Form by Plasma Process Inc, NASA Spin Off: https://spinooff.nasa.gov/Spinoff2011/ip_6.html [cited 7 June 2016]

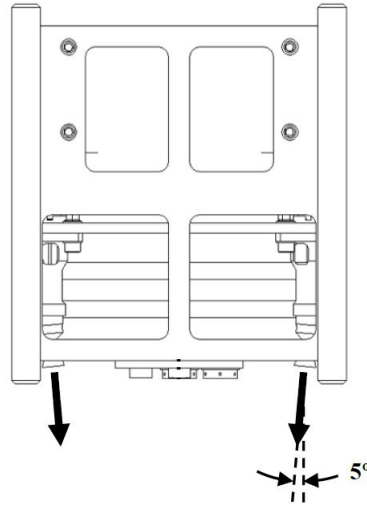


Figure 7.3: Thrust vector shown with adaptable mounting interface

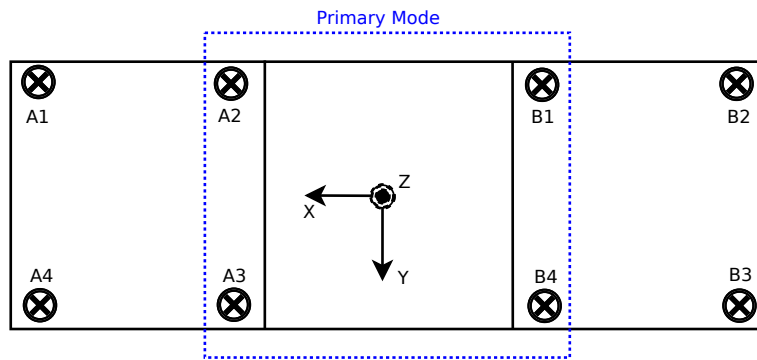


Figure 7.4: Cubesat propulsion

7.4. Mission Operation

In this mission, all segments when the propulsion system operates will be discussed and the firing sequence of thrusters will be discussed. Figure 7.3 shows the layout of the propulsion units. The propulsion system has 1 kg of propellant on board. The propulsion system must operate for three major events in the mission life this can be categorised to three phases as follows;

7.4.1. Orbit insertion phase

In this phase the primary thruster are fired to achieve a ΔV of 121ms^{-1} using the rocket equation it is possible to calculate the mass of propellant required 525 g of propellant. The burn time can be computed using Equation (7.2)

$$F t_b = M_p I_{sp} g_0 \quad (7.2)$$

In Equation (7.2) F defines the total force achieved by the thrusters, for this value a conservative value of 1N [Roc15] per thruster is assumed. The I_{sp} of the system is 240 s [Roc15], M_p is the propellant mass calculated (525 g) and the gravitational acceleration is denoted by g_0 . Using the primary thruster configuration to perform the manoeuvre as shown in Figure 7.4, this will include the thrusters A2, A3, B1 and B4 as shown in Figure 7.4. Each thruster requires a power of <4 W for 2ms to start up (open valve), to remain firing the thrusters will consume <1 W of power [Roc15]. In order to optimise power consumption a thruster fire sequence is adapted. The sequence would be to fire thrusters consecutively starting with A2 then B4 followed up by A3 and finally B1 as shown in Figure 7.4. This sequence will lead to a time lag of 2 ms [SMS11] between each thruster hence to compensate for the resulting forces causing an rolling around Z axis the the thrusters are shut of in the same sequence which will result in counteraction to the rolling motion. The thrust shut of sequence will occur after each individual thruster performs for 309.02s. The shut off sequence is same order of the starting sequence; A2 then B4 followed up by A3 and finally B1. It is important

to note the thruster maximum operative times are not published yet by Aerojet Rocketdyne, depending on this the primary burn needs to be performed in stages if required to reduce the high burn time at one instant.

7.4.2. Reaction Control Phase

The propulsion system needs to be able to provide the AODCS system with that ability to de-saturate the reaction wheels. During the mission it is important to de-saturate the reaction wheels to avoid failure of the reaction control system. The reaction wheels require de-saturation once in two orbits (Chapter 6). The de-saturation is only required in Y axis amount of angular momentum is quantified to be 0.03 Nms (Chapter 6). Using the following relations (7.3) it is possible to account the required performance from the propulsion system to counteract the angular momentum. to counteract this motion two thruster need be fired, this will result in either thruster A1 and A4 or B2 and B3 to operate. The mass of micro after orbit insertion results 9.975 kg

$$H = F b_i t_b \quad (7.3)$$

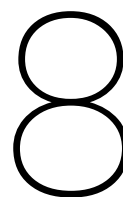
The H denotes the angular momentum that requires to be countered (0.03 Nms) and b_i is the arm length from centre of mass to the force exerted by the thruster, arm length of 14.5cm is used. This results in an impulse of 0.2Ns. If a thruster provide a thrust of 0.8 N then the two thrusters will operate simultaneously for a burn time of 0.129 s. Reaction wheel de-saturation to 55 time during the mission duration. The total propellant used for this phase is accounted to be 80 g and total spacecraft mass 9.895 kg. The minimum impulse bit that can be achieved by an individual thruster is 0.003 N [Roc15]. Hence the thrusters can do precise reaction control.

7.4.3. End of Life

The end of life solution is to maintain the orbit defined in Chapter 5 by providing a ΔV of 30 ms^{-1} . It is taken in to account the changing mass of the MICRO propellant is expelled from the body. Before end of life manoeuvre, the total mass of MICRO would reduce from 10.5 kg to 9.895 kg, with this value the mass of propellant for this manoeuvre is computed to be 125g. Using Equation (7.2) the total amount of burn time of 87.55 s is calculated to be using four primary thrusters (A2, A3, B1 & B4). After end of life manoeuvre is performed, the remaining amount of propellant would be 270 g. It is safe to account the additional propellant for the mission as this can bring more relief for emergency manoeuvres or extended mission operation.

7.5. Recommendations

Currently MICRO uses two MPS-130 propulsion system. It is recommended that for further development of the propulsion subsystem to use a single pressurant tank and fuel tank, this will significantly reduce the mass and increase reliability of the mission (due less components). The propulsion system could implement a thruster in negative Z axis, this could add the ability to reduce ΔV counter any translation to motion encounter when using its reaction control system to dump momentum. The mission doesn't taken into account ΔV for unaccounted perturbations such as collision avoidance. It is advisable to perform thrust optimisation for orbit insertion since the required burn time is 5 minutes and 15 seconds. The propulsion system needs to compensate for misalignment of the centre of mass, for further improvement a typical misalignment scenario must be accounted. Utilising thrusters primary thrusters A2, A3 and B1, B4 can give more precision controlling due to smaller arm length from centre of mass, however this might not be the most efficient way, once the thruster force range is known this can be taken into account.



Command and Data Handling

In this chapter the design of the command and data handling (CDH) subsystem is presented. In the Midterm Report [AFH⁺16] the basic characteristics of the CDH were established and some options were given for components. In this report the design of the subsystem is finalised. First, the functions of the subsystem are given in Section 8.1. Then, the functions and design of the on-board computer is discussed in Section 8.2. Finally, the data interfaces between the subsystems are defined in Section 8.3.

8.1. Functions

The CDH subsystem has multiple functions. The most important ones are listed below based on the requirements imposed on the subsystem. The requirement corresponding to each function is indicated.

- Collecting telemetry [FREQ-SS-CD3, FREQ-SS-CD4, FREQ-SS-CD6, Ch. 15]
- Distributing commands [FREQ-SS-CD11, Ch. 15]
- Data storage and processing [FREQ-SS-CD7, FREQ-SS-CD8, FREQ-SS-CD12, Ch. 15]
- Time-keeping [FREQ-SS-CD10, Ch. 15]
- Failure detection [FREQ-SS-CD5, Ch. 15]
- Changing control modes [FREQ-SS-CD1, FREQ-SS-CD2, Ch. 15]
- Providing data interfaces between subsystems [FREQ-SS-CD9, Ch. 15]

8.2. On-Board Computer

In this section the on-board computer (OBC) of the cubesat is discussed.

8.2.1. Functions

The on-board computer can be regarded as the brain of the cubesat. It is in charge of distributing commands to the other subsystems and managing the functioning of the cubesat.

The OBC is in charge of the correct functioning of the cubesat. At times, this requires receiving commands from the ground control and distributing these to the relevant subsystems. This is also one of the main functional requirements of the whole subsystem. The interface through which these commands are distributed is described in Section 8.3. The OBC also has to provide accurate time-keeping data for the other subsystems. It is especially important to have matching time-stamps on the payload data and the position information provided by the AODCS subsystem so that the science data can be connected to the correct location. The OBC is also in charge of maintaining the correct temperature range in the cubesat. It receives temperature information from the thermistor and if the temperature is under the defined threshold, the OBC sends a command to the propulsion subsystem to produce heat as discussed in Section 11.2. One of the functions of the OBC is also to change the operational mode of the cubesat if commanded to do so by the ground control.

One of the main functions of the OBC is on-board data processing. An important task is processing the data from the scientific payload as the application-specific integrated circuit (ASIC) included with the detector is not capable of it as discussed in Chapter 4. Most of the collected science data has to be compressed in order to reduce the amount of time required to transmit it to the relay satellite. However, occasionally the raw data has to be transmitted for validation purposes which requires no on-board processing. If the on-board processing of the data is found out to be flawed, the software has to be updated by the ground control. The processing of the science data can be done by

most OBC's as it is not computationally intensive [F. Snik, pers. comm. 13th June 2016]. Another important data processing task is the determination of attitude and location based on the sensor input of the AODCS. This processed data has to then be translated into the required actuator action to maintain or change the attitude and to determine the orbit. This is a continuous task and requires a sufficient amount of processing power, which can however be assumed to be available in all COTS OBC's.

In addition to processing data, the OBC also stores it before it can be transmitted. This requires memory and science data is the main driver in sizing the required on-board memory. Also part of the telemetry data has to be stored in case it is sent to Earth for checking the status of subsystems. The effect of this data on the size of the memory is quite small compared to the storage required by the payload data, but it will be taken into account. The map used for the location determination on Mars as discussed in Chapter 6 is also stored in the memory on the OBC and accessed for attitude information.

Due to the radiation environment in outer space, errors in the OBC functions can be caused by single-event upsets. To mitigate this on a fundamental level, the OBC will be placed in the middle of the cubesat bus to the best possible extent. This reduces the received total radiation dose as discussed in Section 11.3. To detect computer failures, a watchdog timer software has to be included in the OBC. The timer has to be reset by the OBC at regular intervals. If this is not done in time, the watchdog timer determines that there is a failure in the OBC and it is reset to an initial configuration. This requires a radiation tolerant storage for the software that allows restoring the system to a functional state when required.

8.2.2. Performance Requirements

The required data storage is one of the most important considerations when selecting an on-board computer. During the mission both housekeeping and payload data have to be stored so they can be sent to the Earth. The amount of data collected for housekeeping cannot be accurately estimated at this phase of the design. It is however estimated based on [sse06] and the Delfi cubesat telemetry data in [Zan13] that the amount of housekeeping data produced is 800 bits s^{-1} . This makes the total amount of housekeeping data that needs to be stored and sent to MRO every orbit approximately 5.656 Mbit considering an orbital period of 7070 s. This data can consist of both analogue and digital measurements, but the analogue values will be digitalised by the OBC. As discussed in Section 4.2, the maximum amount of payload data that has to be stored in the OBC is approximately 399 MB. The combination of housekeeping and payload requires at least 512 MB of non-volatile memory to store the data in case it cannot be processed during the measurements. Having that amount of memory allocated accounts also for the housekeeping data. Additionally, a sufficient amount of RAM is required to efficiently process this data. It is assumed that the same amount of RAM is needed as the amount of non-volatile memory used for storing the data.

Due to the multiple data processing tasks outlined in the previous section, the estimated required processing power is rather high. However, quantifying the required clock speed proved to be quite challenging with the information known. The payload data processing is preferably done after storing the data in the memory temporarily. This requires a high clock speed to ensure the data processing is done effectively. The payload data processing is assumed to be the critical function for the processor speed.

8.2.3. Selection of the On-Board Computer

The selection of the on-board computer was an iterative process based on the available COTS products. At first, the best option that was found was the NanoMind 3200 OBC by GomSpace¹. This is because it is highly compatible with the UHF transceiver chosen in Chapter 9, the NanoCom AX100. Its specifications are also flexible and the available documentation on this OBC is extensive. The main concerns were the maximum clock speed of 64 MHz¹ and the amount of flash memory available. This might lead to an increase in the time it takes to process the payload data and lead to a higher required memory size or a smaller amount of science data obtained during the mission lifetime.

The selection of the AODCS components led to the discovery of an OBC not known previously, due to the fact it is not yet commercially available. The Hyperion Technologies B.V. HT-CP400.85 [S. Engelen, pers. comm. 6 June 2016] is attached to a module with the AODCS components from the same company and has good specifications that outperform the NanoMind OBC. It is however not available to the public at this moment and as such, not all information about it is known. However, based on personal communication the key properties were acquired. It is also known that the computer has a TRL of 7, meaning that it has been tested in an operational environment². The technical readiness can be regarded as sufficient for the mission. Due to the integration with the AODCS subsystem, this computer is a preferable option compared to the NanoMind. The selection of the HT-CP400.85 makes the in-

¹GomSpace NanoMind 3200: <http://gomspace.com/documents/ds/gs-ds-nanomind-a3200-1.6.pdf> [cited 6 June 2016]

²NASA TRL: https://esto.nasa.gov/files/trl_definitions.pdf [cited 6 June 2016]

tegration of the AODCS computing simple and the processing power and memory are more than sufficient for the needs of the mission. The properties of the two on-board computers are shown in Table 8.1. The HT-CP400.85 not only outperforms the NanoMind 3200 but also is the only one out of the two that can be trusted to have good enough specifications. Furthermore, it is already integrated within the AODCS module and thus a convenient choice. For these reasons it is chosen as the OBC for the cubesat.

Table 8.1: Specifications of the NanoMind 3200 and Hyperion HT-CP400.85 on-board computers

Parameter	Value NanoMind 3200	Value HT-CP400.85	Unit
Processor	AVR32	ARMv7-A	[–]
Processing power	n.a.	750	[DMIPS]
Clock speed	8–64	500	[MHz]
RAM	32 (SDRAM)	512	[MB]
Flash memory	128	512	[MB]
Dimensions	65x40x6.5	20x50x10	[mm ³]
Mass	14	10	[g]

For redundancy, an additional OBC is included in the cubesat. This is a cold redundant (not operational) copy that can be switched to in case a failure is detected in the operating computer. This increases the reliability of the subsystem as a whole. The OBC will be placed on the NanoDock motherboard along with the redundant copy³. This should not pose a problem as the option for incorporating third party systems on the motherboard is stated as an option. The data interface options of the OBC include CAN, RS422, RS485, I²C, USB, U(S)ART, SPI and Ethernet. It is also possible to include 7.5 Gbit of radiation tolerant storage in case more memory is required for e.g. software or science measurements [S. Engelen, pers. comm. June 2016].

8.3. Subsystem Data Interfaces

In this section the data interfaces between the subsystems and the OBC are discussed.

8.3.1. Data Bus Selection

One of the most important functions of the CDH subsystem is transmitting telemetry and commands to and from all the subsystems. There are multiple ways to arrange the data architecture to achieve efficient communication between the different subsystems, such as a ring or a bus [WL10, p.653]. The bus structure is the only one considered for this cubesat due to the fact that it requires relatively little wiring and is reliable as the failure of one subsystem does not prevent the flow of the data [WL10, p.653]. For this cubesat, I²C (Inter-Integrated Circuit) and CAN (Controller Area Network) buses are considered due to the fact that most COTS components support them for interfacing and their implementation is not overly complicated for a cubesat.

Both of the standards are serial buses, so the amount of wiring needed is similar. In a serial bus all subsystems are connected to a common wire (or multiple) along which data is transferred in a linear fashion. The I²C standard allows for data speeds up to 400 kbits^{−1}, whereas with CAN rates of 1 Mbits^{−1} can be reached [dJAB08]. The I²C bus is more simple due to the fact that for CAN every node (in this case subsystem) requires additional hardware to implement the protocol. The major advantage of the CAN bus compared to I²C is its robustness against electromagnetic disturbances. This is due to the differential signalling. The reliability is also increased by the error detection included in the CAN protocol⁴. Due to the robustness and higher achievable data rate the CAN bus is selected for use in the CDH subsystem. The additional hardware and complexity of implementing the CAN protocol are accepted in the name of better data transfer performance in space.

CAN Bus Architecture

Using a CAN bus on the cubesat requires some additional hardware in every system connected to the bus. In practice this means that every subsystem on the spacecraft needs a microcontroller and a CAN transceiver. Most subsystems already include a controller of their own, or in case of the AODCS are completely controlled by the OBC itself. The processor requires a CAN controller. In case the subsystems do not already include a CAN interface, a CAN controller with a transceiver can be added, for example the Microchip MCP25625 controller⁵. This ensures that all the messages between subsystems follow the CAN protocol while keeping the subsystem architectures relatively simple.

³GomSpace NanoDock: <http://gomspace.com/index.php?p=products-motherboard> [cited 8 June 2016]

⁴CAN Bus Characteristics: <https://goo.gl/IZdbtH> [cited 3 June 2016]

⁵Microchip CAN Controller: <http://ww1.microchip.com/downloads/en/DeviceDoc/20005282A.pdf> [cited 3 June 2016]

Each subsystem (node) is connected to both of the two CAN lines. This linear bus topology allows the subsystems to communicate with each other without the OBC having to control all the messages. While the nominal data rate is 1 Mbits^{-1} , a large overhead due to the message protocol has to be taken into account [dJAB08]. However, the data rate of the bus should easily be enough to manage the cubesat during all phases of the mission as the payload data is transmitted through a different line.

8.3.2. Payload Data Interface

As discussed in Section 4.2, the amount of data produced during measurements is approximately 2.1 MBs^{-1} . This data has to be stored in the non-volatile memory in real time as the detector electronics do not support storing a large amount of data. The required data rate from the payload to the OBC then vastly exceeds the capacity of the CAN bus and another data interface is required. Due to the high data rate, not many options are available. Out of the interfaces available in the selected OBC [S. Engelen, pers. comm. June 2016], RS485 or Ethernet seem to be plausible options for the payload data interface. The integration of the available OBC interfaces with the interfaces of the SIDECAR ASIC [LBGX07] is not handled at this stage of the design. It is assumed that an FPGA can be included between the ASIC and the OBC with the required interfaces.

8.3.3. Data Handling Diagram

The data connections of the CDH subsystem are shown in Figure 8.1. This figure includes the most important routes of commands and data (e.g. payload and attitude data). The memory sizes, data rates and processor speeds are also indicated. The payload has its own high-speed data link and all the other subsystems are connected to each other and the OBC through the CAN bus. The CPU is connected to both the RAM and flash memories and the payload has a direct link to the flash memory. The functioning of the CPU is constantly monitored by the watchdog.

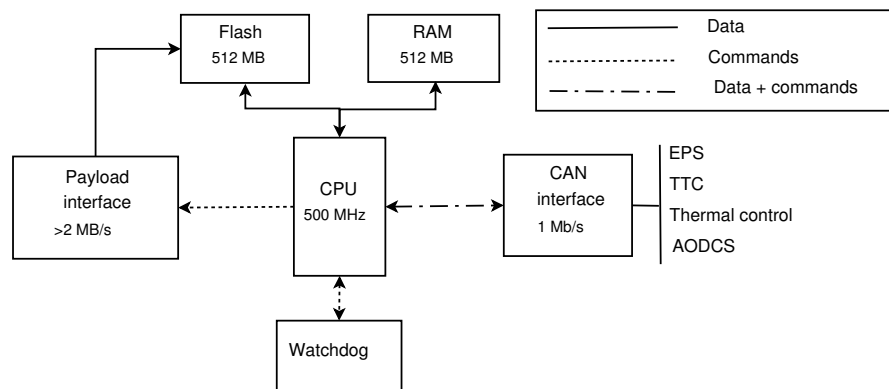


Figure 8.1: Data handling diagram of the CDH subsystem

Telemetry and Communication

The telemetry subsystem represents a critical part of the cubesat mission as it allows communication with ground station. For the MICRO mission, the designed cubesat will be communicating towards the Earth with the use of a relay satellite. This chapter will describe in detail this subsystem through five main parts. First, protocol used for the defining the main characteristics of the communication will be described in Section 9.1. In Section 9.2, the specifications of this subsystem will be explained. Then, Section 9.3 will deal with the transceiver mechanism. Section 9.4 will give a detailed overview of the antenna design. Finally, in Section 9.5, the quality every component used for the telemetry will be studied.

9.1. Proximity 1 Protocol

The Consultative Committee Space Data Systems (CCSDS) has created a set of recommendations for data systems such as the space protocols; which have been adopted by ESA and NASA. These protocols replace the PCM telemetry standard, which used to be followed, in order to improve the interoperability and standardisation.

For this mission, it has been decided to follow the Recommended Standard for proximity space links, i.e. the proximity 1 protocol, defined by the CCSDS. This standard is used for defining specifications of communications links between orbiting satellites and relays, for which the links are defined with a short delay time and/or with a weak signal. Furthermore, it was produced to fit into the space missions requirements in order to have the best efficient data transfer in space; taking into account the different types and features of proximity space links¹.

The Proximity 1 Protocol gives specifications on the communication specifications, as the base band, frequency, modulation and coding, as will be explained in Section 9.2. This protocol conducts also standards for the on-board-computer software, such the Data Link and Physical layers protocol specifications [sse06, p.336]. These layers are part of the Open Systems Interconnection software model, also called the OSI model. This model is a conceptual model describing the communication functions of a telecommunication network. Seven layers can be identified:

- | | | | |
|--------------------|--------------------|-----------------------|----------------------|
| 1. Physical Layer | 3. Network Layer | 5. Session Layer | 7. Application Layer |
| 2. Data Link Layer | 4. Transport Layer | 6. Presentation Layer | |

The design and functions of each layer will be deeply discussed in the Chapter 8, dealing with the Data Handling and Command, where the on-board computer will be described.

9.2. Subsystem Specifications

This section describes the key features of the telemetry subsystem that will be used for this mission.

9.2.1. Base Band and Frequency

The MRO has been considered as the relay satellite for this mission as it has been designed to be the main relay satellite for Mars orbiters and rovers. In addition, MRO has the best communication system that has been sent to deep space at this time. It includes one high gain antenna for communication with the ground station, two low gain antennas for the safe mode and one UHF antenna for its relay function. For a deeper explanation of the MRO communication system, please refer to Chapter 19.

For the proximity space links between the MRO and cubesat entities, a UHF band will be necessary for transmitting and receiving the data [FREQ-SS-TC10, Ch. 15], as advised by the proximity 1 standard and allowed by the MRO relay antenna. The UHF band represents, indeed, the lowest possible band frequency to use in deep space, which has a

¹Proximity-1 Space Link Protocol: <http://public.ccsds.org/publications/archive/211x0b1s.pdf> [cited 1 June 2016]

frequency range of 390- 405 MHz and 435- 450 MHz, for uplink and downlink communications respectively [FREQ-SS-TC11, Ch. 15]. The difference in frequency ranges lies in the range of data to be transferred. Indeed, the receiver system receives only command data, while the forward frequency sends the housekeeping, attitude and payload data.

Once the ranges of frequencies have been determined for the uplink and downlink. The next step is to define the exact frequencies that will be used for the sending and receiving data. Those are defined by the selected channel from the MRO. Selecting the channel is done in two main steps. First, the number of frequencies pairs has to be determined. For this mission, one pair has been selected as it has been decided to have one channel for the hailing and working modes. The ailing channel is used for establishing the initial physical link communication, it corresponds to the CW mode. While the working channel is used for transferring data; this corresponds to the AX.25 mode [FREQ-SS-TC9, Ch. 15]. The second step is to determine the exact channel from the ones available. If one pair of frequencies is used for the UHF band, four possible channels could be used, i.e. channels 0, 1, 2 and 3. The chosen channel, namely the channel 1, is characterised by a frequency of 435.6 MHz for the forward link and 404.4 MHz for the return link. This channel has been selected in order to minimise the use of the UHF bandwidth.

9.2.2. Modulation and Coding

The modulation associated to a specific type of coding are key drivers for the selection of the bandwidth, the consumption and how the system will be implemented inside the cubesat, in other words, it will drive the design complexity². As for the selected band, a modulation is advised by the proximity 1 standard, namely phase shift keying (PSK). More specifically, the pulse code modulation, PCM, biphase level [LWH09].

The PCM modulation allows the conversion of an analogue signal to a digital one through two main phases. The sine wave signal is first sampled using the Nyquist-Shannon sampling theorem in order to avoid aliasing artifacts. The signal is then transformed to a digital one with a certain quantisation; this is done by comparing the sampled signal with a quantising scale. After the quantisation, the data are in the form of a serial stream of data. Therefore, a frame synchroniser will be required for frame alignment, i.e. the data can be organised and labelled with information regarding the time, source, type and other parameters.

Furthermore, a specific coding format is associated to the pulse code modulation format. In this case the biphase level has been selected, as recommended by the Proximity 1 standard. Indeed, for satellite telemetry links, a phase encoded signal is used². The biphase level code also called the Manchester code is composed of the combination of a clock signal and the data bit value. It produces a level change in the half of each bit interval, therefore no DC component will be required². Now that the modulation and coding are defined, the bandwidth required for the reception and transmission can be calculated. Using the appendix J, from the National Telecommunication and Information administrations, the necessary bandwidth, B_n , can be calculated using the bit rate R , shown Equation (9.1) for the PCM.

$$B_n = 1.16R \quad (9.1)$$

For determining the require bit rate, first the total amount of data which can be sent back to Earth per orbit, D_{orbit} , has to be calculated. The amount of data, summarised in Table 9.1, depends on the housekeeping data, the science data and the received commands from Earth. The science data considered for the downlink is the highest that would be needed for this mission. As explained in Section 4.2, the amount of data collected from the Mawrth Vallis per measurements series taken in one orbit will be used.

Table 9.1: Amount of data for uplink and downlink

	Housekeeping [kbit]	Science [kbit]	Received command [kbit]	Total amount [kbit]
Downlink- data processed	5,656	4,612	–	10,268
Downlink- data not processed	5,656	100,663	–	106,319
Uplink	–	–	1000	1000

Then, the communication time available between the cubesat and the MRO has to be determined. From Subsection 5.3.3, the minimum communication time during the mission has been determined as $T_{comm} = 4390$ s, (Chapter 5), from which 80 % will be allocated for the transmission and 20 % for the reception.

²Line Code: <https://upload.wikimedia.org/wikiversity/en/2/2a/DComm.2.C.LineCode.20130920.pdf> [cited 1 June 2016]

$$R = \frac{D_{orbit}}{T_{comm}} \quad (9.2)$$

Table 9.2 gives an overview of the bit rate, found by using Equation (9.2) and of the required bandwidth for the transmission and reception [FREQ-SS-TC13-14, Ch. 15].

Table 9.2: Total bit rate and necessary bandwidth: uplink and downlink communications

Communication	Bit Rate [kbits ⁻¹]	Bandwidth [kHz]
Downlink- data processed	2.924	3.391
Downlink- data not processed	30.273	35.117
Uplink	2.277	2.635

9.3. Transceiver Mechanism

The choice of selecting a transceiver, instead of having the transmitter and receiver systems independent, was for maximising the bandwidth while minimising the size and power of the entire telemetry subsystem. In this section, first a trade-off of the transceivers available will be carried out. Then, the specifications of the selected transceiver will be detailed, followed by its architecture. Furthermore, the architectures of the transmitter and receiver will be detailed and explained. Finally, the integration mechanism of the transceiver will be explained.

9.3.1. Trade-off

If the COTS achieves the required performances, defined in Section 9.2, it would be preferable to select one than designing a new component. It will, indeed, allow to save time and money, e.g. the levels of testing will differ. Therefore, through an analysis of the available transceivers in the market, three have been selected. In order to choose one for the mission, a trade-off was realised, based on four main criteria; the power supply, the mass, the volume and the transceiver antecedents. Each criterion has its own weight, which is described by the width of the corresponding column.

Table 9.3: Trade-off transceivers

Transceiver Type	Power Supply [V]	Mass [g]	Flight Proven [–]	Volume [mm ³]
Si4463	3.6 [G]	[N]	[G]	[N]
NanoCom AX100	3.3-3.4 [E]	24.5 [E]	[G]	65x40x6.5 [G]
ISIS TRXUV	6.5-12.5 [U]	85 [B]	[G]	96x90x15 [B]

Legend [E] Excellent [G] Good [B] Barely acceptable [U] Unacceptable [N] Non available

As can be seen in Table 9.3, the NanoCom AX100 scores the best in overall. Therefore, this transceiver has been selected for the telemetry subsystem of the MICRO mission³.

9.3.2. Selected Transceiver: Specifications

For the mission the NanoCom AX100, which is a configurable radio transceiver, will be used⁴. The mechanism includes a microcontroller, a transmitter and a receiver. The NanoCom AX100 has been selected as it allows a reconfiguration of the bit rate, frequency and modulation type, which will be convenient for the MICRO mission as those parameters have been already defined in Section 9.2. Furthermore, it is an advanced high performance narrow-band transceiver for UHF. The specifications of the NanoCom AX100 are presented in Table 9.4⁵ [FREQ-SS-TC2-3-4, Ch. 15].

³High Performance, Low Current Transceiver: <https://www.silabs.com/Support%20Documents/TechnicalDocs/Si4464-63-61-60.pdf> [cited 5 June 2016]

⁴TRXUV VHF/UHF Transceiver: http://www.isispace.nl/brochures/ISIS_TRXUV_Transceiver_Brochure_v.12.5.pdf [cited 15 June 2016]

⁵High Data Rate Radio Transmitter for Cube Satellites: <http://goo.gl/X9Q23H> [cited 12 June 2016]

Table 9.4: Transceiver specifications

Parameter	Value	Unit
Operational Temperature	-30 to +85	[°C]
Dimensions	65x40x6.5	[mm ³]
Mass	24.5	[g]
Data Rate	0.1 to 115.2	[kbits ⁻¹]
Supply Voltage	3.3 to 3.4	[V]
Maximum Supply Current	1.2	[A]
TCXO stability frequency	2.5	[ppm]
Characteristics		
Glass/Polyimide material		
MCX Antenna Connector		
Multiple data interfaces: I ² C, USART, CAN-Bus		
Configurable bandwidth		
Configurable carrier frequency		
Configurable modulation type		
Automatic frequency control		
Same stability frequency of TCXO over entire range of temperatures		
No need of frequency offset calibration for TCXO after satellite deployment		

9.3.3. Architecture

In order to have a general overview of the transceiver, the architecture of the transceiver has been realised, as can be seen in Figure 9.1.

The transceiver system is the intermediary system between the antenna subsystem and the on-board computer, connected by the use of the CAN bus. The transceiver system is composed of a transmitter and receiver, which will be explained in details later. These last components use the same temperature compensated crystal oscillator, TCXO [FREQ-SS-TC8, Ch. 15]. This instrument allows to regulate the frequency of the oscillator in order to compensate for temperatures variations. Furthermore, the TCXO is good balance between the space and the cost, for achieving a precised frequency source. For further explanations about the TCXO used, please refer to the Appendix C. Both, the receiver and transmitter systems, are linked to the microcontroller [FREQ-SS-TC7, Ch. 15]. This uses a CAN bus connection with the On-Board-Computer [FREQ-SS-TC1, Ch. 15]. The choice of using a CAN bus instead of a USART or a I²C connection has been detailed in Chapter 8. The transmitter and the receiver are connected to the antenna subsystem, that will be detailed in Section 9.4, using a RX/TX switch. This switch has been made robust to handle a severe discrepancy from the antenna and to handle maximum 5 W⁶.

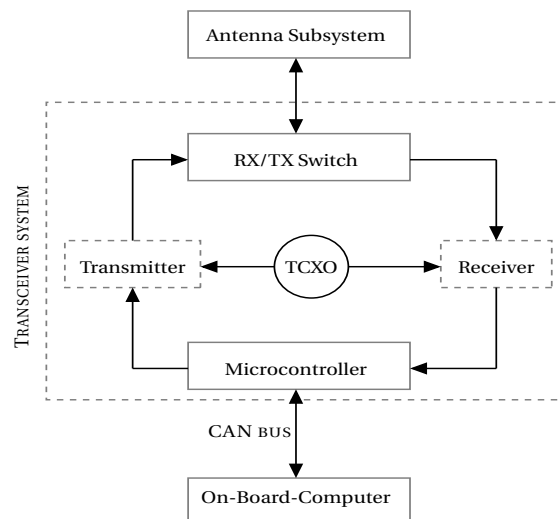


Figure 9.1: Transceiver architecture for the cubesat

⁶Temperature Compensated Crystal Oscillator: <http://goo.gl/uF4d6d> [cited 1 June 2016]

9.3.4. Transmitter

In this subsection, a detailed description of the transmitter used in the transceiver will be realised. The main parameters of the transmitter are listed in Table 9.5.

Table 9.5: Transmitter specifications

Parameter	Value	Unit
Supply Current	0.7-0.85	[A]
Signal bit rate capable	500-115,200	[bits ⁻¹]
Output Power at RF connector	29-31	[dB mW]
Possible Bandwidth	50-500	[kHz]
Synthesizer start up time	5-25	[ms]

Now that the main characteristics are known, the specific architecture of the transmitter can be investigated, this is shown in Figure 9.2. The transmitter architecture can be described by three main parts: the baseband subsystem, the low power radio frequency subsystem and the power amplifiers. Once the data have been collected and stored on the On-Board Computer, as will explained in Chapter 8, these are sent to the micro-controller by the use of a CAN bus. This controller sent the received data to the transmitter. Once in the transmitter, two modes are considered, i.e. the CW for the identification of the satellite by the MRO and the AX.25 mode for the nominal communication such as sending the science data, etc. In the AX.25 mode, the pulse code modulation with a biphas-level is performed; it consists of sampling, quantising, frame synchronising and finally coding the data. The signal leaving the encoder is then amplified by the use of an operational power amplifier before being transferred to the modulator. After the modulator, a thermopad has been installed in order to control the temperature inside the transmitter; indeed, it is a temperature variable attenuator. Before being sent to the antenna subsystem, the signal has to be amplified in order to reach the required output power. The power amplifiers are connected to a power controller providing a specific voltage. In the CW mode, the data follows the same steps as for the AX.25, except in the baseband subsystem; indeed, the data are sent directly to the encoder from the micro-controller.

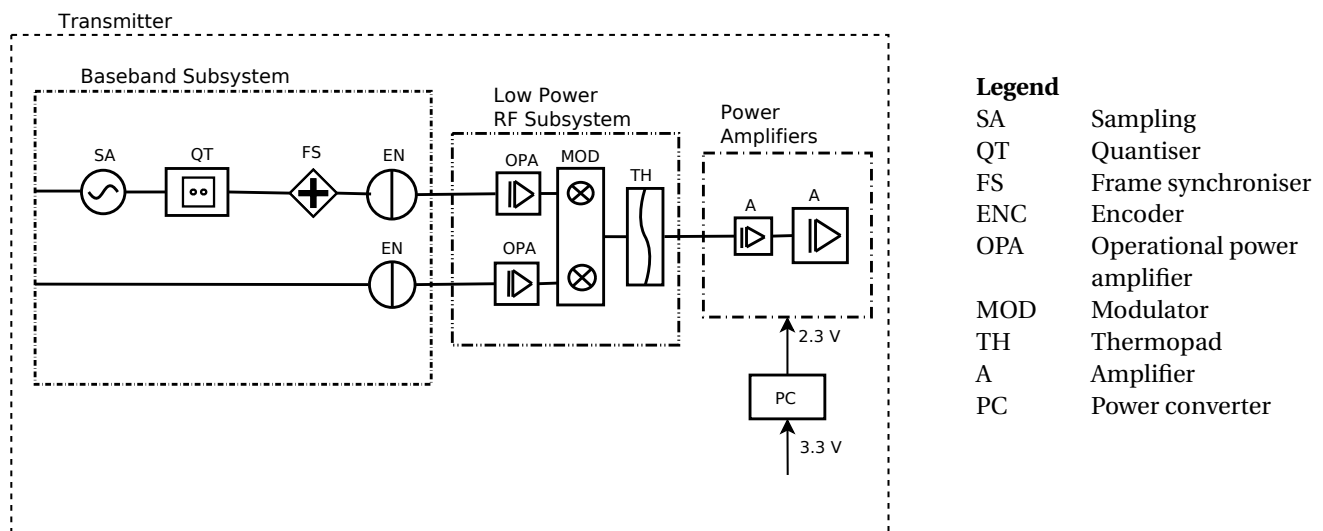


Figure 9.2: Transmitter architecture

For the transmission, the exact link budget has been calculated, using the equations from Appendix D. The values for determining the link budget are listed in Tables 9.6 and 9.7. As can be seen in Table 9.7, the in space transmission is characterised by the thermal noise and the free space loss [FREQ-SS-TC12, Ch. 15]. Therefore, other losses contribution as the radiation and fading have not been included in the link margin calculations for the transmitter and receiver.

Table 9.6: Values used for the link budget: transmitter

Parameter	Value	Unit
Effective area relay antenna	0.068	[m ²]
Effective area cubesat	0.053	[m ²]
Noise temperature	288.15	[K]
Carrier wavelength	0.7418	[m]
Max distance MRO-MICRO	24400	[km]
Bandwidth required	35.117	[kHz]

Table 9.7: The link budget for the transmission part

Parameter	Value	Unit
Transmitter power	3.2	[dB]
Free space loss	172.97	[dB]
Gain transmitter	1.48	[dB]
Gain receiver	2.56	[dB]
Noise	169.36	[dB]
Transmitter loss	0.79	[dB]
Receiver loss	1.14	[dB]
Link margin	1.702	[dB]

9.3.5. Receiver

As in Subsection 9.3.4, the receiver subsection will be analysed in three main parts. First, the specifications of the receiver will be listed. Then, the detailed architecture of the receiver will be discussed. Finally, the link budget for the data reception will be calculated. In Table 9.8, the receiver main features are listed.

Table 9.8: Receiver specifications

Parameter	Value	Unit
Supply Current	0.045-0.12	[A]
Signal bit rate capable	100-115,200	[bits ⁻¹]
Possible Bandwidth	50-500	[kHz]
Synthesizer start up time	5-25	[ms]

As explained earlier, the UHF range of frequencies will be used for receiving the data; however at a frequency of 404.4 MHz. Therefore, the signal received by the antenna subsystem will first pass through a bandpass filter adjusted at $404.4 \text{ MHz} \pm 3\%$ margins, in order to select a specific range of frequencies. Then if the signal is weak or unreliable, it will be amplified by the low noise amplifier which generally consumes between 10 to 100 mA, before being sent to the first mixer. This will create new carrier frequencies from the input signal and the oscillator frequency. The mixer is based on the principle of multiplying two sine waves resulting in two different waves being the sum and the differences of them. For this design, a dual conversion receiver has been selected over the single one, therefore the frequency will be converted twice by the mixers before being demodulated by the pulse code demodulator. For the T&C of the cubesat only two modulating signals are present on the carrier. Therefore, only two filters will be required. The signals resulting from the filters will, then, be sent to the sub-carrier demodulator. In this design, the modulating signal also acts as a carrier. Indeed, extra information can be modulated on the subcarrier, instead of using another modulating signal. The later bit synchroniser ensures that the various signals, after filtering, are still in synchronisation before sending them to the decoder and the frame synchroniser. The entire architecture of the receiver can be seen in Figure 9.3.

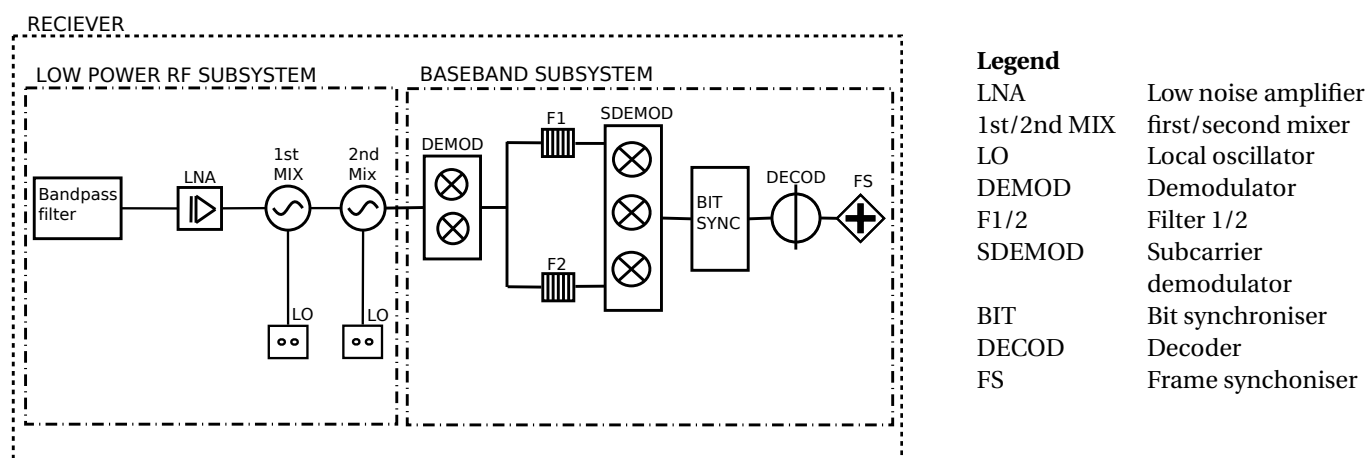


Figure 9.3: Receiver architecture

Tables 9.9 and 9.10 describe the link budget for the reception. As explained for the link budget of the transmitter, the equations from Appendix D have been used.

Table 9.9: Values used for the link budget: Receiver

Parameter	Value	Unit
Effective area relay antenna	0.068	[m ²]
Effective area cubesat	0.053	[m ²]
Noise temperature	288.15	[K]
Carrier wavelength	0.6887	[m]
Max distance MICRO-MRO	24400	[km]
Bandwidth required	2.635	[kHz]

Table 9.10: The link budget for the reception part

Parameter	Value	Unit
Transmitter power	1.46	[dB]
Free space loss	172.32	[dB]
Gain transmitter	1.91	[dB]
Gain receiver	0.84	[dB]
Noise	179.92	[dB]
Transmitter loss	0.79	[dB]
Receiver loss	1.14	[dB]
Link margin	9.87	[dB]

9.3.6. Integration Mechanism

As specified in Subsection 9.3.3, the transceiver is connected to the On-Board-Computer and to the Antenna subsystem. This subsection will deal with the connection mechanisms that will be used among the components of the telemetry subsystem. For the transceiver, in order to see all connectors, the top and bottom views have to be considered.

As shown in Figure 9.4, two connection points have been distinguished, namely H1 and H2, on the top of the AX100. The H1 connection is the one linking the transceiver to the antenna subsystem. This will be done by the use of a RF, radio-frequency, connector of 50 Ω MCX (micro coaxial), connected to cables. These cables shall not be covered by heat shrink tubing. Indeed, in vacuum conditions, the outgassing of the tubing might happen. The H2 allows picoblade connections, for configuring the transceiver. A JTAG, joint test action group, interface, which is a testing printed circuit board, is connected to the interface connector and is used for factory software upload. In Figure 9.5, H3 shows the main connector, which is a 20 positions printed circuit board hard-gold plated. The transceiver is mounted on a motherboard. For this mission, the NanoDock DMC-3, motherboard has been selected, board on which the On-Board-Computer and the transceiver are mounted and, therefore, connected. The transceiver is fastened to the motherboard using four connection screws⁷ [FREQ-SS-TC5, Ch. 15].

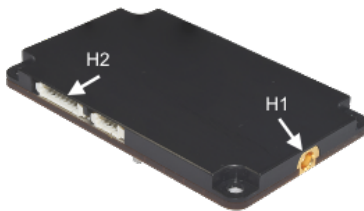


Figure 9.4: Top view of Nanocom AX100

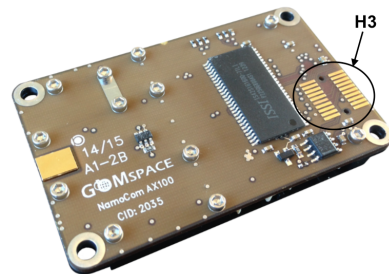


Figure 9.5: Bottom view of Nanocom AX100

9.4. Antenna

In order to select the antenna, first the use of commercial off the shelf antenna has been considered, as designing a new antenna design would require more time and expenditures for the later stages of the mission than taking COTS; e.g. a proper verification and validation tests required. The performances required by the antenna has been first explained and then compared to the COTS performances through a trade-off of the available antennas in the market. Later, the selected antenna will be described.

9.4.1. Characteristics

As explained in the earlier subsections, the defined Proximity-1 standard is used for communication between the relay satellite and the cubesat. Specific communication frequencies have been determined within the UHF band as follows: 1. The forward frequency 404.4 MHz 2. The return band frequency 435.6 MHz

⁷GOM Space: http://www.gomspace.com/raw/Products/AX100_shield_300.png [cited 12 June 2016]

The used frequencies and corresponding wavelength are the key factors for the antenna selection. Furthermore, the antenna has to be selected such as communication is possible in all directions independently of the cubesat orientation.

9.4.2. Trade-off

The available off the shelf antenna that comply with the frequency requirements are the ISIS UHF Turnstile antenna and the GomSpace ANT400 Turnstile. Moreover, both of the above products are compatible with the GomSpace AX-100 transceiver, that will be used.

The turnstile antennae use four monopoles to form one circular polarised antenna. The monopole antenna is a resonant antenna for which the length is found by the quarter wavelength. The wavelength used for determining the standard antenna length should be the longest of the wavelengths used (downlink and uplink), hence the lowest frequency should be selected. Therefore, for the uplink frequency used in this mission, i.e. (404.4MHz), the required antenna length is 0.176m.

In order to determine which antenna to use, a trade off has been realised based on seven criteria, described below:

1. Nominal RF power consumption
2. Deployment power required
3. Maximum length of the monopole
4. Insertion Loss
5. Mass
6. Deployment Mechanism
7. Flight proven
8. Output connector

Each of the criterion has been given a specific weight, shown by the width of the corresponding column, and has been classified using one of the five categories described in the legend.

Table 9.11: Final trade-off for antenna selection

Antenna	Nominal Power [mW]	Mass [g]	Flight Proven [-]	Deployment Mechanism [-]	Deployment Power [W]	Insertion Loss [dB]	Monopole Length [m]	TM Connection [-]
Turnstile	[N]	[N]	[G]	[E]	[N]	[N]	0.55 m [G]	I ² C [G]
ANT400	[N]	30 +1.5/rod [E]	[G]	[U]	2 [G]	1.6 [G]	0.176 [E]	CAN Bus [E]

Legend [E] Excellent [G] Good [B] Barely acceptable [U] Unacceptable [N] n.a.

INTEGRATION MECHANISM/DESIGN

In order to classify the deployment mechanism of each antenna, the following analysis has been carried. The ISIS antenna consists of a deploying mechanism on board. The tape antennae is deployed by the use of thermal wire. the GomSpace requires a separate Mechanism to deploy the antenna. The proposed by GomSpace is the GOMX Interstage which consists of four panels. The panels consists of the antenna attachment and deployment mechanism along with a charging interface and RBF pins. The disadvantage of the GOMX Interstage is that it would have to be placed for panels with deploying mechanism around the cubesat axis, this mechanism stow the antenna which can be released upon a receiving a signal. The GomSpace deployment mechanism would add more weight due to the interstages and will interfere with solar panels during deployment, making this a bad choice of deployment mechanism. Most suited for would be the ISIS antenna.

From Table 9.11, it can be seen that the two COTS studied do not represent the standards expected for the mission. Indeed, having non available values and/or an unacceptable criterion do not allow to pursue the design. Therefore, it has been decided to design a suitable antenna for the MICRO mission.

9.4.3. Selected Antenna

As explained in the earlier subsection, taking a COTS would not achieve the expected performances for the cubesat. For this design, a planar structure has been selected, namely the patches. For the MICRO mission, it has been decided to design a specific configurations of antennae, in order to optimise the antennae performances.

In order to cover all link directions, i.e. having a coverage of 4π sr, six individual square patch antennae should be placed on every face of the cubesat, each of the antenna covering $\frac{2}{3}\pi$ sr, with a beamwidth of 90 deg. However, as explained in Section 18.1, one face of the cubesat dedicated to the propulsion system and the the SPEX instrument, will be always oriented to Mars. Furthermore, the only time when dumbling will occur is after the deployment from

the host mission. However, no communication with the ground station is expected during the stabilisation time. After the phase, the AODCS subsystem of the cubesat will be operational all the mission time, allowing to point the cubesat to Mars. Therefore, having an antenna on this face will not be necessary.



Figure 9.6: Cubesat view

The proposed configuration can be seen in Figure 9.6. This type of antennae is manufactured by PCB techniques with the use of space graded materials. Therefore, radiation will not represent a main issue for the design. However, for the design a half-power beamwidth of 90 deg has been considered as it provides the minimum useful solution.

The patch antenna consists of two main components, namely the patch and the dielectric substrate, this last being the layer between the patch and the cubesat.

The size of each patch should have at least the dimensions found by Equation (9.3)⁸.

$$0.49 \frac{\lambda}{\sqrt{\epsilon_r}} \times 0.49 \frac{\lambda}{\sqrt{\epsilon_r}} \quad (9.3)$$

The highest wavelength required has been selected. Indeed, for a frequency of 435.6 MHz, a free-space wavelength, λ , of 688.7 mm, leading to a patch size of 344.35 x 344.35 mm², using no dielectric strength, $\epsilon_r=1$. As these antenna dimensions exceed the available space on the cubesat faces, two options have been investigated.

First, the dielectric strength has been increased by selecting a specific material for the substrate. Rogers TMM10i, ceramic substrate, has been selected, as it has a ϵ_r of 9.8, with a height of 3.2 mm. However, in order to achieve a reliable performance, two substrates will be required leading to a height of 6.4 mm. On the top substrate, a hybrid coupler will be printed. The hybrid coupler is a printed circuit board, which allows to receive and send signal with the same antenna. The component has four ports: two receiving the signal from the MRO, one receiving the signal from the HPA for transmission. While, the last port transfers the output signal to the receiver inside the transceiver. Using the Equation (9.3), the new dimensions of the patch have been calculated as 107.8 x 107.8 mm². Even if the area has been reduced by $\pm 90\%$, the cubesat antenna will be designed by etching 10 slits, with the same width, on each side of the patch. This design allowed to decrease the area by $\pm 50\%$ leading to a patch dimensions of 76.21 x 76.21 mm², the new length has been calculated using Equation (9.4). The patch being made of the same material, Rogers TMM10i, a height of 3.2 mm has been considered.

$$L_{new} = L_{old} \sqrt{2} \quad (9.4)$$

In order to facilitate the integration of the feed connection, the substrate length has been increased by ± 7.8 mm, leading to the substrate dimensions of 84 x 84 mm². A initial design of the microstrip patch antenna can be seen in Figure 9.7.

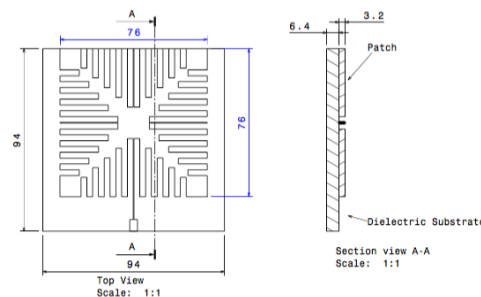


Figure 9.7: Microstrip patch antenna

⁸Patch Antennas and Microstrip Lines: <http://goo.gl/IG2Qxt> [cited 12 June 2016]

The patch antennae do not require any deployment mechanism and therefore, no specific deployment power, which is generally power consuming for the non planar antennae. In order to determine the return loss, RL, of the antenna, the Equations (9.5) and (9.6)⁹ can be used. As can be seen in Equation (9.6), the variable τ is dependent on the feeding source impedance, Z_S , and the input impedance, Z_{in} .

$$RL = -20 \log(\tau) \quad (9.5) \quad \tau = \frac{Z_{in} - Z_S}{Z_{in} + Z_S} \quad (9.6)$$

The input impedance can be calculating based on the material property used for the patch, i.e. ϵ_r . The calculation is shown in Equation (9.7)¹⁰.

$$Z_{in} = 90 \frac{\epsilon_r^2}{\epsilon_r - 1} \quad (9.7)$$

Filling the Equations (9.4) through (9.7) and using feeding source impedance, Z_S , of 50Ω ¹³, the return loss of 0.88 has been found. In Table 9.12, the characteristics of the microstrip patch antenna are listed.

Table 9.12: Microstrip patch antenna characteristics

Antenna	Nominal Power [W]	Mass [g]	Deployment Mechanism [-]	TM Connection [-]	Dimensions [mm]
Microstrip patch	1	20	not applicable	Can bus	84 x 84

9.5. Quality Approach

In this section, the quality approach that will be followed is described, by the application of the quality approach to the different cubesat components of the telemetry and communication, described in Sections 9.3 and 9.4, and will be analysed. No specific standards are available for the space quality of the cubesat. Therefore, the quality approach that will be followed for this design have been described through two main points.

1. Use of COTS circuit already used in previous similar cubesat missions or qualified for this mission.
2. Specific testing methods. These can be defined into three categories, namely the qualification, the acceptance and the pre-launch. A deeper explanation of the testing methods are explained in Chapter 18.

Table 9.13 lists all the components taken off-the-shelf, namely qualified components or used in previous similar missions. If the component is qualified for the mission or if it has been used in a previous mission, the symbol I will be indicated in the corresponding case; otherwise, the symbol O will be used to indicate the opposite.

Table 9.13: COTS components: overview

Component	Qualified	Used in previous mission
RX/TX switch	I	I
TCXO	I	I
Transmitter	I	O
Receiver	I	O
Microprocessor	I	I
CAN Bus	I	I
MotherBoard	I	I
MCX + cables	I	I
Antenna subsystem	I	O

While Table 9.14 gives a clear overview of the testing methods that will be applied to each components of the telemetry and communication subsystem [FREQ-SS-TC6, Ch. 15].

Table 9.14: Testing methods for components of telemetry and communication subsystem

Testing Category	Testing Method	Component
Qualification	Functional & Thermal Vacuum Vibrational & Mechanical Shocks	All components RX/TX switch, TCXO, Transmitter, Receiver Antenna subsystem
Acceptance	Functional	All components
Pre-launch	Functional & Interference	Antenna subsystem, MotherBoard

⁹Electrically Small Microstrip Antennas Targeting Miniaturized Satellites: the CubeSat Paradigm: <http://goo.gl/GPbHa0> [cited 12 June 2016]

¹⁰Antenna Development Corporation: <http://goo.gl/81kMHB> [cited 11 June 2016]

10

Electrical Power Subsystem

This chapter describes the design and trade off process for the power subsystem of MICRO. Section 10.1 summarises the preliminary design choices conducted for sizing the key elements of the power subsystem namely Solar Array, battery and PMDC unit. Section 10.2 defines the probable control operating modes and updates the power requirements for each of the subsystem. Once the power requirement is defined for each of the control operating modes, Solar arrays and batteries are designed in Sections 10.3 and 10.4. Finally a electronic block diagram along with general architecture and interfacing for PMDU is presented in Section 10.5.

10.1. Preliminary Trade-off Choices

To conduct the feasibility of integrating a power subsystem, capable of sustaining an interplanetary cubesat mission, preliminary estimations were conducted in earlier design phases [AFH⁺16]. Results of the preliminary calculations are presented in Table 10.1. Later sections of this chapter will iterate the initial estimates and cater for COTS components to design the power subsystem of MICRO.

Table 10.1: Preliminary electrical power subsystem design

Property	Value	Unit
<i>Astrodynamic characteristics</i>		
Solar radiation range	494.00 - 718.76	[W m ⁻²]
Orbital period	7070	[s]
Sunlit duration	5428	[s]
Eclipse duration	1642	[s]
<i>Subsystem power requirement</i>		
Sunlit phase	0.00	[W]
Eclipse phase	7.50	[W]
Contingency factor	30	[%]
<i>Solar array characteristic</i>		
Cell Type	Azure Space TJ GaInP/GaAs/Ge	[-]
Efficiency	30	[%]
Power generation	44.66	[W]
Panel Area	0.42 - 0.61	[m ²]
Panel Mass	0.20 - 0.41	[kg]
<i>Battery characteristic</i>		
Chemical type	Li-ion	[-]
DOD	65	[%]
Mass	0.10	[kg]
Volume	3.3010 ⁻⁵	[m ³]
Energy density	18.80	[Wh]
<i>Power Distribution Management and Control</i>		
Mass	0.15	[kg]

10.2. Control Operating Modes and Subsystem Power Requirements

To achieve a optimum power subsystem design different control operating modes must be defined. Furthermore, the power consumed by each of the subsystem for individual control operating modes must be quantified. Different control operating modes for a typical satellite mission is defined as follows [WL10, p.357]:

- **Separation:** Mission phase during which the cubesat is detached from the host mission.
- **Insertion:** Mission phase during which the cubesat is brought into its final orbit (Chapter 5).
- **Acquisition:** Initial stabilisation and attitude determination of the cubesat, followed by first contact with the relay satellite.
- **Nominal:** Mission phase during which the cubesat is in orbit and/or performing the scientific mission.
- **Slew:** Represents the trajectory correction manoeuvres for reorienting the spacecraft when necessary.
- **Search:** Mode in which the cubesat loses contact with the relay satellite.
- **Wait:** If the battery fails to distribute power, the cubesat will enter this mode. PMDC unit will limit the power consumption of each subsystem, and wait for sufficient charge/Solarlit orbital phase.
- **Safe:** Used in case of a mode failure or when the system is disabled.
- **Special:** Mode that might be needed due to an unusual upset event e.g. meteoroid impact, single event upset or Solar storms etc.
- **Communication:** Mission phase during which data is transmitted to the relay satellite.

Table 10.2 illustrates subsystem operational status for respective control operating modes, while Table 10.3 indicates the power consumed by separate subsystems during each mode. Since the subsystems consume a standby power they contribute to the power budget even if they are nonoperational. All the subsystems are not continuously active during the control operating modes. Table 10.4 lists down the energy consumed by each of the subsystem for different control operating modes and extrapolates respective power consumption. The average power arising out of the total energy consumption in Table 10.4 is much lower than that of Table 10.3. Since this is still the preliminary design phase, duty cycles of each of the operational modes is not known. Thus the power subsystem is designed for the instance of peak power consumption. Operational mode in Table 10.3 consuming the maximum power is taken as the ultimate scenario for power consumption during the Sunlit phase. The payload is nonoperational during the eclipse period. Thereby payload power consumption is deducted from this value and checked with other power modes with inoperative payload, maximum of the two is taken as ultimate power consumption for eclipse phase. As can be seen in Table 10.3, Slew phase clearly demands the highest power. The power subsystem will be designed for power requirement of 14.34 W during both sunlit and eclipse phase.

Table 10.2: Subsystem operational status for different control operating modes

Subsystem	Modes									
	Separation	Insertion	Acquisition	Nominal	Slew	Search	Wait	Safe	Special	Comm.
TCS							O			
EPS										
AODCS	O	O					O	O		
TT&C					O		O			
P&P	O		O	O		O	O	O	O	O
Payload	O	O	O		O	O	O	O		O
CDH										

Table 10.3: Subsystem power requirements for different control operating modes

Subsystem	Modular Power Budget									
	Separation	Insertion	Acquisition	Nominal	<i>Slew</i>	Search	Wait	Safe	Special	Comm.
TCS	0.00	0.00	0.00	0.00	0.00	0.00	0.00	0.00	0.00	0.00
EPS	1.00	1.00	1.00	1.00	1.00	1.00	1.00	1.00	1.00	1.00
AODCS	1.65	1.65	4.1	4.1	3.4	4.1	1.65	1.51	4.1	4.1
TT&C	1.00	0.01	1.00	1.00	0.01	1.00	0.01	0.01	1.00	1.00
P&P	2.00	8.00	2.00	2.00	8.00	2.00	2.00	2.00	2.00	2.00
Payload	0.00	0.00	0.00	1.50	0.00	0.00	0.00	0.00	1.50	0.00
CDH	0.50	0.50	0.50	0.50	0.50	0.50	0.50	0.50	0.50	0.50
Total Power	6.15	11.16	8.60	10.10	12.91	8.60	5.16	5.02	10.1	8.60
Contingency Power	6.83	12.40	9.56	11.22	14.34	9.56	5.73	5.58	11.22	9.56

Table 10.4: Power requirement arising from energy consumed for different control operating modes

Subsystem	Energy Budget [Ws]									
	Separation	Insertion	Acquisition	Nominal	Slew	Search	Wait	Safe	Special	Comm.
TCS	0.00	0.00	0.00	0.00	0.00	0.00	0.00	0.00	0.00	0.00
EPS	821-2714	821-2714	821-2714	821-2714	821-2714	821-2714	821-2714	821-2714	821-2714	821-2714
AODCS	2709-8956	2709-8956	6732-22255	6732-22255	5583-18455	6732-22255	2709-8956	2479-8196	6732-22255	6732-22255
TT&C	5960-15936	650-1738	5960-15936	5960-15936	650-1738	5960-15936	650-1738	650-1738	5960-15936	5960-15936
P&P	0.006	2368	0.006	0.006	0.024	0.006	0.006	0.006	0.006	0.006
Payload	0.00	0.00	0.00	0.00-570	0.00	0.00	0.00	0.00	0.00-570	0.00
CDH	821-2714	821-2714	821-2714	821-2714	821-2714	821-2714	821-2714	821-2714	821-2714	821-2714
Power [W]	7.0-6.2	5.0-3.8	9.7-8.9	9.7-9.0	5.3-5.2	9.7-8.9	3.4-3.3	3.2-3.1	9.7-9.0	9.7-8.9

10.3. Solar Array Design

Upon determining the power budget for MICRO as illustrated in Table 10.3, the next step involves re-evaluating the mission astrodynamical characteristics and sizing for the Solar arrays. Preliminary calculations are made to estimate the properties of Solar panels for MICRO mission. Later a Solar array drive actuator is chosen to optimise the Solar array size.

10.3.1. Solar Panel Design

Operational environment of the satellite determines the power generation capabilities of the Solar arrays. The mission environment characteristics as illustrated in Sections 5.1.3, 5.2 and 11.2.3 are summarised in Table 10.5. EOL power to be generated by the Solar cells depends on the power required during Solar incident and Solar absent phases of the orbit along with the corresponding durations of those phases. Equation (10.1a) [WL10] is used to determine the EOL power to be generated by the Solar cells. Daylight peak power transmission path efficiency, X_d can be assumed to be 0.8 while that of eclipse phase X_e can be assumed to be 0.6 [WL10].

Table 10.5: MICRO operational environment

Parameter	Value	Unit
Solar intensity range	498.41 – 558.23	[Wm ⁻²]
Orbital Period	7070	[s]
Sunlit duration	5428	[s]
Eclipse duration	1642	[s]
Primary mission orbits	1330	[–]
Primary mission duration	109	[day]
P_{SA}	24.41	[W]

As indicated in Table 10.1, during the initial phase TJ 3G30C¹ from Azure Space were selected. Due to high power consumption accompanied by low surface area of the cubesat, amount of required Solar cells cannot be body mounted to achieve a simultaneous Solar incidence to support the mission. Thereby, deployables will be designed along with Solar array drives to provide an optimum solution w.r.t. mass and volume. The Solar cells must be covered with coverglass to protect the cells against radiation and provided with interconnectors to connect with adjacent Solar cells. Integrating the separate components in house, requires additional qualification testing which adds to the production and development timeline. Therefore Solar cell companies sell CICs (Cells, Integrators and Coverglass) which are readily mountable on cubesats and arrays. During the selection of CICs from Azure Space^{2,3}, better performing CICs were found from Sol Aero Tech.⁴. Both of them will be analysed and a trade off is conducted at the end of this section. Companies like GOM Space⁵ and Clyde Space⁶ offer the flexibility of integrating and testing CICs if the array configuration is provided. First, CICs are designed for required mission power. Later, deployable panels are designed to carry the loads imposed by CICs.

CIC Selection

Table 10.6 lays out the performance features of the CICs. The performance parameters are used to generate the power extraction capabilities of CICs. Equation (10.1b) [WL10] is used to obtain the maximum power extraction

¹TJ 3G30C: <http://www.azurespace.com/index.php/en/products/products-space/space-solar-cells> [cited 14 June 2016]

²Azure Space CIC: http://www.azurespace.com/images/products/HNR_0003805-01-00.pdf [cited 14 June 2016]

³Azure Space CIC: http://www.azurespace.com/images/products/0003401-01-00_DB_3G30A.pdf [cited 14 June 2016]

⁴Sol Aero Tech: <http://solaerotech.com/wp-content/uploads/2015/04/IMM4J-CIC-Datasheet.pdf> [cited 14 June 2016]

⁵GOM Space: <http://gomspace.com/index.php?p=products-p110> [cited 14 Jul 2016]

⁶Clyde Space: <https://www.clyde.space/products> [cited 14 June 2016]

capabilities of CICs. J_M is the Solar intensity at the Beginning Of Life and EOL, while η_{SC} is the CIC efficiency as seen in Table 10.6.

$$P_{SA} = \frac{\frac{P_e T_e}{X_e} + \frac{P_d T_d}{X_d}}{T_d} \quad (10.1a)$$

$$P_O = J_M \eta_{sc} \quad (10.1b)$$

Table 10.6: Performance features of CICs

Solar Cell Type	Operational Temperature T_O [K]	Specific Mass $M_{\delta_{SA}}$ [kgm ⁻²]	Max. Power Min. Avg. Efficiency η_{SC} [-]	Surface Area per Cell [m ²]	Array Design Efficiency $\eta_{array\ design}$ [-]
<i>Azure Space</i>					
3G30A CIC	123.15-523.15 [E]	1.18 [G]	0.30 [G]	0.003018 [E]	0.87 [E]
<i>Emcore/Sol Aero Technologies</i>					
IMM4J CIC	98.15 - 393.15 [E]	0.81 [E]	0.33 [E]	0.003018 [E]	0.87 [E]

Legend [E] Excellent [G] Good [B] Barely acceptable [U] Unacceptable

Once the output power performance P_O is obtained, BOL power P_{BOL} is calculated using Equation (10.2a) [WL10]. Inherent degradation arises due to the CIC design inefficiencies and can be assumed to be 0.77 [WL10]. Solar radiance angle, $\theta \approx 0$ due to the active Solar tracking of Solar arrays. Finally the EOL power consumption, P_{EOL} is calculated using Equation (10.2b) [WL10]. For the selected Solar cells a life degradation factor, L_d of 0.9 is used [FJE⁺, BLK⁺, MSB, MSM08]. P_{EOL} determined is used to obtain the A_{SA} using Equation (10.3a). For the CICs selected in Table 10.6, cell packing efficiency $\eta_{cell\ packing}$ of 0.9 can be achieved [Rau80, BCP⁺, FLE, LES⁺]. Array design efficiency $\eta_{array\ design}$ is calculated using Equation (10.3b). An intercellular gap of 1 mm is used to account for wiring space and design flaws. Mass of the CIC panel, M_{CP} is calculated using Equation (10.2c). Table 10.7 summarises the CIC panel features. Comparing CIC parameters in Table 10.6 and Table 10.7, it can be seen that Advanced Quadruple Junction IMM4J CIC from Sol Aero Tech is the optimum performing option. The CIC was undergoing TRL 8 qualification test as of April 2015. Thus IMM4J from Sol Aero Tech is chosen for the Solar array design. It is important to use diodes in between CICs, to prevent reverse flow of currents and quarantine a cell in case of shadowing. 94 silicon by-pass diodes⁷ from Azure Space are used for 94 CICs with a cumulative mass of 2.82 g.

$$P_{BOL} = P_O I_d \cos(\theta) \quad (10.2a) \quad P_{EOL} = P_{BOL} L_d \quad (10.2b) \quad M_{CP} = A_{CP} M_{\delta_{SA}} \quad (10.2c)$$

$$A_{SA} = \frac{\frac{P_{SA}}{P_{EOL}}}{\eta_{cell\ packing} \eta_{array\ design}} \quad (10.3a) \quad \eta_{array\ design} = \frac{A_{cell\ area}}{A_{area\ consumed} A_{intercellular\ gap}} \quad (10.3b)$$

Table 10.7: CIC panel performance and configuration parameters.

CIC Type	P_O Range [Wm ⁻²]	P_{BOL} Range [Wm ⁻²]	P_{EOL} Range [Wm ²]	CIC Panel Area [m ²]	CIC Panel Mass [kg]	No. of CICs [-]	TRL [-]
<i>Azure Space</i>							
3G30A CIC ⁸	149.5-167.5 [G]	115.1-128.95 [G]	103.6-116.06 [G]	0.28-0.31 [G]	0.25-0.28[G]	103 [G]	9 [E]
<i>Emcore/Sol Aero Technologies</i>							
IMM4J CIC ⁹	164.5-184.2 [E]	126.6-141.8 [E]	114.0-127.7 [E]	0.26-0.29 [E]	0.16-0.18 [E]	94 [E]	7 [G]

Legend [E] Excellent [G] Good [B] Barely acceptable [U] Unacceptable

Deployable Panel Design

Once the CICs are chosen they must be integrated with Solar panels. Panels must be designed to provide radiation, thermal and structural support to the CICs. As indicated in Subsection 11.2.3, due to the absence of magnetic field the Martian radiation is much lower than the radiation around Earth. CMX coverglass used in the CICs provide significant resistance against Solar radiation around Earth. It can be safely assumed that the CICs will show negligible impact of Martian radiation over the short mission period of 109 days.

⁷ Diodes: http://www.azure.space.com/images/pdfs/0002576-00-01_DB.pdf [cited 15 June 2016]

⁸ Azure Space 3G30A: <http://goo.gl/Zdpct7> [cited 15 June 2016]

⁹ Sol Aero Tech IMM4J: <http://goo.gl/Zf1NGW> [cited 15 June 2016]

Since the CICs are sensitive against vibration, an adhesive layer of Kapton tape [Rau80] is used to prevent abrasion of Solar cells against the panel. To save unnecessary mass of shock resisting adhesive layer, an eclipse shaped cutting is made in the Kapton layer under the cells as shown in Figure 10.1.

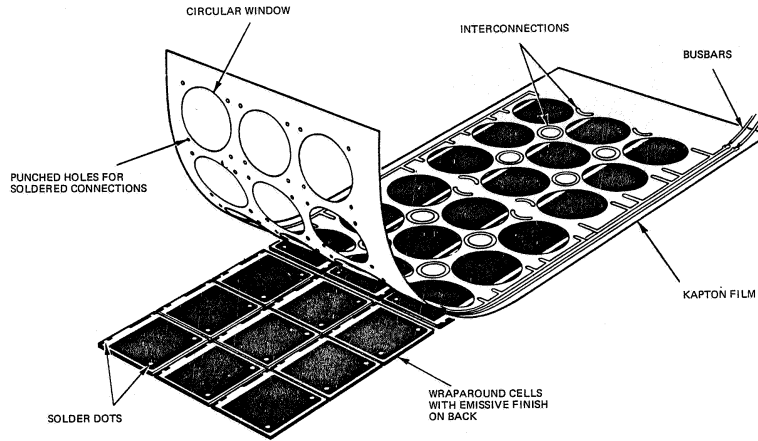


Figure 10.1: Solar panel integration configuration [Rau80]

The ellipses were cut 10 mm away from the CIC edges to provide sufficient padding and attachment area. Thickness of the adhesive layer is determined using Equation (10.4) [Sin]. $\sigma_{\text{allowable}}$ represents the allowable stress of the adhesive. For Kapton tape $\sigma_{\text{allowable}} \approx 62 \text{ MPa}$ ¹⁰, which is the strength at which the adhesive yields. While shear stress τ_{average} arises from the mass of the CIC panel, launch load and the area of adherent in contact with the CIC panel. To ensure the adherent is well below its yield strength during the launch phase, a thickness of 0.1 mm is required. As shown in Figure 10.1, wirings are embedded underneath the Kapton layer and the entire sandwich is consolidated with the supportive panel.

$$\tau_{\text{avg}} = \frac{\sigma_{\text{allowable}} t}{L} \quad (10.4)$$

Since the Solar panels will constantly face the Sun during the Sunlit phase of the orbit, this might result in high temperature swings. The temperature swings will expose different layers of the Solar panel sandwich to variable thermal expansions corresponding to diverse layer properties. Industrial CICs are expected to sustain contact pull strength >300 g; CICs chosen for MICRO can withstand contact pull strength >600 g¹¹. The use of metal panels without special adjustable silicon glues have jeopardized several missions where the cells failed by cracking due to excessive expansion of metal panels. To avoid risk the panels can be constructed with polyimide glass fiber (50% glass fiber). Polyimide glass fiber is high temperature resistant and approximately mimics the thermal expansion coefficient of CICs. Furthermore both GOM Space and Clyde Space can custom design Solar panels with polyimide glass fiber support. Thickness of the panels depends on the fundamental launch frequency of the launcher and the mass it has to support. Based on the orientation of the spacecraft described in Chapter 11.1, the Solar arrays can be assumed to be clamped on one side. Using Equations (10.5a) and (10.5b) thickness of the supportive panels are determined to sustain the fundamental axial and lateral frequency imposed by the launcher. A panel thickness of 1.2 mm can sustain lateral launch frequency of 11.8 Hz, while 0.03 μm can sustain launch frequency of 25 Hz. Thereby, the panel must be designed for thickness >1.2 mm. To conclude a quick overview of the properties of different layers of the Solar panel is presented in Table 10.8.

$$f_{\text{axial}} = \frac{1}{4} \sqrt{\frac{EA}{mL}} \quad (10.5a)$$

$$f_{\text{lat}} = \frac{1.875^2}{2\pi} \sqrt{\frac{EI_{zz}}{mL^3}} \quad (10.5b)$$

¹⁰Kapton Properties: <http://goo.gl/TNPjhV> [cited 25 June 2016]

¹¹IMM4J CIC: <http://solaerotech.com/wp-content/uploads/2015/04/IMM4J-CIC-Datasheet.pdf> [cited 15 June 2016]

Table 10.8: Mechanical and thermal properties of Solar panel

Parameter	Layer Thickness [mm]	Thermal specific heat capacity [J kg ⁻¹ K ⁻¹]
CMX coverglass	0.1	500
Solar cell	0.15	677
Rear contact	0.16	900
Interconnector	0.03	900
Kapton layer	0.11	1250
Polyimide PCB	1.2	1280
Diode	0.16	–
Result	1.74	1061

Thermal specifications of different layers of the panel are presented in Table 10.8. Based on the thickness of each layer, a weighted average of 1061 J kg⁻¹ K for Solar panel's specific heat capacity is obtained. This is used to carry out a thermal analysis on the Solar panel in Subsection 11.2.5.

10.3.2. Solar Array Drive Actuator

To ensure that maximum peak power is generated by the Solar arrays, the arrays must actively track the Sun. For cubesats several novel deployable techniques have been demonstrated, however active Solar tracking for cubesats is relatively new. First and only available active Solar array drive actuator for cubesats was developed by Honeybee Robotics¹² and MMA design¹³ which will fly on first interplanetary cubesat MARCO¹⁴. A schematic representation of the drive actuator is represented by Figure 10.2. Relevant specification parameters of the Solar Array Drive Actuator is summarised in Table 10.9¹⁵. Due to its low radiation tolerance, SADA must be fitted inside the radiation hardened cubesat bus.

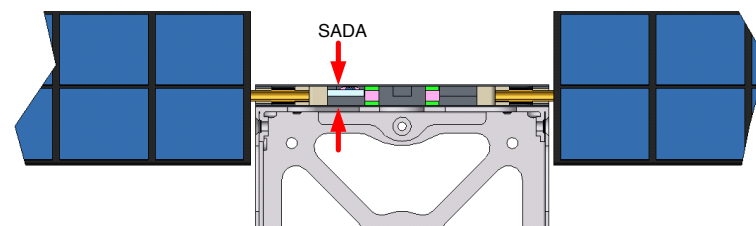


Figure 10.2: Schematic configuration of the Solar array drive actuator manufactured by Honeybee Robotics [PH10]

Table 10.9: Solar array drive actuator performance specifications

Specification	Value	Unit
Mass	180	[g]
Rotational margin	±180	[deg]
Output step angle	0.009	[deg]
Operational temperature	243.15 to 358.15	[K]
Operational power	0.5	[W]
Dimensions	100x100x6.5	[mm]
Radiation tolerance	10	[krad]

10.4. Power Storage

Once the CICs are selected, the next step involves designing a storage medium to store the excess power generated by the Solar cells for respective mission modes. Based on Cadex¹⁶ battery tests, Li-ion batteries provide the highest specific energy densities. Additional power generated during the sunlit phase must be stored in the batteries to sustain cubesat operations during eclipse phase of the mission. During orbit insertion the cubesat might encounter

¹²Honeybee Robotics: <http://goo.gl/MTP0hk> [cited 15 June 2016]

¹³MMA SADA: <https://www.google.ch/patents/US8757554> [cited 15 June 2016]

¹⁴SADA and MARCO: <http://goo.gl/ai8j5j> [cited 15 June 2016]

¹⁵SADA Specs <http://www.honeybeerobotics.com/wp-content/uploads/2013/12/Honeybee-Robotics-cubesat-SADA.pdf> cited 15 Jun 2016

¹⁶Cadex Electronics: <http://www.cadex.com/en> [cited 16 Jun 2016]

delays in orienting itself for the mission. The batteries must be designed to support the mission at least for the first two orbits. As indicated in Table 10.3 the power required during the eclipse phase is 12.91 W. Equation (10.6) is used to determine the energy storage capability of the battery, E_{bat} .

$$E_{bat} = \frac{P_e T_e}{\eta_{bat} DOD} \quad (10.6)$$

Apart from storing the energy, the batteries must deliver the required subsystem power along with the respective voltage and current levels. Depth of Discharge, DOD greatly relies on the life cycle of the battery. Since the cubesat undergoes 1330 orbits in 109 days, the batteries must be designed for 1330 charge-discharge cycles. Based on the DOD vs Life Cycle analysis carried out by Cadex¹⁷, for Li-ion batteries a DOD of 45.9 % is required for 1330 duty cycles. Batteries from Saft¹⁸, Clyde Space¹⁹ and GOM Space²⁰ were chosen and designed for MICRO's power requirements. Table 10.10 represents the performance parameters obtained for different batteries.

Table 10.10: Battery performance specifications

Model Name	DOD/100 [%]	E_{bat} [Wh]	$\eta_{bat}/100$ [%]	Nominal Voltage [V]	Nominal Capacity [Wh]	E_{δ_M} [Wh kg ⁻¹]	E_{δ_V} [Wh L ⁻¹]	Mass incl. circuitry[kg]	Volume incl. circuitry [cm ³]	Heater power Consumption [W]	Batteries required
<i>Saft Batteries</i>											
MP 174565	0.459 [E]	13.44 [E]	0.95[E]	3.75 [E]	18[E]	175 [E]	423[E]	0.103[E]	42.55[E]	–[E]	2 [E]
MP 174565 xtd	0.459 [E]	13.44 [E]	0.95 [E]	3.65 [E]	14.6 [G]	150 [G]	258 [G]	0.097 [G]	56.59 [G]	– [E]	2 [E]
MP 176065	0.459 [E]	13.44 [E]	0.95[E]	3.65 [E]	23.4[E]	174 [E]	303[G]	0.134[E]	77.23 [G]	–[E]	2 [E]
MP 176065 xc	0.459 [E]	13.44 [E]	0.95[E]	3.65 [E]	20.4[E]	150 [G]	264 [G]	0.136 [G]	77.27 [G]	–[E]	2 [E]
MP 176065 xtd	0.459[E]	13.44 [E]	0.95[E]	3.75 [E]	26[E]	178 [E]	375 [G]	0.146 [E]	69.33[G]	– [E]	2 [E]
MP 144350	0.459 [E]	13.44 [E]	0.95 [E]	3.75 [E]	9.75 [B]	143 [G]	344 [G]	0.068 [G]	28.34 [G]	–[E]	3 [E]
<i>GOM Space</i>											
BP4	0.25 [G]	36.19 [G]	0.95 [E]	6-8.4 [E]	38.48 [E]	142.52 [G]	205.84 [G]	0.270 [G]	186.94 [G]	7 [U]	1 [G]
BPX	0.25 [G]	38.11 [G]	0.95 [E]	6-33.6 [E]	77 [E]	154 [G]	241.18[G]	0.50 [G]	319.27 [B]	6[U]	1 [G]

Legend [E] Excellent [G] Good [B] Barely acceptable [U] Unacceptable

Along with the power delivering and energy storage capabilities, batteries must ensure that all subsystems acquire relevant voltage and current. Table 10.11 summarises the current and voltage characteristics of MICRO satellite. The highest voltage required is around 6 V to heat up the propulsion subsystem. The battery must be capable of providing the required amount of voltage to relative subsystem across all operating modes and mission phases.

Table 10.11: I-V characteristics of different subsystems

Device	Max. Voltage [V]	Max. Current [mA]
Sun Sensor	5	2
Star Tracker	5	20
Reaction Wheel	5.1	n.a.
SPEX	0	0
Detector	n.a.	n.a.
Propulsion	6	n.a.
T&C	n.a.	n.a.

The best choice is MP174565 from Saft as indicated in Table 10.10. Combining two batteries generate a total voltage 7.5 V. Both batteries combined can sustain the initial orbit insertion phase for ≈ 2.7 orbits, in case MICRO misses orbit insertion or fails to contact MRO within the primary contact window. Additional energy stored on board can also provide energy in times of Solar storms when the Solar panels are stowed away to protect the Solar cells against harmful radiation impacts.

10.5. Power Management, Distribution and Control Subsystems

Power Management, Distribution and Control (PMDC) Unit comprises of an Array Conditioning Unit (ACU) and a Power Distribution Unit (PDU). PMDC aids in proper management, distribution and control of power through all control operating modes and mission phases.

¹⁷DOD: <http://goo.gl/vcceaS> [cited 16 June 2016]

¹⁸Saft: <http://www.saftbatteries.com/battery-search/mp-small-v1> [cited 16 June 2016]

¹⁹Clyde Space: <https://www.clyde.space/products> [cited 16 June 2016]

²⁰GOM Space: <http://gomspace.com/index.php?p=products-bp4> [cited 16 Jun 2016]

10.5.1. Electronic Block Diagram

Figure 10.3 outlines the electronic block diagram of MICRO. The interface displays the flow and exchange of power in between the subsystems. Motherboard accommodates CDH, Transceiver, Array Conditioning Unit (ACU) and Power Distribution Unit (PDU). Power Management, Distribution and Control unit (PMDC) is composed of ACU and PDU. OBC processes the information from the subsystems and raises a unique flag for individual control operating mode. The flag is read by PMDC unit and EPS is set to perform under the respective control operating mode. In case of safe mode or other power critical modes where OBC fails to raise a flag, PDU possesses the privilege to act as a stand alone processor for the entire satellite. To save power Round Robin scheduling technique is used for T&C. Where each one of the five receivers (threads) is provided power and checked for over a small time interval (order of μ s). If a signal is received by one of the receivers PDU halts the switching of power supply at the receiver until the reception is complete. This reduces the power consumption of T&C by a factor of 5.

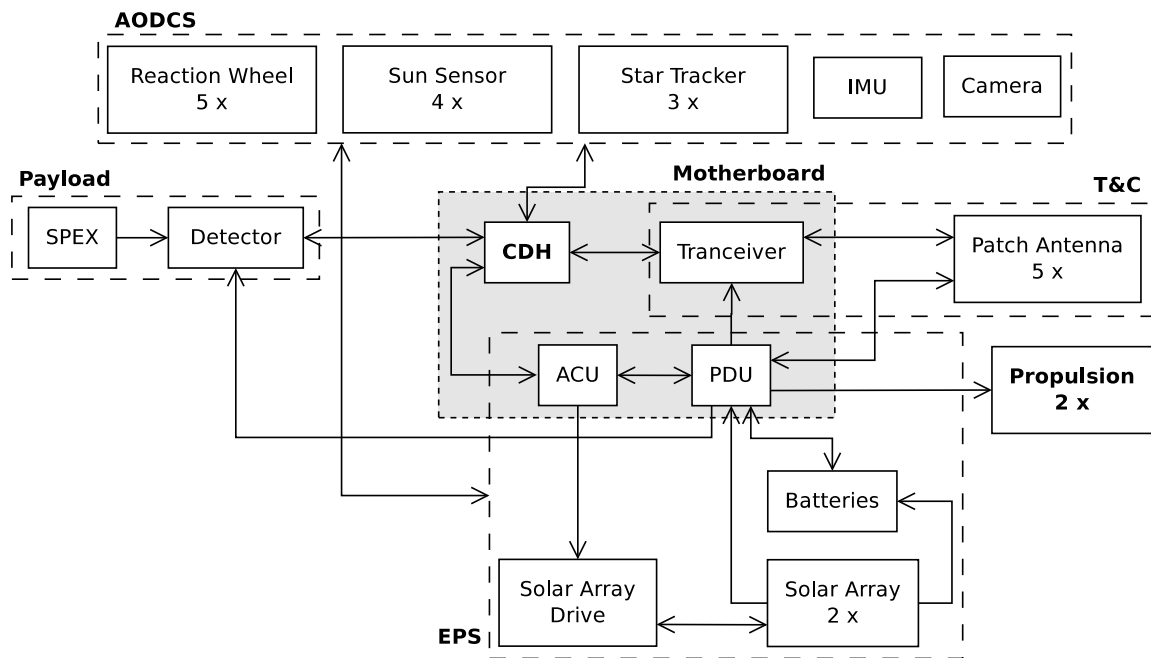


Figure 10.3: Electronic block diagram

10.5.2. PMDC Elements

To avoid the addition of a secondary docking unit/motherboard, components capable of docking with the current motherboard unit are selected. P60 ACU and PDU from GOM Space is selected²¹ to dock with the motherboard chosen in Chapter 8.2. Array Conditioning Unit, ACU works along with SADA. Its general purpose is to maximise the performance of EPS both in times of high and low energy availability. A simplified architecture overview of the ACU is shown in Figure 10.4. It makes use of a Measurement Control Unit, MCU to keep track of the operational status of the Solar cells. It further features 6 Maximum Peak Power Trackers (MPPT) to boost the power harnessing capabilities based on the operational status of the Solar cells and the on-board energy availability. To increase the life cycle of batteries it ensures that batteries are charged at optimum charging levels. In case of shadows casted on Solar cells, ACU ensures that the diodes are functional to prevent the entire series from acting as resistive loads. Furthermore, in an upset event it works along with PDU to combine power flow from batteries and Solar arrays to sustain the power required by the subsystems.

²¹ACU and PDU: <http://gomspace.com/index.php?p=products-p60> [cited 16 June 2016]

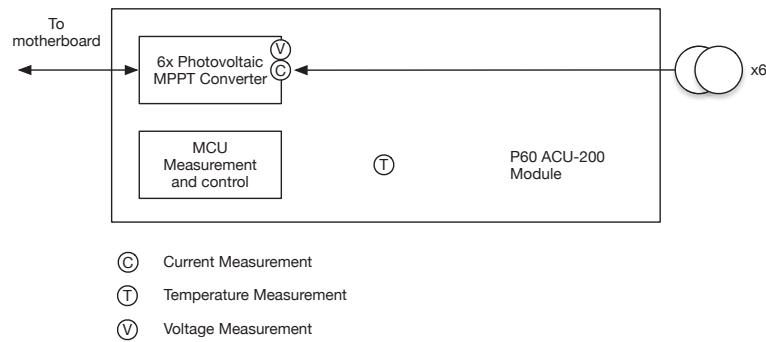


Figure 10.4: Hardware/electronic block diagram of array conditioning unit.

The Power Distribution Unit not only regulates the current and voltage but also ensures an efficient management and distribution of power through different control operating modes across all mission phases. Figure 10.5 demonstrates a simplified architectural overview of the PDU. CDH determines the control operating mode and raises a flag, the flag is read by the PDU to switch to a specific control operating mode. Buck converters play a major role in voltage regulation to meet the varying voltage demands imposed by different subsystems. The PDU architecture features 9 latch up switched over protected current output units. Overprotected current output units protect the on board circuitry against power surges and maintains a smooth power flow. Hardware configuration matrix modulates the subsystem voltage and current requirement based on the control operating mode indicated by motherboard. While the Measurement Control Unit (MCU) analyses the power data and provides the CDH with necessary power housekeeping data.

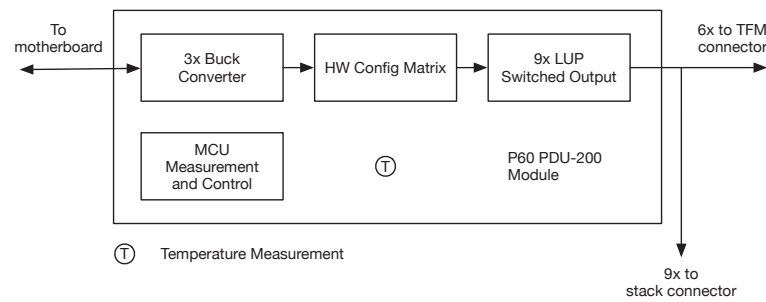


Figure 10.5: Hardware/electronic block diagram of power distribution unit.

Bus Design

In this chapter the cubesat bus will be discussed. The bus is the subsystem that integrates all the other subsystems, provides structural support, shielding for radiation and passively controls the inside temperature. This chapter contains the structural, thermal and radiation design of the spacecraft. First the analysis of the structure is presented in Section 11.1. In Section 11.2 a thermal analysis will be performed in order to make sure the spacecraft will remain within a proper temperature range during the mission. Furthermore in Section 11.3 the radiation environment and shielding is discussed. Finally, in Section 11.4 the verification and validation of the used numerical models is presented.

11.1. Structural Analysis

This section is concerned with the structural design of the spacecraft, which shall ensure that the right material and geometry are selected. The cubesat system will experience certain loads and vibrations, which have to be coped with in a predictable manner and without damage to the host mission or itself. Subsection 11.1.1 describes the environments in which the spacecraft will be operational, after which the structural design is performed in Subsection 11.1.2. This includes the analysis and design of the bus, as well as the configuration of the spacecraft. The frame of reference is defined in Figure 11.2, where the centre of mass coincides with the geometric centre. Note that this reference frame corresponds to the spacecraft frame (SF) described in Appendix A.

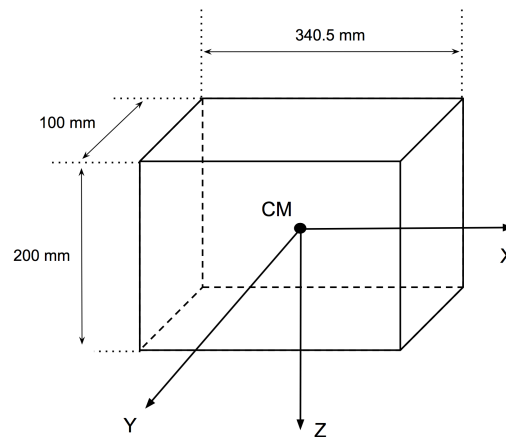


Figure 11.1: Frame of reference

11.1.1. Environments

Three environments will be taken into consideration: take-off, deployment and flight, of which the take-off environment will drive the bus structural design, as the highest loads and the most critical vibration modes are experienced in this phase. Special attention will be dedicated to the mechanical connection (hinge mechanism) between the solar arrays and the bus.

Take-off

The launch of the cubesat will be performed by a host mission as a piggyback option. It has been decided to choose the Mangalyaan 2 mission as the host, as described in Subsection 5.1.2. The proposed launch vehicle for Mangalyaan

2 is the GSLV Mk III, which has yet to be tested for orbital flight, planned early 2017¹. Therefore, for the purpose of performing the structural design and due to the unavailability data for the launcher, the performance parameters have been estimated using three other launchers, that could perform the mission in a similar manner: Atlas V from ULA, Falcon 9 from SpaceX and Proton from ILS.

Due to the loads and vibrations experienced at take-off, the bus should be designed for strength and stiffness such that it survives the stress levels without yielding and such that the fundamental frequency of the cubesat does not dynamically couple with the natural frequency of the launch vehicle [WL11]. During the launch phase, the cubesat will experience axial and lateral accelerations. Axial accelerations are driven by the thrust and drag profile, while the lateral accelerations are caused by wind gusts, thrust vectoring or stage separation events. Table 11.1 contains the performance parameters for the three launchers. The fundamental frequencies of the Atlas V and Proton launcher have been collected from [WL11], while the ones for Falcon 9 are obtained from [Spa15]. The load factors are taken from the launcher user guides, [GS10] for Atlas V, [ILS09] for Proton and [Spa15] for Falcon 9 respectively. The spacecraft structural design process will be dictated by the most critical launcher parameters.

Table 11.1: Launcher performance parameters

	Axial load factor [–]	Lateral load factor [–]	Fundamental axial frequency [Hz]	Fundamental lateral frequency [Hz]
Atlas V	6	2	15	8
Proton	5.1	1.7	25	8.5
Falcon 9	8.5	3	25	10

Deployment

The cubesat will be deployed once the host reaches its nominal mission orbit, after which manoeuvres by the cubesat are necessary in order to insert it into the desired orbit. The deployment mechanism is a system which ejects the cubesat from the payload fairing into a convenient point in space and time, after which the solar arrays will be unfolded and the orbital parameters and the attitude will be adjusted. Pyrotechnics will not be used for deployment because of the increased risk of damaging the host mission or harming the cubesat. The most critical structural aspect is the dynamic fluttering of solar panels upon deployment from the cubesat structure, which will be characterised and counteractive measures will be taken in Section 11.1.2.

Flight

The flight phase of the cubesat is the period of time in which the cubesat performs its scientific mission. No special attention is considered in terms of structural design in this phase as there are no critical aspects added to the cubesat.

11.1.2. Structural Design

Taking into consideration the limit loads experienced during launch, the equivalent axial loads can be computed. A safety factor ($F = 1.25$ [WL11]) is considered at this stage of the design, and the cubesat is modelled as a hollow cantilever beam, which shall take all structural loads. Having an outer shell rather than a truss system alone is also advantageous for radiation shielding, where the shielding layer has to be coated on a surface or a thin layer has to envelop the cubesat. The full spacecraft mass is assumed to be 10 kg, uniformly distributed on the beam. The cross sectional geometry of the load-carrying structure is assumed to be a rectangle with a constant thickness, as outlined in the standard cubesat design from ISIS². Other structural elements include spars for structural strength and the frame, which adds torsional rigidity and also serves for stacking the cubesat components.

Bus Structure

The custom designed bus structure is composed out of a truss system which takes all the bending loads and the normal stresses, and a shell (six aluminium panels) which takes the shear loads. The frame also serves for stacking components inside the cubesat, while the shell contributes to thermal control and radiation shielding, as outlined in Section 11.2 and Section 11.3. The final configuration of the bus is provided in Section 12. For the purpose of estimating the ideal positioning of the deployer in the host, the initial truss system consists of 12 spars (four of which can also serve as rails during deployment), one on each edge of the cubesat.

¹GSLV III: <http://goo.gl/TXUUqX> [cited 27 May 2016]

²6U Cubesat Dimensions: <http://goo.gl/5CMLcp> [cited 31 May 2016]

Material Selection

Table 11.2 outlines common materials used for cubesat manufacturing, alongside their properties, for aluminium alloys 7075-T6³, 6061-T6⁴, 5005⁵ and 5052⁶. The material selection will be performed for the 6 panels covering the bus and the frame (skeleton).

Table 11.2: Material properties

Aluminium	Young's Modulus ⁷ [GPa]	Density [kg m ⁻³]	Tensile Yield Strength [MPa]	Shear Strength [MPa]
7075-T6	71.7	2810	503	331
6061-T6	68.9	2700	276	207
5005	69.0	2700	42	76
5052-H32	70.3	2680	193	138

Compressive strength is directly related to the modulus of elasticity, with a higher value being preferred because the critical buckling load should be as high as possible. Shear loads shall be taken by the six panels covering the skeleton structure, therefore a higher shear strength is also preferred. Thermal expansion is considered identical for all the mentioned aluminium alloys (i.e. $23.6 \mu\text{m m}^{-1} \text{ } ^\circ\text{C}^{-1}$). This is compatible with the deployer material, which considers aluminium alloys for construction [Cor15a], therefore there will not be stress concentrations because of thermal expansion. For this reason, materials such as steel or composites might not be appropriate choices. Taking mass into consideration, the lowest density is ideal, although the difference in mass (w.r.t. the entire cubesat mass) is negligible (i.e. 0.2% for 400 g of material). The material selection criteria are: compressive strength, shear strength and manufacturing ability. The selected material is aluminium 7075-T6, as it offers superior structural properties and manufacturing advantages (i.e. manufacturable thickness is 0.5 mm⁸). This material is also considered common for cubesat manufacturing⁹.

Loads

The ultimate loads experienced by the spacecraft are given by its weight multiplied by the load factor and the safety factor F . Table 11.3 outlines the limit loads for axial, lateral and for a bending moment during take-off. The bending moment does not concern the cubesat, as it is assumed to be taken entirely by the deployer structure.

Table 11.3: Applied loads

Load Type	Weight [N]	Distance [m]	Load Factor [–]	Limit Load [–]
Axial	98.1	-	8.5	1042.4 N
Lateral	98.1	-	3	367.9 N
Bending Moment	98.1	0.17	3	62.5 N m

Stiffness

The fundamental (natural) frequencies are calculated with respect to the position of the cubesat during take-off, as the highest vibrations will be encountered in this environment. The axial natural frequency is calculated using Equation (11.1), as explained in [WL10].

$$f_{axial} = \frac{1}{4} \sqrt{\frac{EA}{mL}} \quad (11.1)$$

The natural axial frequency of the spacecraft shall be equal or higher than the launcher longitudinal fundamental frequency (25 Hz). For a minimum thickness of 0.5 mm, the natural axial frequency is 1928 Hz, much higher than required. The lateral vibration mode is estimated using Equation (11.2).

³Aluminium 7075-T6: <http://asm.matweb.com/search/SpecificMaterial.asp?bassnum=MA7075T6> [cited 31 May 2016]

⁴Aluminium 6061-T6: <http://goo.gl/1CDuc0> [cited 31 May 2016]

⁵Aluminium 5005: <http://goo.gl/6nKBj9> [cited 31 May 2016]

⁶Aluminium 5052-H32: <http://asm.matweb.com/search/SpecificMaterial.asp?bassnum=MA5052H32> [cited 31 May 2016]

⁷Compressive Modulus of Elasticity 2% higher than tensile: <http://goo.gl/OLy0eR> [cited 30 May 2016]

⁸Aluminium 7075: <http://goo.gl/Dvrhlj> [cited 31 May 2016]

⁹SwissCube Structures: <http://goo.gl/ur4Fmz> [cited 9 June 2016]

$$f_{lat} = \frac{1.875^2}{2\pi} \sqrt{\frac{EI_{zz}}{mL^3}} \quad (11.2)$$

Equation (11.2)¹⁰ yields a first lateral frequency of the spacecraft of 3023 Hz, which is far from the lateral fundamental launcher frequency of 10 Hz.

Deployer Positioning

In order to determine the ideal position of the cubesat in the host mission there are three scenarios considered, to be further explained in Table 11.4. For these three possibilities of attaching the deployer to the host, the normal axial stress has been calculated (induced by axial accelerations, Equation (11.3)) and the normal lateral stresses (induced by lateral accelerations, Equation (11.4)). It is assumed that the cubesat is constrained by the deployer on each side and all bending moments and shear stresses are taken by the deployer structure.

$$\sigma_a = \frac{8.5W}{A} \quad (11.3)$$

$$\sigma_l = \frac{3W}{A} \quad (11.4)$$

For the purpose of performing initial stress analysis, a preliminary custom design will be considered. The bus will be covered with the minimum manufacturable thickness aluminium sheet, with the skeleton being represented by 12 spars, each having an 8.5x8.5 mm² cross sectional area. In Equations (11.3) and (11.4), A represents the cross sectional area of the spars and panels, in normal direction. The final design will make use of CATIA to arrive to a more efficient structural design.

Table 11.4: Deployer positioning

Face [–]	Axial direction [–]	Normal axial stress [MPa]	Lateral direction [–]	Lateral normal stress [MPa]
ZX	Y	1	Z	0.4
			X	0.5
ZY	X	1.42	Z	0.4
			Y	0.35
XY	Z	1.15	X	0.5
			Y	0.35

Table 11.4 includes the face on which the deployer will be attached to the host, the axial direction (flight direction) and the normal stresses in axial and lateral directions. The lateral stresses are negligible, therefore the axial stress becomes the tradeoff criteria for the deployer positioning, although they are far from the yield stress of the materials. However, it is necessary to keep the cubesat in a favourable position such that the solar panels do not get damaged. As the panels will be placed on the XZ faces (both sides of the satellite), it is ideal to attach the deployer on the XY face. Although the axial stress is larger with such a configuration (i.e. 15% larger than the minimum), a compromise is advantageous in terms of local stress concentrations as it ensures a larger safety of margin for the cubesat integrity.

Frame Selection

The main selection criteria for the bus frame (structure) is the mass, as the loads and vibrations are far from critical (highlighted in Subsection 11.1.2). There are three main options to be considered: COTS, custom designed, and re-designed COTS frames.

Custom designed frames have the advantage that they can accommodate specific mission needs rather than having a broad, general design. However these frames have a low TRL and they are not space-qualified, making it necessary to perform iterative procedures to arrive to a reliable design. Furthermore, extensive testing and validation are necessary. COTS frames are 'ready-made', meaning that they are not improved in terms of specific parameters but instead are designed for a large range of missions, resulting in higher mass than custom designed frames but also higher TRL. Because of the time and resource limitations of the project, as well as the main selection criteria, it has been decided to redesign already available frames without influencing critical structural components. For this purpose, the ISIS frame¹¹ will be considered as a 'base design', with the redesigned frame being described in Subsection 11.1.2. Table

¹⁰Lateral Natural Frequency: <http://goo.gl/da5LYW> [cited 30 May]

¹¹6U Cubesat STEP File: <http://goo.gl/i8Rw4n> [cited 16 June 2016]

11.5 outlines the available off-the-shelf frames and their mass and the custom designed frame respectively. For the custom designed frame, the mass of the outer shell, consisting of six Aluminium 7075-T6 panels, is found to be 342 g for a 0.5 mm thickness. The 12 struts (rails) weigh 520 g, which does not include component stacking opportunities. An additional 50 g per unit is estimated for the frame, which brings the total mass of the structure to 1162 g.

Table 11.5: Frames

Frame	Custom designed	ISIS ¹²	GomSpace ¹³	ClydeSpace ¹⁴	CubesatKit ¹⁵
Mass [g]	1162	1100	1206 ¹⁶	1083	1231 ¹⁷

Due to the unavailability of 6U cubesat structures, some frames for 3U cubesats are considered. Their mass, translated to 6U, is estimated to increase by a factor of 1.9¹⁸, as empirically seen for ISIS designed structures. The mass values from Table 11.5 includes the skeleton and the shear panels, as well as the stacking elements.

Final Design

The ISIS frame has been redesigned by focusing on mass reduction, without compromising on structural integrity. Figure 11.2 shows a section of the XZ face, in order to illustrate the geometry of the frame. The dimensions account for the skeleton itself, with radiation shielding and thermal control being added on top of the frame. The redesigned frame will be covered with the same six aluminium panels as the custom designed frame, and the actual frame is a monocoque structure, with the skeleton roughly composed out of L-shaped spars. Each spar has a cross sectional area of 165.6 mm². There are six spars going in X direction, twelve in Y direction and eight in Z, with the highest stress experienced on the X face (ZY plane). A preliminary stress analysis for the new structure shows a 44% stress reduction on this face (compared to the 1.42 MPa), while the weight of the frame together with the panels has been reduced by 19%. This increase in efficiency, both in terms of mass and load carrying capabilities, is mainly accounted for the improved geometry of the spars (L-shaped instead of solid square spars) and the addition of extra spars outlining the six units of the cubesat. A CATIA model can be found in Section 12.2. The new frame has a mass of 300 g, bringing the total mass of the structure to 942 g.

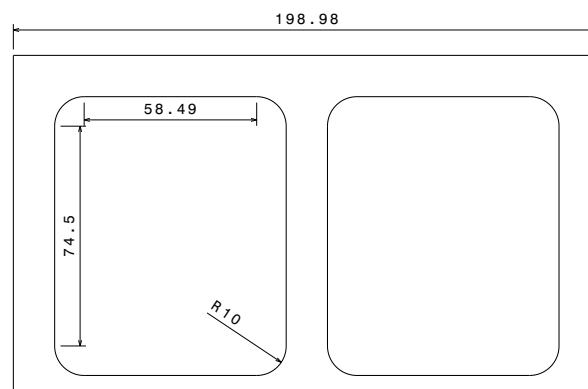


Figure 11.2: Section of the final frame design

11.2. Thermal Control

In this section the thermal control subsystem design is discussed. The thermal control subsystem regulates the internal temperature of all subsystems of the cubesat to stay within operational limits. Large temperature differences can cause distortions of measurements and misalignments of sensors or even cause component failures. Furthermore temperature changes may cause thermal stresses in the structure of the spacecraft. The thermal control subsystem should therefore keep temperatures of all components of the spacecraft within allowable ranges for optimal performance during the lifetime of the mission.

In Subsection 11.2.1 the operational ranges and the survival ranges of the subsystems and payloads are presented.

¹²ISIS 6U Cubesat Structure: <http://www.isispace.nl/product/6-unit-cubesat-structure/> [cited 8 June 2016]

¹³3U GOMX-Platform: <http://gomspace.com/index.php?p=products-platforms> [cited 8 June 2016]

¹⁴3U CS Structure: <https://www.clyde.space/products/1-cs-3u-cubesat-structure> [cited 8 June 2016]

¹⁵3U Solid-wall Structure: <http://www.cubesatkit.com/content/design.html> [cited 8 June 2016]

¹⁶Mass Estimated by Subtracting Already Existing Components (Power, Antenna, Communication, Solar Arrays, Computer)

¹⁷CubesatKit Mass Estimation Done by Importing the 3U CAD Model in CATIA, Multiplying by a Factor of 1.9 and Adding the Mass of the Six Panels

¹⁸Cubesat Shop Structures: <http://goo.gl/vwuP85> [cited 9 June 2016]

Then in Subsection 11.2.2 active thermal control solutions are discussed. In Subsection 11.2.3 the types of radiation and equations used for the simulation are presented. This is followed by the results of the thermal simulation of the bus and solar panels in Subsection 11.2.4 and 11.2.5 respectively. Finally in Subsection 11.2.6 the stresses induced by temperature differences are discussed and in Section 11.2.7 the contingency plan with respect to desired temperature is presented.

11.2.1. Mission Thermal Ranges

In Table 11.6 the operational and survival temperature ranges are documented. The operational range indicates the thermal range in which the subsystems and payloads can operate properly. The survival range is the ultimate temperature range in which the components do not get damaged. The spacecraft should stay within the operation temperature range during the operational phase of the mission. The temperature of the spacecraft has to stay within the survival range during all phases of the production, launch, transfer and the operational mission phase. The combined range is the range in which the component with the highest minimum and the component with the lowest maximum are still able to operate. This is the range in which each subsystem and payload overlaps in terms of thermal range, this range of -5 to +27 °C is therefore the design space for the thermal subsystem [FREQ-SS-TH1, Ch. 15]. The survival temperature range is assumed to be -10 to +30 °C [FREQ-SS-TH2, Ch. 15]. If the survival temperature is not specified for a certain component, the operational temperature is assumed to be critical. The minimum operational temperature of the propulsion system is set at -5 °C because the propellant will freeze at lower temperatures. This is not a critical survival temperature, since frozen propellant can be unfrozen. Therefore in order to be conservative, the operational temperature range of SPEX is the leading survival temperature range.

Table 11.6: Operational and survival temperature ranges for sub-systems and payload

Component	Operational Temperature [°C]	Survival Temperature [°C]
SPEX	-10 to +30	n.a.
Detector	-30 to +27	-30 to +60
Battery	-20 to +60	-50 to +60
Propulsion Subsystem	-5 to +50	n.a.
Solar Arrays	-175 to +120	-175 to +120
Cubesat Deployment Mechanism	-40 to +65	n.a.
Telemetry & Command	-30 to +85	n.a.
On-Board Computer	-25 to +60	-45 to +85
Star Sensors	-20 to +40	n.a.
Sun Sensors	-30 to +85	-40 to +90
Combined Range	-5 to +27	-10 to +30

11.2.2. Active Thermal Control

An dedicated active thermal control system severely increases the complexity of the cubesat, increases the power usage, reduces volume available for other subsystems and often requires telemetry resources. Furthermore, an active thermal control system increases the total spacecraft mass due to the need of more components. The preliminary temperature estimations performed during the Midterm Report [AFH⁺ 16] indicate that passive solutions are adequate options to regulate a viable temperature range in which all subsystems and payload can operate properly. Passive thermal control will therefore be the preferable solution. Consequently active thermal control will not be used in the cubesat design. Furthermore, the components that require to be cooled, such as the transceiver for the communication has an integrated internal thermal control system. Therefore an external active thermal control is not necessary for this cubesat.

11.2.3. Thermal Equilibrium

In this section a thermal equilibrium simulation procedure is described. In Table 11.7 constant Martian parameters are listed. These parameters are relevant to obtain a temperature equilibrium calculation. All the relevant planet parameters are obtained from NASA fact sheets^{19 20}. The cubesat in orbit will receive three significant types of radiant energy that will increase the temperature. These types of radiation are solar radiation received directly from the Sun, planetary albedo radiation and planetary infrared radiation received from Mars. Furthermore, the temperature is affected by internal energy dissipation, caused by heat generated by electrical equipment. The method and equations presented in this section can be found in [WL10].

¹⁹Mars Fact Sheet: <http://nssdc.gsfc.nasa.gov/planetary/factsheet/marsfact.html> [cited 4 May 2016]

²⁰Sun Fact Sheet: <http://nssdc.gsfc.nasa.gov/planetary/factsheet/sunfact.html> [cited 9 May 2016]

Table 11.7: Relevant thermal parameters

Parameter	Symbol	Value	Unit
Stephan Boltzmann Constant	σ_b	5.67×10^{-8}	$[\text{Wm}^{-2}\text{K}^{-4}]$
Black-body Temperature Mars	T_M	209	[K]
Average Radius Mars	r_M	3.39×10^6	[m]
Albedo Factor	b	0.17	[–]
Sun Power Output	P_{Sun}	3.828×10^{26}	[W]
Perihelion Mars	r_p	206.62×10^9	[m]
Aphelion Mars	r_a	249.23×10^9	[m]

Solar Radiation

The amount of solar radiation received at any distance from the Sun can be computed with Equation (11.5a). Due to the eccentricity of Mars' orbit, seasonal changes give rise to different values for the solar flux at Mars during its orbit around the Sun. In a Martian orbit the solar flux has a minimum and maximum value of 490 Wm^{-2} at the aphelion and 714 Wm^{-2} at the perihelion, respectively. The thermal subsystem has to be designed for a range of incoming solar flux. As described in Chapter 5 the cubesat will arrive at Mars on the 15th of February of 2021. At the time of arrival the distance between Mars and the Sun is 1.567 AU. This distance will then gradually increase until 1.659 AU when the end of the mission is expected. This results in a solar flux range of $554\text{--}495 \text{ Wm}^{-2}$ during the mission life time. The direct solar radiation is the largest contributor to the flux received by the spacecraft and has to be accounted for [FREQ-SS-TH6, Ch. 15]. The absorbed radiation due to solar flux can be computed with Equation (11.5b).

$$J_{Sun} = \frac{P_{Sun}}{4\pi d^2} \quad (11.5a)$$

$$\dot{Q}_{\text{absorbed}_{Sun}} = \alpha_s J_{Sun} A_{i,Sun} \quad (11.5b)$$

The radiation received from the sun is only absorbed by the sides of the cubesat directed towards the sun. Therefore, $A_{i,Sun}$ depends on the orientation of the cubesat. The effective area receiving solar radiation is not constant, it changes during the orbit. The minimum area that will receive solar radiation is 0.02 m^2 when the spacecraft is above one of the poles. The maximum effective area receiving solar radiation is 0.03405 m^2 when the spacecraft is above the equator.

Albedo Radiation

Albedo radiation is a fraction of the incident radiation from the Sun which is reflected by the planet on the cubesat, this contributes to the temperature and has to be designed for [FREQ-SS-TH4, Ch. 15]. The albedo flux reflected from the surface is given by Equation (11.6a). The average albedo factor for Mars is 0.17. The absorbed radiation by the spacecraft as a result of albedo radiation can be calculated with Equation (11.6b). This equation uses the albedo flux obtained with Equation (11.6a).

$$J_b = J_{Sun} b F \quad (11.6a)$$

$$\dot{Q}_{\text{absorbed}_b} = \alpha_s J_b A_{i,b} \quad (11.6b)$$

The visibility factor is dependent on the angle between the local vertical and the Sun's rays. Since the spacecraft is nadir pointing, the effective area receiving the albedo flux is the side that is facing Mars at all times. The area facing the surface of Mars is 0.03405 m^2 .

Infrared Radiation

Mars is a black-body radiator which emits infrared radiation, this is the final relevant external temperature source where the thermal solution needs to account for [FREQ-SS-TH5, Ch. 15]. The average black-body temperature of Mars is presented in Table 11.7. The infrared flux emitted by Mars can be determined with Equation (11.7a). Consequently, the absorbed radiation due to infrared planet radiation can be found using Equation (11.7b).

$$J_{ir} = \sigma_b T_M^4 \left(\frac{r_M}{r_O} \right)^2 \quad (11.7a)$$

$$\dot{Q}_{\text{absorbed}_{ir}} = \epsilon_{ir} J_{ir} A_{i,ir} \quad (11.7b)$$

The amount of infrared flux received from the planet depends on the orbit altitude of the cubesat due to the J2 effect. The altitude will vary between 336 km and 473 km during the mission. The absorption factor, ϵ_{ir} for infrared absorption is different than the absorption factor for the visible spectrum. It is however the same as the infrared emission factor ϵ , due to the Kirchhoff radiation law. The area receiving the infrared flux is similar to the area receiving albedo flux.

Emission

Heat can only be transferred into space by means of radiation. The spacecraft emits heat into space as a black-body. The amount of heat radiated by the spacecraft into space can be computed by Equation (11.8). The temperature in deep space is 2.7 K and this has to be subtracted from the spacecraft temperature. The entire surface area of the cubesat can be used for radiation of heat. The amount of radiation through each surface is dependent on the coating and insulation used at each side of the cubesat.

$$\dot{Q}_{\text{emitted}} = \epsilon_{\text{ir}} \sigma_b (T_c - T_0)^4 A_e \quad (11.8)$$

Equilibrium Temperature

Receiving and dissipating radiation will result in an equilibrium temperature, this equilibrium condition can be described by Equation (11.9). In this equation the heat radiated out of the spacecraft is in equilibrium with the heat absorbed from the Sun, albedo, Mars and the internally dissipated power.

$$\dot{Q}_{\text{emitted}} = \dot{Q}_{\text{absorbed}_{\text{sun}}} + \dot{Q}_{\text{absorbed}_b} + \dot{Q}_{\text{absorbed}_{\text{ir}}} + P_{\text{dissipated}} \quad (11.9)$$

The internal equilibrium temperature can be determined by Equation (11.10). The values for the absorbed heat due to the Sun, albedo and infrared radiation can be obtained by Equations (11.5b), (11.6b) and (11.7b) respectively. After substituting these values in Equation (11.9) the equation for the cubesat equilibrium temperature, Equation (11.10), can be extracted.

$$(T_c - T_0)^4 = \frac{\alpha_s J_{\text{Sun}} A_{i,\text{Sun}} + \alpha_s J_b A_{i,b} + \epsilon J_{\text{ir}} A_{i,\text{ir}} + P_{\text{dissipated}}}{\epsilon \sigma_b A_e} \quad (11.10)$$

Temperature Change

While the spacecraft is in the eclipse region it does not receive direct sunlight radiation nor does it receive albedo radiation. The only form of radiation the spacecraft receives is the black-body radiation emitted from Mars. Furthermore, the spacecraft shall not be fully operational during the eclipse and therefore less dissipating power will be present. This will cause the spacecraft to decrease in temperature during the eclipse period. During the period in which the spacecraft does receive Sunlight the amount of temperature radiated outwards is less than the received radiation, hence the temperature will increase again. This causes the spacecraft to fluctuate around a certain equilibrium temperature. The amount of temperature gain and loss the spacecraft will endure during a orbit can be computed with Equation (11.11).

$$\Delta T = \frac{\dot{Q} \Delta t}{MC} \quad (11.11)$$

11.2.4. Simulation Results

In Table 11.8 the relevant simulation input parameters are presented. The heat capacity of the cubesat is assumed to be similar to the heat capacity of the aluminium 7075-T6²¹ bus. The illuminated areas are based on the orientation of the spacecraft as indicated in Chapter 6, the spacecraft is nadir pointing and the $0.2 \text{ m}^2 \times 0.3 \text{ m}^2$ side is never facing the Sun. The amount of power dissipation is based on values obtained in Chapter 10. The visibility factor is set to 0.50 based on the inclination angle and altitude of 92.5 deg, obtained in Chapter 5.

Table 11.8: Bus simulation parameters

Parameter	Symbol	Value	Unit
Heat Capacity	C	960	$[\text{J kg}^{-1} \text{K}^{-1}]$
Dissipated Power Nominal	$P_{\text{dissipated}}$	10	[W]
Dissipated Power Eclipse	$P_{\text{dissipated}}$	8.5	[W]
Cubesat Mass	m	10	[kg]
Sunlight Absorption Area	$A_{i,\text{Sun}}$	0.03405-0.02	$[\text{m}^2]$
Albedo Absorption Area	$A_{i,b}$	0.03405	$[\text{m}^2]$
Infrared Absorption Area	$A_{i,\text{ir}}$	0.03405	$[\text{m}^2]$
Emission Area	A_e	0.2443	$[\text{m}^2]$
Separation Temperature	T	280	[K]
Visibility Factor	F	0.50	[-]

²¹Aluminium 7075: http://www.qfaluminum.com/products_detail/&productId=26.html [cited 31 May 2016]

Using the equations from Subsection 11.2.3 a simulation can be performed on what the spacecraft temperature will be during its mission life time. The performed simulation incorporates the fact that the amount of solar flux present at Mars changes during the mission due to the change in distance between the Sun and Mars. These changes are visualised in Figures 11.3 and 11.4. The gradual change in solar intensity can be observed in Figure 11.5 and 11.6, here the temperature gradually changes over the mission duration due to this effect. The simulations also accounts for the fact that the orbital height of the spacecraft changes throughout each orbit and throughout the mission. The change in orbit height is plotted in Figure 5.4. The change in orbit altitude has an effect on the amount of infrared radiation received. Furthermore, since the surface area facing the Sun changes throughout the orbit, the effective radiated area changes throughout each orbit of the simulation, the change in illuminated area is incorporated in the simulation, as well.

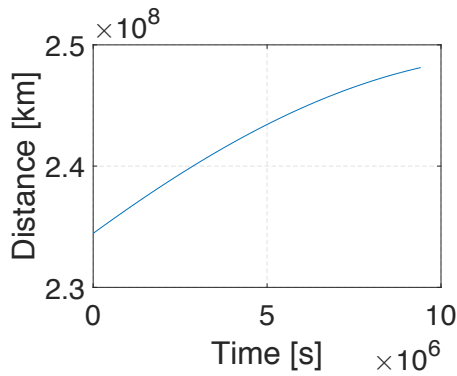


Figure 11.3: Distance between Mars and the Sun

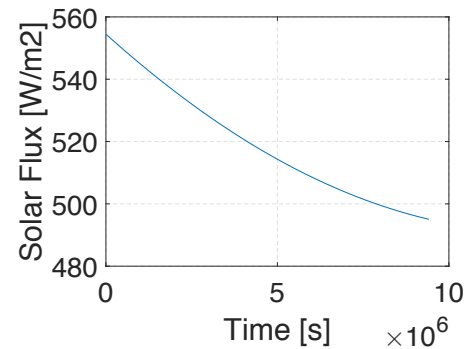


Figure 11.4: Solar flux at different distances

In Table 11.9 two suitable coating materials are listed that would be able to reach the required temperature. The properties of Electroless nickel are taken from the Lockheed thermal catalogue [GCSS78]. The properties of a black irridite coating are from the NASA thermal catalogue [Low77].

Table 11.9: Equilibrium temperature for different surface finishes

Parameter	Absorption Factor	Emission Factor	Equilibrium Temperature	
	[-]	[-]	[K]	[°C]
Electroless Nickel	0.45	0.17	287	+14
Black Irridite	0.62	0.17	297	+24

From the two different materials that have been found suitable to assure a spacecraft temperature in which all the components will survive and can operate electroless nickel has been selected as the preferred material. This has two main reasons, firstly the equilibrium temperature is lower than that of black irridite coating. This is preferable since the equilibrium temperature has the tendency to increase during the mission, even though the spacecraft moves further away from the Sun during the mission. The reason for this is that the absorption factor increases over time due to material degradation. The material degradation is not accounted for in the simulation and is therefore not incorporated in Figure 11.5 and 11.6. Furthermore, the power subsystem can be used as an extra source of temperature generation if necessary, as described in Subsection 11.2.7. An extra advantage is that more information is available on electroless nickel than on black irridite. Properties of the coating material²² that will be used can be found in Table 11.10. For the coating it is assumed that the thickness of the material can be manufactured to be 1 mil.

Table 11.10: Material properties of electroless nickel

Material	Density	Thickness		Area	Mass
	[gcm ⁻³]	[mil]	[mm]		
Electroless Nickel	8.52	1	0.0254	0.2443	52.9

Combining the previously described effects plotted in Figures 11.3 and 5.4 with the Equations from Subsection 11.2.3, Figure 11.5 and 11.6 can be created, here the temperature during the first 100 orbits is plotted. These figures shows the temperature transition from the point of separation until the equilibrium temperature is reached. The separation temperature is the temperature the host will have during the transfer. It is assumed that the temperature of the

²²Electroless Nickel Properties: <https://goo.gl/t3iLfK> [cited 6 June 2016]

cubesat will be the same as the host temperature during transfer and before separation and that this temperature complies with the cubesat temperature requirements, defined in Table 11.6. The temperature at separation is not relevant for the results, since the temperature converges towards the same equilibrium temperature irrespective of the initial state. In both figures the (blue) line in the middle is the expected temperature for which the mission is designed. In Figure 11.5 the sensitivity of the design with respect to the launch date is included. This figure shows the bus temperature if the spacecraft arrives at solar maximum or solar minimum. It can be observed that the bus temperature stays within the operational ranges irrespective of the time of arrival. Figure 11.6 shows the sensitivity with respect to the dissipated power, it can be observed that an increase or decrease of 1 W of dissipated power affects the spacecraft temperature severely. This has to be dealt with carefully and the approach to handle a change in power dissipation is described in Subsection 11.2.7.

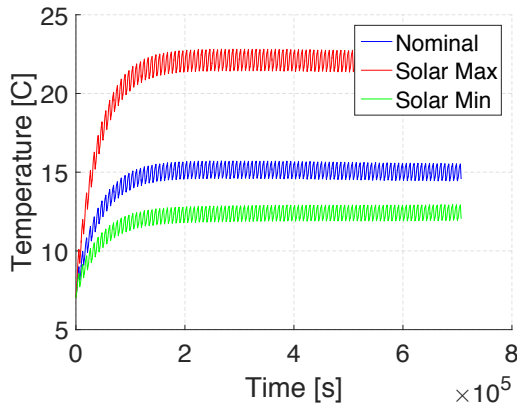


Figure 11.5: Bus temperature with launch date sensitivity

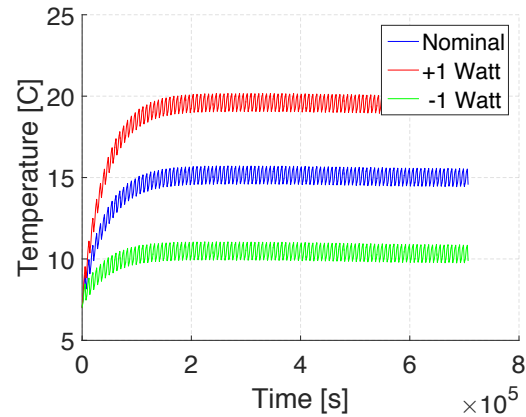


Figure 11.6: Bus temperature with power dissipation sensitivity

11.2.5. Solar Panel Temperature Range

Since the solar panels are outside of the bus and have a large area the temperature swings will be significant. The temperature simulation for the solar panels is conducted similarly as for the bus. The difference is that it is assumed that no power dissipation occurs in the arrays. Furthermore, since the solar arrays consist of different materials, the specific heat capacity is assumed to be the weighted average of these materials. In Table 11.11 the parameters used for the simulation are presented. The sunlight absorption area will remain constant during each orbit because the solar panels have rotational capabilities and will always be pointing towards the Sun. The albedo and infrared absorption area does not remain constant but an average value is assumed as they are not crucial factors for the equilibrium temperature.

Table 11.11: Solar panel simulation parameters

Parameter	Symbol	Value	Unit
Heat Capacity	C	1061	$[\text{J kg}^{-1} \text{K}^{-1}]$
Array Mass	m	0.738	$[\text{kg}]$
Sunlight Absorption Area	$A_{i,\text{Sun}}$	0.136	$[\text{m}^2]$
Albedo and IR Absorption Area	$A_{i,b}$	0.0962	$[\text{m}^2]$
Emission Area	A_e	0.2720	$[\text{m}^2]$
Absorptivity Front	α_S	0.90	$[-]$
Emissivity Front Side	ϵ_{IR}	0.85	$[-]$
Emissivity Back Side	ϵ_{IR}	0.64	$[-]$

In Figure 11.7 the temperature swing of a solar panel is plotted. This simulation accounts for the fact that the front and back of the panel consist of different materials and therefore a weighted average of the front and back emissivity is used. The simulation is performed for 25 orbits. The temperature varies between 215 K and 290 K. This is not a problem for the solar panels because this is within their operational temperature as can be seen in Table 11.6.

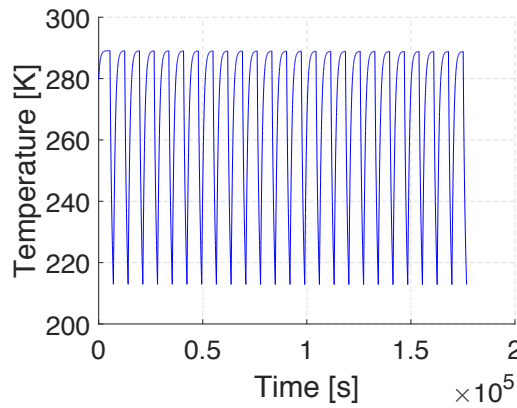


Figure 11.7: Temperature difference in the solar panels during 25 orbits

11.2.6. Thermal Expansion

Thermal expansion is an important aspect of thermal design. If large temperature differences arise stress in the material will occur. Stresses caused by temperature differences can be determined with Equation (11.12), the parameters used in this formula can be found in Table 11.12. The equilibrium temperature is approximately 14 °C whereas the minimum and maximum survival temperature are −10 °C and 30 °C. Assuming a temperature difference of 50 K in order to be conservative, the maximum thermal stress is found to be 91.8 MPa.

$$\sigma = E\alpha_T\Delta T \quad (11.12)$$

Table 11.12: Thermal stress in the bus structure

Material	Young's Modulus [GPa]	TEC [$\mu\text{m m}^{-1} \text{ } ^\circ\text{C}^{-1}$]	Temperature Difference [K]	Stress [MPa]
Aluminium 7075-T6	71.7	25.2	50	91.8

11.2.7. Thermal Redundancy

The power dissipation inside the spacecraft is one of the main contributors to the equilibrium temperature. However, the amount of power dissipated by the subsystems and payload is a large unknown which is not constant and varies for each control operating mode. All power that is used in the spacecraft will be dissipated into heat, except for the power that is transmitted by for example the antenna [J. Bouwmeester, pers. comm. June 2016]. The amount of power that is converted in each phase can only be determined by exhaustive testing. For the thermal simulation the nominal power usage is assumed, which generates a power dissipation of 9 W during the operational period and 9 W during the eclipse. If these values are not reached the spacecraft will have a lower equilibrium temperature. Furthermore, from Figure 11.5 and 11.6 it can be concluded that the equilibrium temperature gradually decreases since the distance between Mars and the Sun increases during the mission. A combination of these two effects may cause the temperature to decrease too rapidly. Should this problem arise, the propulsion system can be used to increase the temperature [FREQ-SS-TH3, Ch. 15]. The valve coil of the propulsion system can also function as a heater if the voltage in the system is maintained below the pull-in level for the valve [SMS11]. If the temperature decreases below a certain threshold, a voltage below 6 V will be applied to the valve until the desired temperature is reached again. Thermistors²³ will be installed to measure the temperature inside the spacecraft, the data will then be processed by the OBC. In order to process the scientific data temperature data of the payload should be known. Therefore 1 thermistor will be placed between HAWAII H1RG and SPEX and two on the bottom side of SPEX, 1 on each large panel facing the outside of the cubesat. Furthermore 1 thermistor will be placed on the propulsion system, since it is one of the leading components in terms of temperature. The weight of a single thermistor is less than 0.5 g. The OBC determines if the temperature is within the desired limit and it will activate the heater functionality of the propulsion system if necessary. If the dissipated power becomes more than what is designed for, the OBC should cut off power in order to decrease the temperature.

11.3. Radiation

During the Midterm Report [AFH⁺16], radiation was only briefly discussed. For the trade-off between the mission concepts it was not really considered important as it will be approximately the same for the missions. It is however a

²³Thermistor: http://www.meas-spec.com/product/temperature/ESCC_Epoxy_Coated_Thermistors.aspx [cited 14 June 2016]

crucial factor for the final spacecraft design. This is due to the dependency on off-the-shelf components for nominal cubesat missions, which usually operate in Low Earth Orbits. Space missions in these orbits are protected against harmful radiation that originates from space by the Earth's magnetic field.

11.3.1. Radiation in General

The Midterm Review has already discussed the failure modes that can be caused by particle radiation and the counter measures that could be used to prevent these failure modes. These are all briefly summarised in Table 11.13.

Table 11.13: Radiation failures and counter measures

Main Failure Modes	Counter Measures
Charging	Hardening
Sparking	Shielding
Ionisation	Redundancy
Single-Event Upsets	
Latch-Ups	

All the different failure modes can be prevented by minimising the amount of radiation that reaches the components of the spacecraft. This amount of radiation is also known as the total ionising dose and is expressed in rad. When considering the possible counter measures as already mentioned, redundancy is not a proper option as the redundant device or system will be exposed to the same amount of radiation as the primary component. Hence, in terms of radiation, redundancy only accounts for extra weight as the redundant components might fail even earlier than the main component. Hardening and shielding of the bus can definitely be considered. However, existing components cannot be hardened and thus new components should be designed. Therefore it is checked how well the bus can be shielded. From these results it can be checked if extra shielding of some sensitive components is necessary.

11.3.2. Graded Shielding

For structural purposes, the bus consists of aluminium panels with a width of 0.5 mm as determined in Section 11.1. These panels shield the components within the bus to some extent, but unfortunately do not block enough radiation. This will be thoroughly discussed in Subsection 11.3.4

Therefore other methods for the shielding of the bus should be considered. A good other option which is considered for space missions is graded shielding. This method combines certain Low-Z and High-Z materials, which have different characteristics with regard to particle radiation.

Low-Z materials are commonly known as light materials, which include relatively less protons in the nucleus, such as aluminium. These type of materials usually have a high stopping power per unit mass, resulting in a large deceleration of penetrating particles due to inelastic collisions with the bound electrons within the Low-Z material.

High-Z materials are heavy materials, which have a larger amount of protons within the nucleus, like tungsten, lead and tantalum. High-Z materials are more efficient at scattering incoming particles, but do generate 'Bremsstrahlung', which is electromagnetic radiation produced by the deceleration of the incoming radiation by the atomic nucleus. Graded shielding combines these type of materials and thus their characteristics, such that the penetrating amount of radiation is greatly reduced.

11.3.3. Methodology

The chance that the different failure modes, as mentioned in Subsection 11.3.1, will occur depends on the total amount of particles that penetrate through the shielding of the cubesat over its mission lifetime. This total amount of dose is commonly called the total ionisation dose. Therefore it is important that this total dose is determined. The nominal off-the-shelf component dose limit is about (10 krad), hence the total dose within the shield should be lower than this value.

ESA's Space Environment Information System (SPENVIS)²⁴, a collection of different useful tools, has been used to acquire these desired ionising doses, which will be thoroughly discussed in Subsection 11.3.4. The different tools that have been used are described in this section. The acquired doses using these models can be found in Section 11.3.4.

Step 1: Generating the orbit

Orbit generator: Firstly the orbit of the cubesat should be generated. Radiation wise, the most important factor is the distance from the Sun as this is the main source of radiation at Mars. SPENVIS has a very convenient tool to provide this orbit, developed by the European Space Operations Centre at ESA.

The main input is the duration of the mission (including the transfer to Mars). This should be approximately one year

²⁴SPENVIS: <https://www.spenvis.oma.be/> [cited 1 June 2016]

as determined in Chapter 5. Also, the distance from the Sun is important, which is approximately 1.5 AU. It should be noted that during the transfer this distance varies from 1 AU to 1.5 AU. However, after discussing this matter with an expert [A. Menicucci, pers. comm. 30 May 2016] and by checking it in SPENVIS, it is sufficient to fix the distance at 1.5 AU to obtain a proper dose baseline. The output of this simulation is an orbit model which the upcoming simulations can utilise.

Step 2: Generating the radiation models

Trapped Particles: For some space missions, trapped particles should also be considered. These are particles that are captured by anomalies in space such as a magnetic field. Fortunately, due to the lack of these type of anomalies around Mars, it can be safely assumed that no trapped particles are present. This is confirmed when running the trapped particle models from SPENVIS.

Solar Particle Fluxes: The dose of radiation received over the duration of the mission can be determined. Both the short-term and long-term solar particle fluxes can be determined using models (CREME-96 and ESP-PSYCHIC) developed by the GODDARD Space Flight Centre at NASA. The CREME-96 model is based on average observed fluxes and the ESP-PSYCHIC uses solar proton event data from the last 3 solar cycles²⁵. The only input for these simulations is the orbit model and the preferred ion range (which for this mission is the entire spectrum). The calculated radiation doses have all been determined for a solar maximum to be as conservative as possible. Solar flares also have been accounted for.

GCR Spectra: Next to the solar particle fluxes, the Galactic Cosmic Ray (GCR) fluxes should be determined. SPENVIS provides a model (ISO-15390) developed by the Lomonosov Moscow State University and the Royal Belgian Institute for Space Aeronomy. This model also uses the orbit model and ion range as inputs.

The ISO-15390 model is the international standard for estimating the radiation impact of galactic cosmic rays. It also accounts for variations of these fluxes due to variations in solar activity²⁶.

Step 3: Shielding Simulations

Ionisation Dose Models: From all the radiation models, a total ionisation dose model can be determined. SPENVIS includes a model (SHIELDDOSE-2) developed by the National Institute of Standard and Technology (NIST). SHIELDDOSE-2 uses the different radiation specifics which result from the previous models, together with the material properties of aluminium, to determine the radiation dose behind aluminium sheets with different thicknesses.

MULASSIS: Finally, when all the required variables are calculated, different set-ups of graded shielding can be tested. This is done using SPENVIS's Multi-Layered Shielding Simulation (MULASSIS), developed by the Royal Belgian Institute for Space Aeronomy. As it is not physically feasible to solve the shielding simulation, it uses Monte Carlo simulations to obtain the total ionizing dose behind the different shields. These simulations use a large amount of random sampling to obtain doses for all the different material layers and thicknesses. As obtaining the desired doses takes a lot of simulations, one million samples have been used per data point. To obtain more precise doses, up to several million or billion simulations could be executed per data point. However, due to time constraints this has not been possible for the doses found in this report. It has to be noted that for most of the calculated doses errors are within acceptable margins (between 0.1 and 0.5 percent).

MULASSIS can be used if the results from SHIELDDOSE-2 are not sufficient. It is possible to define more layers of shielding, different materials and custom thicknesses of the different layers. The main principle is the same as for SHIELDDOSE-2. Using the material properties and the calculated radiation doses, the dose behind a layer of material is determined.

11.3.4. Results

When applying the methodology from Section 11.3.3, different results are obtained. In this Section it is calculated how thick the aluminium panels should be to decrease the radiation dose to allowable levels. Also the same is done, but by combining the aluminium panel of the bus with different High-Z metal coatings.

Pure Aluminium

Firstly, a panel consisting of solely aluminium is considered. After determining the radiation models, as discussed in Subsection 11.3.3, MULASSIS is used to determine all the individual data points for the curve in Figure 11.8. Also the nominal off-the-shelf component dose limit (10 krad) is added as a horizontal line. This has been included as not all the components have a known radiation tolerance and this results in a conservative approach. It should be clear that the total ionising dose generated behind the aluminium panel should drop below the off-the-shelf component

²⁵ CREME-96 Model: <https://goo.gl/raZayz> [cited 31 May 2016]

²⁶ ISO-15390: <https://www.spenvi.soma.be/help/models/gcr.html> [cited 31 May 2016]

dose limit for the mission to become feasible with respect to radiation. When observing the plot, it can be concluded that the total ionising dose behind the aluminium panel becomes feasible at 2.1 mm thickness. At this thickness, the total ionising dose drops below 10 krad and all components within the cubesat should be able to withstand all radiation for at least a year. Other factors should still be accounted for as there are several budget restrictions for the cubesat. These factors are the cost, volume and mass of the shield. During these considerations, the added amount of thickness with respect to the original bus value (0.5 mm) will be considered, hence 1.6 mm.

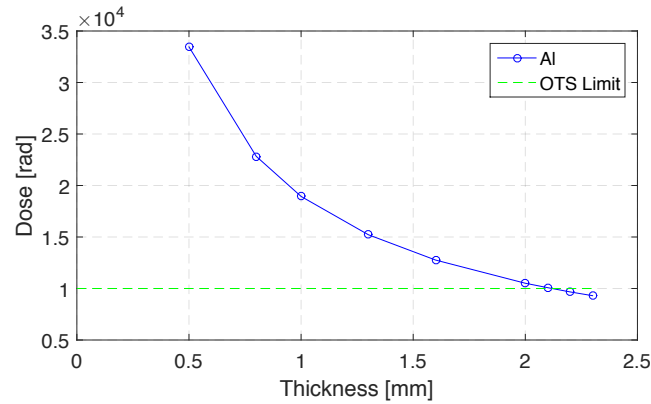


Figure 11.8: Total Ionising dose behind a pure aluminium shield.

Cost: The cost of an aluminium panel of 1.6 mm thickness is 166 euro for a single 300 mm × 300 mm panel and 209 euro for two of these panels²⁷. When taking into account the dimensions of the cubesat (340.5 × 200 × 100 mm), it can be calculated how many panels are necessary to cover the inside walls of the bus. Firstly the total area of the cubesat panels has to be calculated. This is done using Equation (11.13), where A is the total area and L, D and W are the length, depth and width of the cubesat.

$$A = 2(LW + LD + WD) \quad (11.13)$$

When considering the area of a single panel (300 × 300 mm) and dividing the total area (244 300 mm²) by this value it is obtained that 2.72 panels are needed. As panels come as a whole, 3 panels should be bought. This gives a total cost of 369 euro, which will not cause any problem for the budget of 10 million euro.

Volume: The volume added can be determined by multiplying the total area of the panels (244 300 mm²) by the thickness of the panels (1.6 mm). This is equal to 390 880 mm³. The total volume available in the cubesat is 6 810 000 mm³ (length × width × depth). This results in a decrease of 5.74 percent of available volume for all subsystems.

Mass: To determine the mass of the added aluminium panels, the density of aluminium is considered. This has been determined in Section 11.1 and is equal to 2.81 g cm⁻³. Then the added mass is determined by multiplying this density with the acquired volume of the added panels (390 880 mm³). This results in a total weight addition of 1098 g. The allowed maximum mass of the cubesat equals 12 kg. This results in a decrease of 9.15 % of available mass for all subsystems.

Conclusion: With a pure aluminium panel, the total ionising dose can be decreased below the off-the-shelf dose limit. However, when checking the volume and especially the mass which the panels will require, it becomes clear that this method of shielding is definitely not preferred. This is due to the fact that both of especially the mass budget is already really strict and it is not feasible to add a shield which decreases available mass by 9.15 %.

Graded Shielding

As already discussed in Subsection 11.3.2, graded shielding is an interesting alternative to the pure aluminium shielding. It utilises the 0.5 mm aluminium of the bus and combines it with different High-Z materials. The most interesting High-Z materials are lead, tantalum and tungsten [A. Menicucci, pers. comm. 30 May 2016]. All results obtained using these material combinations can be found in Figure 11.9.

Cost: Firstly the possible manufacturing foil thicknesses and their costs for all the High-Z metals have been considered²⁷. The total cost as a function of the thickness can be found in Figure 11.9a, this total cost has been calculated using the method from Subsection 11.3.4. The cost has a big variance. Thin foils are expensive, but as the thickness increases the foils become a lot cheaper. The most expensive foils will cost a total of almost 200,000 euro, thicker foils

²⁷ Panel Costs: <http://www.goodfellow.com/> [cited 6 June 2016]

only cost several thousand euro. Therefore it is important that the cost will be accounted for in the final comparison of the different shields.

Weight: The densities of tantalum, tungsten and lead can be found in SPENVIS and are equal to 16.7, 19.3 and 11.3 g cm^{-3} respectively. By multiplying these densities with the corresponding thickness and the total area of the panels as found in Subsection 11.3.4, the added weight for the different panels is obtained. These results can be found in Figure 11.9b. It seems that all the different shield consistencies do not add a lot of weight to the aluminium bus. These weights do however vary from 2 g to 120 g and are therefore also considered in the final comparison.

Volume: These High-Z metals have a high density and thus, in comparison to the mass impact, the volume impact is small. This was already twice as small for a Low-Z metal and thus it is not considered important for the trade-off between these High-Z materials. It will be calculated for the final chosen shielding at the end of this chapter.

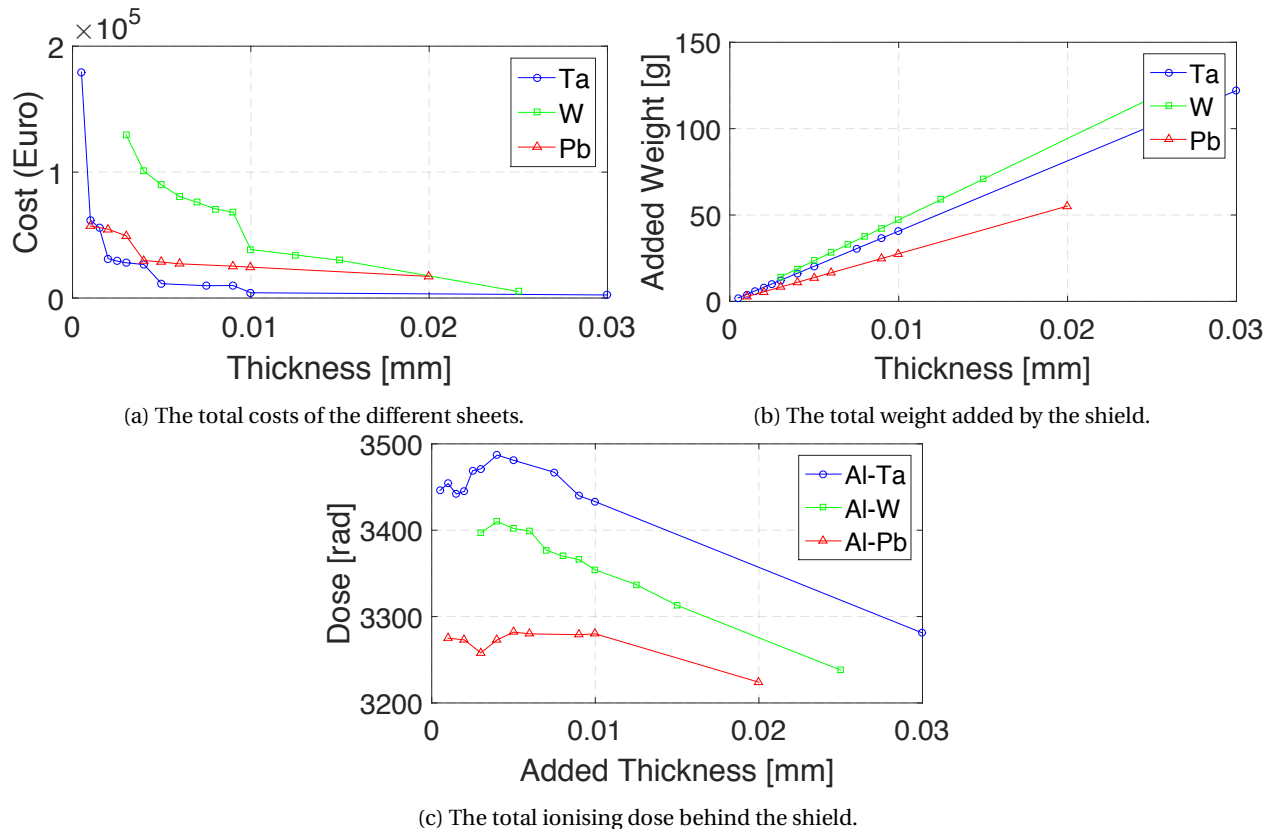


Figure 11.9: Results for different graded shielding set-ups.

Radiation: To determine the ionisation doses behind the shielding, the methodology from Subsection 11.3.3 has been applied. Figure 11.9c shows these calculated doses for the different added thicknesses. It must be noted that this dose is calculated behind the entire shield, hence behind the 0.5 mm of aluminium and the added High-Z metal as shown in Figure 11.9c. The x-axis however only shows the added thickness due to convenience.

It can directly be seen that all the values for the radiation are way below the threshold value of off-the-shelf components. With an ionising dose of only 3200-3500 rad, all chosen components should be able to operate for the estimated mission lifetime. It should be noted that in Figure 11.9c the doses behind the shields sometimes increase briefly at certain thicknesses. This is due to the increments between these thicknesses being extremely small, resulting in a very small change in dose per step. When keeping in mind that the Monte-Carlo simulations, as described in Subsection 11.3.3, give a small error as percentage of the total dose, these errors can be slightly higher as these small step differences. When considering the mission and the type of radiation received, this large decrease in dose due to only a thin layer of High-Z foil can be explained. It is due to two main factors. First, the mission duration of one year is very short. Therefore the amount of ionisation dose will be limited. Second, the main radiation source is the Sun. This primarily expels protons and heavy ions which, due to their energy levels, do not easily penetrate through High-Z metals (As these metals have a lot of protons within the nucleus).

-Final Conclusions: For the final comparison the overall cost, added weight and dose of the different materials have been compared for the different thicknesses. Another important factor which also should be taken into account is

sustainability. From a sustainable point of view it becomes clear that lead is not an optimal solution as it is poisonous if not properly handled (more on sustainability in general can be found in Chapter 20). From Figure 11.3.2 it is observed that tungsten is a lot more expensive as tantalum, it is also slightly heavier but the components of the cubesat do experience lower doses behind this shield. However, also for tantalum these doses are only a third of the required minimum of 10 krad. Therefore, especially due to the high cost of tungsten, tantalum is chosen as the final material for the High-Z part of the shield.

Now the optimal thickness for this tantalum shield has to be determined. The dose behind the shield is no problem for all thicknesses. The weight varies from a few grams to 120 grams, which is not a large impact, but should be taken into account as the weight budget is strict. For cost four clear jumps can be observed in Figure 11.9a. Really thin panels are extremely expensive and should therefore be avoided. When observing Figure 11.9a it is observed that the cost of the panels decreases significantly until a thickness of 0.01 mm has been reached. If this thickness would be chosen, the added weight would be equal to only 42 grams. Therefore this thickness of tantalum as High-Z component of the final graded shield will be the optimal solution from the results as presented in Figure 11.9.

Now a final conclusion can be made with regard to the radiation shielding. A graded shield, consisting of 0.5 mm aluminium with 0.01 mm tantalum covering the inside will be utilised during the mission. This shield adds 42 grams of weight and will approximately cost 4800 euro.

11.4. Verification and Validation of Numerical Models

In this section the verification and validation of the numerical models used in the bus design will be discussed. In Section 11.4.2 the verification of the thermal simulation is discussed. In Section 11.4.3 the verification and validation of the radiation simulation software is elaborated on.

11.4.1. Structure

In order to verify that the custom-designed structure complies with the requirements defined in Chapter 15, several tests are suggested (Section 18.3). Of these, the EMC tests are not necessary as the structure does not have electro-magnetic components. As a result of the testing, the design requirements can be validated and the structure can be iterated towards a more efficient design. Furthermore, if more time and resources were available, the frame and the general bus structure would be even more efficient in taking predefined loads. Events such as shocks are difficult to design for, as they are generally described as high-loads that take place in very short time frames. Therefore it is self evident that extensive testing and iteration would lead to a better design.

11.4.2. Thermal Control

The verification of the simulation used to determine the temperature was carried out in the following manner. First simple equilibrium calculations were performed for the coldest and hottest extremes without any time and position dependent variables. The real simulation had to stay within these extremes, this test was conducted successfully. The second test was to determine if the temperature would always converge towards the same equilibrium temperature regardless of the separation temperature. This was always the case and therefore this was verified. Furthermore all the relevant time dependent parameters were plotted and examined to see if the values and trend of the values are in compliance with their expected results. An overview of the verification procedure is presented in Table 11.14.

Table 11.14: Verification of thermal simulation

Parameter	Expectation	Compliance
Sun - Mars distance	Increasing	✓
Solar Flux	Decreasing	✓
Altitude	Fluctuating around 400 km	✓
Illumination Area	Fluctuating between 0.02 and 0.03405m ²	✓
Absorbed Solar Flux	Decreasing	✓
Absorbed Albedo Flux	Decreasing and about 10% of Solar Flux	✓
Absorbed Infrared Flux	Fluctuating and same order of magnitude as Albedo Flux	✓
Temperature Hot Case	Higher than Simulated Temperature	✓
Temperature Hot Case	Lower than Simulated Temperature	✓
Converging Equilibrium Temperature	Similar irrespective of Separation Temperature	✓

11.4.3. Radiation

The models which are briefly discussed in Subsection 11.3.3 are extensively used worldwide. An example is the recent space mission Rosetta, which also used SPENVIS to model the radiation environment²⁸. Verification and validation

²⁸Rosetta Radiation: <http://space.irfu.se/rosetta/sci/radbelts.html> [cited 30 May 2016]

is impossible for radiation effects at Mars. All models have been created and are utilised by different well-known organisations around the globe. These organisations have also extensively tested these models, thus all models can be considered verified and validated.



Configuration and Layout

This chapter discusses all aspects related to the internal and external layout of the cubesat. It will show the physical appearance of MICRO. However, the deployment mechanism (or dispenser) is firstly treated in Section 12.1 since it is linked to the external layout of the cubesat (needs to fit into the deployer). Then, Section 12.2 will discuss the internal and external layout of MICRO and illustrate these using CAD-renderings.

12.1. Deployment Mechanism

MICRO will spend the majority of the mission duration in hibernation mode. It spends approximately 270 out of 379 days ($\approx 71\%$ of the time) (see Chapter 5) inside a dispenser installed on the host satellite, Mangalyaan 2. The dispenser should safeguard the cubesat during the launch phase, its transfer to Mars and has to deploy MICRO safely into space after Mangalyaan 2 reaches its science orbit, resulting in requirement [OREQ-M-HO3, Ch. 15].

12.1.1. Trade-off

Since the majority of the cubesat industry focuses on 3U or lower unitary cubesats, only few reliable deployers are available to select from. Table 12.1 illustrates the major 6U cubesat dispensers along with their corresponding performance parameters. In case data is missing with respect to a certain parameter, the property is labelled as n.a. (Not Available) and highlighted in yellow. Parameters hindering the storage of the cubesat with respect to the available internal volume are highlighted in red. Thus, the 6-POD [ISI16][Uni16] cannot be used due to the dimensional restrictions imposed by MICRO. The mass of the deployer plays a crucial role for the host mission. Since the total mass of deployer and cubesat together is set as a limit by the host mission. A reduction in deployer mass accommodates the possibility to increase the mass of the cubesat or reduce launch costs. As indicated in Table 12.1, the Canisterized Satellite Dispenser (CSD) [Cor13, Cor15a, Cor15b, Cor16] is the lightest option compared to the other left over available options. CSD also offers the highest cubesat accommodation volume. Deployer mounting orientation affects the vibrational loadings on the cubesat. Both CSD and Nanosatellite Launch Adapter System (NLAS) [Pla16] provide flexible mounting capability on all faces. Since all the dispensers have been launched before and performed successful deployment of a cubesat, they share a TRL of 9. CSD provides a lower ejection force than NLAS, which is less detrimental for the cubesat in case of misaligned orbit insertion.

To summarise, 6-POD cannot be chosen due to dimensional constraints of MICRO and Nanoracks [Nan13] can be discarded due to a lack of available data. Finally, CSD outperforms NLAS over the majority of the performance specifications and is therefore selected as the dispenser for the MICRO mission.

Table 12.1: Performance specifications for deployment mechanisms [Cor15b]

Dispenser	Properties								
	Deployer mass [kg]	Payload mass [kg]	Payload Length [mm]	Payload Height [mm]	Payload Width [mm]	Payload Volume [$1 \times 10^{-3} \text{ m}^3$]	Mountable sides [N]	TRL [–]	Ejection force [N]
CSD	4.54 [E]	12.00 [E]	366.00 [E]	239.40 [E]	109.70 [E]	9.61 [E]	6 [E]	9 [E]	16.07 [E]
NLAS	5.40 [G]	14.00 [E]	336.30 [U]	226.30 [E]	100.00 [E]	7.61 [E]	6 [E]	9 [E]	81.2 [E]
6-POD	2.75 [E]	12.00 [E]	340.50 [E]	176.00 [U]	90.00 [U]	5.39 [U]	n.a. [B]	9 [E]	n.a. [B]
Nanoracks	n.a. [B]	16.971 [E]	340.50 [E]	201.20 [E]	100.60 [E]	6.89 [U]	n.a. [B]	9[E]	n.a. [B]

Legend [E] Excellent [G] Good [B] Barely acceptable [U] Unacceptable

12.1.2. Canistered Satellite Dispenser

This subsection describes the selected deployment mechanism in more detail. The Canisterized Satellite Dispenser (CSD) [Cor15a] will be used to fully encapsulate the cubesat during launch and the transfer to Mars until the host mission reaches Mars (see Figure 12.2). Then, the cubesat will be deployed in the hosts' nominal orbit using a spring mechanism. The CSD is deemed reliable since it is at Technology Readiness Level 9 and has proven its reliability during the POPACS Mission¹. In Table 12.2, additional relevant specifications of the deployer are presented while its base specifications were already shown in Table 12.1.

Table 12.2: Specifications CSD [Cor15a]

Parameter	Value	Unit
Payload Ejection Energy	5.4	[J]
Max Rotation Rate After Ejection	10	[deg s ⁻¹]
Operational Temperature Range	-45 – + 90	[° C]
External Height	263.53	[mm]
External Width	157.66	[mm]
External Length	402.1	[mm]

The mass of the deployer is not taken into account for the mass budget of the cubesat since it is not a part of the cubesat itself. However, it must be taken into account when evaluating the launch costs which will be discussed in Chapter 14. The mass of the cubesat is important since requirement [OREQ-M-EB1, Ch. 15] follows from the maximum payload mass described in Table 12.1. The payload ejection energy results from the energy stored in the two springs. Using the kinetic energy equation², the maximum ejection velocity of the cubesat with a mass of 10 kg, is 1.04 ms⁻¹. This can be assumed negligible compared to the ΔV -budget for orbit insertion defined in Subsection 5.1.3. The spring force is also assumed to have a negligible effect on the cubesat when comparing this to the launch loads it can cope with as described in Section 11.1. The maximum rotation rates will be coped with by the ADCS subsystem as described in Chapter 6. Finally, the operational temperature range for the deployer is well within the thermal operating range described in Section 11.2.

The maximum external dimensions of the deployer are given in Table 12.2 and the maximum internal dimensions of the cubesat in order to fit into the deployer are given in Table 12.1. These maximum internal dimensions comply with the dimensions of the cubesat shown in Figure 11.2. However, this is just the base external frame of the cubesat. Some additional external components and deployables are also present which need to fit as well. On the negative z-face, an actuation mechanism is present of 6.5 mm thickness and an antenna next to it of 9.6 mm thickness. This increases the cubesat height to 209.6 mm. On both the positive and negative y-faces, a stacked solar panel is present with a thickness of 4.8 mm. This results in an extended cubesat width of 109.6 mm. Finally, two antennas are present at both the x-faces which extends the length of the cubesat to 359.7 mm. When comparing these maximum external dimensions to Table 12.1, the cubesat dimensions satisfy with the internal volume available.

On top of these general specifications which all comply with the mission and the cubesat design, the CSD has some additional features compared to other dispensers which are beneficial to the mission success:

- During integration of the payload with the CSD, the cubesat will be attached to two preloaded tabs running the length of the ejection axis. The CSD will grab these to ensure a secure, modelable and preloaded junction. This prevents vacillation of MICRO which could harm MICRO (see Figure 12.1) and is essential in predicting loads on critical components. On top of that, the act of closing the door automatically preloads the tabs. The tabs will be manufactured before integrating the cubesat with the deployer out of 7075-T7 aluminium and run the entire length of MICRO. This satisfies requirements [FREQ-SS-ST6, Ch. 15] and [FREQ-SS-ST7, Ch. 15].
- All six sides are mountable. Since no information is present on the exact dimensions or layout of the Mangalyaan 2 mission or on GSLV III, this increases the flexibility of mounting the deployer to the host. This feature makes the mission comply with requirement [OREQ-M-HO1, Ch. 15].
- An electrical connector allows communication and charging between the cubesat and the host before, during and after launch.
- Option to constrain moving parts of the cubesat, but needs custom tailoring of the CSD.
- A P-POD compatible mechanical interface ensures compatibility with existing structures. This also satisfies the required flexibility with respect to the host mission and its launcher.
- A full length, constant force ejection spring ensures a constant force is applied to the cubesat during ejection.

¹POPACS: <http://tinyurl.com/zrv8dke> [cited 7 June 2016]

²Kinetic Energy Equations: <http://tinyurl.com/2ew634d> [cited 7 June 2016]

- Two independent electrical circuits and a triple redundant commutator incorporates electrical redundancy to ensure deployment of the cubesat even if there are faults in the wiring harness.
- No pyrotechnics are used to deploy the cubesat which reduces the risk of harming MICRO or Mangalyaan 2, satisfying requirement [FREQ-SS-ST1, Ch. 15].

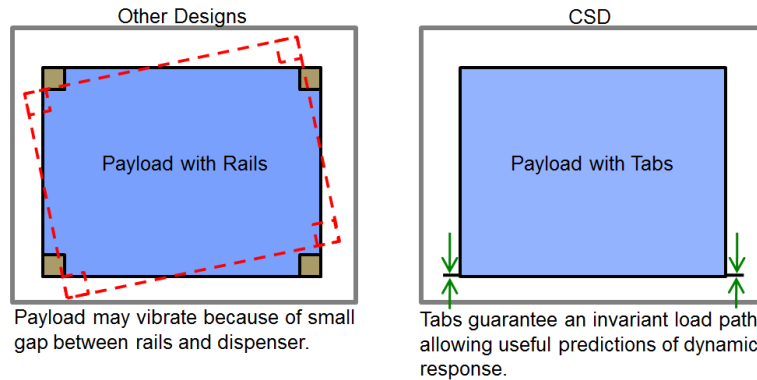


Figure 12.1: Benefit of using tabs [Cor15a]

12.1.3. Host Interaction

One of the benefits of selecting the CSD is the electrical interface it offers between the cubesat and the host and between CSD and the host. The former connection is via a electrical connector and the latter via a DB-9 socket connector both indicated in Figure 12.3. This enables the possibility of charging the cubesat as well as running diagnostics.

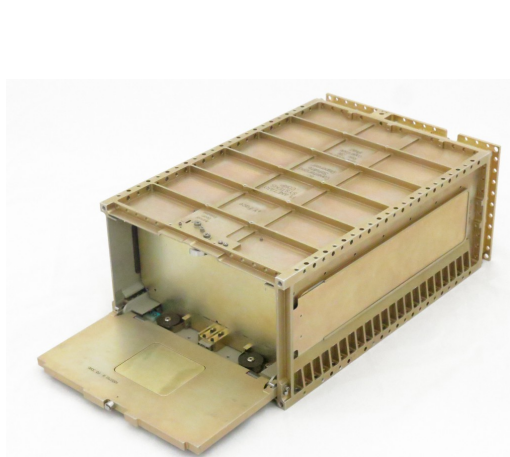


Figure 12.2: 6U Canistered satellite dispenser [Cor15a]

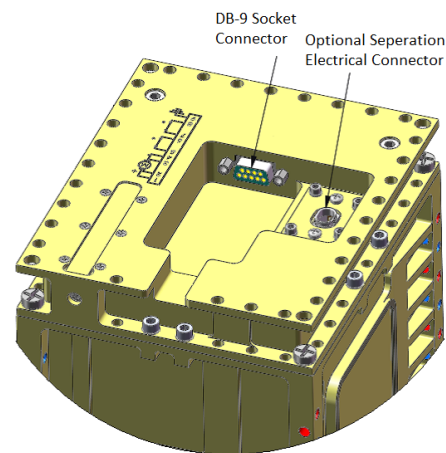


Figure 12.3: Electrical interface between the host and the CSD and an optional connection between the host and MICRO. Note that this shows the connection for the 3U CSD, but the configuration for the 6U CSD is similar [Cor15a]

The electrical connection between the host and the deployer is required to activate the deployment mechanism. When Mangalyaan 2 is in its nominal mission orbit, a signal is sent from Earth to the host satellite to activate this mechanism and deploy MICRO. The electrical connection between the host and the cubesat is an optional one. It could be used to run diagnostics on MICRO after launch to check if its systems are still functional. If this would not be the case, MICRO could be ejected early into a parking orbit around Earth. This way, the host does not have to carry MICRO all the way to Mars which would save fuel for Mangalyaan 2 and results in a more sustainable host mission. Additionally, ejecting a satellite into parking orbit would result in a rapid decay of this satellite due to the low altitude of this orbit [Noo15b]. This would limit the time that the cubesat is space-debris which also increases the sustainability aspect of the mission.

The electrical schematic of these electrical interfaces can be found in [Cor15a]. It shows the schematic when the cubesat is deployed and when it is installed. The separation electrical connector is an in-flight disconnect (IFD) and is provided by PSC³ which will be used to disconnect the interface when MICRO is deployed. The plug and cables

³Separation Connector: http://www.planetarysystemscorp.com/?post_type=product&p=451 [cited 8 June 2016]

of the connector part of the cubesat are connected to its on-board computer. The available connections on the computer are RS422, USB, U(SART), SPI and even ethernet as described in Subsection 8.2.3. When the cables are installed in the cubesat and connected to the on-board computer, an interface to interface module can be custom designed for this connection. This is because the type of connection of the electrical connection is unknown.

12.2. CAD Design

Now that all dimensions are known, all components have been selected and positioning has been determined, a proper CAD model can be created. This model will consist of an external configuration, which will be discussed in Subsection 12.2.1 and an internal configuration, which will be discussed in Subsection 12.2.2.

12.2.1. External Configuration

The external configuration of the cubesat consists of four main components: the bus, the antenna patches, the solar array and the sun sensors. All these components are visualised in Figures 12.4 and 12.5.

The bus is a rectangular box with dimensions of 340.5 x 200 x 100 mm and consists of different layers. The outside layer consists of electroless nickel due to thermal purposes as discussed in Section 11.2. Behind the thin thermal layer there is the main structure consisting of 0.5 mm aluminium, which has been determined in Section 11.1. This aluminium layer is coated on the inside by 0.01 mm of tantalum, as determined in Section 11.3, to protect all internal components against particle radiation. Within this final layer the frame can be found which will provide support for different loads and hold all components. This frame has been designed in Section 11.1. The antenna patches have been designed in Chapter 9. These patches can be found on all sides of the cubesat except for the side facing Mars. These antenna's have dimensions of 94 x 94 x 9.6 mm. The solar array consists of six individual solar panels, hinges and an actuator drive system. Each panel consists of individual cells, diodes and connectors. This entire system has been determined in Chapter 10 and is able to be stowed next to both of the 340.5 x 200 mm sides of the cubesat as illustrated in Figure 12.5. The panels are stowed such that the patch antenna's fit underneath them. The entire array is also free to rotate about two axis when deployed such that they can be utilised as efficient as possible during the entire mission. Finally some components of the AODCS, as designed in Chapter 6 are marked in sky-blue. The oval shaped components are the sun sensors and the circles just sticking out of the hull are the star trackers.

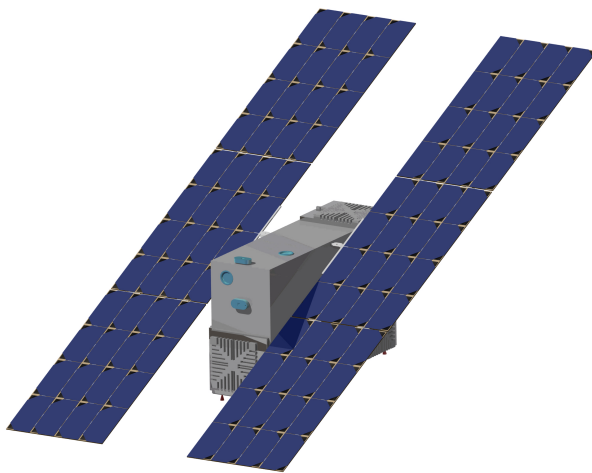


Figure 12.4: External configuration, solar panels deployed

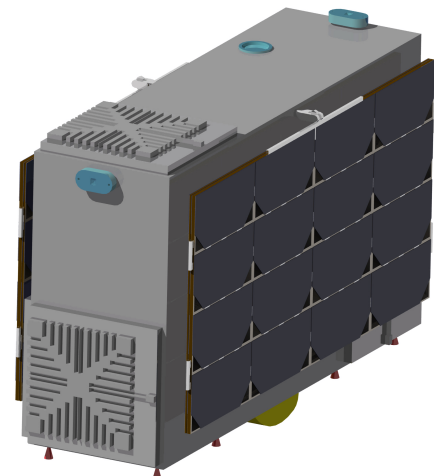


Figure 12.5: External configuration, solar panels stowed

12.2.2. Internal Configuration

Also the internal configuration of the cubesat has been designed. In Figure 12.6 and Figure 12.7 all the subsystems have been marked with a different colour. Within this section, this colour will be used in the documentation to show the location of the respective subsystem in the figures. For illustration purposes the solar panels and a set of side panels have been hidden from view in both figures.

Within the aluminium bus and radiation shield, which were already discussed in subsection 12.2.1, the main frame (orange) is placed. This frame accounts for the structural integrity of the cubesat and connects all components to the bus. The frame includes two stacking units, found in the upper right and left corners of the cubesat in Figure 12.6. The final inner design has primarily been driven by the size of some components (SPEX + propulsion) and the ability of these components to point out of the fuselage. Both propulsion units are just over 1u in height, which allows for unitary stacking above them. SPEX however has really exotic dimensions, especially with the detector on top of it.

Therefore in the middle 2u it has not been possible to stack other components except for a star tracker.

Both propulsion units are included (red) and have dimensions of approximately $100\text{ mm} \times 100\text{ mm} \times 110\text{ mm}$. In the middle of the cubesat interior the main payload (yellow) can be found. This consists of SPEX with a detector on top. There is a 1 cm gap left between the two on purpose due to possible heating effects of the detector on SPEX. The inner power subsystem (dark blue) consists of two large batteries which can be found on the right lower stack, the actuator of the panels (top middle) and an ACU and PDU which both can be found on the lower left stack. The transceiver and processor units (light green) can be found on the same motherboard (dark green) as the PDU and ACU at the bottom of the left stacking unit. Finally, the AODCS (sky-blue) consists of three star trackers, which all point out of the bus in different directions, four reaction wheels, placed about different axis and an IMU. All these components can be found on the upper stacks at both sides of the cubesat. It should be noted that one star tracker is placed directly on top of SPEX to obtain a pointing efficiency which is as high as possible.

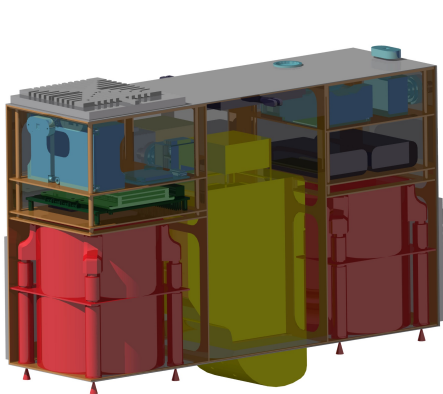


Figure 12.6: Internal configuration

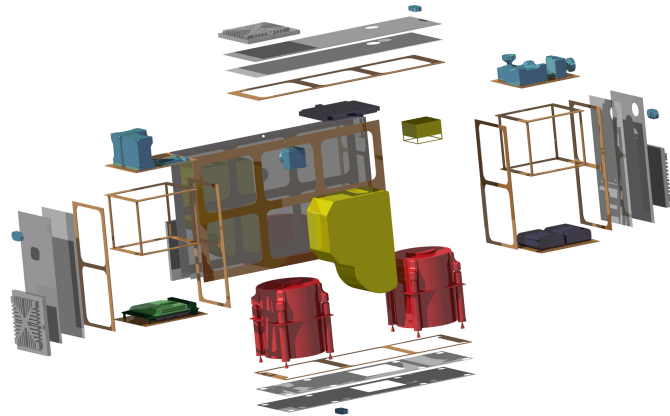
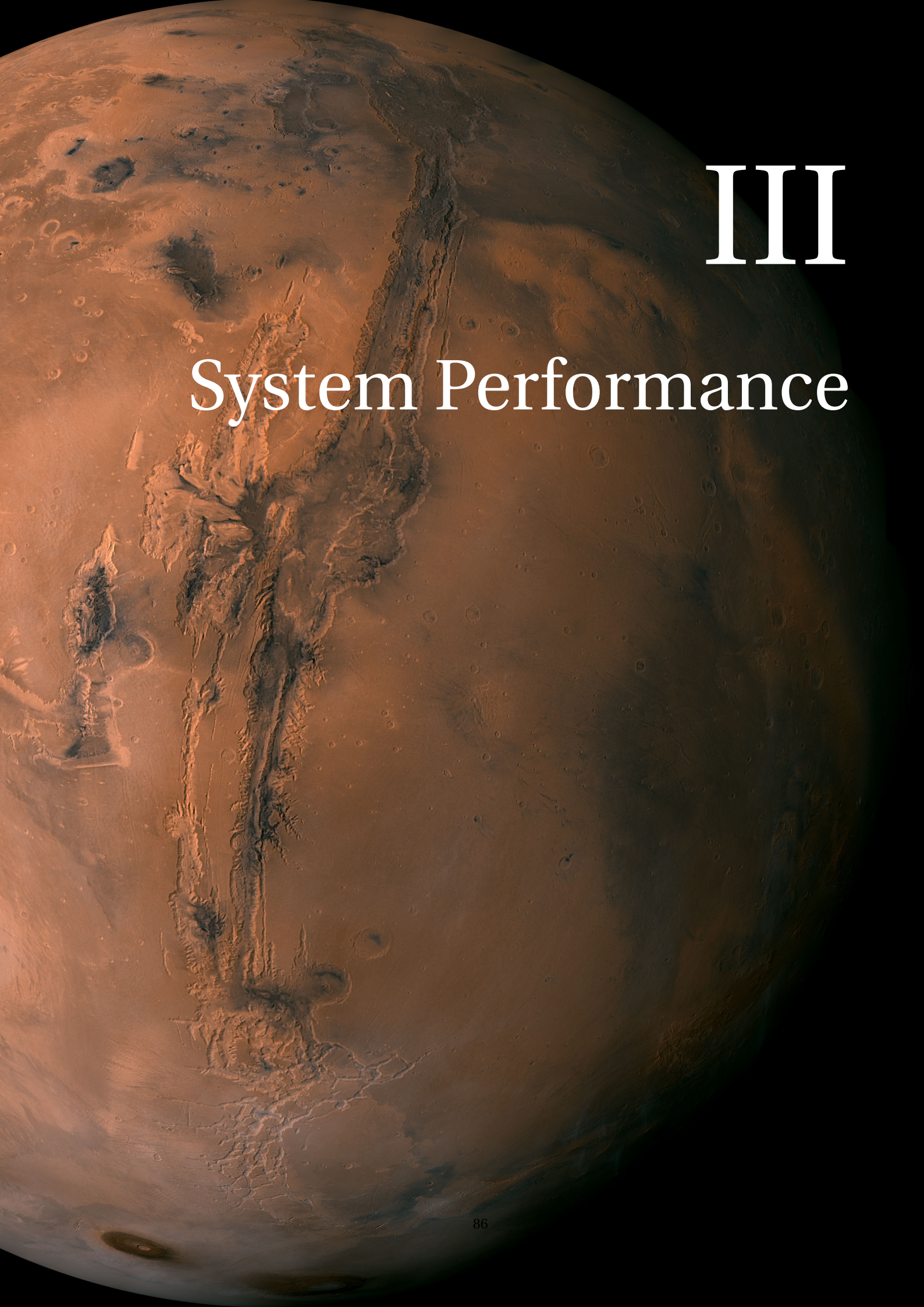


Figure 12.7: Exploded view



III

System Performance

13

Technical Budgets

In this chapter, two main budgets formed by the subsystems of the MICRO mission will be described. Section 13.1 will give an overview of the mass budget while Section 13.2 will describe the volume budget. In Section 13.3, the influence of every subsystem on the budget will be analysed.

The seven subsystems described in Part II have been taken into consideration for the budget estimations. One has to keep in mind that the structure subsystem includes the frame and shielding effect.

13.1. Mass Budget

From the different subsystems forming the cubesat, a final mass budget has been determined. It is important to notice that the propellant needed for the mission is included within the mass budget for the propulsion subsystem. In Table 13.1, the values estimated in an initial phase of the design [AFH⁺16] and the updated values, namely the final estimations, are listed.

Table 13.1: The mass budget resulting from all subsystem designs

Value	Payload	Propulsion	Power	AODCS	Structure	Thermal	TC	CDH	Total	Unit
Initial Estimation	2000	1100	650	264	1200	170	420	100	5904	[g]
Final Estimation	941	4800	1976.64	1150	982.7	52.9	124.5	150	10177.74	[g]

It can be observed that the propulsion, power, AODCS and CDH subsystems, representing 50 % of the total subsystems, are heavier than expected, leading to an increase of 72 % of the expected total mass. However, the final mass found of 10.178 kg complies with the requirement [OREQ-M-EB1, Ch. 15]. Indeed, the maximum mass defined for the nano-satellite is defined as 12 kg, which gives a contingency factor of 1.18¹.

13.2. Volume Budget

From all the subsystem designs, the final volume budgets for all the missions can be determined. It represents one of the most crucial budget, indeed, as a 6U cubesat is volume constraint, i.e. 1U= 10x10x11.4cm³. Furthermore, the volume budget and the sizing of each subsystem is important for the internal and external lay-out of the cubesat. The corresponding budget for the MICRO mission can be found in Table 13.2.

Table 13.2: The volume budget resulting from all subsystem designs

Value	Payload	Propulsion	Power	AODCS	Structure	Thermal	TC	CDH	Total	Unit
Initial Estimation	1101	1134	420	270	500	n.a.	252	100	3777	[cm ³]
Final Estimation	1141.7	2280	219.1	590	230.2	6.2	16.9	20	4504.13	[cm ³]

As for the mass budget, several changes from the initial estimations can be seen in Table 13.2. It can be observed that some subsystems take up more volume than expected and some decrease by a factor of 15. Besides, at an initial stage of the design [AFH⁺16], it was not possible to get a proper volume estimation of the thermal subsystem. As shown in Table 13.2, the final volume of 4504.13 cm³ respects the volume constraint of the 6U cubesat. Indeed, the total volume found represents ± 53 % of the allowed volume of a 6U, which provides contingency for the future development and the cabling for MICRO, that was not determined at this stage of the design.

¹Nano/Microsatellites market assessment: http://www.sei.aero/eng/papers/uploads/archive/SpaceWorks_Nano_Microsatellite_Market_Assessment_January_2014.pdf [cited 23 June 2016]

13.3. Comparison

In this section, the influence of every subsystem on the budgets analysed in Sections 13.1 and 13.2 will be analysed and the critical components for the design will be pointed.

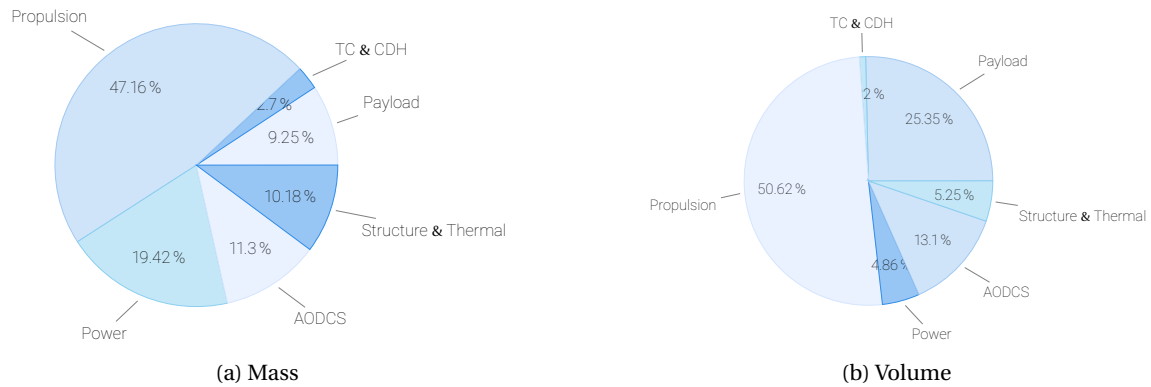


Figure 13.1: Mass and volume breakdown: subsystems

the left diagram representing the mass distribution while the right represents the volume distribution, As can be seen in the diagrams of Figure 13.1, the propulsion subsystem can be distinguished as the most critical subsystem as it represents 47.16 % and 50.62 % of the cubesat mass and volume, respectively. The structure part, thermal part and the AODCS have nearly the same influence on both budgets. While, the payload subsystem is light (9.25 %) and requires a considerable volume (25.35 %). The discrepancy in volume/mass for the power subsystem is explained by the fact that the mass includes the solar panels and the electronics inside the cubesat. While, the volume budget studied is only considering the inside volume of the cubesat; and therefore, not the solar panels system volume. Indeed, the purpose of this budget is to monitor the space inside the structure. The volume budget of the cubesat outside determined by the 6U frame, antennae and solar panels, has been explained in Chapter 12, as it is a key driver for selecting the deployer.

13.4. ΔV Budget

In this section, the ΔV budget will be detailed. Determining the total ΔV for this mission is a key driver for designing the propulsion subsystem, i.e. the I_{sp} available should allow a certain ΔV . Table 13.3 summarises the ΔV values, that have been determined in Chapters 5 and 6.

Table 13.3: ΔV budget for MICRO mission

Value	Orbit Insertion	EOL Manoeuvre	Orbit Maintenance	Attitude Control	Total	Unit
First Estimation	106	11	0	17	134	[m s^{-1}]
Final Estimation	121	30	0	19	170	[m s^{-1}]

Based on the values found in Table 13.3, an increase of 27 % of the initial total ΔV can be seen. As explained in Chapter 7, the propulsion selected has an exhaust velocity of 248 m s^{-1} , which results in 38.5 % contingency for future development.

14

Cost Budget

For the MICRO mission, ten million € have been allocated, as specified by the requirement [CREQ-M-C1, Ch. 15]. In order to satisfy this requirement, the cost budget had to be studied meticulously throughout the design. In this chapter, the cost budget of this mission will be described. Section 14.1 will give a cost overview of the different components. In Section 14.2, a study of the cost budget will be carried out, using the total cost budget described in Section 14.1.

14.1. Cost Description

In Table 14.1, the total cost of the mission is shown as well as the contribution of each part into the total one. It is expected that the MICRO mission will reach a total cost of 7841 k€, which meets the requirement CREQ-M-C1 and allows room for future development with a contingency cost of 2159 k€.

Table 14.1: Mission costs

	Bus And Payload	Development	Operation	Launch	Sustainability	Total	Unit
Cost	5852	1086	380	207	316	7841	[k€]

As can be seen in Table 14.1, the cost of a mission can be described into five different categories:

- *Bus and Payload cost:*
This cost regroups all the costs of the subsystems and the cabling. A detailed overview of the cost of each subsystems can be seen in Table 14.2.

Table 14.2: Bus and payload costs

Bus And Payload Cost										
	Payload	Propulsion	Power	AODCS	Thermal	Structure	TC	CDH	Cabling	Unit
Cost	5200	105	171	220	6	10	67	58	15	[k€]

- *Development cost:*
It represents the cost necessary for the project since the design starts until the beginning of operation. In this category, four subcategories have been distinguished, as shown in Table 14.3. The administration includes the costs related to the design approval (i.e. space proven component for the component that have to be designed), the channel purchase, etc. The personnel regroups the total cost of the employees working on the SPEX. Two subcategories for the personnel have been distinguished. The Personnel TU cost is for the employees of Delft University of Technology working on the SPEX. The low cost is mainly due to the active participation of the students for the assembly, as explained in Chapter 18. While the Personnel Other cost is dedicated for hiring experts from outside TUDelft environment, who would be needed for specific part of the project process. The facilities subcategory includes the material needed for the integration and assembly of the cubesat, and the use of specific testing material and the clean rooms. The last subcategory considered in the development cost is the transport. It includes the transportation of the components to the assembly place and the one necessary to reach the launch place.

- *Operation cost:*

As described by its name, the operation cost describes the cost of the operations, namely the mission after the launch. In this category, two main parts have been considered, first, the data analysis which is the cost required for processing the data on the ground station. This cost can be translated into the rent of the ground stations equipment and the systems required. The personnel needed to analyse the data has also been considered as the second main part.

Table 14.3: Development and operation costs

	Development Cost					Operation Cost		Cost
	Administration	Personnel TU	Personnel Other	Facilities	Transport	Personnel	Data Ana.	
Cost	450	256	120	200	60	280	100	[k€]

- *Launch cost:*

As explained in Chapter 5, the cubesat will be piggyback into an initial orbit. Therefore, the launch cost includes the launcher and the deployer, which has been explained in Chapter 12. As can be seen in Table 14.3, the launcher selected, GSLV III, allows to reach Mars at a extremely low cost compared to the market prices.

- *Sustainability cost:*

As can be seen in Table 14.4, it represents the cost needed for the development of the sustainable strategy, explained in Chapter 20. Indeed, it has been decided to plant trees in the world based on the carbone dioxide emission created by the MICRO mission on Earth.

Table 14.4: Launch costs

	Launch Cost		Sustainability Cost	Cost
	Launcher	Deployer	Treelogical	
Cost	132	75	316	[k€]

14.2. Cost Analysis

In this section, the cost evolution throughout the project time will be analysed. It will consist of the planned value of the project and will be a basis value for the project management. Indeed, during the next steps of the project progresses, the actual cost and earned value should be added to Figure 14.1, in order to see how well the project. For this graph, the different phases of the mission explained in Section 18.4 have been delimited by dotted lines. Furthermore, two more phases, than the ones from Section 18.4, can be distinguished in the Figure 14.1 which correspond to the mission lifetime once launched and the sustainability strategy of planting trees, corresponding to phases 5 and 6, respectively.

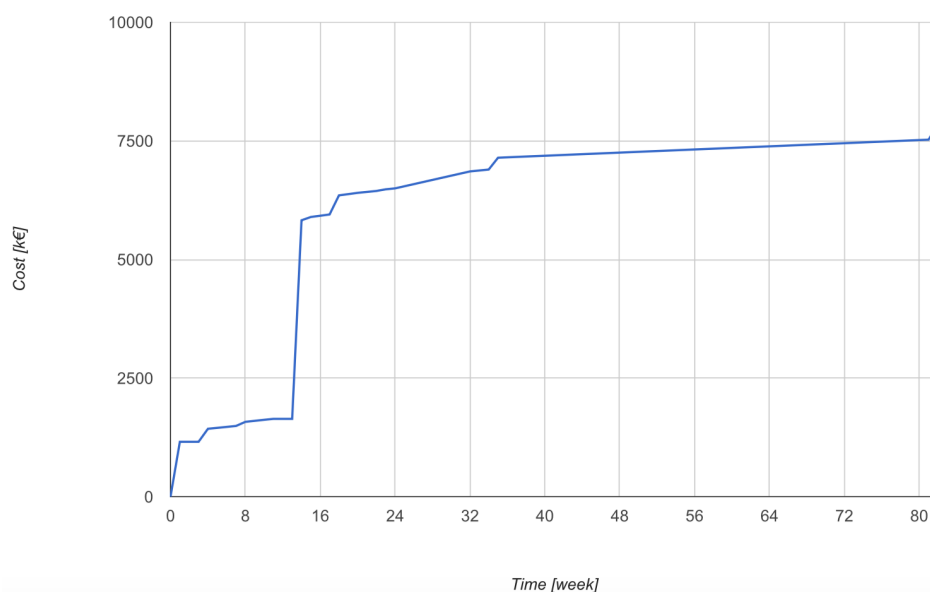


Figure 14.1: Planned value of the MICRO mission

15

Requirements

Requirements are a very important part of a space mission design. In this chapter, the requirements for the MICRO mission will be listed, in Section 15.1. Together with the requirements, the compliance matrices are given. Section 15.2 will give an overview of the methods that are generally used to verify requirements. Finally, in Section 15.3 an analysis of the components used for the design of the MICRO cubesat will be done, to determine which components need to undergo verification.

15.1. Requirements and Compliance Matrices

In this section, the requirements for the cubesat mission will be described. A main division of the requirements has been done producing three parts, namely the functional, operational and constraints requirements. Functional requirements describe how well the system must perform, whereas the operational ones describe the way the system must operate and its interactions with the users. Constraints requirements, on the other hand, will put the emphasis on the limits on the cost, schedule and implementation techniques [WL10, p.16].

According to requirement standards [ECS09a], each requirement shall be given a distinct identifier (ID). To comply with these standards, requirements of the MICRO mission are given an ID based on the following template:

$$\underbrace{\text{XREQ}}_{\text{type}} - \underbrace{\text{YY}}_{\text{depth}} - \underbrace{\text{ZZ}}_{\text{subsystem}} \underbrace{\text{N.M}}_{\text{number}}$$

Character X represents the type of requirement. It can be either F, O or C, representing functional, operational or constraint requirements, respectively. Furthermore, the depth character, namely YY, describes to which level the requirement applies. These letters can be either M, S or SS, which correspond to mission, system or subsystem levels. Then, the ZZ characters are substituted by the acronym of the subsystem, which were already introduced in the list of abbreviations. Finally, the number of the requirement is given at the place of N.M. The number in place of M is optional, and is only specified in case the same requirement applies to more control operating modes.

In the following pages, the functional, operational and constraint requirements will be given, together with their compliance. With the use of the phrase “during all control operating modes” it is meant during all the control operating modes in which the subsystem is active.

Finally, validation of requirements is not going to be treated in this report, since all the requirements were checked to agree with all the VALID criteria [AFH⁺16].

15.2. Verification Methods

Verification has the purpose to demonstrate that the product being inspected meets the specified requirements. Verification is performed by one or more of the processes listed below [ECS09b, Cer16, Gue08], as it was already explained in the Midterm Report [AFH⁺16].

- **Testing and Demonstration**

Testing and demonstration consist of measuring the performance of the product under conditions that simulate the mission environment.

- **Analysis, Similarity and Simulation**

Analysis, similarity and simulation were put under the same category of verification methods, since they are all based on the same principle. The latter being the execution of theoretical or empirical evaluations, to conclude whether the design meets the specified criteria. In particular, the similarity analysis have the role of providing evidence that an already qualified product fulfils the requirements.

- **Review of Design**

ROD consists of unambiguously proving that the requirements are met by using approved documents such as technical reports and engineering drawings.

- **Inspection**

The final verification method is inspection. This procedure comprises the visual determination of the physical characteristics of the component. The characteristics that are usually taken into consideration are physical conditions, hardware conformance to drawings, constructional features, et cetera.

These methods are in the order that usually provides more confidence in the results. For instance, in case a requirement is verified only by analysis or ROD, a risk assessment should be organised to determine the severity of the impact of this requirement on the mission [ECS09b, p.17]. This evaluation has to be reported in the System Verification Plan, or SVP, along with the specifications of all the procedures scheduled [WL11, p.719]. As it will be explained in Section 15.3, these tests not need to be performed only on non-off-the-shelf components

15.3. Cubesat Components

The verification of COTS is done during their development. The COTS components used for the design of the cubesat are listed in Table 15.1. The TRL of each component is also shown. For components whose TRL could not be found (or was not given in the specifications), it is assumed to be at TRL 8 or higher, since they are already in the market. In addition, for components with a TRL of 6 or more, it is known that they have already been tested¹, thus they do not have to go through the verification and validation process.

Table 15.1: Components used for the design of MICRO

Subsystem	Component	Name	TRL
AODCS	Star tracker	HT-ST-200	9
	Sun sensor	nanoSSOC-A60	9
	IMU	MASIMU02	9
	Reaction wheel	HT-RW400.30	6
	Camera	HT-IM-200	9
Bus	Radiation shielding	Tantalum	9
	Structural frame	Custom designed frame	2
	Bus panels	Aluminium 7075-T6 shear panels	2
CDH	On-board computer	HT-CP400.85	7
	Motherboard	NanoDock DMC-3	9
Deployer	Deployer	CSD-6U	9
EPS	Batteries	Saft MP174565 Integration	9
	Solar array drive	Honeybee cubesat SADA	8
	Array Conditioning Unit	GOM Space P60 ACU	8
	Power Distribution Unit	GOM Space P60 PDU	8
	CICs	Sol Aero Tech IMM4J	7
Payload	Instrument	SPEX	6
Propulsion	Thruster module	MPS130	6
T&C	Transceiver	NanoCom AX100	7
	Microstrip patch antenna	n.a.	3

As can be seen in Table 15.1, all the components have a TRL higher or equal to 6, except for three, which are going to be custom designed. Verification and validation of these component are treated in their respective chapters. For the components with TRL 6+, it means that, according to the definitions of TRL, they are ready to be used in space. However, it is likely that before assembly and integration starts (scheduled for August 2018, as clarified in Chapter 23), most of the components will have reached a higher TRL level. This is true except for SPEX, since so far this mission is its only space application. Therefore, this mission (if successfully performed) will raise the TRL of SPEX to 7.

¹NASA TRL: https://esto.nasa.gov/files/trl_definitions.pdf [cited 6 June 2016]

²NASA Mission Design & Planning: <https://goo.gl/HVLV5a> [cited 13 June 2016]

³UN Office for Outer Space Affairs: <http://goo.gl/4jDqum> [cited 22 June 2016]

⁴Dutch Laws Governing Space Activities: <http://goo.gl/Hvk2zC> [cited 22 June 2016]

Table 15.2: Functional requirements I

Class	ID	Requirement	Reference	Compliance
AODCS	FREQ-SS-AO1	The attitude control of the spacecraft shall be provided by the ADCS during all control modes.	6.5	✓
	FREQ-SS-AO2	The attitude determination of the spacecraft shall be provided by the ADCS during all the control modes.	6.5	✓
	FREQ-SS-AO3	The pointing accuracy shall be at least 360 arcsec with 3σ .	4.1.2, 6.1.2	✓
	FREQ-SS-AO4	The ADCS design shall conform to the total lifetime covering expected combinations of the mission phases.	6.5	✓
	FREQ-SS-AO5	The ADCS shall be able to counteract the tumbling of the S/C after release from the host satellite.	6.1.2	✓
	FREQ-SS-AO6	The attitude determination shall be done in real time by the spacecraft.	6.3	✓
Bus	FREQ-SS-AO7	The ODS shall be able to determine the location of the spacecraft with an accuracy of at least 7 km during all control modes.	4.1.2, 5.2, 6.2.2	✓
	FREQ-SS-ST1	The spacecraft shall not allow the use of pyrotechnics.	12.1.2	✓
	FREQ-SS-ST2	The bus shall fit into the deployment mechanism as defined in [Cor15b].	[Cor15b]	✓
	FREQ-SS-ST3	The bus structure shall not yield under the launch limit loads.	11.1.1	✓
	FREQ-SS-ST4.1	The bus structure shall have an axial natural frequency higher than 25 Hz.	[Spa15]	✓
	FREQ-SS-ST4.2	The bus structure shall have a lateral natural frequency higher than 10 Hz.	[Spa15]	✓
	FREQ-SS-ST5	The cubesat bus shall protect all internal components against solar radiation.	11.3.2	✓
	FREQ-SS-ST6	The deployer tabs shall be 100% continuous 7075-T7 aluminium alloy.	12.1.2	✓
	FREQ-SS-ST7	The deployer tabs shall run the entire length of the cubesat.	12.1.2	✓
	FREQ-SS-ST8	Dimensions and tolerances defined in [Cor15b] shall be maintained under all temperatures.	[Cor15b]	✓
CDH	FREQ-SS-ST9	The maximum dimensions stated in [Cor15b] are the payload's dynamic envelope and shall include all load cases.	[Cor15b]	✓
	FREQ-SS-CD1	Ground control shall be able to command the entry into safe mode [ECS13, p.18].	8.1	✓
	FREQ-SS-CD2	Ground control shall be able to command the exit from safe mode [ECS13, p.18].	8.1	✓
	FREQ-SS-CD3	TM shall be able to monitor the energy resources during all the control operating modes [ECS08a, p.19].	8.1	✓
	FREQ-SS-CD4	TM shall be able to monitor the source temperatures during all the control operating modes [ECS08a, p.19].	8.1	✓
	FREQ-SS-CD5	The spacecraft subsystems TM shall allow to locate failures impacting the mission performance and reliability [ECS08a, p.19].	8.1	✓
	FREQ-SS-CD6	The CDH subsystem shall collect the telemetry data from all subsystems.	8.1	✓
	FREQ-SS-CD7	The CDH subsystem shall store the payload data before transmission to the MRO.	8.1	✓
	FREQ-SS-CD8	The CDH subsystem shall process the payload data on board.	8.1	✓
	FREQ-SS-CD9	The CDH subsystem shall provide a data interface between the subsystems in the cubesat.	8.1	✓
EPS	FREQ-SS-CD10	The CDH subsystem shall provide the time.	8.1	✓
	FREQ-SS-CD11	The CDH shall distribute commands to the subsystems.	8.1	✓
	FREQ-SS-CD12	The CDH shall process the AODCS sensor data to provide attitude and location information.	8.1	✓
	FREQ-SS-E1	The EPS shall power all subsystems during respective control operating modes.	10.2	✓
	FREQ-SS-E2	The EPS shall store at least 13.91 Wh for operation during the eclipse phase.	10.4	✓
	FREQ-SS-E3	The EPS shall generate at least 24.41 W at EOL.	10.3.1	✓
	FREQ-SS-E4	The solar cells shall supply at least EOL power of 127.66 W m^{-2} .	10.3.1	✓
	FREQ-SS-E5.1	The interface of the EPS shall regulate the power supplied to the subsystems.	10.5	✓
	FREQ-SS-E5.2	The interface of the EPS shall regulate the voltage supplied to the subsystems.	10.5	✓
	FREQ-SS-E5.3	The interface of the EPS shall regulate the current supplied to the subsystems.	10.5	✓
EPS	FREQ-SS-E6.1	The EPS shall provide a peak power of 14.34 W during the sunlit phase of the mission.	10.2	✓
	FREQ-SS-E6.2	The EPS shall provide a peak power of 14.34 W during the eclipse phase of the mission.	10.2	✓

Table 15.3: Functional requirements II

Class	ID	Requirement	Reference	Compliance
EPS	FREQ-SS-E7	The EPS shall not interfere with the other subsystems and payload.	10.5 [ECS08a, p.7] 10.4 10.3.1 10.2	✓
	FREQ-SS-E8	The EPS shall be rechargeable.		✓
	FREQ-SS-E9	The EPS shall be redundant.		✓
	FREQ-SS-E10	The EPS shall conform to mechanical loads during all control operating modes.		✓
	FREQ-SS-E11	The EPS design shall conform to the total lifetime covering expected combinations of the mission phases.		✓
Payload	FREQ-SS-PL1	The payload shall measure the flux, DoLP and AoLP simultaneously using spectral modulation encoder technology.	4.1 4.1 4.1 4.1 4.1 4.1	✓
	FREQ-SS-PL2	The payload shall measure the spectral range from at least 400 to 800 nm.		✓
	FREQ-SS-PL3	The payload shall have a spectral resolution of at least 20 nm.		✓
	FREQ-SS-PL4	The payload shall have at least 5 downward viewing apertures for ground measurements.		✓
	FREQ-SS-PL5	The payload shall have at least 2 limb-viewing apertures to analyse clouds.		✓
	FREQ-SS-PL6	The payload shall provide knowledge on the aerosol microphysical properties on mars.		✓
Propulsion	FREQ-SS-PR1	The propulsion subsystem shall provide a ΔV of 120.9 m s^{-1} for orbit insertion.	7.2 7.2 7.2 7.2 7.2 7.2 7.2	✓
	FREQ-SS-PR2	The propulsion subsystem shall provide a ΔV of 18.9 m s^{-1} for attitude control.		✓
	FREQ-SS-PR3	The propulsion subsystem shall provide a ΔV of 30 m s^{-1} for end-of-life manoeuvre.		✓
	FREQ-SS-PR4	The propulsion subsystem shall not exceed power of 10 W.		✓
	FREQ-SS-PR5	The propulsion subsystem shall have maximum mass of 55 % of the cubesat 30 m s^{-1} for end-of-life manoeuvre.		✓
	FREQ-SS-PR6	The propulsion subsystem shall provide reaction control system to the spacecraft.		✓
	FREQ-SS-PR7	The propulsion subsystem shall have a maximum volume of 2.4U.		✓
T&C	FREQ-SS-TC1	The output voltage of the LCL within the nominal range of $<4b> V$ shall be confirmed by the ON/OFF status of the LCL.	[ECS16, p.28], 9.3.3 [ECS16, p.28], 9.3.2 [ECS16, p.28], 9.3.2 [ECS16, p.42], 9.3.2 [ECS08a, p.19], 9.3.6 [ECS08a, p.19], 9.5 [ECS08a, p.19], 9.3.3 [ECS08a, p.19], 9.3.3 9.2.1 9.2.1 [LWH09, p.397], 9.2.1 9.3.4 9.2.2	✓
	FREQ-SS-TC2	The current telemetry shall be provided by the LCL.		✓
	FREQ-SS-TC3	The full scale TM current shall be at least equal to the maximum limited LCL current.		✓
	FREQ-SS-TC4	The current TM offset shall be at least equal to $\pm 4\%$ of the full scale value in safe mode.		✓
	FREQ-SS-TC5	The spacecraft subsystems TM shall allow to retrace all the reconfigurable elements.		✓
	FREQ-SS-TC6	The spacecraft subsystems TM shall allow to locate failures impacting the mission performance and reliability.		✓
	FREQ-SS-TC7	TM shall be able to monitor the energy resources during all the control operating modes.		✓
	FREQ-SS-TC8	TM shall be able to monitor the source temperatures during all the control operating modes.		✓
	FREQ-SS-TC9	The CS shall be operational in every control operating mode.		✓
	FREQ-SS-TC10	The spacecraft shall communicate with the data relay satellite with a UHF.		✓
	FREQ-SS-TC11	The spacecraft shall have a transmitter frequency in the range of 390-450 MHz.		✓
	FREQ-SS-TC12	The EIRP shall be at most in the range of 0.6 – 1.87 dBW.		✓
	FREQ-SS-TC13	The downlink data shall have a rate in the range of a UHF bandwidth, i.e. between 10 – 300 kbits s^{-1} depending on the control operating modes.		✓
TCS	FREQ-SS-TC14	The uplink data shall have a rate of a UHF bandwidth, i.e. between 10 – 300 kbit s^{-1} depending on the control operating modes.	9.2.2	✓
	FREQ-SS-TH1	The TCS shall keep the temperature in the bus within -5 and +27 °C range during the operational phase.	11.2.1 11.2.1 11.2.7 11.2.3 11.2.3 11.2.3	✓
	FREQ-SS-TH2	The TCS shall keep the temperature in the bus within -10 and +30 °C range at all times.		✓
	FREQ-SS-TH3	Heater capabilities of the propulsion system shall be used if the temperature decreases below +7 °C.		✓
	FREQ-SS-TH4	The spacecraft shall be designed for the albedo radiation of Mars.		✓
	FREQ-SS-TH5	The spacecraft shall be designed for infrared radiation of Mars.		✓
	FREQ-SS-TH6	The spacecraft shall be designed for solar radiation.		✓

Table 15.4: Operational requirements

Class	ID	Requirement	Reference	Compliance
Host	OREQ-M-HO1	The S/C shall not interfere with the deployment of the host satellite.	12.1.2	✓
	OREQ-M-HO2	The S/C shall piggyback Mangalyaan 2 in July 2020.	5.1.2	✓
	OREQ-M-HO3	The spacecraft shall be deployed when Mangalyaan 2 is in its nominal mission orbit.	5.1.1, 12.1	✓
EB	OREQ-M-EB1	The spacecraft mass shall be less than 12 kg.	12.1.2	✓
	OREQ-M-EB2	The spacecraft shall not exceed 6U in volume.	[VDW16]	✓
Orbit	OREQ-M-OR1	The spacecraft orbit shall have an altitude range of 300 to 500 km during the nominal mission phase with 3σ .	5.3.3	✓
	OREQ-M-OR2	The spacecraft orbit shall have an inclination between 92.4 deg and 92.6 deg during the nominal mission phase with 3σ .	5.1.3	✓
	OREQ-M-OR3	The spacecraft orbit shall have a right ascension of the ascending node between 226 deg and 228 deg during the nominal mission phase with 3σ .	5.3.2	✓
	OREQ-M-OR4	The spacecraft shall avoid impacting Mars over a time period of 50 years with a probability $< 1 \times 10^{-2}$.	5.4	✓
Verification	OREQ-S-V1	Random vibration testing shall be performed on the structure.	18.3.1	✓
	OREQ-S-V2	Sine vibration shall be performed on the structure during testing.	18.3.1	✓
	OREQ-S-V3	Mechanical shock testing shall be performed on the structure during testing.	18.3.1	✓
	OREQ-S-V4	Fatigue testing shall be performed on the spacecraft structure.	[WL11, p.676]	✓
	OREQ-S-V5	The spacecraft shall be tested using thermal-vacuum techniques.	[WL11, p.676]	✓
	OREQ-S-V6	The spacecraft shall be tested using thermal-cycling techniques.	[WL11, p.676]	✓

Table 15.5: Constraint requirements

Class	ID	Requirement	Reference	Compliance
Safety	CREQ-M-SA1	The cubesat shall not endanger the host mission.	[VDW16]	✓
Cost	CREQ-M-C1	The cost of the project shall not exceed 10 million euros.	[VDW16]	✓
Regul.	CREQ-M-R1	The cubesat shall comply with the regulations on Outer Space from the UN.	3	✓
	CREQ-M-R2	The cubesat shall comply with the regulations from the Dutch Space acts.	4	✓
Schedule	CREQ-M-SC1	The launch of the spacecraft shall take place with the GSLV III rocket of ISRO.	5.1.2	✓
	CREQ-M-SC2	The preliminary design of the S/C shall take no more than 10 weeks.	[VDW16]	✓
	CREQ-M-SC3	The assembly, integration and testing of the S/C shall take no more than 34 weeks.	18.4	✓
	CREQ-M-SC4	The spacecraft shall have a scientific mission duration of at least 109 days.	5.2	✓

Sensitivity Analysis

In this section the sensitivity analysis of the design is discussed. This is done by investigating what the influence is on the parameters of the design once a major sub-system's parameters change. The sensitivity analysis is performed in order to determine the robustness of the design and to establish the degree of feasibility. In Section 16.1 a general sensitivity analysis with respect to power is performed. Afterwards in Section 16.2 the sensitive with respect to the launcher are discussed. Furthermore in Section 16.3 the sensitivity with respect to the orbit insertion is elaborated on. Finally the degree of feasibility and robustness of the design is discussed in Section 16.4.

16.1. Power Sensitivity Analysis

In Figure 16.1 the interconnections of the power influences of all subsystems are presented. This figure shows what subsystems experience a change in parameters due to the change of another subsystem's power requirement. An increase in required power for a certain subsystem will have a slight effect on most other subsystems and a significant effect on the thermal control solution which may require a reiteration of the design concept.

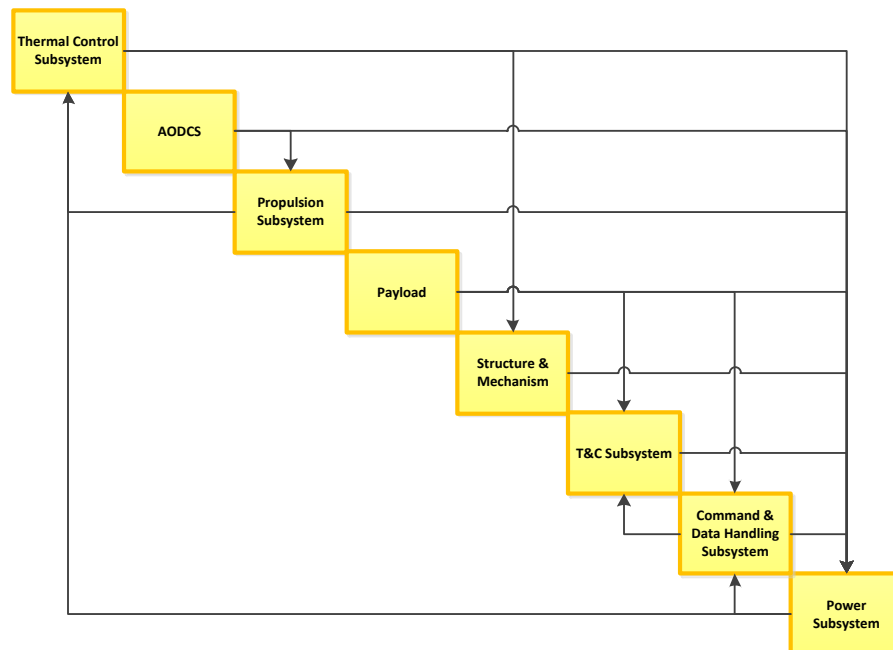


Figure 16.1: Power sensitivity analysis

An increase or decrease in power will have an effect on the thermal control subsystem, since a fluctuation in power dissipation will generate a change in thermal energy inside the spacecraft, consequently increasing or decreasing the temperature. This has a severe impact on the design concept, a change of 1 W in dissipated power causes the equilibrium temperature to change by roughly 5 °C as can be seen in Figure 11.6 in Chapter 11. A different coating, thermal strategy or even active thermal control might be necessary to maintain the desirable temperature range.

16.2. Launch Window Sensitivity

Since the cubesat mission will piggyback with the Mangalyaan 2 mission the design is highly dependent on the host mission. The launcher choice and the orientation of the deployer can effect the mass of the structure of the cubesat since it drives the fundamental frequency of all structures. Apart from that the time of launch also effects the design. The thermal coating as well as the power subsystem are designed for a specific range of incident solar flux. If the cubesat arrives at Mars during a period where the solar intensity is different due to the position of Mars with respect to the Sun, the temperature of the cubesat changes as can be seen in Figure 11.5 in Chapter 11. The temperature does stay within the operational limit irrespective of the distance between Mars and the Sun.

16.3. Host Mission Orbit Altitude

As explained in Subsection 5.1.3, it is assumed that MICRO will be deployed in an altitude range of 200-500 km. Based on reference missions, this is a valid assumption. However, there is no guarantee that this will be the case and it is therefore crucial to investigate what the impact would be on the mission if MICRO reaches an orbit outside of this altitude range.

Firstly, the insertion of MICRO into a lower orbit than 400 km is accounted for in the ΔV -budget. Therefore, this will not negatively impact the mission. However, the insertion of MICRO into a higher orbit can cause several issues regarding the mission success. For SPEX to be able to function, the maximum orbital altitude is 698 km. This is derived from the fact that the outer viewing angles of SPEX are 56 degrees with respect to the nadir of MICRO. If MICRO is at a higher altitude, these outer viewing angles do not reach the surface of Mars anymore. This followed from basic geometry. On top of that, from the nominal mission simulation presented in Subsection 5.3.3, oscillations of the orbit eccentricity can cause the altitude to increase with 73 km at some times. Therefore, the maximum orbit altitude is 625 km to account for these oscillations.

The maximum altitude of 625 km is the maximum altitude of the target orbit for the mission to still be successful. However, the deployment orbit can be higher since the cubesat has a ΔV -budget that used for orbit insertion. The propulsion system can provide a total ΔV of 235 ms^{-1} of which 197 ms^{-1} can be used for that purpose. The highest possible deployment orbit to achieve the highest target orbit is 1300 km, calculated for a Hohmann transfer. If the cubesat is deployed in an orbit with an altitude higher than 1300 km, the cubesat won't be able to reach the maximum possible altitude of 625 km and cannot perform the mission.

Ideally, the final orbit has an altitude of 400 km. In the worst case scenario where MICRO is deployed at an altitude of 1300 km and can only reach the altitude of 625 km, it is important to analyse what impact this has on the orbital characteristics and how this can impact the subsystems and the scientific output of the mission. A comparison between the relevant orbital parameters for the ideal target and the worst case scenario is presented in Table 16.1.

Table 16.1: Altitude sensitivity analysis

Altitude [km]	Period [s]	Eclipse Time [s]	Normalised Eclipse Fraction [–]	Swath Width [km]	Scanning Length [km]
400	7070	1642	1	49	7
625	7710	1720	0.96	76	11

The altitude increase has the biggest influence on the spatial resolution of SPEX. Both the swath width and the scanning length increase proportionally to the altitude increase. This would result in less accurate output data, which is not beneficial for the scientific gain of the mission. A decrease in spatial resolution also results in less data obtain by MICRO and to be sent to MRO. Furthermore, since the eclipse time barely increased with respect to the increase in orbital period, communication with MRO is therefore expected to be less of a constraint to the mission. Additionally, since the altitude of MICRO is higher, a negligible amount of drag will be experienced which eliminates the need for an EOL-manoeuvre.

The increase in altitude also has an impact on the power subsystem. The orbital period and the eclipse time are both increased. However the ratio of eclipse time over sunlit time decreases with increasing altitude. The decreasing ratio indicates that less energy has to be generated by the solar panels for increasing altitudes. Nevertheless, the general increase in eclipse time demands higher energy storage, which results in an increase of battery mass. The reduction in solar panel mass per unit increase in altitude surpasses the gain in battery mass. This results in an overall decrease of EPS mass with increase in altitude. No other EPS component apart from solar panel and batteries are affected by this change. Figure 16.2 illustrates the effect on solar panel and battery mass along with their combined mass for increasing altitude. With respect to the thermal subsystem, some more challenging issues may arise. Since the orbital

period and eclipse time are both increased, the amplitude of the thermal oscillations of MICRO can increase as well, which could result in the need of an active thermal control subsystem.

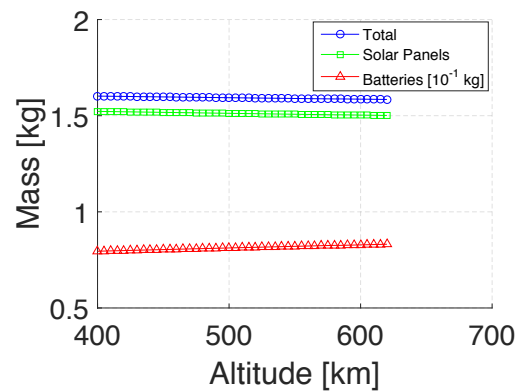


Figure 16.2: EPS mass sensitivity for increase in orbit altitude

It can be concluded that MICRO can still perform its mission when it is deployed into an altitude below 1300 km. However, if deployed at this maximum altitude, the scientific gain of the mission is slightly decreased and the thermal subsystem would require some additional analysis.

16.4. Feasibility and Robustness of the Design

This mission has one main assumption that could undermine the entire feasibility of the design. That assumption is that the cubesat can use the Mangalyaan 2 as a host mission. If the hypothetical piggyback functionality is deemed impossible by the ISRO the MICRO mission cannot be executed. Furthermore if the orbit insertion is not executed properly the scientific gain will decrease. Finally the insertion of the orbit should at least be above 230 km otherwise the cubesat will crash due to atmospheric drag within 109 days.

Spacecraft System Characteristics

In this chapter the system characteristics of MICRO will be described. In Section 17.1 the overall flow diagram for the entire mission is presented, as well as a detailed flow diagram for the operational phase of the mission. This is followed by a functional breakdown diagram which describes the primary function of each subsystem, the payload and the deployer in Section 17.2. Finally, in Section 17.3 an overview of the mission and cubesat specifications is presented.

17.1. Mission Functional Flow Diagram

In this section the functional flow diagram of the mission will be presented and elaborated on. In Figure 17.2 the functional flow diagram for this mission is portrayed. This diagram indicates the logical chronological flow of all actions performed by or on the spacecraft from after the launch onwards. Figure 17.1 describes the operational mission. This is a detailed portrayal of block 3.1.1 of the Figure 17.2. During the operational mission the attitude and thermal control loops will be active constantly and run in parallel with the scientific data acquisition. Furthermore, the cubesat will be able to receive operational commands from the ground station during the operational mission. Finally the processed data and the housekeeping data will be send to the MRO. The functions described in Figure 17.1 will be repeated until the mission is completed.

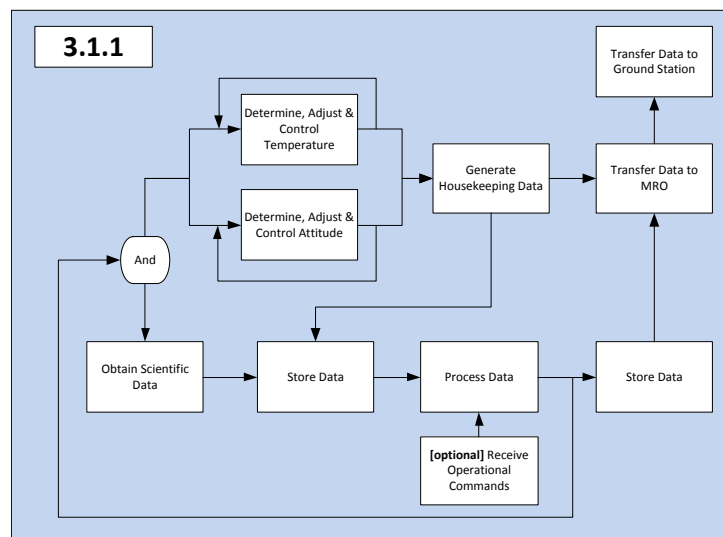


Figure 17.1: Operation flow diagram

In Figure 17.1 the overall mission flow is described. Right after the launch when the host satellite is in Earth's parking orbit an initial system check will be performed by the cubesat to see if it survived the launch. This information will be transferred to the host and then to the ground station. If the cubesat does not show any problems the mission will be executed according to plan, however if it is concluded that the cubesat did not survive the launch it may be decided to separate it from the host and abort the mission. A post-launch system check has a number of advantages: the host will save fuel, the defective cubesat shall not endanger the host and the ground station does not need to wait for nine months to find out the spacecraft did not survive the launch.

When the host is at the right location the cubesat will be ejected. After the separation the cubesat will turn on and the initialisation process will start. The initialisation process will be succeeded by a crucial test. During the test it is determined if the payload is initialised properly, if this is not the case the assessment of the problem is transmitted to the ground station. The ground station will then decide if the problem is crucial or fixable. If no problems occur during the initialisation, initial measurements will be taken. The data will be sent to the MRO which will send the data back to Earth. The ground station analyses the data and determines whether or not the data is acquired correctly. If problems arise with the data acquisition, depending on if its correctable, a degraded mission will be performed or the end-of-life phase is initiated.

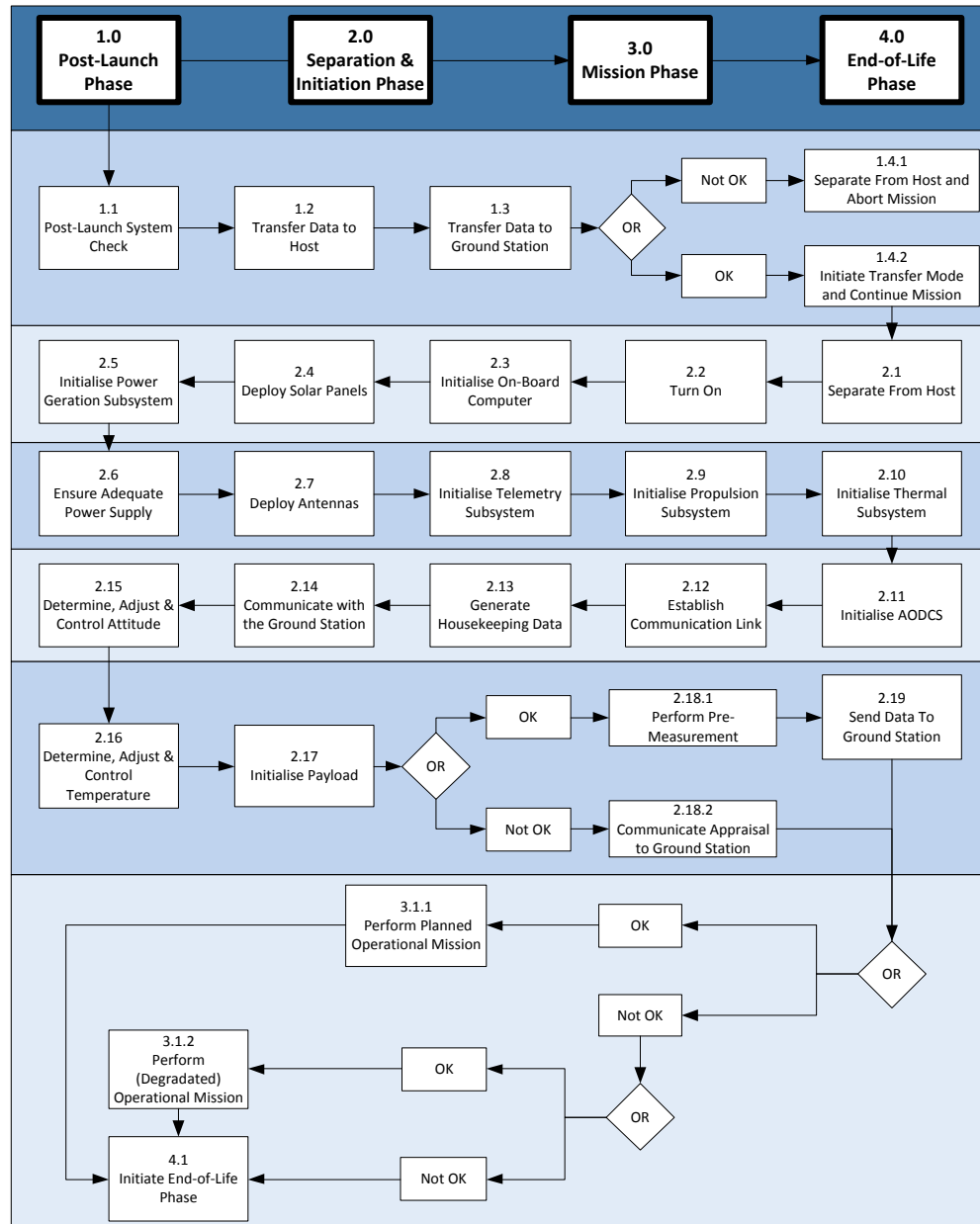


Figure 17.2: Mission flow diagram

17.2. Cubesat Functional Breakdown Diagram

In Figure 17.3 a global overview of the functions of the subsystems and deployer that will be performed during the mission are portrayed. More detailed block diagrams can be found in the corresponding chapters. The first level in the figure defines all subsystems and then break down in the crucial operations to be performed by the respective subsystems.

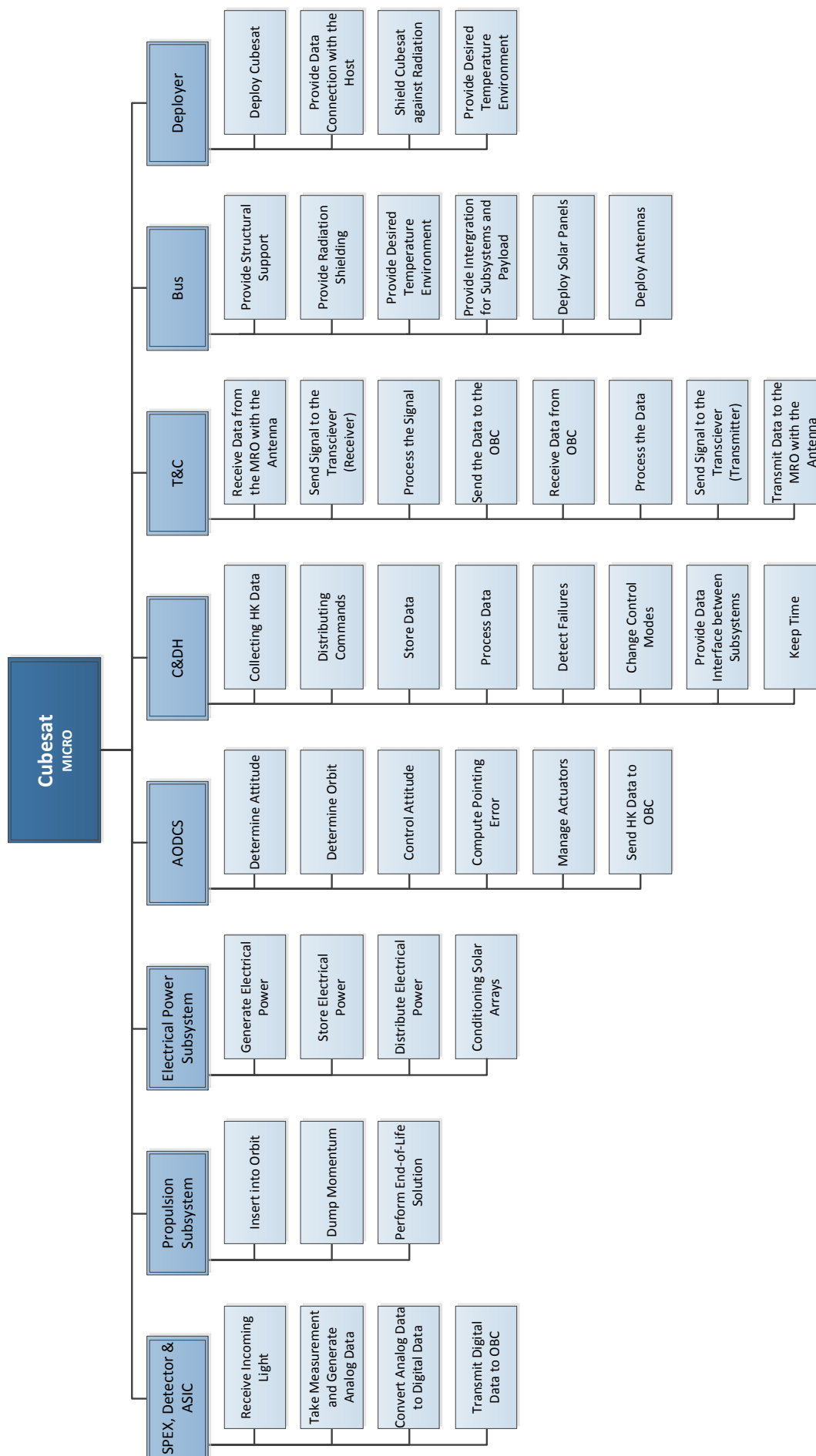


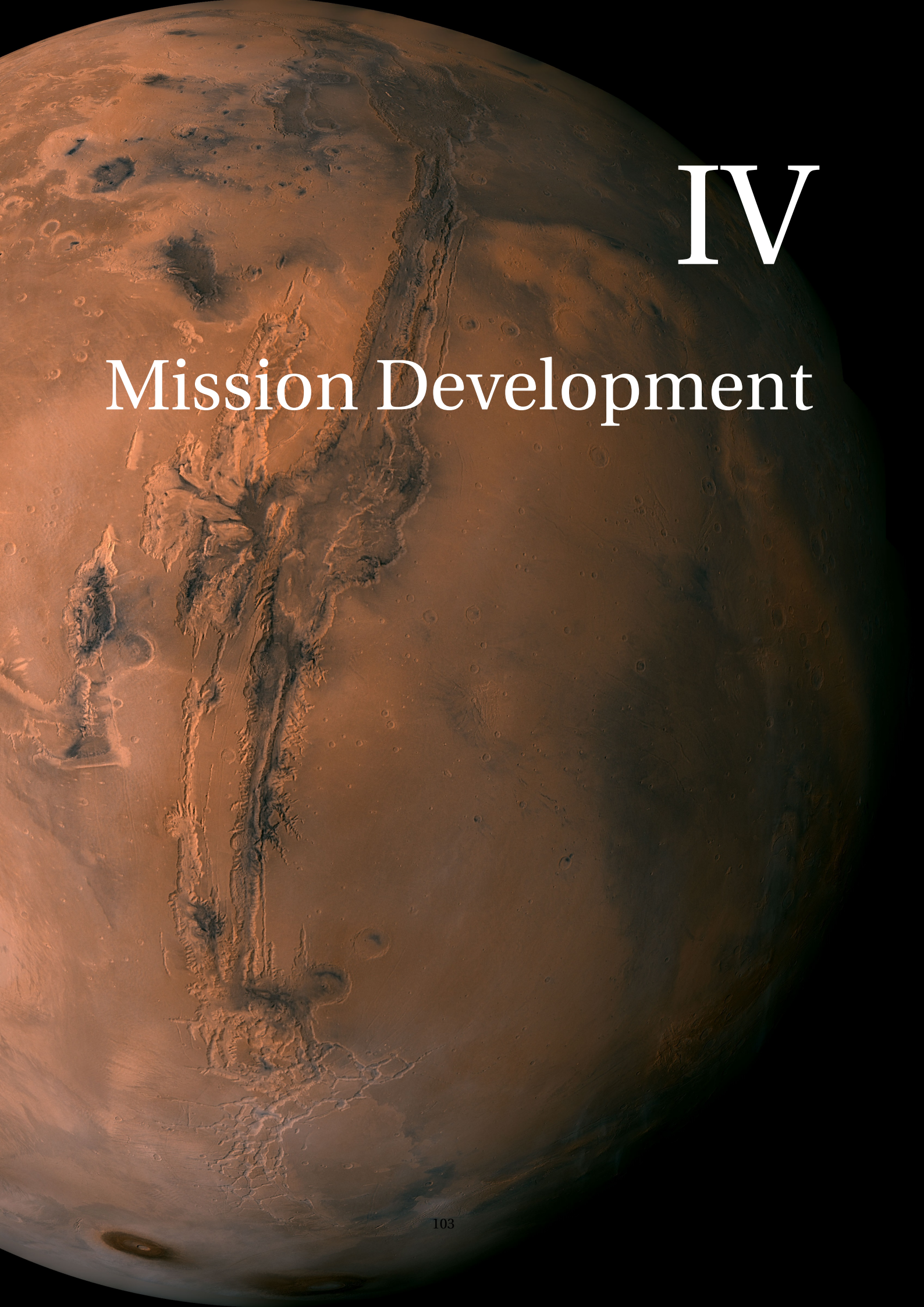
Figure 17.3: Cubesat functional breakdown diagram

17.3. MICRO Specification Sheet

Table 17.1: Specification summary of MICRO satellite

(a) Sheet I			(b) Sheet II		
Property	Value	Unit	Property	Value	Unit
AODCS			EPS 2		
Pointing accuracy	30	[arcsec]	Solar panel mass	1.48	[kg]
Slew tolerance	0.3	[deg s ⁻¹]	Battery mass	0.206	[kg]
Drift	12	[arcsec s ⁻¹]	TC		
Momentum storage	120	[mN m s]	Relay-satellite	MRO	[–]
Rotation rate	5000	[rpm]	Uplink frequency	404.4	[MHz]
ΔV attitude control	18.7	[m s ⁻¹]	Downlink frequency	435.6	[MHz]
Bus			Uplink data rate	2.277	[bit s ⁻¹]
Max Radiation Dose	12.5	[krad]	Downlink data rate	30.273	[kbit s ⁻¹]
CDH			Propulsion		
Processing speed	750	[DMIPS]	Propellant Mass	1	[kg]
RAM	512	[MB]	I_{sp}	240	[s]
Flash memory	512	[MB]	Impulse bits	21321	[cm ³]
EPS 1			Thermal		
Li-ion Battery	2x3.75	[V]	Operation temperature range	+5 to +27	[°C]
Energy capacity	2x18	[Wh]	Survival temperature range	-10 to +30	[°C]

(c) Sheet III		
Property	Value	Unit
Astrodynamics		
Transfer type	piggybacking	[–]
Host mission	Mangalyaan 2	[–]
Launcher	GSLV III	[–]
Expected launch date	July 2020	[–]
Expected arrival date	February 2021	[–]
Nominal mission duration	109	[day]
Minimum total orbit time	167	[year]
Orbit type	quasi-polar Sun-synchronous	[–]
Altitude range	336 – 473	[km]
Inclination	92.5	[deg]
Right ascension	227	[deg]
Solar radiation range	494.00 – 718.76	[W m ⁻²]
Orbital period	7070	[s]
Eclipse duration	1642	[s]
Communication time per orbit	4390	[s]
ΔV orbit insertion	120.9	[m s ⁻¹]
ΔV EOL	30	[m s ⁻¹]
Payload		
Maximum power consumption	1.5	[W]
Total viewing angles	9	[–]
Spectral range	400 – 800	[nm]
Resolution for polarisation	20	[nm]
Resolution for intensity	2	[nm]
FOV along-track	1	[deg]
FOV cross-track	7	[deg]
Viewing directions	0, ± 14 , ± 28 , ± 42 , ± 56	[–]
Sensor type	CMOS	[–]
Resolution	1024x1024	[–]
Raw data size	16778	[kbit]
Processed data size	18.9	[kbit]



IV

Mission Development

Assembly, Integration and Test

In this chapter, the assembly, integration and testing of MICRO will be explained. The assembly of MICRO along with the critical subsystems; scientific payload, UHF patch antennae and solar arrays are detailed in Section 18.1. The components of MICRO are made functional through the integration process, detailed in Section 18.2. Testing and verification of the subsystems are done throughout the assembly and mission phase to perform analysis and provide knowledge on the system, as described in Section 18.3. The logistic diagram for assembly, integration and testing of MICRO is given in Section 18.4.

18.1. Assembly

Assembly is the action in which components are integrated together to form larger subsystems. The assembly of these larger subsystems in turn form the complete cubesat. There are different phases to finalise the assembly phase, this will be described in Subsection 18.1.1. During the assembly phase, cleaning of the components and system is an important aspect of assembly and will be done throughout the whole assembly phase. The cleaning procedure will be described in Subsection 18.1.2. Special attention has to be given to the attachment of the payload, UHF patch antenna and solar arrays as they are not COTS. The assembly of these components are elaborated in Subsections .

18.1.1. Assembly Phases

The assembly phases of a cubesat are described in this subsection from [dC09]. The assembly of components and cleaning can be done in the TU Delft facilities available: cleanroom, mechanical workshop, climate chamber, electronics assembly at EWI and a heat treatment facility at 3ME [BUVH08]. The cleanroom at Space Systems engineering is suitable to do fabrication, assembly, integration and testing in a sterile environment¹. It is recommended to take a photograph of every component before assembly, during assembly, the location of the assembly and the final step in the assembly of each subsystem. Photographs allow for inspection of the internal of the cubesat and aid in the integration process, in order to avoid dismantling [BUVH08]. Assembly of the SPEX payload, UHF patch antennae and solar arrays happen during the test assembly phase.

1. **Structural inspection** to ensure the structures meet engineering specifications and no sharp corners and burrs are present in the TU Delft cleanroom. Specifically the mass property should be measured of all components to ensure the mass budget is not exceeded.
2. **Cleaning of structures** to remove dust and particles in the TU Delft cleanroom. Specific care has to be put on the SPEX instrument, to ensure there are no particles on the lens and detector which can interfere with the measurements.
3. **Fit-check** to ensure compatibility of tools and hardware available in order to assemble all the components.
4. **Test assembly** according to assembly procedures, including harness routing validation and wire length determination. Most of the interfaces and electrical component assembly can be done at the electronics assembly hall at EWI. Programming of the individual subsystems is done at this phase.
5. **Cleaning for flight** of all components in the TU Delft cleanroom.
6. **Harness fit-check** of all pin-out for integration with the CSD.
7. **Flight-like test assembly** by completing the assembly of the satellite and flight harness integration. This phase is performed simultaneously with integration of the subsystems.
8. **Flight assembly** of the complete cubesat including all inspection, full functional testing and staking procedures.

¹ TU Delft Cleanroom: <http://goo.gl/WIOvN3> [cited 9 June 2016]

Payload Assembly

SPEX is the scientific payload of MICRO and is custom made. The payload is situated in between the two thrusters. The SPEX is encased by an aluminium housing, designed to, among others, handle the launch vibrations. Whilst taking scientific measurements, the thrusters will be off. However, to minimise the effect of vibrations due to thrusting, the SPEX instrument should not be attached or touch the propulsion system on either sides. The aluminium housing shall be attached to the structural frame such that the payload is rigidly connected. The SIDECAR ASIC, part of the payload, is attached to the OBC. Cleanliness is of extra importance between the attachment of the SPEX with the HAWAII-H1RG and for the 9 apertures, as impurities could affect the quality of the measurements. The detector should not be directly attached to the SPEX instrument as it might slightly heat up SPEX, it should be decoupled. Therefore a frame, housing the detector has to be assembled such that a buffer of 10 mm is in between the SPEX and the detector.

UHF Patch Antennae Assembly

The microstrip patch antennae are placed on the panels of the cubesat. A bonding compound has to be used for attachment between the patch, dielectric substrate and the aluminium side panel. A few spots are available for applying adhesive between the patch and dielectric substrate. After applying the adhesive bonding, a thin layer of air will be in between the patch and dielectric substrate due to the adhesive thickness. A connection has to be formed between the patch antenna and transceiver, this is done by means of photo etching one end of the feed line onto the dielectric substrate. The feed line then goes along the perimeter of the dielectric substrate and is fed through a coaxial connector. A hole has to be drilled through the aluminium panel. The coaxial connector is fit through the hole and acts as an insulator against conductivity.

Solar Array Assembly

Power required by MICRO cannot be sustained by body mounted solar cells alone. Due to the lower surface area of 6U, deployables are required to cater for optimum power generation requirements. In house building of solar panels results in additional testing and quality assurance procedure. Upon delivering a configuration of the solar panels and the chosen CICs companies like GOM Space² can provide design and integration solutions. Integration and quality testing is conducted by the manufacturers. Solar panels in general consist of four major layers namely CIC, adhesive, wiring and supportive panel. CICs chosen for MICRO consist of one CMX coverglass layer embedded around front metal grids. Followed by four layers of Ga-compound solar cells supported on a metal plate interconnector and substrate. The CICs are welded in desired configuration and with the aid of adhesives like Kapton tape attached onto the panel. The adhesives have an embedded lining of wirings. The panel can be of various configuration and material, in case of MICRO a flat panel of Polyimide glass fiber (50% glass fiber) was chosen. The entire sandwich is integrated by the contractor and tested to meet space qualifications.

18.1.2. Cleaning Procedures

Cleaning of the structure and components is important throughout the whole assembly phase, as dust particles can interfere or possibly harm the cubesat. Therefore a cleaning procedure has to be established and performed to ensure proper assembly. The order is given in Table 18.1 from [dC09]. Cleaning and storage of components is possible at the TU Delft cleanroom facility.

Table 18.1: Cleaning procedure

Order	Process	Tools
1	Blow all surfaces with filtered compressed air.	Filtered air compressor
2	Bathe all objects for 10 minutes. Do not do this for electrical components.	Ultrasonic cleaning bath
3	Clean all surfaces and holes such that no visible contamination are present.	Clean-room wipes swabs
4	Perform final cleaning to remove residual contamination left.	Filtered air compressor
5	Perform visual inspection. Repeat any step until the items are sufficiently clean.	
6	Storage the items in the clean room	

18.2. Integration

In this section, the integration procedures of MICRO are described. Integration is defined as the process by which the cubesat, composed of a collection of assembled components, is made functional through the use of an interconnection medium [dC09]. Integration looks similar to assembly, but is different in the sense that it turns the assembled spacecraft into a functional system by interconnecting all its components. Hence, it is making sure that all the defined interfaces work properly by interconnecting the different components and control hardware through the use

²GOM Space: <http://gomspace.com/index.php?p=products-p110> [cited 16 June 2016]

of a wiring harness. Additionally, system level testing requires a fully integrated cubesat. First, Subsection 18.2.1 describes the facility that will be used to perform the integration procedure. Secondly, Subsection 18.2.2 discusses the size limit of the different components and how this challenge will be handled with respect to integration. Finally, the entire integration procedure is described generally in Subsection 18.2.3.

18.2.1. Facility

All the integration activities to be performed on the cubesat will take place at the cleanroom at Space Systems Engineering [dC09] (Faculty of Aerospace Engineering, TU Delft). It has a cleanliness of 100.000 particles³ and its temperature and humidity are monitored continuously. On top of that, all the standard tooling is available for satellite assembly and integration.

18.2.2. Size Limit

An aspect that needs to be taken into account during system integration is the size limit [Kik07] imposed by the cubesat structure. All the components and subsystems need to fit into the cubesat housing. To achieve this, it is crucial to identify the exact dimensions of the components. Then, they are all fit together into the desired configuration. A CAD-model of the cubesat and its constituent parts helps identify whether everything fits perfectly (see Chapter 12). Additionally, there is volume left over in the housing as a means of contingency. So, when integrating all the subsystems, there is extra room left for cabling, a wiring harness, parts which were not taken into account during the design et cetera. Contingency is a major aspect of the design philosophy to assure a successful mission. When all the subsystems and parts are properly assembled, they can be easily fit into the cubesat housing because of this contingency.

18.2.3. Integration Procedure

The main integration steps are described below in this section. The subsystems are integrated with increasing complexity. Most of the integration can be performed by students with the supervision of experts. The steps are the following and the subsystems are placed in the frame according to the CAD-model of Chapter 12:

1. Integrate the two on-board computers, the power management and control unit and the transceiver with the motherboard. The power management and distribution control unit will be connected to the PJ-unit of the motherboard which is used for on-ground interface testing. Throughout the entire integration phase, external power will be used. The interfaces between these components will be checked first. Diagnostic cabling could also be attached to the motherboard to perform a functional test on the on-board computers.
2. The first complete subsystem to be integrated with the on-board computer is the AODCS since this subsystem is bought in one module with the on-board computer. Therefore, the integration of the on-board computer with the AODCS is expected to go smoothly. It is attached to the cubesat frame and connected to the CAN bus using wiring. Then, the algorithms supplied by the AODCS provider are run to check the functionality of the interface between the on-board computer and the AODCS.
3. Place the thermal sensors in their designated positions onto the frame and connect to the CAN bus using wiring. Activate the sensors and check if the output of the thermal sensors to the on-board computer is accurate by comparing the data with a validated thermometer in the cleanroom.
4. Run thermal sensors and AODCS at the same time to check if on-board computer can handle different data flows at the same time.
5. Attach both propulsion units through wiring to the on-board computer without propellant. This requires a microcontroller to synchronise both propulsion units properly. Activate the units and check if they provide the required output data to the on-board computer. Use dedicated software to manage the AODCS in combination with the propulsion units, the AODCS outputs can be simulated to check whether the right thrusters are activated at the right time to dump momentum. Additionally, the orbit insertion and end-of-life manoeuvres can be simulated and it can be checked whether the propulsion units perform as desired. Note that these functional tests do not include any pressurant or propellant. They check the electronic and data interfaces between the different subsystems.
6. Special attention needs to be paid to the telecommunications and telemetry subsystem because it is custom made and is assembled out of a lot of different components. It is not an off-the shelf module like the AODCS subsystem. The transceiver is already installed in the first step of the integration. However, the installation of the antennas and the other components of the telecommunications subsystem is required. Then, the telecommunication software is integrated to the on-board computer after which the telecommunication software interface with the simulation environment is tested [GH16b]. Now, the interface between the hardware and the on-board computer can be tested. The final step is to generate signals similar to those received by the cubesat

³Cleanroom SSE: <http://tinyurl.com/zfwuwuh> [cited 9 June 2016]

to check the entire telecommunications interfaces and to transmit signals using the transmitter of the subsystem to verify whether these output signals comply with the required standards of MRO.

7. Integrating the SPEX-instrument should be done with caution. It needs to be fixed properly to the cubesat structure. Also, the connection between the detector of SPEX and the on-board computer is via a separate high-speed connection that allows the transmission of high data rates. The interface between the on-board computer, the detector and SPEX is checked by activating the payload and analysing the output data of the instrument.
8. The final integration step is integrating the rest of the power subsystem. Before, all the subsystems were tested and integrated with an external power feed. Now, the actual electronics of the spacecraft with the power supply and storage (distribution is already integrated) are integrated and tested. The solar array drive actuator, solar panels and batteries are installed and their interfaces with the other subsystems and the PMDC are tested and verified. Now, the cubesat is ready for full system testing.

After the full system tests are performed and the cubesat is flight-ready, the cubesat can be integrated into the CSD before launch according to the standards prescribed in [Cor15b] and [Cor16]. The propellant and pressurant can be loaded in the propulsion subsystem as a final integration step. All the integration steps mentioned above are to be performed in a chronological manner. In Figure 18.1, system integration is expected to take 8 weeks, on average one week per integration step. This is expected to be more than enough for all the steps to be performed properly. Furthermore, since students will aid in the intergration of the cubesat, a broad time-frame is required.

18.3. Verification Phases

Verification is carried out throughout the mission lifetime and on different levels. The verification stages (in **bold**) and levels (in *italic*) are defined as [ECS09b, p.19-21]:

- **Qualification** for *elements* and *subsystems*

Qualification is usually applied to single components and complete subsystems. Its goal is to verify that the requirement set for said components are met. In case the actual product to be verified is not available, qualification should be implemented on hardware or software that is representative of the final configuration. Every product is given a category, based on its classification. For commercial off-the-shelf components that have not been modified by the user, the corresponding category is A. This implies that no qualification is necessary. The opposite applies to custom designed or custom made components. In fact, they belong to category D, the lowest possible. These components require a full qualification.

- **Acceptance** for *elements* and *subsystems*

The acceptance stage is also carried out on single elements or whole subsystems. It consists of checking the product for production or assembly errors and making sure that they are ready for operational use. Again, acceptance is conducted on both hardware and software and the same categories apply as for qualification. Thus, COTS components that have not been modified do not need to go through acceptance, as they have already been space proven.

- **Pre-launch** for the *overall system*

Pre-launch is the stage whose aim is to make certain that the product is properly configured and that is ready to function for launch and early operations. The pre-launch verification phase is performed on the overall system, once all the components have been assembled and connected together.

- **In-orbit** for the *overall system*

In-orbit verification occurs after insertion in orbit at Mars, since no transmission to Earth is occurring during the transfer. This final step is to make sure that no degradation took place during launch and the transfer to Mars. This stage concludes once the scientific mission starts. Finally, since this mission is the first space application of the instrument SPEX, this phase will also be a verification that it will work in environmental conditions that cannot be modelled or simulated on the ground.

The pre-launch and in-orbit phases are the ones that focus will be put on in this chapter. They will be described in the following subsections.

18.3.1. Pre-launch Testing Stage

The pre-launch testing stage is performed right after assembly and integration of the spacecraft and concerns both hardware and software elements. Key tests that have to be performed are listed below, in chronological order [WL11, Gue08, BUVH08, Bag10, dC09, GH16a, SC99]. Furthermore, Table 18.2 shows the location where the tests will be performed. The locations for the tests were based on the facilities used for the Delfi-C³ cubesat [BUVH08].

- **Integration Tests**

These tests comprise of short duration tests, which can be performed at various stages of integration, to verify

the proper functioning and installation of the components. These elements include electronics, sensors, actuators, propulsion system, deployable devices and all other subsystems, excluding the payload. The objective of this test is, however not to verify the performance criteria of the single components, since this was already done in the qualification stage.

- **Comprehensive System Tests**

These tests are very similar to the tests performed in the stage above. Nevertheless, now the emphasis is put on the payload. Again, these tests only focus on proper integration and installation, not on verifying the meeting of requirements.

- **Vibration Tests** [OREQ-S-V1, OREQ-S-V2, Ch. 15]

The vibration test simulates the low frequency vibrations caused by the rocket at launch⁴. Since no data about the GSLV III launcher could be found, designing for vibration resistance (as well as acoustic, as described below) has to be done by using reference data from the Falcon 9 rocket, as found in Table 11.1 from Subsection 11.1.1. The test is carried out by generating sinusoidal and random vibrations on each axis and making sure that the natural frequency of the cubesat's structure is not reached.

- **Acoustic Tests**

Acoustic tests are similar to vibration tests, but they try to recreate the vibrations caused by noise generated during launch⁵. Using again Falcon 9 as reference, the design noise is of approximately 131 dB [Spa15, p.25]. Again, the eigenfrequency of the bus structure must not be attained, to avoid dynamic coupling with the launcher.

- **Thermal Vacuum Tests**

Thermal vacuum tests are used to simulate the changes in solar radiation exposure (hence temperature) and vacuum that the cubesat experiences in orbit⁶. The purpose of these tests is to verify that the satellite can still operate normally in vacuum, that thermal expansion does not affect the functioning of the spacecraft and that no material out-gassing or fuel leakages occur.

- **Shock Tests** [OREQ-S-V3, Ch. 15]

Shock tests are meant to simulate the launch phases when large accelerations are generated. Such an example is during stage separations or detachment from the launcher. These shocks are characterised by their broad frequency content and the short duration.

- **Quasi-Static Tests**

Quasi-static tests are vibrational tests at low frequencies far below the eigenfrequencies of the spacecraft. Their purpose is to see how the satellite responds to static loading⁷.

- **EMC Tests**

Electromagnetic compatibility, or EMC, test ensures that the different subsystems do not interfere with each other or the launch vehicle. This is especially important to prevent damage in the sensitive electronics.

- **Mass Properties Measurements**

These measurements include the accurate determination of the mass, centre of gravity and mass moments of inertia of the spacecraft. This knowledge is crucial for the control of the spacecraft.

The facilities chosen for testing the cubesat are all located in the Netherlands, mostly in Delft. The Spacecraft Systems Engineering department at the faculty of Aerospace Engineering in TU Delft has a cleanroom with multiple test facilities that can be used for this cubesat. Some tests can not be conducted with the facilities available at the university. Fortunately, there are multiple companies that can offer the required facilities nearby. These include NLR and TNO, the latter of which has its required facilities in Delft. The facilities for each type of testing are listed in Table 18.2. It should be noted that bus and vehicle system tests are conducted during the integration of the system and thus are done in the general assembly location. Furthermore, acoustic testing is included in vibrational tests.

⁴NSO Vibration Test: <http://goo.gl/EoMYu8> [cited 8 June 2016]

⁵NSO Acoustic Test: <http://goo.gl/8l6aCN> [cited 8 June 2016]

⁶NSO Thermal Vacuum Test: <http://goo.gl/7ZjpYx> [cited 8 June 2016]

⁷Gaia Vibration Testing: <http://sci.esa.int/gaia/49071-gaia-payload-module-vibration-testing-completed/> [cited 9 June 2016]

Table 18.2: Pre-launch verification phase [BUVH08]

Test	Location	Facility
Integration Tests	AE	Cleanroom
Comprehensive System Tests	AE	Cleanroom
Vibration	TNO	Shaker table
Thermal Vacuum	NLR	Thermal vacuum chamber
Shock	TNO	Shaker table
Quasi-static Load	AE	Cleanroom
EMC	NLR	N/A
Mass Properties	AE	Cleanroom

18.3.2. In-orbit Stage Testing

The in-orbit phase testing consists of tests conducted after the cubesat has been detached from the host mission. This includes both checking the health status of the different subsystems and the functioning of the payload. Additionally, the communication link between the cubesat and MRO has to be checked. It is important to check the functioning of SPEX as it has never flown in space before and its performance in the operational conditions is not known. This is done by taking some measurements and sending them back to Earth for analysis. If the measurements contain expected results, the science mission can go on as planned. If there is a problem with the payload, calibration can be done before continuing with the mission.

18.4. Logistics Diagram

The logistic diagram follows from the concurrent assembly, integration and testing phases. The flow diagram shows the expected time-line, which includes contingency for unforeseen circumstances, such as re-ordering certain parts or tools that are missing. The logistic diagram will be used for the design and development logic in Section 23.1. Based on this time-line, the assembly, integration and testing shall take no more than 34 weeks as specified by requirement [CREQ-M-SC3, Ch. 15].

Phase 1: obtaining components

Phase 1 will consist of physically obtaining every subsystem component from the respective manufacturer or developer. Some subsystems take more time to obtain, as they have to be custom made and certain aspects of IRPCS; inspection, repair, programming, cleaning and storage, take up more time. During this phase, qualification and acceptance testing is performed (if required) after obtaining each component.

Phase 2: test-assembly and integration of subsystems

Phase 2 consists of the preliminary assembly phase of the cubesat. First, fit-check has to be performed to ensure the correct tools are present after obtaining the tools. Following that, the test assembly phase can take part. During the test assembly phase, integration of the subsystems happen. Finally the cubesat has to be inspected and cleaned to prepare for the pre-launch testing phase. In phase 2, obtaining the official papers for transportation, testing and qualification is initialised.

Phase 3: flight assembly and integration of system

Phase 3 consists of finalising the assembly for launch. First a harness fit-check has to be performed, to ensure that the pin-outs can be integrated with the CSD. Afterwards, a flight-like test assembly has to be done such that all the subsystems are integrated towards a fully functioning system. The flight-like test assembly then goes through pre-launch testing to ensure that the cubesat is properly configured. During the testing phase, if unforeseen events or mistakes are encountered, these should be taken care of and fixed. The outcome of the pre-launch testing will determine the amount and types of work which have to be performed during the final flight assembly. Phase 3 ends with finalising the testing of the flight assembly of MICRO, it is ready for launch and operation.

Phase 4: transfer to launch

After flight-assembly, the cubesat has been tested and assembled. The cubesat is ready to be launched. The final phase is thus transferring the cubesat to the launcher. Finalisation of the official papers, documents and formalities have to be done during this phase. After transferring and integrating the cubesat into the CSD, MICRO is ready to be launched.

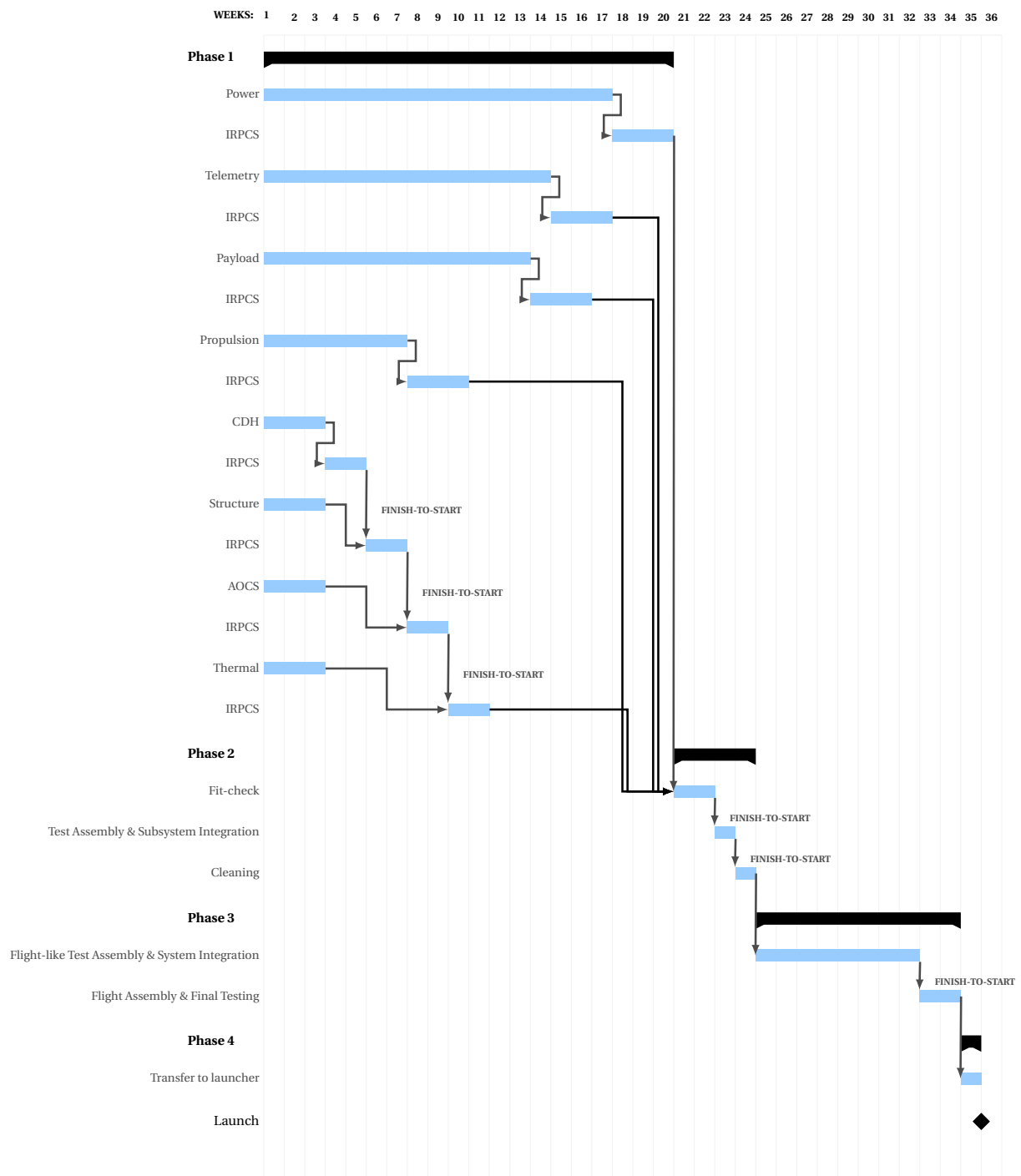


Figure 18.1: Logistics Gantt chart

19

Operations

This chapter will elaborate on the communication part between the ground station and the MRO, through four main steps. In Section 19.1, the communication flow diagram between the two entities will be described. Then, in Sections 19.2 and 19.3, the ground stations and the relay satellite will be developed, respectively, into the hardware, architecture and software used. Finally, Section 19.4 will analyse the correlation between the ground station and the relay satellite, through a link budgets study. The main focus of this chapter is on operations which is considered to be one of the most crucial elements in a space mission.

19.1. Communication Flow

In Figure 19.1 the communication flow diagram detailing the way the MRO communicates with the ground station is shown.

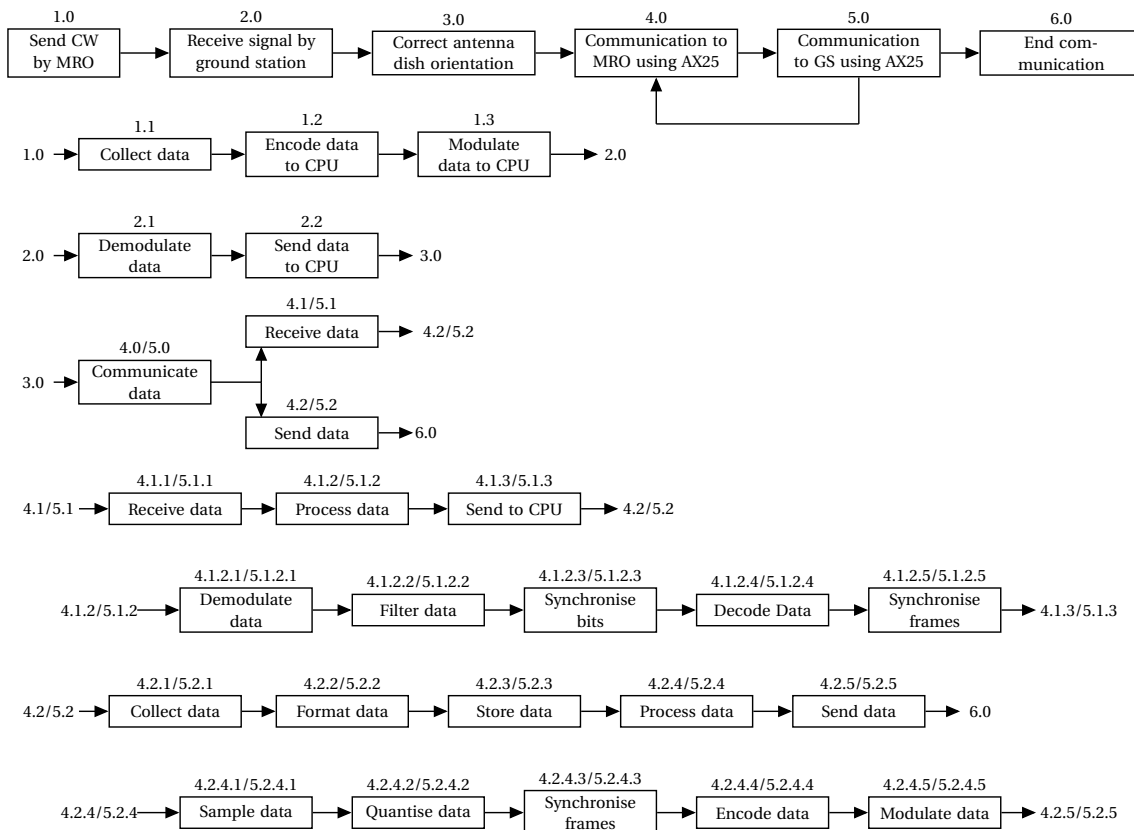


Figure 19.1: Communication flow diagram

The top row shows the top level functions and the three rows below show the functions a level below. The last three rows go another level into detail. The top level functions are self-explanatory. The feedback loop between 4.0 and 5.0 implies that data is sent in both directions. The next two rows go more into detail on the process of sending and

receiving signals. The fourth row presents the option of either sending or receiving data, by either the MRO or the ground station. The two rows below it go into further detail on the functional flow of receiving data, whereas the last two rows outline the sending of data.

19.2. Ground Stations

In this section, the ground stations will be described through three main parts. First, the different types of antenna and the complexes available will be detailed. Then, the architecture of the antenna will be explained. Lastly, the software used by the ground stations will be analysed.

19.2.1. Hardware

The antennae of the ground stations support several functions such as the telemetry and commanding capabilities [sse06, p.478]. The antennas communicating with the MRO shall be operating at X-/Ka- frequencies: namely the X-band for transmission and reception and Ka-band for reception, as the MRO is already using these frequencies (the most common frequency used being the X-band). The MRO being operational (in orbit) and using a deep space network with the 70 m antenna, the 34 m beam-waveguide antenna and the 34 m high-efficiency antenna located on the three DSN complexes (in Spain, Australia and California). The second antenna is used for the majority of the mission phases of the MRO, while the 70 m antenna is used for the MOI and the safe operating control modes, as it is the most sensitive type of ground based antennae. The last type of antenna is alternatively used for non Ka-band frequency; because of the low noise amplifier, the G/T is improved by ± 1 dB.

Using a relay satellite already in orbit for the communication between the Earth and the cubesat allows to avoid the design of new antennae on ground, and therefore reduce the cost and the design time [TLS06].

Table 19.1 gives an overview of the antenna types characteristics, describing the location, name identification, frequencies, gain and EIRP of the antennae.

Table 19.1: Deep space network antennas [WL11, p. 884]

Type	Location	Transmission frequency [MHz]	EIRP [dBW]	Received Frequency [MHz]	Gain [dB K ⁻¹]
34 m BWG	Goldstone	X-band: 7,145-7,235	89.5-109.5	X-band:8,400-8,500	68.2/53.9
	Canberra	X-band: 7,145-7,235	89.5-109.5	X-band:8,400-8,500	68.2/53.9
	Madrid	X-band: 7,145-7,235	89.5-109.5	X-band:8,400-8,500	68.2/53.9
	Goldstone	n.a.	n.a.	Ka-band:25,500-27,000	76.5/58.6
	Goldstone	n.a.	n.a.	Ka-band:31,800-32,300	78.4/60.8
	Canberra	n.a.	n.a.	Ka-band:25,500-27,000	76.5/58.6
	Canberra	n.a.	n.a.	Ka-band:31,800-32,300	78.4/60.8
	Madrid	n.a.	n.a.	Ka-band:25,500-27,000	76.5/58.6
	Madrid	n.a.	n.a.	Ka-band:31,800-32,300	78.4/60.8
	Madrid	n.a.	n.a.	Ka-band:31,800-32,300	78.4/60.8
34 m HEF	Goldstone	X-band: 7,145-7,190	89.5-109.8	X-band:8,400-8,500	68.2/53.1
	Canberra	X-band: 7,145-7,190	89.5-109.8	X-band:8,400-8,500	68.2/53.1
	Madrid	X-band: 7,145-7,190	89.8-109.8	X-band:8,400-8,500	68.3/53.1
70 m	Goldstone	X-band: 7,145-7,190	95.8.5-115.8	X-band:8,400-8,500	74.5/61.3
	Canberra	X-band: 7,145-7,190	95.8.5-115.8	X-band:8,400-8,500	74.5/61.3
	Madrid	X-band: 7,145-7,190	95.8.5-115.8	X-band:8,400-8,500	74.5/61.3

19.2.2. Architecture

As can be seen in Figure 19.2, the telemetry subsystem of the ground station can be studied into two parts, namely the reception and transmission of the data.

The signal received by the antenna structure a console which controls if the received respects the constraints and transmission characteristics. This console is linked to the antenna controller, which controls the antenna and the transmission lines carrying the signals. Once received and analysed by the antenna system, the signal is sent to the receiver system. The ground station is able to receive in both CW and AX.25 modes. The carrier in the AX25 mode will have four modulations, two regarding the relay satellite and two the cubesat. Indeed, each satellite has two modulations, one for the position information and one for the scientific data. After the filters, the data are then processed through a subcarrier demodulator, a bit synchroniser, in order to verify if the various signals are still in synchronisation. Then, these are sent to a storage unit before being decrypted inside the decoder. A storage unit is necessary as in every ground station, the received data are stored for future reference. The data is stored together with the time stamp of reception. After the decoding and a final sample synchronisation, the signals are sent to the computer system which transmits the data to the user interface.

For the transmission part, the data collected in the computer system are processed in three main steps before being encoded and modulated. First, the continuous signal is transformed to a set of values, with a consistent time intervals. The signal is then reconstructed into a discrete signal through the so-called quantisation process. The last step of the command formator is the frame synchronisation. Once modulated, the signal can be transmitted to the antenna structure, with the correct band and frequency.

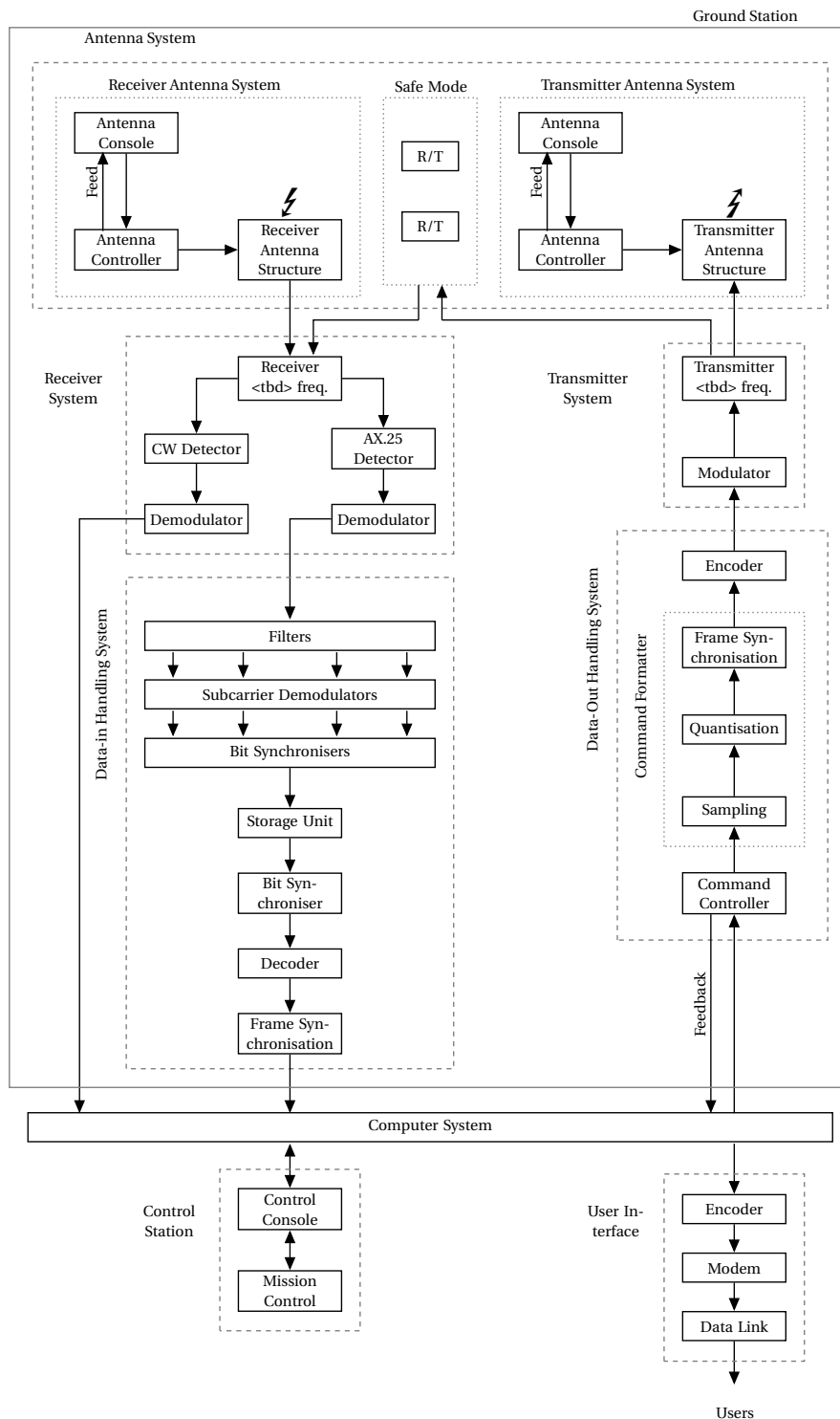


Figure 19.2: Network diagram for the ground station

19.2.3. Software

At the beginning of the mission, the requirements related to the ground station are mainly based on the types of software used. For this mission, two types of software operating at the ground station have been distinguished. These are the pre-reception software and the post-reception software.

Pre-reception Software

As its name suggests it, the pre-reception software includes the operations that need to be done before gathering the data from the science mission. Three software categories are required for the pre-reception [sse06, p. 486]. In contrast to the Mid-term report [AFH⁺ 16], orbit determination and prediction are not required as the spacecraft can do it autonomously.

- **Observation Planning and Scheduling**

Having an observation schedule planned is essential for the mission. Knowing the sites of interest enables scheduling the science measurements. This also requires up-to-date knowledge on the orbit of the cubesat. In addition to planning the schedule of the observations, the duration of each of them has to also be planned. This information is then sent to the cubesat so that the measurements can be taken.

- **Command List Generation**

The command list generation contains a list of commands and instructions that need to be followed during the actions when the data has to be loaded into a computer memory. This data can be a new satellite plan or the tracking data. This command list, also called the reception schedule, shall be constructed as far ahead from the real time mission as possible, and shall be constructed automatically using a set of default options.

- **Simulation**

A simulator software is used for debugging and troubleshooting. Therefore, a simulator for the complete end-to-end ground system should be provided before the launch phase of the mission. This simulation should be of the spacecraft housekeeping data and of the instrument data.

Post-reception Software

Once the data from the satellite has been received, the ground station can start analysing the data. This analysis consists of three tasks [sse06, p. 490], namely:

- **Data Processing**

Data processing consists of the operations carried out by the DATA-IN HANDLING SYSTEM, whose function is to process the received data so that it can be analysed. Once the data has been processed, it is used to execute the following tasks.

- **Health Assessment**

The telemetry data from the subsystems has to be assessed to monitor the health of the cubesat. The results of this analysis might lead to additional operational commands having to be uplinked to the cubesat.

- **Data Analysis**

Data analysis consists of checking the quality of the reduced scientific data received. Furthermore, in this phase, the data is distributed to the users for analysis. To analyse the data, the SPEX measurements, the corresponding attitude, the location information and the temperature of SPEX are needed. These are correlated with the included time stamps. The completeness of the data is checked regarding all the listed variables before the data is forwarded to the users. Ideally, the information required for analysis is derived from the raw instrument data before the data is distributed. The correct functioning of the data reduction algorithm is checked at regular intervals by comparing the science data extracted from the reduced data to the results from the full raw data.

19.3. Relay Satellite

In this section, the relay satellite used for the MICRO mission will be analysed through three aspects. First, the antennas composition inside the MRO will be described. Then, the interactions between the main elements of the MRO telemetry subsystem will be explained through a clear architecture. Finally, the specific communication software used will be briefly discussed.

19.3.1. Hardware

The MRO has three main antennas for communication with Earth. One HGA designed as the main antenna for sending and receiving data. Two low gain antennae mounted on the high gain antenna dish allows to communicate during the safe and special modes. These antennae have an receiver-transmitter system, including amplifiers: two for transmitting 100 W signal in the X-band and one for the 35 W signal in the Ka-band. Furthermore, the MRO is equipped of an UHF antenna designed for its relay function.

19.3.2. Architecture

The data received by the MRO from either the cubesat or the ground station cannot be relayed forward as is. This is due to the fact that the RF bands the MRO uses for Earth-communication are the X- and Ka-bands, while UHF is used to communicate with the cubesat. Hence, data processing is required to be able to transmit the data successfully. This requires multiple steps that are outlined below for an example case of receiving data from the cubesat and

relaying it to Earth. This process is shown in Figure 19.3.

The cubesat transmits data at 404.4 MHz and this is received by the AX.25 detector of the MRO. The received signal is then demodulated and filtered by at least two filters: one for the science data and one for the housekeeping data. It should be noted that also at least two filters are used for receiving signals from the Earth, one for commands to the MRO and the other for the messages to be forwarded to the cubesat. If there is information modulated onto the modulating signal (subcarrier) that is then demodulated. After the demodulation has been done the bit synchronisers ensure that all signals are still in sync. Before storage onto the on-board computer the data is decrypted by the decoder and organised for housekeeping purposes by the frame synchroniser. The data is then stored on the OBC until it can be transmitted to Earth.

When it is possible for MRO to transmit data to the ground station, a very similar sequence is followed but in reverse. The data is encrypted and modulated according to the type of message being sent. First, the CW mode is used to establish contact. To communicate with the Earth, X-band is used. For the data sent back to Earth, the AX.25 emitter is used. Through the transmitter the data is relayed to the antenna.

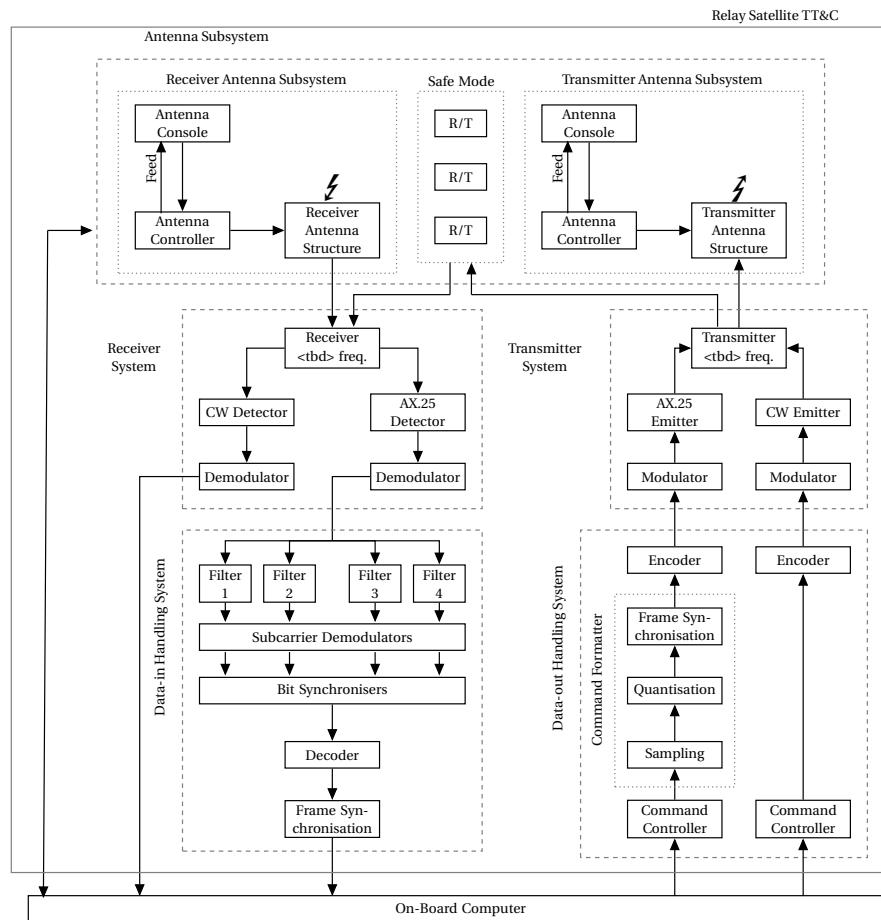


Figure 19.3: Network diagram for relay satellite, MRO

19.3.3. Software

This satellite has the best communication system sent to deep space so far. Indeed, the MRO is equipped with next generation space qualified processors and with a 160 Gbit data recorder (i.e. 700 memory chips with a 256 Mbit memory each). The software on the MRO includes relay sequence generating software¹ that integrates the relay operations with the other operations of the MRO. The software also initiates the relay sessions. This ensures that the MRO can be used as a relay effectively and makes the data link to Earth available.

19.4. Link Budgets

In this section, the link budget for the communication between the relay satellite and the ground station is discussed. The equations used are summarised in Appendix D. For this section, references [TLS06], [Rei08] and [Dur08] have

¹MRO Data Relay Software: <http://www.techbriefs.com/component/content/article/5692> [cited 10 June 2016]

been used for comparison and confirmation.

Table 19.2 displays values relative to the 34 m BWG antenna in X-band and Ka-band. The main difference between the two obviously stands in the wavelength of the carrier and the bandwidth of the signal. The effective areas for the antennae ($A_{T,e}$ and $A_{R,e}$) represent the surface area of the antennae corrected by a scaling factor, to account for the difference from the physical area². Furthermore, for the determination of the values in Table 19.2, the worst case scenario is used (implying that the largest distance D is taken).

Table 19.2: Values used for the link budget – Ground Station Antennas

Parameter	34 m BWG Value X-band	34 m BWG Value Ka-band	34 m HEF Value X-band	70 m Value X-band	Unit
Carrier wavelength	0.0356	0.0116	0.0356	0.0356	[m]
Bandwidth	1×10^6	3.46×10^6	1×10^6	1×10^6	[Hz]
Effective area ground antenna	662.8	662.8	771.7	2809.4	[m ²]
Effective area relay satellite	4.77	4.77	2.3	2.3	[m ²]
Common Parameters					
Distance		4.01×10^{11}			[m]
Boltzmann constant		1.38×10^{-23}			[m ² kg s ⁻² K ⁻¹]
Noise temperature		28			[K]

For determining the link budget as shown in Table 19.3, Equations (D.1a) through (D.1d) were used, as explained in Appendix D. Table 19.3 lists the main communication characteristics leading for the link budget of each type of antenna used by the MRO.

Table 19.3: The total link budget for X-band antennas

Parameter	34 m BWG Value X-band	34 m BWG Value Ka-band	34 m HEF Value X-band	70 m Value X-band	Unit
Transmitter power	20.00	15.44	20.00	20.00	[dB]
Free space loss	283.02	291.77	283.02	283.02	[dB]
Gain transmitter	46.65	56.4	43.64	43.64	[dB]
Gain receiver	68.18	77.92	68.84	74.45	[dB]
Noise	-154.13	-147.78	-154.13	-154.13	[dB]
Transmitter to antenna loss factor	-0.97	-0.97	-0.97	-0.97	[dB]
Transmission path loss factor	-0.46	-0.46	-0.46	-0.46	[dB]
Reception feeder loss factor	-0.97	-0.97	-0.97	-0.97	[dB]
Antenna pointing loss	3.16	9.00	3.16	3.16	[dB]
Link margin	6.71	12.38	4.36	9.97	[dB]

²Communication with Mars Curiosity Rover: <https://goo.gl/vr0uoG> [cited 10 May 2016]

20

Sustainable Development

MICRO mission is a trend setter, it uses state of the art sustainable technology. It is the first planned interplanetary cubesat which aims to fly with significant COTS products, including a green propulsion system on board. In Section 20.1 sustainable aspect of COTS products are addressed followed by Section 20.2 discussing the advantage of the green propulsion system of MICRO. Section 20.3 discusses the measures taken to avoid contaminating Mars. Cubesat industry has shown a significant growth over the last decade. The interest keeps growing mainly due to the technological miniaturisation. Mission capabilities of cubesat are increasing due to low cost and lower complexity. The expected trend in future is to have a growing number of cubesat missions, hence the MICRO mission strives to be an example to look up to in terms of sustainability. In Section 20.4 the MICRO green initiative is presented.

20.1. Sustainability of COTS

MICRO subsystems use a wide range of instruments which are commercially developed. Even though MICRO is a unique interplanetary mission, the possibility to use COTS products shows the feasibility of miniaturised technology. This can be used to the advantage of the sustainability of the design of the 6U cubesat.

If MICRO required unique subsystem components, it would have to be designed, developed, manufactured and tested before being qualified to implement; this would be a large toll on sustainability. Using COTS products eliminates the necessity to perform research and development as it has been already conducted. Some COTS components are being produced at relatively high turn-over rate, this makes the whole process more sustainable and significantly low cost. In-house design of subsystems requires development and testing cost, which in turn decreases the sustainability aspect of the design.

20.2. Green Propellant Advantage

The use of green mono-propellant AF-M315E enables MICRO to perform higher than any of the other propellants in its class. This propellant enables MICRO to achieve an I_{sp} of 240 s making the propulsion process high-performance compared to other mono-propellants such as hydrazine. Hence the acceleration is achieved with a lower expulsion of propellant: this is an advantage to reduce overall mass of the system. Low mass will directly result in the benefit of lower launch mass. The green propellant has low toxicity [RAS13], hence inexpensive in handling and storage methods that could be utilised. AF-M315E is safe to be handled in open containers¹, this makes it ideal to be handled by students. This opens the ability to make the MICRO mission lower in cost in terms of employees.

20.3. Planetary Protection

In the process of designing MICRO, top level design constraints addressing sustainability were established and remained fixed throughout the design process. This included the prevention of forward contamination and mitigating impact risk on Mars or another satellite. Apart from these constraints the implementation of radioisotope thermoelectric generators (RTG) and radioisotope heater units (RHU) were prohibited as this could cause a radiation threat to the system and the host mission and would impose a threat to environment in the case of mission failure. The end-of-life of the mission is designed with the capacity to sustain the orbit for 167 Earth years. This satisfies the COSPAR requirement of 50 Earth years². The propulsion system has a 30% excess of propellant which can be used for unaccounted and critical changes, this would include collision mitigation. There is estimated to be 75 m s^{-1} of ΔV left at the end of the mission.

¹Green Propellant Infusion Mission Project: <https://goo.gl/Qu5pio> [cited 15 June 2016]

²Planetary Protection Provisions for Robotic Extraterrestrial Missions: <https://goo.gl/IXOPDd> [cited 15 June 2016]

The MICRO mission undergoes sterilisation and this is proposed to be handled with industry standards at all phases of the mission, one primary reason being prevention of forward contamination to Mars. This is to comply with COSPAR standards [Nat06]. This is performed to address sustainability of Mars and prevent any possible forward contamination from Earth to Mars.

20.4. MICRO Green Initiative

One of the unfortunate realities of the world we live in today is global warming causing climate change. The people that live on Earth have a responsibility towards future generations to ensure that the impact of this is limited and that it perhaps can be stopped over a considerable time period. The MICRO team believes that every little step made towards achieving this goal is worthwhile. In order to not only have a limited impact but even a positive one on the environment, a goal has been set to make the entire launch CO₂-neutral. It is clear that this is a very ambitious goal. However, sustainability and ensuring prosperity of future generations is deemed to be one of the key goals of this generation. The obstacles caused by past generations need to be overcome with high priority.

Practically, the CO₂ emission of the launch will be estimated using a conservative approach. Then, trees will be planted such that the the same amount of CO₂ will be absorbed by these trees over a span of 10 years. This is a pioneering approach towards sustainability in the space sector since it has never been done before for any space mission in history. However, it does already happen for making the distance travelled by car CO₂-neutral by using help from Treecological³. This company will be contacted to do the same for the MICRO mission.

The estimated CO₂ emission for the space-shuttle launch is 28 metric tons⁴. This spacecraft could carry a payload of 24 metric tons⁵. The GSLV III launcher that will be used to also carry MICRO can carry payload up to 8 metric tons⁶. It can be assumed that the CO₂ emission of the Space Shuttle launch is at least the amount emitted by the GSLV III launch. Hence, by accounting for a CO₂ emission of 28 metric tons, the entire launch can be made CO₂-neutral.

The cost to absorb 1 kg of CO₂ is estimated to be 11.3 euro⁷ over 10 years time according to treecological. This results in a total cost of 316 k€ to make the launch CO₂-neutral. This requires approximately one square kilometer of forest to be planted and maintained over the course of 10 years.

³Turning Travel Into Trees: <http://www.treecological.be> [cited 15 June 2016]

⁴CO₂ Emission Space Shuttle: <http://www.treecological.be> [cited 19 April 2016]

⁵Space Shuttle Payload Mass: <http://goo.gl/BLDDQ5> [cited 19 April 2016]

⁶Payload Launch Mass GSLV III: <http://isro.gov.in/launchers/lvm3> [cited 15 June 2016]

⁷Cost of CO₂-absorption: <http://www.treecological.be> [cited 15 June 2016]

Risk Management

Although it is rare for cubesat missions to have risk management plans, a successful mission is statistically characterised by an early risk identification and by good planning methods. For cubesat missions, due to the low amount of resources available and the short lifespan, it is usually preferred to avoid using expensive and detailed risk management methods [BL13, p.147]. This will become clear in Section 21.1. Failure mode for many cubesats is identified as DOA, or Dead on Arrival, because of poor testing techniques and poor risk management. Handling of risks for this mission was divided in 4 stages [Dep06, ECS08b]: risk identification, treated in Section 21.2, risk analysis, in Section 21.3, risk mitigation, in Section 21.4 and risk tracking, in Section 21.5.

21.1. Statistics

Taking a look at statistics from the first 112 cubesats, the most likely cause of failure (with a probability of almost 50%) is improper integration and assembly [Swa13, p.221]. This is followed by failure of T&C and EPS (both at 18%) and then by mechanical problems (at 8%). It is clear that these statistics, being only based on the very first cubesats ever launched do not represent well the actual failure criteria cubesats are subject to. This is because since 2012 (the year of the launch of the 112th cubesat), reliability of cubesats and manufacturing techniques are expected to have increased. On the other hand, there is still a valuable lesson to learn. Assembly and integration is a crucial part in the design of a cubesat. For this report, these topics are treated in Chapter 18. Furthermore, analysing the other sources of failure, one can assume that T&C and EPS still remain the most critical parts of a cubesat design. Emphasis of the risk analysis should be put on these components, then.

21.2. Identification

As stated earlier in the chapter, every subsystem manager or task supervisor shall perform risk identification activities. These risks will be reported to the risk manager, which shall state them in a standard form: “Given that [CONDITION], there is a possibility of [DEPARTURE] adversely impacting [ASSET], which can result in [CONSEQUENCE]”, as suggested in [DBE⁺11].

- **Condition:** phrase which describes the situation or the environment that is causing concern, uncertainty or anxiety.
- **Departure:** represents the possible deviation from the predefined activity, task, project or performance goal; made credible by the condition.
- **Asset:** main mission element or resource which is affected by the individual risk.
- **Consequence:** phrase which describes the negative impact on the performance of the project.

Once the risks have been identified with the method above, their root cause has to be identified. The root causes can be either *hardware*, *software* or *programmatic* [BL13]. A further classification can be done, to simplify the consequent risk mitigation processes. Hardware and software issues can be divided in [Dep06, p.9]:

- **Requirements** or REQ, hence those risks that represent the sensitivity of the mission to uncertainty in requirements and system description.
- **Testing** or TES, risks that represent the capability of the testing techniques used.
- **Modelling** or MOD, risks that represent the degree to which the models and simulations used represent reality.
- **Technology** or TEC, risks that represent the capacity of the components chosen to meet the requirements (usually expressed as 1, 2 or 3σ).

Finally, the programmatic issues are split in [Dep06, p.9-10]:

- **Assembly** or ASS, thus those risks that represent the point to which the assembly can comply with cubesat standards.
- **Cost** or COS, risks that represent the ability of the mission to not exceed the cost budget.
- **Schedule** or SCH, risks that represent the ability of the mission to not exceed the scheduled time frames.
- **Budget** or BUD, risks that represent the sensitivity of the program to take variations and reductions into account.
- **External factors** or EXT, risks that arise from external stakeholders.

Table 21.1 (on the next page) provides an overview of the identified risks, stated in the standard form which has been earlier defined. In the table, **L**, **C** and **P** refer to likelihood, consequence and priority, respectively. These parameters will be explained in Section 21.3.

21.3. Analysis

After the risks have been collected and divided in their respective categories, as described in Section 21.2, it is time to analyse the risks and assess their severity. The first step to undertake is to rank each risk. The ranking is done by giving each risk a number from 1 to 5 for both likelihood and consequence. The first two columns of Table 21.2 show the description of the numbers assigned.

Conditions can arise that indicate individual sources of significant risk, for which only a limited time frame exists for effective risk management response. Such situations must be responded to quickly, on a shorter time scale than that required for quantitative risk analysis, so that the window of opportunity for response is not lost [DBE⁺11]. Therefore risks are analysed on urgency as well, such that there is no unnecessary risk growth due to late handling. A suggested priority ranking for the project can be found in the last column of Table 21.2 [Rad13].

Table 21.2: Risk rankings

Rank	Likelihood	Consequence	Priority
1	Very low	Trivial	Very long term
2	Low	Minor	Long term
3	Moderate	Moderate	Mid term
4	High	Significant	Near term
5	Very high	Extreme	Imminent

Now that the ranking criteria have been established, they can be applied to each risk, for the construction of the L-C chart, otherwise known as risk map. It can be found in Table 21.3. The risk map shows on the horizontal axis the severity of consequences and on the vertical axis the probability of the event happening. Since risk is defined as the product of these two axes, the highest risks can be found in the upper right corner of the matrix and are given a red colour. On the other hand, the lowest risks can be found in the lower left corner and are identified with a green colour. In particular, the following definitions have been given to the three colours present in the matrix:

- **Low** or [L] as **Green**: Has little or no potential for increase in cost, disruption of schedule, or degradation of performance.
- **Medium** or [M] as **Yellow**: May cause some increase in cost, disruption of schedule, or degradation of performance.
- **High** or [H] as **Red**: Likely to cause significant increase in cost, disruption of schedule, or degradation of performance.

The risk map does not account for the overall risk of the project, nor does it take into account interactions between individual risks. Its main purpose is to inform the reader about the specific risk status, in order to facilitate risk discussion and decisions.

Furthermore, for a preliminary quantification of the risk, its value can be found by using Equation (21.1).

$$R = LC \quad (21.1)$$

In Equation (21.1), R is the risk and L and C are still likelihood and consequence, as defined before.

Table 21.1: Risk identification

Code	No.	Condition	Departure	Asset	Consequence	L	C	P
REQ	1	The S/C endangers the host mission	Undesired interaction	S/C; launch vehicle	Mission failure; cost overrun; host mission failure	1	5	2
	2	The S/C does not follow regulations	Endangering the mission	The mission	Mission cancellation	1	4	5
	3	The S/C disposal fails	Contributing to space debris	Other S/C	Damage to other S/C	4	2	1
	4	The requirements are poorly defined	Improper design	The S/C; the mission	Subsystem failure; mission failure	2	3	4
TES	5	There is a fuel leak	Fuel depletion	The mission	Subsystem failure; under-performance	2	4	4
	6	The V&V methods are not well defined	Improper design	The S/C	Reduced performance; mission failure	2	4	5
MOD	7	The Martian system is not well know	Unexpected environment	The S/C	Loss of S/C	3	5	5
	8	Unforeseen radiation levels might arise	S/C damage	The S/C	Reduced performance; S/C failure; mission failure	4	4	3
	9	The orbital parameters are incorrect	Acquiring the wrong orbit	The mission	Fuel depletion; subsystem failure; mission failure	1	4	5
	10	Presence of global dust storm throughout the mission	Unexpected environment	The mission	No position information	2	4	3
	11	Unknown temperature of host satellite	Unexpected environment	The S/C	Inaccurate thermal control; mission failure	2	4	2
TEC	12	The orbit insertion is incorrectly performed	Fuel depletion	Mission performance	Inadequate attitude control; mission failure	1	4	4
	13	The S/C fails to deploy from host	Failure to conduct mission	The mission	Mission failure; damage to host	2	5	2
	14	Data handling subsystem fails	Incomplete scientific data	The mission	Mission failure	2	3	1
	15	Communication with S/C is lost	Losing track of the S/C	The mission; the S/C	Mission failure	5	5	5
	16	Power is not distributed to all subsystems	Subsystem failure	The S/C	Reduced performance; subsystem failure; mission failure	4	3	4
	17	The solar arrays degrade	Insufficient electrical power	Subsystem	Reduced performance	5	2	2
	18	The S/C does not survive the launch	Structural damage	The S/C; the subsystem	Lack of scientific data; subsystem failure; mission failure	2	5	5
	19	The science payload malfunctions	Lack of scientific data	The mission	Lack of scientific data	3	4	3
	20	Technology development is delayed	Launch delay	The mission	Schedule and cost overrun	3	4	5
	21	Heating up of SPEX detector	Inaccurate measurements	The mission	Lack of scientific data; mission failure	4	4	2
ASS	22	Damage to SPEX detector's pixels	Inaccurate measurements	The mission	Lack of scientific data; mission failure	2	4	2
	23	SADA gets stuck	Improper power generation	Subsystem	Mission failure; schedule delay	1	4	2
	24	The solar arrays fail to deploy	Improper power generation	Subsystem	Mission failure; lack of scientific data	1	4	4
	25	The battery overheats	Increase in the bus temperature	The S/C	Incapability of maintaining the operating bus temperature	2	3	2
	26	There is a short circuit	Power subsystem failure	The S/C	Mission failure	2	4	3
	27	Contaminated of the S/C with Earth organics	Planetary contamination	Future science mission	Unreliable scientific data; cost overrun	2	4	5
COS	28	The production quality is insufficient	Reduced performance	The S/C	Subsystem failure	1	4	5
	29	The labour costs might rise	Cost increase	The mission	Cost overrun	3	2	2
SCH	30	The materials exceed the expected costs	Cost increase	The mission; the S/C	Design change; cost overrun	2	2	2
	31	Premature end of mission	Incomplete scientific data	The mission	Mission under-performance	4	4	1
BUD	32	The budgets are not well defined	Budget overrun	The mission	Cost overrun; schedule delay	3	3	5
	33	Host mission not available	Mission delay	The mission	Schedule delay and cost overrun	2	4	5
EXT	34	Unexpected financial penalties	Cost increase	The mission	Cost overrun	1	1	1
	35	Unexpected political issues affecting the mission	Launch delay or cancellation	The mission	Mission delay; cost increase	3	4	3
	36	The S/C collides with another object	S/C damage	The S/C	Subsystem failure; loss of S/C	1	5	1

Table 21.3: Risk map

Likelihood	1	2	3	4	5
5	[L]	17 [M]	[H]	[H]	15 [H]
4	[L]	3 [M]	16 [M]	8, 21, 27 [H]	[H]
3	[L]	29 [L]	28 [M]	7, 19, 20, 31 [M]	[H]
2	[L]	30 [L]	4, 14, 25 [L]	5, 6, 10, 11, 22, 24 27, 29 [M]	13, 18 [M]
1	30 [L]	[L]	[L]	2, 9, 12, 23, 24, 28 [L]	1, 32 [M]
Consequence					

Table 21.4: Risk map with mitigation

Likelihood	1	2	3	4	5
5	[L]	17 [M]	[H]	[H]	[H]
4	[L]	3 [M]	8, 16 [M]	[H]	[H]
3	[L]	29 [L]	28 [M]	7, 19, 20, 31 [M]	[H]
2	[L]	30 [L]	4 [L]	6, 10, 11, 21, 27, 27, 29 [M]	13, 15, 25 [M]
1	30 [L]	[L]	5, 14, 23, 24 [L]	2, 9, 12, 22, 26, 28 [L]	1, 18, 32 [M]
Consequence					

21.4. Mitigation

This section deals with risk minimisation and avoidance strategies, by reallocating resources, improving or changing the design, increasing redundancy or identifying the elements of the design that are the main contributors to the lack of reliability. As the design process will become more detailed, the risk management and mitigation procedures

will in turn be more specific. General suggestions for minimising risk are provided in Table 21.5, while Table 21.4 shows the mitigation results. Depending on the risk level and its nature, the following labels are assigned:

- **Accept:** the risk level is within predefined risk tolerances; no response is required.
- **Mitigate:** positive action has to be taken to reduce the risk impact.
- **Watch:** the risk driver will be further monitored and observed until uncertainty is at an acceptable level.
- **Research:** further research on the risk driver is required, for better understanding and reducing uncertainty at an acceptable level.
- **Close:** risk is considered insignificant and it can be discarded.

Table 21.5: Risk handling

No.	Label	Mitigation Proposal
1	Watch	
2	Close	
3	Watch	
4	Watch	
5	Mitigate	Design a robust fuel system; insulate electronics and instruments against fuel leaks
6	Watch	
7	Research	Design for higher than expected radiation levels
8	Mitigate	
9	Watch	
10	Watch	
11	Watch	
12	Research	
13	Watch	
14	Mitigate	
15	Mitigate	Add redundancy; choose most reliable data storage method
16	Research	Use a relay satellite; have redundancy in the design
17	Watch	
18	Mitigate	Perform structural and vibrational tests; define a sufficient safety factor
19	Research	
20	Watch	
21	Mitigate	Separation of detector from external environment by air-tight capsule
22	Mitigate	Extra pixels are added to the detector
23	Mitigate	Reallocate arrays to preferred position
24	Mitigate	Have body mounted CICs
25	Watch	Double insulate all electronic components
26	Mitigate	
27	Watch	
28	Accept	
29	Close	
30	Accept	
31	Mitigate	Make use of redundancy in the design
32	Watch	
33	Accept	
34	Close	
35	Accept	
36	Research	

21.5. Tracking

The risk mitigation that was portrayed in Table 21.4, refers to the very initial steps of risk mitigation. This stage of risk management, continues throughout the mission. After every milestone, as defined in Chapter 23, risk identification, analysis and mitigation are performed again, to see whether new risks have arisen or if the criticality of some risks have changed.

Reliability, Availability, Maintainability and Safety

In this chapter the reliability, availability, maintainability and safety characteristics of the mission are discussed. Section 22.1 includes the reliability aspects of the design. In Section 22.2 the availability is briefly discussed. Maintainability is assessed in Section 22.3 and safety critical characteristics are discussed in Section 22.4.

22.1. Reliability

Reliability is the probability that a system has sufficient performance under operating conditions in a certain amount of time [HvT06]. The reliability of the system depends on the components and the way they are integrated. The formulae that can be used to calculate the reliability of the whole system are presented in Subsection 22.1.1. The general methods used during the design are outlined in Subsection 22.1.2. The redundancy policy applied is presented in Subsection 22.1.3.

22.1.1. Reliability Assessment

The reliability of the whole cubesat can be calculated based on the individual reliabilities of the subsystems and, on a more detailed level, components. The resulting system redundancy depends largely on the way components and subsystems include redundancy. For a system consisting only of non-redundant subsystems in a series the redundancy is calculated with Equation (22.1) [WL10, p.754]. In case redundancy is included in the design of a subsystem, its reliability is found with Equation (22.2) [WL10, p.754]. The reliability of a system consisting of a series of redundant subsystems is again calculated with Equation (22.1). Since the designed cubesat is an intricate combination of redundant and non-redundant components, the total reliability of the system is calculated as a combination of both equations where relevant.

$$R_s = \prod_{i=1}^n R_i \quad (22.1)$$

$$R_{s,p} = 1 - \prod_{i=1}^n (1 - R_i) \quad (22.2)$$

The reliability of each component over time depends on its expected failure mode. For electrical components, the failure rate can be assumed to be random and it can be modelled with an exponential distribution. A Weibull distribution can be applied when the failure rate of the component increases over time due to wearing out [WL10, p.753]. At this stage of the design, the reliability of individual components or the system cannot be quantified.

22.1.2. Reliability Considerations

Reliability has been taken into account in multiple ways in the development of the cubesat. In this section the fault avoidance methods are discussed. At a later stage of the project, a Failure Modes and Effects Analysis should be conducted to identify the critical points of the design.

Contingencies have been taken into account when defining the functional requirements of the spacecraft. While this means that the cubesat is over-designed, it also increases the system reliability as unexpected situations can be handled. For example, the amount of propellant is 30% higher than the expected amount needed during the mission

lifetime and the power subsystem has been designed with a 10% contingency in power. In a further development phase the detailed component design will be done that includes e.g. cabling and bolts. These parts will be selected such that their expected loads are much lower than their capacity.

Reliability of the components has been taken into account when selecting the hardware for the various subsystems. All major subsystems consist of proven space qualified components with high enough technical readiness levels to trust their reliability. The requirements imposed on the system regarding the survivability in space are listed in Chapter 15. Additionally, a lot of testing is planned to ensure that each part of the spacecraft meets the requirements. The complete system will also be extensively tested as outlined in Chapter 18.

Software on board the cubesat is protected against errors by being stored in radiation tolerant memory for the whole duration of the mission. To increase the reliability, the operating system included with the OBC has been modified to better tolerate the radiation environment of outer space [S. Engelen, pers.comm. June 2016].

22.1.3. Redundancy Policy

Redundancy is the main method to increase the system fault tolerance and hence reliability [WL10, p.764]. While the cubesat design is not fully redundant, in some subsystems redundancy has been introduced. The applied redundancies are discussed in this subsection alongside with the known single points of failure.

The subsystem and bus design of the spacecraft includes multiple redundant systems. In the CDH subsystem redundancy is applied by including a cold redundant OBC to switch to in case the original computer encounters a fatal issue. The radiation shielding of the cubesat is quite redundant from the point of view of radiation tolerance as a smaller thickness of the protective material would meet the radiation requirements. The AODCS subsystem includes redundant sensors to avoid single points of failure that would lead to the loss of attitude information on the cubesat.

Some aspects of the mission not included in the design of the cubesat itself also have redundancy. From a mission astrodynamics point of view, there is redundancy in the observation opportunities for the science payload. Each location on Mars can be observed twice during the planned mission lifetime. Additionally, the critical components of the deployer, as described in Chapter 12, are redundant to ensure that the cubesat detaches from the host without issues.

Some subsystems have been designed without redundancy due to mass or volume constraints. For example the payload is a singular system that relies on its inherent reliability to successfully complete the mission. Contrary to the attitude control, the orbit determination system has no redundancy. The thermal subsystem is passive and thus cannot be made redundant; if the system had more material than it does, the thermal characteristics would not be within the specifications.

22.2. Availability

In this section the availability of the cubesat is discussed. Availability is the probability that the system is ready for use when required [HvT06]. In case of an interplanetary cubesat, this refers to the ability to take science measurements and communicate with the MRO, which also has to be able to communicate with the ground station. Availability relates to reliability and maintainability as maintenance time has to be deducted from the operational time.

The ability to do science measurements at any given moment depends on the lighting conditions the cubesat is subjected to and the on-board memory available. The ability to communicate in any direction depends on the position of MICRO and the MRO with respect to each other, as well as the position of the MRO with respect to the Earth. The only quantifiable probability at this point of the design is the ability to transmit data between MICRO and MRO. Conservatively approximated, this can be done 62% of the time as discussed in Chapter 5.

22.3. Maintainability

Maintainability is the ability of a system to be maintained [HvT06]. A cubesat located at Mars cannot be physically maintained during its mission. This makes it important to design the cubesat in such a way that single-point failures are minimised. However, some maintenance activities for the mission can be identified. Software maintenance is discussed in Subsection 22.3.1 and ground maintenance is briefly assessed in Subsection 22.3.2.

22.3.1. Software Maintenance

The software on-board the cubesat can be updated from the ground station if so required. This applies both to the software running the spacecraft as well as the algorithms used for processing the payload data. The software required for operations is included on the cubesat at launch and stored on the radiation-tolerant memory of the on-board computer. This includes both the operating system code and the algorithms for handling tasks aboard the cubesat. However, if some functions of the cubesat have to be changed or new operational modes are included, the software has to be updated to take this into account. The new code has to be uplinked from the ground station based on the received housekeeping data.

Another software maintenance task is the update of the payload data processing algorithm. As discussed in Chapter 4, raw data from SPEX is sent to Earth at regular intervals to check whether the data processing on-board is working as intended. If discrepancies are detected, the algorithm can be updated by the scientists analysing the data and sent to the cubesat. It is crucial for the science return to process the data in a way that does not lead to loss of useful data.

22.3.2. Ground Maintenance

While the cubesat can only be maintained in a limited way, the ground station used for the operations (most likely located at TU Delft) can and should be regularly maintained. This applies for both the hardware and the software of the ground station. The hardware maintenance should be scheduled to prevent reduced operational time due to e.g. the wear-out of components. The software used at the beginning of the mission is assumed to be sufficient for the whole lifetime, but if flaws are detected the software should be able to be updated. Doing this should not interfere with the operation of the mission.

22.4. Safety

Safety is defined as lack of hazards to people and equipment [HvT06]. For this mission, it is relevant to avoid damage to the host mission and Mars in addition to keeping MICRO functional. Some of the most critical hazards to the equipment or environment are listed in Table 22.1. For each failure mode found, a category is indicated: this could be a specific subsystem or a mission characteristic. The possible consequences are also presented along with corrective actions that are taken to prevent them. The severity of the hazard is indicated as low, medium or high depending on the consequences and the ability to mitigate them.

Table 22.1: Mission hazard overview

Category	Failure mode	Consequence	Corrective action	Severity
Propulsion	Fuel leak	Damage to cubesat	Robust fuel system	High
End-of-life	Failed EOL manoeuvre	Environmental contamination	Controlled EOL	Medium
Deployment	Deployment failure	Damage to cubesat and/or host	Reliable deployer, testing	Medium
Subsystems	Overheating	Component damage	Thermal control	Medium
Power subsystem	Solar panel actuator failure	Loss of power	Testing	High
Bus	Structural failure	Cubesat damage	Structural reinforcement	High

23

Project Design and Development Logic

In this chapter the project design and development logic of the mission is described. This chapter elaborates on how the transition from the design until the actual product will be conducted. In Section 23.1 the development process will be described in terms of phases, following from Chapter 18 and in Section 23.2 the general process is presented in the form of a Gantt chart.

23.1. Design and Development Logic

In order to make progress and meet the industry standards it is required to have a proper design and development logic established for the whole project. This is defined at that start of the project using in the process of project management, this gives the blueprint of the project in a sequential manner. For the MICRO project the ECSS-M-30-01A standards defined by ESA are used. Using these standards it is possible to interlink the goals of project management and engineering.

At this phase of the project it is important to note the significant progress has been achieved, with this report the MICRO design meets the preliminary design review. So far of this mission it can be concluded that Phase 0 is achieved as defined in the Figure 23.1. The remaining seven phases can be identified as milestones of the mission. Each component in a phase defines a set of activities to be performed. Complying with this procedure will give an optimum and a clear track to reach the mission goal.

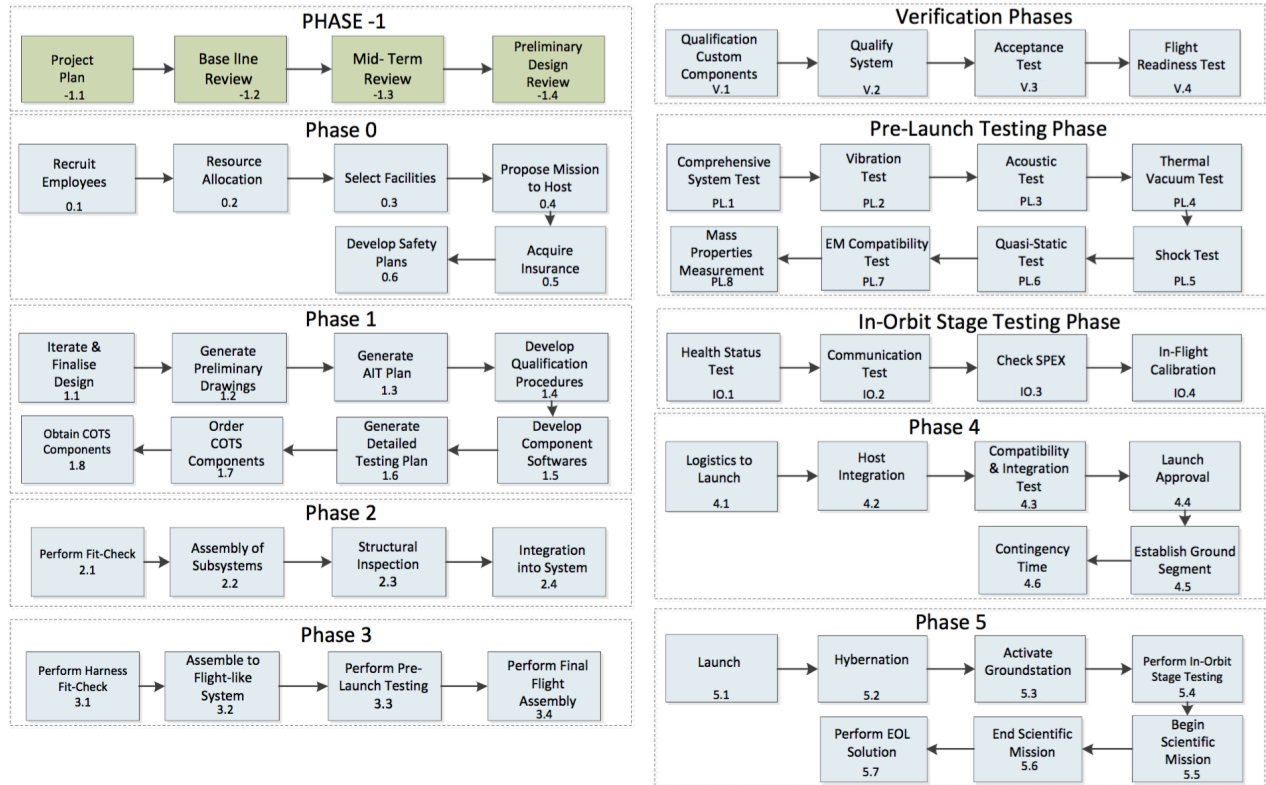


Figure 23.1: Project development logic

The phases follow from the logistic diagram from Chapter 18. A short description is given of the phases. Phases 1 to 4 are detailed in Section 18.4 and will be explained in short.

- **Verification Phases** the verification phases are carried out throughout the mission lifetime and on different levels.
- **Phase -1** defines what the work performed in the DSE project for the MICRO mission. The end of this phase results in a preliminary design for the mission.
- **Phase 0** define the immediate establishment of the project after DSE activities. This segment includes many non technical task, project management plays a vital role at this phase in terms of employee recruitment (block 0.1) and resource allocation and selecting facilities.
- **Phase 1** is the critical design phase of the mission. This would result in a detail design, series of plans for AIT, qualification and testing and finally software development for subsystems and ordering COTS components. The phase ends with obtaining the COTS components.
- **Phase 2** is dedicated for test system assembly and integration of sub-systems, in this phase each subsystem is assembled. Once the modules are ready, they are assembled to form the MICRO system.
- **Phase 3** is dedicated to flight-assembly and integration of the system. First a harness-fit check is performed. After assembly, the flight-like system has to undergo the pre-launch testing phase. After pre-launch testing, unforeseen events or mistakes have to be corrected for to complete the final flight assembly of MICRO.
- **Phase 4** is dedicated to integrating and bringing the cubesat to the launcher. Furthermore the ground segments have to be set-up to support the mission.
- **Phase 5** is performing the mission. It is initialised by launching MICRO. After reaching the destination, MICRO performs in-orbit stage testing to ensure that the subsystems work. When technical deficiencies are encountered, the ground systems have to do in-flight calibration to make everything work. A final check-up is done and the scientific mission can begin. After ending the scientific mission, MICRO goes into EOL-manoevre.

23.2. Post-DSE Project Gantt Chart

In Figure 23.2 the different phases described in Section 23.1 are presented in the form of Gantt chart. In this chart an overview is given about the time frame of the design, development, testing and mission is presented.

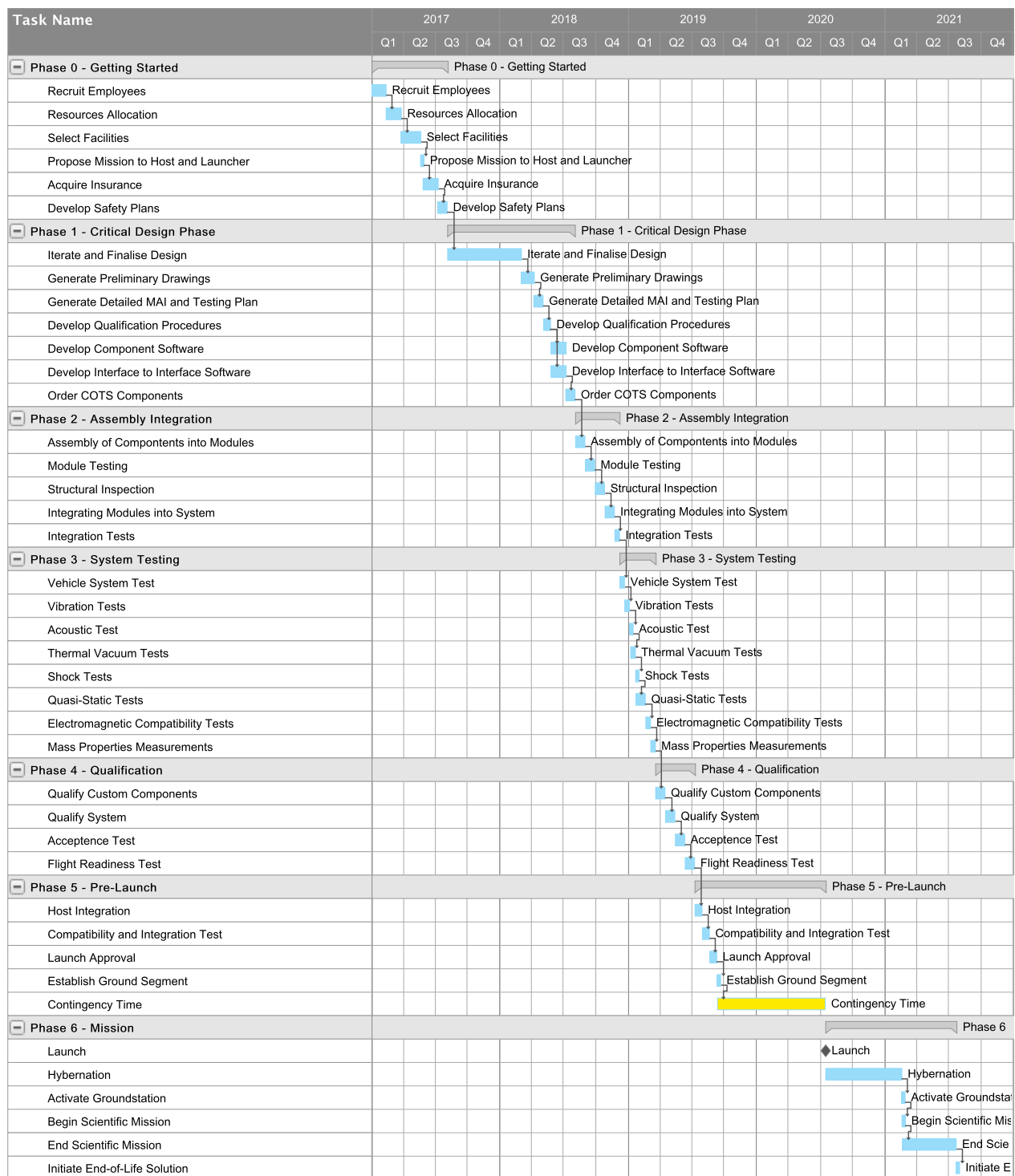


Figure 23.2: Post-DSE Gantt chart

Conclusion and Recommendations

The main conclusion that can be drawn from this report is that a scientific 6U cubesat mission to Mars is feasible within the specified constraints and assumptions. All the top level system requirements that were set at the beginning of the project are met by the mission and cubesat design of the Mars Interplanetary Cubesat and Research Orbiter (MICRO).

MICRO will perform a scientific orbit mission and provide unique science measurements while orbiting Mars. The composition and spatial distribution of dust on Mars will be analysed using the Spectropolarimeter for Planetary EXploration (SPEX) as its scientific payload. The scientific data is unique because it would be the first time that spectropolarimetry data is obtained for Mars. The composition and spatial distribution of dust on certain locations of Mars will be analysed along with the detection of ice particles in the Martian atmosphere. This way, we will learn more about the possible effect dust can have on equipment on Mars and subsequently provide data to plan future Martian settlements. Additionally, the effect of dust and ice particles on the Martian weather system could be characterised since aerosols can act as cloud condensation particles, having an effect on and increasing the formation of clouds. All this information is useful to the scientific community and a necessity if human occupation of Mars is made a reality. The fact that it is feasible for a cubesat to contribute to the scientific community can be considered a profound accomplishment and could have an impact on the development of future interplanetary cubesat missions. However, it can be concluded that SPEX is not ideal in terms of the internal layout of the cubesat since it is not a modular payload designed for cubesat standards and has a considerable price-tag of 5.2 million euro. Nonetheless, the scientific gain that SPEX provides easily outweighs these disadvantages and without the work of all the people involved in the development of SPEX, the MICRO mission would not have been possible.

Apart from the scientific value that the mission adds, it also demonstrates new cubesat technologies. It will be the first interplanetary cubesat that performs a scientific mission and uses a relay-satellite, the Mars Reconnaissance Orbiter (MRO), to communicate with Earth. This allows the design of a relatively simple telecommunications subsystem embodied by the fact that patch antennas are used. Nonetheless, it can be concluded that telecommunication through MRO poses constraints on the scientific output of the mission. The data rates to send data to MRO are limited as well as the communication times per orbit. Therefore, the initial intention to map the entire Martian surface cannot be met and the mission restricts itself to scientifically interesting locations on Mars.

Furthermore, MICRO incorporates sustainability throughout its mission and cubesat design. It has a 2U propulsion subsystem which uses green mono-propellant AF-M315E. This decreases the impact on the environment and on top of that, it is not hazardous to humans. With respect to the emissions of greenhouse gases expelled during launch, measures are taken to plant trees that absorb the same amount of greenhouse gases over the period of ten years which makes the entire launch energy neutral. On top of that, the cubesat does not pose a hazard to the host mission through the use of the Canistered Satellite Dispenser and complies with the Committee on Space Research (COSPAR) recommendations for planetary protection by through end-of-life manoeuvre. It can be concluded that the mission's sustainability approach limits the environmental impact to an absolute minimum.

Lastly, it is important to emphasise that the mission success depends on external factors. MICRO will piggyback the Mangalyaan 2 mission and uses MRO as a relay-satellite. This results in the necessity of collaboration with the National Aeronautics and Space Administration and the Indian Space Research Organisation. Because of the reliability on external factors, it can be concluded that the outcome of this report confirms the feasibility of an interplanetary cubesat mission and its preliminary design rather than serving as an actual mission proposal.

Based on the conclusions drawn in general for the design of the interplanetary cubesat mission and MICRO, certain recommendations can be made for future work. The next paragraph contains recommendations for the design of future interplanetary cubesat missions, followed by recommendations for the further development of the MICRO mission. Finally, a recommendation is made in the last paragraph for the space industry and space agencies in general.

If the goal is to design an interplanetary cubesat mission that is intended to be developed and launched, it is recommended to first find a feasible launch opportunity or piggybacking option before starting the design of the mission. After the selection of the launch opportunity, the design of the mission can start. This is essential because interplanetary cubesat missions or piggybacking options are almost non-existent to this day. This contrasts with the Earth-bound cubesats in the sense that there are multiple launch opportunities for these cubesats every year. Moreover, the cost breakdown structure should start earlier throughout the design of the cubesat. It was discovered relatively late that the payload has a cost of 5.2 million euro. This might have played a crucial role in the selection process of the payload and was not considered in the Midterm Report.

For the development of this mission specifically, it is recommended to make the SPEX instrument fit in 1U. This would result in additional volume left for other subsystems or could even result in a smaller cubesat entirely. Despite the unfortunate dimensions of SPEX, a considerable amount of volume is still left to ensure sufficient contingency for further development of the cubesat. It is recommended to investigate the possibility of carrying a secondary payload that could use this volume to increase the scientific gain of the mission. On top of the aforementioned general recommendations, specific recommendations can be made with respect to the technical aspects of the design of the MICRO mission. In general, all subsystems require further detailed development:

- Command and Data Handling: perform a more detailed analysis on the high-speed data link between SPEX and the on-board computer, the data processing algorithms and processing time
- Telemetry and Telecommunications: develop simulations for the coverage area of MICRO's antennas, consider different substrate materials to be used for the manufacturing of the antenna's in order to increase the dielectric strength, model exact transmission and reception between MICRO and MRO and develop simulations on the effect of using microstrips for the patch antennas
- Attitude and Orbit Determination and Control simulation: add kalman filters, control operating modes, thruster misalignments and variation of solar radiation pressure area to the simulation as well as the addition of the rotation of the cubesat around the y-axis, the tetrahedral configuration of the reaction wheels and the J2 effect of Mars
- Power: carry out detailed analysis on the control operating modes (i.e. duty cycle of different modes, detailed energy analysis to optimise the power generation requirements), investigate power generation if solar array drive actuator gets stuck, design for super-capacitors to ensure a more optimised battery design and optimise the solar panel mass and volume by using mesh structures or flexible printed circuit boards
- Propulsion: design the propulsion system such that it uses one propellant tank, one pressurant tank and one feed system to increase its efficiency analyse and investigate the use of helium as pressurant to possibly decrease the mass of the propulsion system
- Thermal Control: determine absorptivity and emissivity of components on the outside of the cubesat like the patch antenna's, the thrusters and SPEX by analysing the thermal properties of the materials used for these components, analyse the effect of the temperature of internal components on the overall cubesat temperature by using a heat model for the satellite and applying finite element methods, include the conduction of heat between the solar panels and the cubesat bus and figure out how the visibility and albedo factors vary per orbit
- Radiation: run more Monte Carlo Simulations with a larger number of iterations to obtain more accurate results, optimise for single event upsets in more detail and consider more materials in the trade-off for radiation hardening
- Structure: a finite element analysis in combination with extensive testing could result in a lighter structure, more detailed analysis with respect to vibrational loads and shocks is recommended and composite materials could be considered in future work

This project has proven the feasibility of an interplanetary cubesat mission. In addition, it will be the first time that universities and students worldwide can actively contribute to interplanetary space exploration. The challenges that were posed at the beginning of the project like radiation, communication and decreased solar power have been overcome through the design of MICRO. Consequently, it is recommended for space agencies and private space companies to invest in interplanetary cubesat missions and take the next leap towards the expansion of space exploration such that the advantages of miniaturisation, already proven by Earth-bound cubesats, can be extrapolated to interplanetary space missions.

rule, based on the rotation of the spacecraft. Again, the $\hat{\mathbf{y}}^{PF}$ unit vector, or $\hat{\mathbf{q}}$, is such that the system results right-handed. Equation (A.2) [Cur05, p.174] shows the transformation necessary to go from inertial to perifocal frame.

$$\mathbb{T}_{IF \rightarrow PF} = \begin{bmatrix} \cos \Omega \cos \omega - \sin \Omega \cos i \sin \omega & \sin \Omega \cos \omega + \cos \Omega \cos i \sin \omega & \sin i \sin \omega \\ -\cos \Omega \sin \omega - \sin \Omega \cos i \cos \omega & -\sin \Omega \sin \omega - \cos \Omega \cos i \cos \omega & \sin i \cos \omega \\ \sin \Omega \sin i & -\cos \Omega \sin i & \cos i \end{bmatrix} \quad (\text{A.2})$$

The transformation consists of three rotations, first about $\hat{\mathbf{z}}^{IF} \equiv \hat{\mathbf{z}}^{IF'}$ by ω , then about the $\hat{\mathbf{x}}^{IF'} \equiv \hat{\mathbf{z}}^{IF''}$ by i and finally about $\hat{\mathbf{z}}^{IF''} \equiv \hat{\mathbf{z}}^{PF}$ by Ω .

Orbital Frame

The orbital frame is a rotating system. It follows the spacecraft along the orbit and has its $\hat{\mathbf{x}}^{OF}$ unit vector always pointing along the velocity vector \mathbf{V} , $\hat{\mathbf{z}}^{OF}$ pointing in the same direction as $\hat{\mathbf{z}}^{PF}$ and the $\hat{\mathbf{y}}^{OF}$ unit vector follows from the right-hand rule. Transformation from the perifocal axis-system to the orbital frame is given by Equation (A.3).

$$\mathbb{T}_{PF \rightarrow OF} = \begin{bmatrix} -\sin(\vartheta + \gamma) & \cos(\vartheta + \gamma) & 0 \\ -\cos(\vartheta + \gamma) & -\sin(\vartheta + \gamma) & 0 \\ 0 & 0 & 1 \end{bmatrix} \quad (\text{A.3})$$

From Equation (A.3) it is clear that the transformation consists of a rotation about the $\hat{\mathbf{z}}^{PF}$ -axis by $\vartheta + \gamma + \pi/2$. To better visualise the orbital frame, Figure A.2 can be used. It is important to realise, however, that the frame in this figure is missing the rotation by γ . Hence to obtain the OF, a rotation about the $\hat{\mathbf{h}}$ -axis of the figure by γ is necessary, such that the $\hat{\mathbf{u}}_r$ -axis becomes the negative $\hat{\mathbf{y}}^{OF}$ -axis and the $\hat{\mathbf{u}}_\perp$ -axis becomes the positive $\hat{\mathbf{x}}^{OF}$ -axis. γ is the angle between the perpendicular to the true anomaly line and the velocity vector along the path. Its value is given by Equation (A.4)¹.

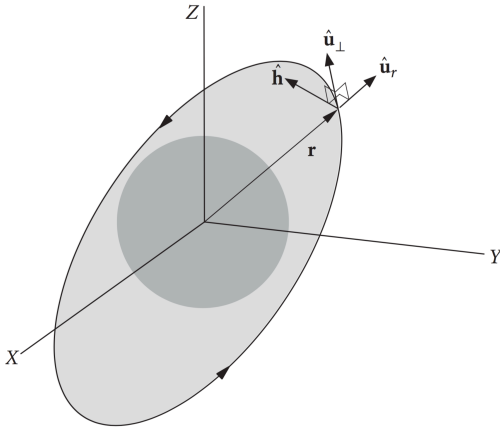


Figure A.2: Orbital frame [Cur05, p.178]

$$\gamma = \tan^{-1} \frac{e \sin \vartheta}{1 + e \cos \vartheta} = \cos^{-1} \frac{\mathbf{V} \cdot \mathbf{d}}{Vd} \quad (\text{A.4})$$

Spacecraft Frame

The final reference frame is the spacecraft frame, or SF. It is defined along the dimensions of the spacecraft and centered at the center of mass, with the $\hat{\mathbf{z}}^{SF}$ -axis parallel to the 3U side and pointing toward Mars (in the nominal operating mode) and the $\hat{\mathbf{x}}^{SF}$ -axis pointing along the 1U side and parallel to the velocity vector \mathbf{V} , again this is valid only when the satellite is in the nominal mode. Finally, as always, the $\hat{\mathbf{y}}^{SF}$ -axis follows from the right-hand rule. To transform to the spacecraft frame, a rotation about the $\hat{\mathbf{x}}^{OF}$ -axis by $-\pi/2$ is necessary. The transformation matrix is displayed in Equation (A.5).

$$\mathbb{T}_{OF \rightarrow SF} = \begin{bmatrix} 1 & 0 & 0 \\ 0 & 0 & -1 \\ 0 & 1 & 0 \end{bmatrix} \quad (\text{A.5})$$

Of course the above transformation is valid under the assumption that the attitude of the spacecraft is continuously corrected. If the spacecraft were to be left under the influence of disturbances, the direction of the SF axes would be different at every instant. As a final remark it should be important to emphasise that throughout the report, whenever x -, y - and z -axis are mentioned, they refer to the spacecraft frame.

¹Rocket and Space Technology – Orbital Mechanics: <http://goo.gl/tMGdV> [cited 31st May 2016]

B

Parameters

This appendix contains tables that include various parameters (mostly used for astrodynamics and the AODCS) used for calculations and simulations used throughout the report. This allows for the results to be reproduced by the reader.

Table B.1: Parameters used for calculations and simulations throughout report

(a) Astrodynamic parameters			(b) AODCS parameters		
Symbol	Value	Unit	Symbol	Value	Unit
g_0	9.81	[m s ⁻²]	A	0.274	[m ²]
μ_S	132.712×10^6	[km ³ s ⁻²]	m	8.5	[kg]
r_M	3385	[km]	l_x	340.5	[mm]
m_M	0.6417×10^{24}	[kg]	l_y	100	[mm]
μ_M	0.042828×10^6	[km ³ s ⁻²]	l_z	200	[mm]
J_{2M}	1960.45×10^{-6}	[–]	I_{xx}	0.238	[kg m ²]
a_M	227.9×10^6	[km]	I_{yy}	0.497	[kg m ²]
$T_{M_{sol}}$	24.6597	[hours]	I_{zz}	0.238	[kg m ²]
h_{MIC}	400	[km]	C_d	2.2	[–]
a_{MIC}	3785	[km]	q	0.14	[–]
e_{MIC}	0	[–]	U_S	5	[g mm]
i_{MIC}	92.5	[deg]	U_D	5	[g mm ²]
T_{MIC}	7070	[s]	$\omega_{RW, max}$	5000	[rpm]
$T_{MIC_{ecl}}$	1642	[s]	I_{sp}	215	[s]
T_{MS}	686.98	[days]	l_{prop}	0.1	[m]

C

TCXO Instrument

In this appendix, an overview of the temperature compensated crystal oscillator will be given through three main parts, namely the temperature effect, the architecture and the performance of TCXO¹.

Temperature Effect

As discussed in Subsection 9.3.3, the TCXO includes a thermal compensations that allows to improve the effectiveness of the oscillator. Indeed, even if the crystal oscillators are relatively stable kind of oscillators, they are highly dependent on the temperature. For example, a basic crystal oscillator will have a stability frequency of 30 [ppm], while the TCXO will have one of 2.5 ppm, for the same operational temperature, i.e. -20 to 85°C .

Architecture

In Figure C.1, the typical architecture of the TCXO is shown¹.

The compensation network produces a voltage inversely proportional to the temperature measured. The voltage generated is then sent into the crystal pulling circuit, which pulls the crystal oscillator frequency, before transferring the signal to the crystal oscillator. This is similar to a standard circuit with some adjustments for the crystal. Finally, the signal is sent to a buffer amplifier which amplifies the output signal.

The voltage regulator, connected to every parts described above, will allow to avoid external voltages variations leading to undesirable frequency shifts, while not introducing a temperature change inside the system.

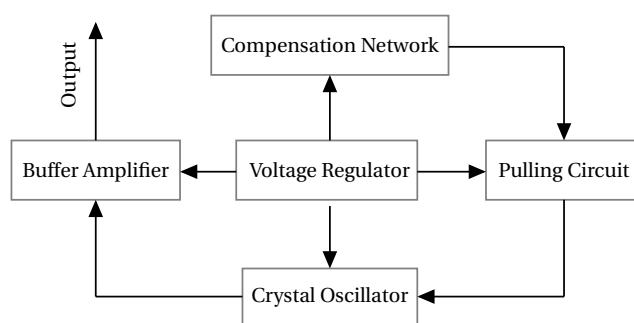


Figure C.1: TCXO typical architecture

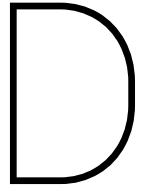
Table C.1: TCXO characteristics

Parameter	Value	Unit
Volume - possibility 1	5x3.2x1.5	[mm]
Volume - possibility 2	5x3.5x1	[mm]
Power	3	[V]
Supply Current Draw	2	[mA]
Oscillator Stabilisation time	>100	[ms]

Performance

As mentioned earlier, the control on the temperature of the TCXO allows a better performance than a regular crystal oscillator. Indeed, the improvement is between 100 % and 400 %, depending on the temperatures operating range. However, the TCXO has a higher power dissipation than an ordinary oscillator system. An overview of the characteristics of the TCXO can be seen in Table C.1¹.

¹Temperature Compensated Crystal Oscillator: <http://goo.gl/wgTUcU> [cited 1 June 2016]



Link Budget Calculations

In this Appendix, the equations used for calculating the link budget are described. The initial sizing of the Telemetry and Command subsystem is to determine the link budget needed between the relay satellite and the cubesat.

The link budget is a key element for the design of the telemetry part. Indeed, it gives an indication on the strength of the signal sent once it will be received by the receiver. If the effect of the noise is too high (i.e. the ratio of signal over the noise is lower than 1), then the signal will not be received properly. Therefore, the telemetry should be redesigned in order to avoid this situation when the mission will be on-operation.

The equations used for the calculations for the link budget are shown in Equations (D.1a) through (D.2b).

$$L_{FS} = \left(\frac{4\pi D}{\lambda} \right)^2 \quad (D.1a) \quad G_T = \frac{4\pi A_{T,e}}{\lambda^2} \quad (D.1b) \quad G_R = \frac{4\pi A_{R,e}}{\lambda^2} \quad (D.1c) \quad N = k B_n T \quad (D.1d)$$

Where,

$$\lambda = c/f \quad (D.2a) \quad B_n = 1.16R \quad (D.2b)$$

To obtain the final link margin, the values have been multiplied/divided or added/subtracted depending on their state (SI or dB). These link margins have been determined using the formulae in Equations (D.3) for the SI units and (D.4) for the decibel values.

$$LM|_{SI} = \frac{P_T G_T G_R}{L_{FS} L_T L_R N} \quad (D.3)$$

$$LM|_{dB} = P_T - L_{FS} + G_T + G_R - N - L_T - L_R \quad (D.4)$$

Bibliography

- [AFH⁺16] M. E. Akel, M. Facchinelli, G. Hirlav, Y. Q. F. Hu, E. Korhonen, S. Mast, A. Nawaz, K. Samarawickrama, M. V. Strien, and D. Tol. Midterm Report: Piggyback to Mars. Technical report, Delft University of Technology, 2016.
- [And10] D. Anderson, J. *Fundamentals of Aerodynamics*. McGraw-Hill, 2010.
- [BAB⁺11] R. Blank, S. Anglin, J.W. Beletic, et al. THxRG Family of High Performance Image Sensors for Astronomy. Technical report, University of Hawaii, Institute for Astronomy, 2011.
- [Bag10] L. A. Baghal. Assembly, Integration, and Test Methods for Operationally Responsive Space Satellites. Master's thesis, Air Force Institute of Technology, 03 2010.
- [BBG⁺08] J.W. Beletic, R. Blank, D. Gulbransen, D. Lee, et al. Teledyne Imaging Sensors: Infrared imaging technologies for Astronomy & Civil Space. Technical report, Teledyne Imaging Sensors, 2008.
- [BCP⁺] R. Bardfield, P. Clapper, D. Peterson, K. Bui, et al. LEONE (>50cm²) Space Solar Cells: Qualification, Production, Cost Reduction. Technical report, Spectrolab.
- [BL13] K. M. Brumbaugh and E. G. Lightsey. Application of Risk Management to University CubeSat Missions. *Journal of Small Satellites*, 2(1):147–160, 2013.
- [BLK⁺] J. Boisvert, D. Law, R. King, E. Rehder, et al. High efficiency inverted metamorphic (imm) solar cells. Technical report, Spectrolab.
- [Bro59] D. Brouwer. Solution of the problem of the artificial satellite without drag. *Astronomical Journal*, 64, 1959.
- [BUVH08] G. F. Brouwer, W. J. Ubbels, A.A. Vaartjes, and E.T. Hennepe. Assembly, integration and testing of the delfi-c3 nanosatellite. In *Proc. of the 59th Astronautical Congress, Glasgow, UK*, pages 1–14, 2008.
- [Can07] B. A. Cantor. MOC observations of the 2001 Mars planet-encircling dust storm. *Icarus*, 186(1):60–96, 2007.
- [Cer15] A. Cervone. Introduction to electrical power systems and rocket propulsion. AE2230-II: Power and Propulsion: Lecture 08: Introduction to Electrical Power Systems and Rocket Propulsion, 2015. Delft University of Technology.
- [Cer16] A. Cervone. Verification & Validation for Spacecraft Propulsion. Lecture 7: AE3221-I: Systems Engineering and Aerospace Design, 2016. Delft University of Technology.
- [CGMM04] E. Canalias, G. Gomez, M. Marcote, and J. J. Masdemont. Assessment of mission design including utilization of libration points and weak stability boundaries. *ESA Advanced Concept Team*, 2004.
- [Cho02] V. A. Chobotov. *Orbital Mechanics*. AIAA, 1801 Alexander Bell Drive, Reston, Virginia 20191-4344, United States of America, 3 edition, 2002.
- [Cor13] Planetary Systems Corporation. *Separation Connector Data Sheet*. Planetary Systems Corporation, 2303 Kansas Ave, Silver Spring, MD, 20910, United States, July 2013.
- [Cor15a] Planetary Systems Corporation. *Canisterized Satellite Dispenser (CSD) Data Sheet*. Planetary Systems Corporation, 2303 Kansas Ave, Silver Spring, MD, 20910, United States, August 2015.
- [Cor15b] Planetary Systems Corporation. *Payload Specification For 3U, 6U, 12U and 27U*. Planetary Systems Corporation, 2303 Kansas Ave, Silver Spring, MD, 20910, United States, August 2015.
- [Cor16] Planetary Systems Corporation. *CSD Operating and Integration Procedure*. Planetary Systems Corporation, 2303 Kansas Ave, Silver Spring, MD, 20910, United States, January 2016.
- [CSD01] A. A. Chacos, P. A. Stadter, and W. S. Devereux. Autonomous navigation and crosslink communication systems for space applications. *Johns Hopkins APL Technical Digest*, 22(2):135–143, 2001.
- [CSOM12] C. Carpenter, D. Schmuland, J. Overly, and R. Masse. Mission Application of MRS 142 Cubesat High-Impulse Adaptable Monopropellant Propulsion System. 2012.
- [CSOM13] C. Carpenter, D. Schmuland, J. Overly, and R. Masse. Cubesta Modular Propulsion System Product Line Development Status and Mission Applications. 2013.
- [CSOM14] C. Carpenter, D. Schmuland, J. Overly, and R. Masse. Test Results for the MPS-120 and MPS-130 Cubesat Propulsion System, 2014. Aerojet Rocketdyne.

- [Cur05] H. D. Curtis. *Orbital Mechanics for Engineering Students*. Elsevier, 2005.
- [DBE⁺11] H. Dezfuli, A. Benjamin, C. Everett, G. Maggio, et al. NASA Risk Management Handbook. Technical report, National Aeronautics and Space Administration, 11 2011.
- [dC09] G. de Carufel. Assembly, integration and thermal testing of the generic nanosatellite bus. Master's thesis, University of Toronto, 2009.
- [Dep06] Department of Defense. *Risk Management Guide for the DoD Acquisition*. USDoD, 6 edition, 2006.
- [DGA⁺10] S. Daphne, R. Gathier, S. Atreya, D. Banfield, et al. SPEX: A Spectropolarimeter for the ExoMars Orbiter. Technical report, SRON, 04 2010.
- [dJAB08] S. de Jong, G.T. Aalbers, and J. Bouwmeester. Improved Command and Data Handling System for the Delfi-n3Xt. 2008.
- [Dur08] G. Durgin. ECE6390 Project: Communication System. *Georgia Institute of Technology*, 2008.
- [ECS08a] ECSS. Space engineering: Electrical and electronic. Technical report, European Cooperation for Space Standardization, 08 2008.
- [ECS08b] ECSS. Space project management: Risk management. Technical report, European Cooperation for Space Standardization, 07 2008.
- [ECS09a] ECSS. Space engineering: System engineering general requirements. Technical report, European Cooperation for Space Standardization, 03 2009.
- [ECS09b] ECSS. Space engineering: Verification. Technical report, European Cooperation for Space Standardization, 03 2009.
- [ECS13] ECSS. Space engineering: Satellite attitude and orbit control system (AOCS) requirements. Technical report, European Cooperation for Space Standardization, 08 2013.
- [ECS16] ECSS. Space engineering: Electrical design and interface requirements for power supply. Technical report, European Cooperation for Space Standardization, 04 2016.
- [Eye90] C. E. Eyerman. A Systems Engineering Approach to Disturbance Minimization for Spacecraft Utilizing Controlled Structures Technology. Master's thesis, Massachusetts Institute of Technology, 1990.
- [FJE⁺] C. Fetzer, B. Jun, K. Edmondson, S. Khemthong, et al. Production ready 30% efficient triple junction space solar cells. Technical report, Spectrolab.
- [FKS⁺99] D. C. Ferguson, J. C. Kolecki, M. W. Siebert, D. M. Wilt, and J. R. Matijevic. Evidence for Martian electrostatic charging and abrasive wheel wear from the Wheel Abrasion Experiment on the Pathfinder Sojourner rover. *Journal of geophysical research*, 104(E4):8747–8789, 1999.
- [FLE] N. Fatemi, J. Lyons, and M. Eskenazi. Qualification and production of emcore ztj solar panels for space missions. Technical report, Emcore, NASA GSFC and ATK Space Systems.
- [GCSS78] R. E. Gaumer, F. J. Clauss, M. E. Sibert, and C. C. Shaw. Materials Effects in Spacecraft Thermal Control. 1978.
- [GH16a] E. Gill and T. Hoevenaars. Risk management & reliability engineering. Lecture 8: AE3221-I: Systems Engineering and Aerospace Design, 2016. Delft University of Technology.
- [GH16b] E. Gill and T. Hoevenaars. Verification and Validation for the Attitude and Orbit Control System. Lecture 6: AE3221-I: Systems Engineering and Aerospace Design, 2016. Delft University of Technology.
- [Gre12] P. Grego. *Mars and How To Observe It*. Springer, 2012.
- [GS10] M. Wilkins G. Sowers. *Atlas V Launch Services User's Guide*. United Launch Alliance, revision 11 edition, 2010.
- [Gue08] L. Guerra. Verification Module. Lecture Slides: Space Systems Engineering, 2008. University of Texas.
- [H⁺11] G. V. Harten et al. Prototyping for the Spectropolarimeter for Planetary EXploration (SPEX): calibration and sky measurements. Technical report, 2011.
- [HB07] K. Hill and G. Born. Autonomous interplanetary orbit determination using satellite-to-satellite tracking. *Journal of guidance, control, and dynamics*, 30(3):679–686, 2007.
- [HL69] M. Harris and R. Lyle. Spacecraft Gravitational Torques. Technical report, National Aeronautics and Space Administration, 1969.

- [HLB06] K. Hill, M. W. Lo, and G. H. Born. Liaison navigation in the sun-earth-moon four-body problem. In *Proceedings of the AAS/AIAA 16th Spaceflight Mechanics Meetings held January*, pages 22–26, 2006.
- [How84] Kathleen Connor Howell. Three-dimensional, periodic, 'halo' orbits. *Celestial Mechanics*, 32(1):53–71, 1984.
- [HQC⁺14] S. P. Hughes, R. H. Qureshi, D. S. Cooley, J. J. K. Parker, and T. G. Grubb. Verification and Validation of the General Mission Analysis Tool (GMAT). Technical report, NASA Goddard Space Flight Center, August 2014.
- [Hug15] H. P. Hughes. General Mission Analysis Tool (GMAT): GMAT Application to GSFC Mission Design, March 2015. NASA.
- [HvT06] R. J. Hamann and M. J. L. van Tooren. Systems Engineering and Technical Management Techniques – Part II. Lecture Notes AE3S01, 2006. Delft University of Technology.
- [ILS09] ILS. *PROTON Launch System Mission Planner's Guide*, revision 7 edition, 2009.
- [ISI16] ISI Space, Molengraaffsingel 12-14, 2629 JD. Delft, The Netherlands. *ISIPOD Cubesat Deployer*, January 2016.
- [JHWK09] M. Jah, S. Hughes, M. Wilkins, and T. Kelec. The general mission analysis tool (gmat): A new resource for supporting debris orbit determination, tracking and analysis. 2009.
- [Kik07] T. Kikugawa. Systems Integration and Stabilization of a Cubesat, 2007. University of Hawaii at Manoa.
- [Laa09] E. Laan. The Spectropolarimeter for Planetary EXploration - SPEX. VSV Symposium on Small Satellites in the Netherlands Delft, 2 2009. TNO Science & Industry.
- [LBGX07] M. Loose, J. Beletic, J. Garnett, and M. Xu. High-Performance Focal Plane Arrays Based on the HAWAII-2RG/4RG and the SIDECAR ASIC. Technical report, Teledyne Imaging Sensors, 2007.
- [LES⁺] Daniel C. Law, K.M. Edmondson, N. Siddiqi, A. Paredes, et al. Lightweight, Flexible, High Efficiency III-V Multijunction. Technical report, Spectrolab.
- [Low77] James R. Lowery. Solar Absorption Characteristics of Several Coatings and Surface Finishes. 1977.
- [LW11] Anders Larsson and Niklas Wingborg. *Advance in Spacecraft Technologies*. InTech, 2011.
- [LWH09] W. Ley, K. Wittmann, and W. Hallmann, editors. *Handbook of Spacecraft Technology*. John Wiley & Sons, 2009.
- [LWS⁺04] M. T. Lemmon, M. J. Wolff, M. D. Smith, R. T. Clancy, et al. Atmospheric imaging results from the mars exploration rovers: Spirit and opportunity. *Science*, 306(5702):1753–1756, 2004.
- [mar95] The JPL Mars Gravity Field, Mars50c, Based Upon Viking and Mariner 9 Doppler Tracking Data. Technical report, National Aeronautics and Space Administration, February 1995.
- [mar01] Mars transportation environment definition document. Technical report, National Aeronautics and Space Administration, March 2001.
- [MSB] S. Makhann, G. C. Sun, and J. C. Bourgoïn. Modelling of solar cell degradation in space. Technical report, Elsevier.
- [MSM08] A. F. Meftah, N. Sengouga, and A. M. Meftah. Prediction of the performance degradation of GaAs solar cells by electron irradiation. Technical report, Laboratory of Metallic and Semiconducting Materials, University of Biskra, October 2008.
- [MvSvdV⁺13] J. A. Mulder, W. H. J. J. van Staveren, J. C. van der Vaart, E. de Weerd, et al. *Lecture Notes Flight Dynamics AE3202*. Delft University of Technology, 2013.
- [Nan13] NanoRacks, NanoRacks, LLC 18100 Upper Bay Road, Suite 150 Houston, TX 77058. *NanoRacks CubeSat Deployer (NRCSD) Interface Control Document*, December 2013.
- [nas01] Mars Transportation Environment Definition Document. Technical report, National Aeronautics and Space Administration, 2001.
- [Nat06] National Research Council. Preventing the forward contamination of mars. 2006.
- [Noo15a] R. Noomen. AE2230-I, lecture hours 19-20: Eclipse, manoeuvres. Lecture Slides, 2015. Delft University of Technology.
- [Noo15b] R. Noomen. AE2230-I, lecture hours 21-24: Interplanetary flight. Lecture Slides, 2015. Delft University of Technology.
- [NZW⁺04] G. A. Neumann, M. T. Zuber, M. A. Wieczorek, P. J. McGovern, et al. Crustal structure of mars from gravity and topography. *Journal of Geophysical Research*, 109, August 2004.

- [PH10] M. Passaretti and R. Hayes. Development of a solar array drive assembly for cubesat. May 2010.
- [Pla16] Planetary Systems Corporation. *Tyvak Nanosatellite Launch Adapter System (NLAS) Mk. II User Guide*, January 2016.
- [QMC14] M. K. Quadrino, D. Miller, and K. Cahoy. Testing the Attitude Determination and Control of a CubeSat with Hardware-in-the-Loop. Technical report, Massachusetts Institute of Technology, 2014.
- [Rad13] A. Rad. Geostationary operational environmental satellite (goes) - goes-r series risk management plan. Technical report, U.S. Department of Commerce (DOC); National Oceanic and Atmospheric Administration (NOAA); NOAA Satellite and Information Service (NESDIS); National Aeronautics and Space Administration (NASA), 08 2013.
- [RAS13] Scott Kimbrel & Chris McLean Ronald A. Spores, Robert Masse. GMPIM AF-M315E Propulsion System. 2013.
- [Rau80] H. S. Rauschenbach. *Solar Cell Array Design Handbook: The Principles and Technology of Photovoltaic Energy Conversion*. Springer, 1980.
- [Rei08] M. S. Reid, editor. *Low-noise systems in the deep space network*, volume 1. Jet Propulsion Laboratory, 2008.
- [Roc15] Aerojet Rocketdyne. Mps-130 top-level specification sheet. 08 2015.
- [SC99] S. N. Shtangey and S. C. Cook. Integration and Test Activities for the FedSat Communications Payload. 1999.
- [Sin] J. Sinke. AE3211-II Production of Aerospace Systems. Reader. Delft University of Technology.
- [SK15] Sejin Kwon Shinjae Kang. Difficulties of catalytic Reactor for Hydroxylammonium Nitrate. *Journal of Spacecraft and Rockets*, 5(5):1508–1509, 2015.
- [SMS11] D. T. Schmuland, R. K. Masse, and C. G. Sota. Hydrazine Propulsion Module for Cubesats. 2011.
- [Spa15] SpaceX. *Falcon 9 Launch Vehicle PAYLOAD USER'S GUIDE*, revision 2 edition, 2015.
- [sse06] *Spacecraft System Engineering*. Wiley, 3 edition, 2006.
- [SSL08] F. Snik, D. Stam, and E. Laan. SPEX, An in-orbit spectropolarimeter for planetary exploration. 7010(15-1), 2008.
- [Swa13] M. Swartwout. The First One Hundred CubeSats: A Statistical Look. *Journal of Small Satellites*, 2(2):213–233, 2013.
- [The] The Royal Academy of Engineering. The study of root mean square (rms) value. The Study of Root Mean Square (RMS) Value.
- [The15] The GMAT Development Team. *General Mission Analysis Tool (GMAT): User Guide*. NASA, r2015a edition, 2015.
- [TLS06] J. Taylor, D. K. Lee, and S. Shambayati. Mars Reconnaissance Orbiter Telecommunications. *Descanso Series on Design & Performance Summary*, (12), 2006.
- [TLZC13] M. Tasy, D. Lafko, J. Zwahlen, and W. Costa. Development of Busek 0.5N Green Monopropellant Thruster. 2013.
- [UNA13] B. Udrea, M. Nayak, and F. Ankersen. Analysis of the pointing accuracy of a 6u cubesat mission for proximity operations and resident space object imaging. 2013.
- [Uni16] California Polytechnic State University. 6u cubesat design specification. Technical report, CubeSat Program, 04 2016.
- [VDW16] W. Van Der Wal. Project Guide Design Synthesis Exercise: Piggyback to Mars, 13 April 2016. Delft University of Technology.
- [vH14] G. van Harten. Spectropolarimetry for Planetary Exploration. Master's thesis, Universiteit Leiden, 12 2014.
- [VMH⁺11] R. Voors, S.G. Moon, S. Hannemann, J. Rietjens, G. van Harten, F. Snik, M. Smit, D.M. Stam, C.U. Keller, E.C. Laan, A.L. Verlaan, W.A. Vliegthart, R. ter Horst, R. Navarro, and K. Wielinga. Spectropolarimeter for planetary exploration (SPEX): performance measurements with a prototype. 8176(81760-D), 2011.
- [WL10] J. R. Wertz and W. J. Larson. *Space Mission Analysis and Design*, volume 8. Space Technology Library, 2010.
- [WL11] J. R. Wertz and W. J. Larson. *Space Mission Engineering: the New SMAD*. Space Technology Library, 2011.
- [YTY05] R. Yang, P. Thakre, and V. Yang. Combustion, explosion, and shock waves. *Thermal Decomposition and Combustion of Ammonium Dinitramide*, 41(6):657, 2005.
- [Zan13] B. T. C. Zandbergen. *Aerospace Design & System Engineering Elements I – Spacecraft Design and Sizing*. Delft University of Technology, 2013.